A STUDY OF
THE MEAN AND FLUCTUATING PROPERTIES
OF A TURBULENT HYPERSONIC BOUNDARY LAYER

Ronald Peter Bartlett B.Sc.

APRIL 1981

A thesis submitted for the degree of
Doctor of Philosophy of the University of London
and for the Diploma of Imperial College.

Department of Aeronautics,
Imperial College
Prince Consort Road,
London, S.W.7. 2BY.

ABSTRACT

The mean and fluctuating properties of hypersonic turbulent compressible boundary layer have been investigated in a Gun Tunnel at a freestream Mach number of 9 and over a range of Re_θ from 2800 to 12000, under conditions of severe wall cooling, $T_w/T_{oe} = 0.28$, and negligible pressure gradient.

The first part of the investigation comprised a study of the mean properties of the flat plate boundary layer at two freestream unit Reynolds number conditions, including detailed surveys of pitot pressure and total temperature at several chordwise stations. Valuable data has been obtained in a boundary layer which at low Re_θ exhibited the so called 'low Reynolds number effects', whereas at high Re_θ was typical of a turbulent boundary layer nearing equilibrium.

The second part of the investigation was a study to assess the feasibility of measuring density in the turbulent hypersonic flow at high molecular number density, around 10^{18} molecules cm^{-3}, using the non-intrusive electron beam fluorescence technique. This aspect of the study proved successful and the technique developed to enable preliminary measurements of mean and fluctuating density to be made in the M=9 boundary layer. Good agreement was obtained between the mean density profile measured with the electron beam probe and that derived from conventional instrumentation. Power spectra of the density fluctuations appeared typical of turbulent flow. Recommendations are made for improvements to the electron beam system for future applications in high density turbulent flow.

A versatile digital data acquisition system has been developed in the course of this investigation to enable the acquisition of the high frequency signals, around 1MHz, associated with the electron beam probe and to provide a substantial increase in the throughput and accuracy of data from the Gun Tunnel.

ACKNOWLEDGEMENTS

I wish to express my thanks to my supervisor, Dr. J. K. Harvey, for his invaluable guidance, assistance and encouragement throughout the course of this research.

I also wish to thank Dr. R. Hillier for his interest through all the stages of the work and, in particular, for his guidance during the calibration of the total temperature probes. I am indebted to Lt. A.J. Edwards RN for developing the survey total temperature probes, for performing the total temperature profile, heat transfer, Preston tube and surface pressure measurements at the high Reynolds number tunnel condition and for allowing me to use these raw data in this thesis. I wish to thank Dr. G.T. Coleman for allowing me to include his heat transfer data.

My thanks go to all the technical staff of the Aeronautics Department of Imperial College under the supervision of Mr. G.W.D. Cunningham. In particular, I wish to thank Mr. E.F. Turner for his untiring efforts in the Hypersonics Laboratory over many years and Mr. K. Sage for his careful construction of the aerodynamic models and the electron beam equipment. I wish to thank the various Ministry of Defence Contract Monitors for their interest and help over the period of this study.

My thanks go to my wife, Susan, for her support and encouragement during the course of this work and for the typing of my thesis.

This project was funded by the Procurement Executive, Ministry of Defence under Agreement AT/2037/084.

CONTENTS

		PAGE
	ABSTRACT	2
	ACKNOWLEDGEMENTS	3
	LIST OF SYMBOLS	9
	LIST OF FIGURES	16
1.0	INTRODUCTION	21
2.0	REVIEW OF LITERATURE	29
	2.1 Introduction	29
	2.2 Laminar Compressible Boundary Layer	30
	2.2.1 Velocity-temperature relationships	30
	2.2.2 Exact solutions	31
	2.3 Transition	32
	2.4 Turbulent Compressible Boundary Layer	34
	2.4.1 Velocity-temperature relationships	34
	2.4.2 Transformation methods	36
	2.4.3 Van Driest effective velocity method	37
	2.4.4 Law of the wall	38
	2.4.5 Law of the wake	39
	2.4.6 Outer law	40
	2.4.7 Determination of skin friction and heat transfer.	41
	2.4.8 The time-averaged data	44
	2.5 Fluctuating Properties of Turbulent Compressible Boundary Layers	51
	2.5.1 Fluctuating quantities	51
	2.5.2 Turbulence modelling	54
	2.5.3 Turbulence properties from time-averaged conservation equations	54

PAGE

2.5.4 Turbulence measurements 56

2.5.4.1 Hot wire aneomometer 56

2.5.5 The turbulence data 58

3.0 EXPERIMENTAL DETAIL 63

3.1 The Imperial College No. 2 Hypersonic Gun Tunnel 63

3.2 Wind tunnel models 64

3.2.1 Large modular flat plate model 64

3.2.2 Inclined flat plate 64

3.2.3 Boundary layer transition trips 65

3.3 Instrumentation 65

3.3.1 Digital data acquisition system 65

3.3.2 Transducers 66

3.3.3 Preston tubes 66

3.3.4 Surface pressure 67

3.3.5 Heat transfer 67

3.3.6 Boundary layer survey probes 68

3.3.6.1 Pitot probes 68

3.3.6.2 Total temperature probes 68

3.3.7 Stagnation pressure measurement 70

3.3.8 Freestream total temperature measurement 70

3.4 Signal Processing 70

3.5 Estimates of Accuracy 70

4.0 ELECTRON BEAM SYSTEM 72

4.1 Introduction 72

4.2 Historical 73

4.3 Background Theory 77

4.3.1 Excitation-emission mechanisms 77

4.3.2 Fluorescent light intensity dependence 80

PAGE

4.3.3 Spatial resolution and frequency response 81

4.4 Electron Beam Equipment 84

4.4.1 Model 84

4.4.2 Model support 85

4.4.3 Drift tube and differentially pumped block 85

4.4.4 Electron beam gun 86

4.4.5 Optical detection system 86

4.4.6 Signal acquisition and processing 87

4.5 Calibration 88

4.5.1 Calibration equipment and technique 88

4.5.2 Calibration results 89

4.6 Application to Boundary Layer Measurements 90

4.7 Conclusions and Recommendations 92

5.0 RESULTS AND DISCUSSION 94

5.1 Flowfield Two-dimensionality 95

5.2 Transition position 96

5.3 Surface pressure 97

5.4 Heat Transfer 97

5.5 Surface Impact Pressure 98

5.6 Pitot Pressure Profiles 101

5.7 Mach Number Profiles 102

5.8 Total Temperature Profiles 103

5.9 Velocity Profiles 104

5.10 Velocity-Temperature Relationships 106

5.11 Integral Quantities 110

5.12 Compressibility Transformation 111

5.12.1 Law of the wall 112

5.13 Outer Law 113

PAGE

5.14 Wake Component 118

5.15 Turbulent Transport Properties 120

5.16 Electron Beam Density Measurements 127

5.16.1 Time-averaged density profile 128

5.16.2 Comparison with time-averaged density profile from conventional instrumentation 128

5.16.3 Fluctuating density 129

5.16.3.1 Fluctuating density Profile 131

5.16.3.2 Comparison with available data 132

5.16.3.3 Power spectral density 134

5.16.3.4 Correlation measurements 137

6.0 CONCLUDING REMARKS 139

APPENDIX A : DIGITAL DATA ACQUISITION SYSTEM 149

A1.0 Digital Data Acquisition System 149

A2.0 Minicomputer System 150

A2.1 Minicomputer 151

A2.2 MOS Operating System 151

A3.0 Hypersonic's Control Program 153

A3.1 Hardware 153

A3.2 Software 154

A3.2.1 Initialisation functions 154

A3.2.2 Input-output functions 155

A3.2.3 Floating point arithmetic 155

A3.2.4 Master console tasks 156

A4.0 Gun Tunnel Data System 156

A4.1 Acquisition System 156

A4.2 Gun Tunnel Application Tasks 159

A4.2.1 Task G 159

PAGE

A4.2.2 Task P 160

A4.2.3 Task Q 161

A4.2.4 Task F 161

APPENDIX B : TOTAL TEMPERATURE PROBE CALIBRATION 163

B1.0 Total Temperature Probes 163

B2.0 Probe Calibration and Results 164

REFERENCES 169

TABLES

Table 1: Gun Tunnel Operating Conditions 179

Table 2: Properties of LP Condition Tripped Boundary Layer 180

Table 3: Properties of HP Condition Natural Transition Boundary Layer 181

FIGURES 182

List of Symbols

A	constant in Eq. 2.11, Eq. 2.23 and Eq. 5.15
A_1	constant in Eq. 4.4
A_2	constant in Eq. 4.5 and Eq. 4.9
B	constant in Eq. 2.11, Eq. 2.24 and Eq. 5.15
B_1	constant in Eq. 4.4
B_2	constant in Eq. 4.5 and Eq. 4.9
c_p	specific heat at constant pressure
c_v	spacific heat at constant volume
C	constant, (= 5.10), in law of the wall
C_1	constant in Eq. 4.4
C_2	constant in Eq. 4.5 and Eq. 4.9
C_f	skin friction coefficient, $\frac{\tau_w}{\frac{1}{2}\rho_\infty U_\infty^2}$
$\overline{C}_f$	incompressible skin friction coefficient
d	diameter of thermocouple wire (Appendix B)
d_o	diameter of electron beam at wall
D	constant in Eq. 4.5
e	output voltage signal of HWA
f	frequency (Hz)
$f(^*U)$	function in Eq. 5.13
f_1	focal length of lens
F	Reynolds analogy factor, $\frac{2St}{C_f}$
$F(k)$	power spectral density function
F_c	function in Eq. 2.23
F_θ	function in Eq. 2.24
G	function in Eq. 5.13, $(\gamma-1)M_e^2$

h enthalpy

$^{*}h$ enthalpy ratio, h/h_e

H total enthalpy

$^{*}H$ total enthalpy ratio, H/H_e

H_i altitude

H_{n2} shape factor, δ_n/δ_2 where $n = 1, 3$ or 4

H_{12K} kinematic shape factor, δ_{1K}/δ_{2K}

i_b electron beam current

I_n normalised fluorescent light intensity, I_{ul}/i_b

I_{ul} fluorescent light intensity

k constant in the law of the wall, (= 0.40)

or

thermal conductivity

or

wavenumber, $\frac{2\pi f}{U}$

k_g thermal conductivity of gas in Eq. B1

k_w thermal conductivity of wire in Eq. B1

ℓ mixing length

l_g length of electron beam in boundary layer

L length of thermocouple wire (appendix B)

m lens magnification

or

ratio of fluctuating to mean mass-flow, $\frac{(\rho u)'}{\rho U}$

M Mach number

n molecular number density

N exponent in $\frac{U}{U_e} = \left[\frac{y}{\delta_u}\right]^{1/N}$

Nu Nusselt number

p pressure

p_r surface impact pressure from Preston tube

p_t pitot pressure

$P(f)$ power spectral density function, $\overline{\rho'(f)}/\overline{\rho'}$

Pr Prandtl number, $\mu c_p/k$

q turbulent heat flux, $k\frac{\partial T}{\partial y} - \rho\overline{v'T'}\,c_p$

Q heat transfer rate

$Q(T)$ collision cross-section function, Eq. 4.3

r recovery factor

R gas constant

Re Reynolds number, $\frac{\rho U}{\mu}$

Re_{cr} critical Reynolds number

Re_{3d} Reynolds number in total temperature probe based on wire diameter and stagnation conditions

Re_θ momentum thickness Reynolds number, $\frac{\rho_e U_e}{\mu_e}\delta_2$

$\overline{Re}_\theta$ incompressible momentum thickness Reynolds number

$Re_{\delta 2}$ momentum thickness Reynolds number, $\frac{\rho_e U_e}{\mu_w}\delta_2$

R_{mt} correlation coefficient in Eq. 2.39

St Stanton number, $\frac{Q}{\rho_\infty U_\infty (H_r - H_w)}$

S_{T_o} sensitivity coefficient in Eq. 2.39

$S_{\rho u}$ sensitivity coefficient in Eq. 2.39

t ratio of fluctuating to mean total temperature, T_o'/T_o

t_r Gun Tunnel steady run time

T temperature

T_b thermocouple bead temperature

T_i thermocouple initial temperature

T^* reference temperature in Eq. 2.21 and Eq. 2.22

T_r recovery temperature, $T_e(1 - \frac{(\gamma-1)}{2} r M_e^2)$

U velocity in the x-direction

$^*U$ velocity ratio, U/U_e

$\overline{U}^*$ effective velocity from van Driest method, Eq. 2.11 and Eq. 5.15

U_τ friction velocity, $(\tau_w/\rho_w)^{\frac{1}{2}}$

$\Delta\frac{\overline{U}^*}{U_\tau}$ strength of wake component

V velocity in y-direction

V_a electron beam gun acceleration voltage in Eq. 4.6

w_b half-intensity width of beam in Eq. 4.6

W velocity in z-direction

$W(y/\delta)$ wake function, $1 - \cos(\pi y/\delta)$

x distance from the leading edge

y distance normal to the surface

z distance along surface normal to flow direction

Z constant in Eq. 5.13

Greek symbols

α function in Eq. 2.23

α_1 function in Eq. 2.41

β function in Eq. 2.23

β_1 function in Eq, 2.41

γ ratio of specific heats, c_p/c_v

Γ non-dimensional temperature function, $\frac{T_b - T_i}{T_r - T_i}$

δ boundary layer thickness

$\delta_1(\delta^*)$ dispacement thickness, $\int_o^{\delta_p} (1 - \frac{\rho U}{\rho_e U_e})\, dy$

$\delta_2(\theta)$ momentum defect thickness, $\int_o^{\delta_p} \frac{\rho U}{\rho_e U_e}(1 - \frac{U}{U_e})\, dy$

δ_3 kinetic energy defect thickness, $\int_o^{\delta_p} \frac{\rho U}{\rho_e U_e}(1 - \frac{U^2}{U_e^2})\, dy$

δ_4 total enthalpy defect thickness, $\int_o^{\delta_p} \frac{\rho U}{\rho_e U_e}(1 - \frac{T_o}{T_{oe}})\, dy$

δ_{1K} incompressible displacement thickness, $\int_o^{\delta_p} (1 - \frac{U}{U_e})\, dy$

δ_{2K} incompressible momentum thickness, $\int_o^{\delta_p} \frac{U}{U_e}(1 - \frac{U}{U_e})\, dy$

δ_i^* incompressible displacement thickness (δ_{1K})

δ_u boundary layer thickness where, $U = 0.995U_e$

δ_p boundary layer thickness where, $p_t = 0.99p_{te}$

Δ constant in Eq. 5.13

Δ^* boundary layer thickness defined by Eq. 2.19

ϵ small parameter in Eq. 5.13, $1 - Pr$

θ momentum thickness

θ_t non-dimensional temperature function, $\frac{T_o - T_w}{T_{oe} - T_w}$

λ function in Eq. B1

λ_c bandwidth of interference filter

μ viscosity

ν kinematic viscosity, μ/ρ

ξ eddy viscosity

ξ_1 radiation parameter in Eq. B1

ξ_w emissivity of wire (Appendix B)

$\overline{\Pi}$ wake paramter in Eq. 2.15, $\frac{k}{2}\Delta\left[\frac{\overline{U}^*}{U_\tau}\right]$

ρ density

τ shear stress, $\tau_t + \tau_1$

τ_t turbulent shear stress

τ_1 laminar shear stress

τ_w shear stress at the wall

ψ non-dimensional temperature function, $\frac{T_r - T_w}{T_{oe} - T_w}$

ψ_1 function in Eq. B1

ω angular frequency, $2\pi f$

Ω function in Eq. 5.13, $5/2N$

Superscripts

' fluctuating quantity

$\bar{\ }$ mean or time-averaged quantity

$\overline{(\ )}^2$ mean squared quantity

$\langle\ '\rangle$ root mean square (rms) quantity

Subscripts

aw adiabatic wall

e conditions at edge of boundary layer

o stagnation conditions

w conditions at wall

x distance from leading edge

∞ freestream

δ at $y = \delta_p$

eb electron beam

vd van Driest

List of Figures

1-1 Velocity-Altitude Plot for Typical Re-Entry Trajectories

1-2 Mach Number-Reynolds Number Plot for Re-Entry Trajectories

3-1 Schematic of the No. 2 Hypersonic Gun Tunnel

3-2 Performance Envelope of the No.2 Gun Tunnel

3-3 Photograph of the Modular Flat Plate Model

3-4 Photograph of Rake of Four Pitot Probes

4-1 Schematic of the Electron Beam Fluorescence Probe System

4-2 Excitation-Emission Processes for Nitrogen

4-3 Schematic of Optical Detection System

4-4 Photograph of Drift Tube and Differentially Pumped Block

4-5 Photograph of Electron Beam Gun

4-6 Photograph of Optical Detection System

4-7 Dependence of Fluorescent Light Intensity on Density for the Boundary Layer Detectors

4-8 Quenching Effect of Oxygen on Fluorescent Light Intensity

5-1 LP Condition Surface Pressure Distribution along Centreline

5-2 HP Condition Surface Pressure Distribution along Centreline

5-3 HP Condition Centreline Heat Transfer Distribution

5-4 LP Condition Centreline Heat Transfer Distribution

5-5 LP Condition Surface Impact Pressure Distribution(Preston Tube)

5-6 LP Condition Skin Friction Coefficient from Preston Tubes

5-7 HP Condition Surface Impact Pressure Distribution(Preston Tube)

5-8 HP Condition Skin Friction Coefficient from Preston Tubes

5-9 LP Condition Pitot Pressure Profiles

5-9a x = 260mm

5-9b x = 360mm

5-9c x = 560mm

5-10 LP Condition Mach Number Profiles

5-10a x = 260mm

5-10b x = 360mm

5-10c x = 560mm

5-11 HP Condition Pitot Pressure Profiles

5-11a x = 360mm

5-11b x = 410mm

5-11c x = 460mm

5-11d x = 510mm

5-11e x = 560mm

5-12 HP Condition Mach Number Profiles

5-12a x = 360mm

5-12b x = 410mm

5-12c x = 460mm

5-12d x = 510mm

5-12e x = 560mm

5-13 LP Condition Total Temperature Profiles

5-13a x = 260mm

5-13b x = 360mm

5-13c x = 560mm

5-14 LP Condition Corrected Total Temperature Profiles

5-14a x = 260mm

5-14b x = 360mm

5-14c x = 560mm

5-15 HP Condition Total Temperature Profiles

5-15a x = 360mm

5-15b x = 460mm

5-15c x = 560mm

5-16 HP Condition Corrected Total Temperature Profiles

5-16a x = 360mm

5-16b x = 460mm

5-16c x = 560mm

5-17 LP Condition Velocity Profiles

5-17a x = 260mm

5-17b x = 360mm

5-17c x = 560mm

5-18 HP Condition Velocity Profiles

5-18a x = 360mm

5-18b x = 460mm

5-18c x = 560mm

5-19 Dependence of Velocity Power Law Exponent N with Re_θ

5-20 LP Condition Comparison with Linear Crocco Temperature-Velocity Relationship, Eq. 5.10

5-21 HP Condition Comparison with Linear Crocco Temperature-Velocity Relationship, Eq. 5.10

5-22 LP Condition Comparison with Pr ≠ 1 Crocco Temperature-Velocity Relationship, Eq. 5.6

5-23 HP Condition Comparison with Pr ≠ 1 Crocco Temperature-Velocity Relationship, Eq. 5.6

5-24 LP Condition Velocity Profile 'Transformed' by the Van Driest Method, Eq. 5.16

5-24a x = 260mm

5-24b x = 360mm

5-24c x = 560mm

5-25 HP Condition Velocity Profiles "Transformed' by the Van Driest Method, Eq. 5.16

5-25a x = 360mm

5-25b x = 460mm

5-25c x = 560mm

5-26 LP Condition Comparison with Maise and McDonald Outer Law,Eq. 5.18

5-27 HP Condition Comparison With Maise and McDonald Outer Law,Eq. 5.18

5-28 Data of Watson et al (1973) Compared with the Fernholz Outer Law, Eq. 5.19

5-29 LP Condition Comparison with the Fernholz Outer Law, Eq. 5.19

5-30 HP Condition Comparison with the Fernholz Outer Law, Eq. 5.19

5-31 Method of Evaluating Strength of Wake Component, $\Delta(\overline{U}^*/U_\tau)$

5-32 LP and HP Conditions Comparison with the Available Strength of the Wake Component Data

5-32a Adiabatic Wall

5-32b Isothermal Wall

5-33 HP Condition Total Shear Stress Distribution at x = 460mm

5-34 HP Condition Mixing Length Distribution at x = 460mm

5-35 HP Condition Comparison with the Available Mixing Length Data

5-36 HP Condition Eddy Viscosity Distribution at x = 460mm

5-37 HP Condition Comparison with the Available Eddy Viscosity Data

5-38 LP Condition Fluorescent Light Intensity Profile at x = 560mm

5-39 LP Condition Mean Density Profile at x = 560mm

5-40 LP Condition Comparison with Mean Density from Conventional Probes

5-41 LP Condition Comparison with Static Temperature Profile from Conventional Probes

5-42 LP Condition RMS Density Profile at x = 560mm

5-43 Comparison of Present Data with Available RMS Density Data from Hot Wire Aneomometer Studies

5-44 Comparison of Present Data with Available RMS Density Data from Electron Beam Studies

5-45 LP Condition Power Spectral Density at x = 560mm

5-45a $y/\delta_p = 0.1$

5-45b $y/\delta_p = 0.2$

5-45c $y/\delta_p = 0.3$

5-45d $y/\delta_p = 0.6$

5-45e $y/\delta_p = 0.8$

5-45f $y/\delta_p = 1.0$

5-46 Comparison of Power Spectral Density Distribution with the Data of Sandborn (1974) Plotted on Wavenumber Basis

5-47 LP Condition Correlation between Fixed and Traversing Detector both Focused at $y/\delta_p = 0.10$

5-48 LP Condition Correlation between Fixed Detector ($y/\delta_p = 0.10$) and Traversing Detector ($y/\delta_p = 0.6$)

A1 System Configuration (Schematic)

A2 Core Map

A3 Master Task Flowchart

A4 Gun Tunnel Data System (Schematic)

A5 Timing Diagram

A6 P_o Pressure Trace

A7 Organisation of Channel Calibration Data (Task G)

A8 Task P Flowchart

A9 Task Q Flowchart

A10 Task Q Data File Format

A11 Task F Flowchart

B1 Schematic of Calibration Total Temperature Probes

B2 Variation of Probe Reynolds Number with Incidence

B3 Calibration data for the Three Probe Types

1.0 Introduction

With the advent of vehicles designed to fly at high velocity in the upper atmosphere, such as the Space Shuttle, it is important to understand thoroughly the physics of the flow around such bodies at hypersonic Mach numbers. This requirement is further emphasised by the trend of higher flight Mach numbers at relatively low altitudes, for example the development of tactical air-carried missiles with low hypersonic Mach number capabilities, or perhaps, even by the development of future manned hypersonic vehicles. Flight at hypersonic Mach numbers is generally confined to a 'flight corridor' usually bounded by vehicle design constraints of sufficient lift and maximum acceptable heat load, as illustrated by the velocity-altitude plot, fig. 1-1. A ballistic re-entry trajectory is also shown in fig. 1-1; in this case the requirement is for high terminal velocity, hence high accuracy at the target, implying a low drag, slender projectile with adequate thermal protection to withstand the extreme levels of aerodynamic heating. The corresponding Mach number-Reynolds number plot, fig.1-2, shows more clearly the different flow regimes that a vehicle may experience on a typical trajectory. The similarity parameter, $M_\infty/\sqrt{Re}_\infty$, is often used to characterize the boundaries between the different flow regimes, and the criterion, $M_\infty/\sqrt{Re}_\infty = 0.01$, is commonly used to define the change from continuum to non-continuum flow that occurs with increasing altitude.

At altitudes below about 40km, air behaves as a continuum and the flow field produced by a vehicle will be characterized at high Mach numbers by the thin Rankine-Huginiot bow shock, the viscous boundary layer adjacent to the surface of the body and the inviscid flow region in between the shock and the boundary layer. The boundary layer gives rise to skin friction and aerodynamic heating effects and also influences the inviscid flow by its

displacement effect. The magnitudes of these effects are dependent on the local state of the boundary layer for example laminar, transitional or turbulent. At hypersonic Mach numbers, M>5 say, the boundary layer thickness will be much greater than the equivalent boundary layer at the same Reynolds number in subsonic or supersonic flow. The bow shock also lies relatively close to the body at high Mach number and the boundary layer thickness may no longer be small compared to the distance between the body and the shock. This can lead to an interaction between the viscous boundary layer and the inviscid flow giving rise to additional displacement effects, for example at or near the leading edge of a flat plate at hypersonic speeds or at the shock-boundary layer interaction occuring at a compression corner. This mutual interaction of the boundary layer with the external flow is known as viscous interaction, an effect that becomes more important with increasing Mach number.

In order to assess the aerodynamic performance of a hypersonic vehicle, the designer requires accurate predictions of the properties of a compressible, turbulent boundary layer over the range of Mach number, Reynolds number and heat transfer rate encountered on a typical trajectory. Complete wind tunnel simulation of these flow parameters over such a wide range is generally not practical with existing hypersonic wind tunnel facilities especially if non-equilibrium effects such as real gas, high enthalpy or low density effects are present. However, it is possible to investigate the structure of these hypersonic boundary layers on simple shapes in existing facilities over a limited range of flow conditions. The data obtained from investigations of simple aerodynamic models, such as flat plates or axisymmetric bodies, can be used to derive and test empirical or semi-empirical correlation methods and, of course, help to develop the numerical prediction methods. In this way relevant information can be obtained for application to more complex shapes without exactly matching flow conditions.

At high Mach number the boundary layer shows certain phenomenological differences from low speed boundary layer flow. For instance, with increasing free-stream Mach number the onset of transition is delayed and the extent of the flow regimes between the end of a laminar boundary layer and the formation of an equilibrium turbulent layer, i.e.'the transition region and the low Reynolds number turbulent region', increases. In the low Reynolds number region the boundary layer is statistically turbulent, but not yet in equilibrium and the local boundary layer properties are highly dependent on the local Reynolds number. Much of the available data has been obtained in the boundary layer formed on a wind tunnel nozzle wall. Long lengths of flow are available to generate fully developed, equilibrium boundary layers but with the distinct possibility of significant upstream history, transverse curvature or pressure gradient effects. As boundary layer flow on hypersonic vehicles can be expected to be turbulent for much of the flight and often preceded by long lengths of transitional flow, there is a specific need for reliable data in this region, especially from flows of known origin on highly cooled walls, the only conditions of practical flight interest. Due to compressibility effects the turbulence structure of hypersonic boundary layers, $M>5$ say, is also different from that of a low speed flow. It is possible for significant fluctuation levels in velocity, temperature, density and pressure to co-exist. Little turbulence data is available at these Mach numbers particularly under conditions of significant heat transfer and there is a requirement for such data to develop the numerical prediction methods.

Many numerical prediction methods are available for the solution, with varying success, of the two-dimensional or axisymmetric, laminar or turbulent compressible boundary layer equations, see for example Bushnell, Cary and Harris (1976) for a critical review. These methods often use finite difference techniques with various assumptions to close the system of controlling

equations. The simplest approach is the so called 'mean-field closure' method using either an eddy viscosity or mixing length approach. For example, the mixing length model would relate the turbulent shear stress to the velocity field and, using a turbulent Prandtl number, the temperature field to the velocity field. At present there is considerable effort to develop higher-order turbulence closure models based on the Reynolds-stress equation, see for example Marvin (1977) or Rubesin et al (1977). It is hoped that the more intricate higher-order methods will provide a more realistic modelling of complex flows. At M>5 there are few studies which have yielded turbulence data on which to base the development of the turbulence models required in the prediction methods. For the more sophisticated prediction methods not only is the time-averaged information needed, but further investigations to obtain time-resolved data are also required to assess the effects of flow conditions such as Mach number, Reynolds number, pressure gradient or heat transfer on the turbulence structure. At hypersonic Mach numbers where the interpretation of the hot wire aneomometer signal in the presence of pressure fluctuations proves intractable without questionable simplifying assumptions, it is necessary to employ newer non-intrusive techniques such as the laser-doppler aneomometer or the electron beam fluorescence technique which measure directly, without ambiguity, a single flow parameter namely the velocity or density respectively.

In the present study, performed in the No. 2 Gun Tunnel at Imperial College, the boundary layer studied was formed on the wall of a large flat plate model at a nominal freestream Mach number of 9. The objective of this study has been to obtain systematic experimental data in a two dimensional turbulent boundary layer on a cold wall, $T_w/T_{oe} \simeq 0.3$, at Reynolds numbers typical of flight conditions $Re_x \simeq 10^7$. The compilation of compressible turbulent boundary layer data recently published by Fernholz and Finley (1977) showed

the range of Mach and Reynolds number of the present experiment, i.e. $M_e \simeq 9$ and $Re_\theta \simeq 2800$ to 12000, filled a gap in the available time-averaged data. The experiment was divided into two distinct phases.

Firstly, the mean properties of the boundary layer were studied in detail at two freestream unit Reynolds numbers. At the lower Reynolds number, with forced transition, the flow conditions were typical of those at which the so called 'low Reynolds number effects' might be expected. In contrast at the higher Reynolds number, with natural transition, the flow approached an equilibrium turbulent boundary layer toward the trailing edge of the model. At both freestream Reynolds numbers profile measurements of pitot pressure and total temperature were taken at three stations and wall distributions of heat transfer rate, static pressure and skin friction (inferred from Preston tubes) were measured along the model centreline. Velocity profiles have been calculated and compared with several of the current velocity-temperature correlations and, after compressibility transformation, with the well known incompressible results. Using an assumption of local similarity, it is possible to calculate the turbulent transport properties using the experimental mean flow data and the time-averaged conservation equations. This approach has been used to calculate the total shear stress, mixing length and eddy viscosity distributions which have been compared with the available models and previous data. This method is valuable in view of the shortage of direct measurements of turbulence quantities at hypersonic Mach numbers.

The second phase of the experiment consisted of a feasibility programme using the electron beam fluorescence technique to make preliminary measurements of instantaneous and mean density in a turbulent boundary layer. The electron beam technique has been applied mainly to rarefied laminar

flows at high Mach number with considerable success and the present study is one of the highest density turbulent flows to which it has been applied so far. It is a non-intrusive method in which a relativistic electron beam is fired into the test gas flow, usually air or nitrogen, and the resulting ultra-violet radiation observed with optical detectors. Due to the inherent high frequency response, coupled to the high spatial resolution that can be obtained using an optical detection system, it is possible to measure the fine details of the turbulent structure making significant improvements on hot-wire aneomometry. An assessment of the accuracy has been obtained by comparing the time-averaged density measurements made in the first phase of the study (using conventional instrumentation) with the electron beam results. It became apparent early in the electron beam probe development programme that with the available equipment it was not possible to make measurements in the high Reynolds number condition, natural transition layer as initially hoped. This was due to beam attenuation at the higher density condition coupled with inadequate differential pumping of the electron beam gun. Therefore, the electron beam study was limited to the tripped boundary layer at the lower Reynolds number running condition, although it must be re-emphasised that even at this condition the number density represented one of the highest to which the technique had been applied successfully. Most of the previous high Mach number investigations containing fluctuating data have been made with the hot wire aneomometer technique which is sensitive to mass-flux or total temperature fluctuations according to overheat ratio, and cannot match the frequency response of the essentially optical electron beam technique.

Due to inevitable time constraints the electron beam study was limited to one flat plate station, but it was sufficient to demonstrate the

feasibility of the application of the technique to the present turbulent flow. In addition to time-averaged and rms density profiles, preliminary correlation measurements were made using two detectors, one fixed and one traversing the boundary layer normal to the surface. Estimates of power spectral density for each detector and the coherence between the detectors were made using a fast Fourier transformation technique to convert the data into the frequency domain. Although preliminary, due to the paucity of measured fluctuating data, the present results are valuable since together with the mean data it is hoped that an improved understanding of the structure of turbulent compressible boundary layer flow will result eventually leading to the formation of better analytic models of the turbulent transport properties.

A third aspect of the investigation has been the development of a data acquisition and processing system which was essential for handling the high frequency signals of approximately 1MHz associated with the fluctuating density measurements. This system was also used for the time-averaged measurements with conventional instrumentation, such pitot tubes and total temperature probes, to give greater accuracy than achieved previously. The digital system is capable of digitizing one channel at 4×10^6 samples/second or up to 24 channels at slower rates, thus providing a system that accommodates all the data acquisition needs of the Gun Tunnel. This data acquisition system which is linked to the Departmental minicomputer has been successfully incorporated into an overall data processing system for the Hypersonics Laboratory, i.e. Gun and Nitrogen Tunnels, a task that entailed considerable software development in Assembly Language.

This thesis contains the following sections. In Section 2.0, a general review of the literature relevant to the turbulent compressible boundary layer at

supersonic and hypersonic Mach numbers is presented. Section 3.0 contains a description of the No. 2 Gun Tunnel facility and the instrumentation used to obtain the time-averaged profile and wall data. The development and calibration of the electron beam system is fully described in Section 4.0, which also contains a brief historical and theoretical background to the technique together with suggestions for the improvement of the system. The results from all the phases of the study are discussed and evaluated in Section 5.0. Conclusions to the validity of the present results and suggestions for further work are given in Section 6.0.

2.0 Review of the Literature

2.1 Introduction

An investigation of the available literature shows that most studies of hypersonic, turbulent boundary layers have been limited to time-averaged measurements. In contrast to the numerous studies at low speeds containing time-resolved information there are few investigations containing fluctuating data in supersonic or hypersonic flow and there are no systematic studies to investigate the effects of Mach number. This situation exists due to both experimental difficulties, compounded at the higher speeds, and the subsequent problems in data analysis due to the interactions between the various fluctuating modes. In consequence most investigations have concentrated on the time-averaged measurements and much effort has gone into developing the techniques to transform the flow to an equivalent incompressible flow.

In the survey it is proposed to discuss the laminar, compressible boundary layer and the transition from laminar to turbulent flow in brief and then to discuss the turbulent, compressible boundary layer in detail. The discussion of the turbulent case will be divided into the time-averaged properties and the fluctuation (or time-resolved) properties. In the case of the time-averaged properties, the common methods for analysing and interpreting the data will be discussed initially, to be followed by a review of some of the important contributions to the data. The same approach will be taken with the time-resolved properties with an additional discussion of one of the most important measurement techniques, i.e. the hot wire aneomometer.

2.2 Laminar Compressible Boundary Layer

With increasing Mach number the effects of compressibility, i.e. the effects of varying density, must be considered in the differential equations of the laminar boundary layer.

2.2.1 Velocity-temperature relationships

Two solutions of the energy equation were derived by Busemann (1931) and independently by Crocco (1932) for the relationship between the temperature and velocity fields. The first solution corresponds to a Prandtl number of unity and an adiabatic wall:

$$\frac{T}{T_\infty} = 1 + \frac{(\gamma-1)}{2} M_\infty^2 \left[1 - \left[\frac{U}{U_\infty} \right]^2 \right] \qquad \text{(Eq. 2.1)}$$

The molecular Prandtl number, a property of the gas, is defined as:

$$Pr = \frac{\mu c_p}{k}$$

The second solution is valid for a zero pressure gradient flow with unity Prandtl number on an isothermal wall:

$$\frac{T}{T_\infty} = \frac{T_w}{T_\infty} + \left[1 - \frac{T_w}{T_\infty} \right] \frac{U}{U_\infty} + \frac{(\gamma-1)}{2} M_\infty^2 \left[1 - \frac{U}{U_\infty} \right] \frac{U}{U_\infty} \qquad \text{(Eq. 2.2)}$$

From the solution of the energy equation for zero pressure gradient and unity Prandtl number, the well known Reynolds analogy between the rate of heat transfer and the rate of momentum transfer can be shown to exist. The Reynolds analogy can be expressed in terms of the skin friction coefficient and Stanton number as, for a Prandtl number of unity:

$$St = \tfrac{1}{2} C_f \qquad \text{(Eq. 2.3)}$$

or in general terms for a non-unity Prandtl number as:

$$St = \tfrac{1}{2} C_f \, Pr \qquad \text{(Eq. 2.4)}$$

2.2.2 Exact Solutions

Exact solutions of the laminar compressible boundary layer equations have been made possible by the elegant transformation methods such as the analysis of Illingworth (1946) and Stewartson (1949) which relate the compressible laminar boundary layer to the equivalent incompressible layer. This transformation, known as the Illingworth - Stewartson method, has formed the basis of several exact solutions using similarity concepts such as those of Li and Nagamatsu (1953, 1955); the similarity assumption relies on the fact that it is possible to scale velocity profiles to be congruent at different x-stations. The exact solutions using these concepts are valuable for testing against the approximate methods which are usually based on the momentum integral equations of the boundary layer.

The various approximate solutions have been reviewed by Walz (1969) and Stewartson (1964). The methods are usually based on one of three approaches:

i) Modification of the exact compressible similar solutions.

ii) Extension to compressible flow of the integral momentum and energy relations.

iii) Finite difference computation of the exact compressible, laminar boundary layer equations.

The advent of powerful digital computers has made the last approach more attractive in recent years e.g. Cebeci and Smith (1970).

2.2.3 Reference Temperature Methods

The reference temperature concept is an empirical method that has been used

widely to evaluate local compressible flow properties from the approximate formulae successful in incompressible flow. In detail, the reference temperature, or intermediate temperature, method involves evaluating the transport properties, such as viscosity, and the density at a temperature somewhere between the wall and freestream temperatures. The approximate low speed formulae can then be used with the transport properties evaluated at the reference temperature. The reference temperature is determined from one of the empirical methods such as those due to Young and Janssen (1952), Eckert (1955) or Sommer and Short (1955).

Detailed descriptions of the structure and calculation of the laminar, compressible boundary layer are available in Schlichting (1968), White (1974) or Stewartson (1964).

2.3 Transition

The factors effecting the transition from a laminar to a turbulent boundary layer are numerous and complex. At subsonic speeds the structure of the transition region has been widely investigated and four distinct regions have been noted:

a) Region of Tollmien - Schlichting waves.

b) Region of spanwise vorticity.

c) Three dimensional vortex breakdown.

d) Region of turbulent spots.

There are many factors which can influence the critical Reynolds number, Re_{cr}, above which the instabilities in the boundary layer will grow eventually resulting in transition to turbulent flow. These factors include pressure gradient, suction, fluid injection, heat transfer, freestream turbulence, noise, roughness and streamwise curvature. Mach number is also a factor which

influences transition. In addition to the effects of compressibility, there is often significant heat transfer associated with high speed flows, and this in general has been found to produce a stabilising effect, i.e. increases the critical Reynolds number.

Stability theory has proved useful in the study of transition in incompressible flow, notably the solution of the Orr-Sommerfelt equation. The addition of compressibility greatly increases the complexity of stability theory due to the existence of fluctuations in density and temperature. Mack (1975) has produced numerical solutions to the stability equations which reveal simultaneous oscillations or modes each of which is composed of waves propagating at different angles to the local mean flow vector. The experimental verifications of stability theory at high Mach number has been confused by the high noise levels found in most supersonic or hypersonic facilities primarily emanating from the nozzle wall boundary layer. It is thought that in most facilities transition is triggered acoustically but free stream turbulence may be the cause especially at lower Mach numbers. It is also difficult to assess the effects of Mach number due to the widely varying unit Reynolds number achievable in different wind tunnels. Mack (1975) suggests that the first effect of compressibility is to reduce the critical and transition Reynolds numbers to a minimum at $3<M_e<5$, followed by an increase at higher Mach number. Recent experimental investigations by Kendall (1974) and Demetriades (1974) have shown good agreement with the calculations of Mack.

The topics of stability and transition of high speed flows have been widely reviewed by Reshotko (1975), Mack (1969) and in particular by Morkovin (1969).

2.4 Turbulent Compressible Boundary Layer

As in the case of the laminar compressible boundary layer, the effects of varying density must be taken into account in the turbulent flow case. In addition to the velocity fluctuations present in the incompressible case, significant fluctuations in density, hence temperature, are possible in the compressible turbulent boundary layer. At high Mach number, it is also possible that pressure fluctuations will exist hence all four fluctuation modes may co-exist. Exact solutions of the turbulent boundary layer equations have not proved feasible for either the incompressible or compressible boundary layer and much effort into obtaining experimental data for input to, or to test against, the many numerical solutions. In the compressible flow case, most investigations have concentrated on time-averaged measurements of profile or wall quantities, and the methods for analysing this data has relied heavily on concepts successful in the analysis of incompressible turbulent flows. Fluctuation, or turbulence, measurements have been limited by the experimental difficulties but are vital to form the necessary turbulence models for input to the calculation methods. The technique most frequently used has been the hot wire aneomometer, but the newer non-intrusive methods are becoming inceasingly popular. In this section, the time-averaged and the time-resolved (fluctuation) properties of the compressible turbulent boundary layer are discussed and a review presented of the important contributions to the data.

2.4.1 Velocity-Temperature Relationships

The Crocco-Busemann relationship between velocity and temperature, derived for the compressible laminar boundary layer (Crocco (1932) and Busemann (1931)), has been extended to the compressible turbulent case by van Driest (1951). The original Crocco relationship is based on an exact solution of

the energy equation and is valid for the following conditions: molecular Prandtl number of unity, isothermal wall and zero pressure gradient. To account for a non-unity Prandtl number, van Driest modified the Crocco relationship to include a recovery factor. In the turbulent flow case, the recovery factor, r, is found to be,

$$r \simeq \sqrt[3]{Pr} = 0.89 \quad \text{(turbulent,air)}.$$

The Crocco relationship, modified by van Driest, for $0.8 < Pr < 1$ is:

$$\frac{T}{T_e} = \frac{T_w}{T_e} + \frac{U}{U_e}\left[1 - \frac{T_w}{T_e}\right] + \frac{r(\gamma-1)}{2} M_e^2 \frac{U}{U_e}\left[1 - \frac{U}{U_e}\right], \qquad \text{(Eq. 2.5)}$$

which can be re-written in terms of the recovery temperature T_r as

$$\frac{T_o - T_w}{T_{oe} - T_w} = \frac{T_r - T_w}{T_{oe} - T_w}\left[\frac{U}{U_e}\right] + \frac{T_{oe} - T_r}{T_{oe} - T_w}\left[\frac{U}{U_e}\right]^2, \qquad \text{(Eq. 2.6)}$$

where,

$$T_r = T_e\left[1 + \frac{r(\gamma-1)}{2} M_e^2\right].$$

For unity Prandtl number and unity recovery factor, the relationship simplifies to the original linear Crocco solution:

$$\frac{T_o - T_w}{T_{oe} - T_w} = \frac{U}{U_e} \qquad \text{(Eq. 2.7)}$$

If the wall condition is adiabatic, i.e. $T_r = T_w$, rather than isothermal, the relationship reduces to a quadratic:

$$\frac{T_o - T_w}{T_{oe} - T_w} = \left[\frac{U}{U_e}\right]^2 \qquad \text{(Eq. 2.8)}$$

It is usual to compare compressible turbulent velocity-temperature data with the linear and quadratic relationships. The non-unity Prandtl number solution Eq. 2.5, deviates only slightly from the linear solution, Eq. 2.7, and has shown good agreement with data from zero pressure gradient flows with little upstream influence especially on cold walls, see for example Bushnell et al (1969). The quadratic relationship, Eq. 2.8, which is also known as the

Walz form of the Crocco solution has shown good agreement for flow with non-zero pressure gradients, e.g. nozzle wall boundary layers. In the case of adiabatic or near adiabatic wall flows the simple relationships above do not predict the velocity-temperature distribution, see Sturek and Danberg (1971). Recently Whitfield and High (1977) have produced an analytic relationship which predicts an increase in Prandtl number approaching the wall within the viscous sublayer, by including an approximate model for the turbulent shear stress distribution. Earlier Meier and Rotta (1971) produced a similar solution using a numerical approach with a variable Prandtl number distribution through the boundary layer.

2.4.2 Transformation Methods

The prime objective of the compressibility transformation method is to derive a set of functions which relate a compressible flow to a corresponding constant density flow. For example, it is possible to derive an exact solution in the case of a laminar compressible boundary layer which transforms the flow to a corresponding subsonic flow e.g. the Illingworth-Stewartson transformation (Schlichting (1968) p324). At present in the compressible turbulent case there is no available exact solution, and all the available transformation methods require assumptions usually based on experimental data. Early work on transformation methods can be traced back to von Karman (1935) but the first attempt to transform the partial differential equations of turbulent flow was by Mager (1958). The method due to Coles (1962) is one of the best known methods and is based on the earlier work of Mager. He assumed that the turbulent shear stress is invariant under the transformation but Coles modified the method with a more rigorous 'law of corresponding stations' for compressible adiabatic flow. This law is based on the assumption that certain of the terms in the transformation are functions of x only (see for example Bradshaw (1977)). The Coles method is derived for zero pressure gradient flows on adiabatic

walls and many later workers have attempted to extend the method to flows with pressure gradient or heat transfer, e.g. Crocco (1963), Baronti and Libby (1966) and Lewis, Kubota and Webb (1970).

2.4.3 Van Driest effective velocity approach

The effective velocity method of van Driest (1951) has been extensively used to 'transform' the compressible turbulent boundary layer to an equivalent incompressible flow. Although applied to the whole layer this method is strictly valid in the inner layer; the method is based on similarity concepts using a modified Prandtl mixing length theory in conjunction with a Crocco-Busemann temperature distribution. The Prandtl mixing length theory is based on the assumption that the turbulent shear stress in the boundary layer can be expressed as:

$$\tau_t = \rho \overline{v'u'} = \rho \ell^2 \frac{dU}{dy} \left|\frac{dU}{dy}\right| \qquad \text{(Eq. 2.9)}$$

Prandtl found that the mixing length, ℓ, was proportional to y, i.e. $\ell = ky$. To relate the density to velocity, van Driest assumed a perfect gas and used the Crocco-Busemann relationship for unity Prandtl number:

$$\frac{\rho_w}{\rho} = \frac{T}{T_w} = 1 + \left[\frac{T_{aw}}{T_w} - 1\right]\frac{U}{U_e} - \frac{(\gamma-1)}{2}M_e^2 \frac{T_e}{T_w}\left[\frac{U}{U_e}\right]^2 \qquad \text{(Eq. 2.10)}$$

If Eq. 2.9 is substituted into Eq. 2.10 and assuming that $\tau \simeq \tau_t \simeq \tau_w$, van Driest was able to integrate the resulting equation to obtain an effective velocity in terms of U/U_e. Keener and Hopkins (1973) have proposed a form of the van Driest relationship incorporating a temperature distribution based on a turbulent recovery factor to allow for a non-unity Prandtl number.

The van Driest effective or 'transformed' velocity is then , after integration given by

$$\frac{\overline{U}^*}{U_\tau} = \frac{1}{A\sqrt{\frac{1}{2}C_f\,(T_w/T_e)}}\left[\sin^{-1}\left[\frac{2A^2(U/U_e) - B}{\sqrt{4A^2 + B^2}}\right] + \sin^{-1}\left[\frac{B}{\sqrt{4A^2 + B^2}}\right]\right] \qquad \text{(Eq. 2.11)}$$

where $U_\tau = (\tau_w/\rho_w)^{\frac{1}{2}}$ and is known as the friction velocity,

and

$$A^2 = \frac{T_e}{T_w}\frac{(\gamma-1)}{2}M_e^2 \qquad B = \frac{T_e}{T_w} + A^2 - 1 \qquad \text{(Eq. 2.12)}$$

2.4.4 Law of the wall

The analysis of the incompressible turbulent boundary layer has relied heavily on the multi-layer concept of the boundary layer, see for example Bradshaw (1976a). In this description the layer is divided into a viscous sublayer, a buffer layer and the log-layer, whereas the outer region is divided into an outer layer and a superlayer.

The inner region is characterised by the so-called 'law of the wall' which has had so much success in correlating low speed velocity data, e.g. Cebeci and Smith (1974), and much effort has been expended on establishing the law of the wall in compressible flow. The effective velocity approach of van Driest has been extensively used to transform the compressible flow velocity profiles for comparison with the law of the wall. The law of the wall using the van Driest method, Eq. 2.11, is usually modelled as:

$$\frac{\overline{U}^*}{U_\tau} = \frac{yU_\tau}{\nu_w} \qquad \text{(IN SUBLAYER)} \qquad \text{(Eq. 2.13)}$$

$$\frac{\overline{U}^*}{U_\tau} = \frac{1}{k}\ln\left[\frac{yU_\tau}{\nu_w}\right] + C \qquad \text{(LOG LAYER)} \qquad \text{(Eq. 2.14)}$$

Where k is the von Karman constant, Schlichting (1968), and C is a function dependant on heat transfer rate and skin friction.

The values of k and C are still subject to uncertainty, Bradshaw (1977) recommends k = 0.41 and C = 5.2, whereas Fernholz and Finley (1977) suggest k = 0.40 and C = 5.1 (based on their critical comparison of available data). The van Driest method has shown considerable success in correlating data over a wide range of Mach number from both adiabatic and cooled wall boundary layers e.g. Laderman (1978).

2.4.5 Law of the Wake

Coles (1956) proposed a function which represented the wake-like behaviour of the outer region of the boundary layer in incompressible turbulent velocity profiles; this hypothesis is commonly known as the Law of the Wake. A wake function can be incorporated into the law of the wall and extended to the compressible case using the van Driest method for transforming the velocity profile:

$$\frac{\overline{U}^*}{U_\tau} = \frac{1}{k} \ln\left[\frac{yU_\tau}{\nu_w}\right] + C + \frac{\overline{\Pi}}{k} W(y/\delta) \qquad \text{(Eq. 2.15)}$$

The wake is represented by a wake parameter $\overline{\Pi}$ and a function $W(y/\delta)$ which is approximated by:

$$W(y/\delta) \simeq 1 - \cos(\pi y/\delta) \qquad \text{(Eq. 2.16)}$$

This function has a value of zero at the wall and equals 2 at $y = \delta$. Coles defined the strength of the wake component as $\Delta(\overline{U}^*/U_\tau)$ which represents the maximum overshoot of the velocity profile from the log-law region. The wake parameter is related to the strength by:

$$\overline{\Pi} = \frac{k}{2} \Delta\left(\frac{\overline{U}^*}{U_\tau}\right) \qquad \text{(Eq. 2.17)}$$

Coles found that the strength, $\Delta(\overline{U}^*/U_\tau)$, was zero at $Re_\theta<500$ and reached a maximum value of $\Delta(\overline{U}^*/U_\tau) \simeq 2.8$ at $Re_\theta>5000$. Fernholz and Finley (1979) have concluded that the wake component shows similar characteristics in supersonic flow as in the incompressible flow case but the large scatter in the available wake strength data is probably due to a combination of difficulties in evaluating it from the experimental data, and to factors such as three dimensional effects, free stream turbulence, upstream influences or other as yet unknown factors.

2.4.6 Outer law

Many attempts have been made to extend the outer law or the velocity defect law to compressible flow, e.g. Coles (1953), Stalmach (1958) or Maise and McDonald (1968). Using the van Driest method and incorporating a wake function, the outer law is usually represented by:

$$\frac{\overline{U}_\delta^* - \overline{U}^*}{U_\tau} = -\frac{1}{k} \ln (y/\delta) + \frac{\overline{\Pi}}{k} (2 - W(y/\delta)) \qquad \text{(Eq. 2.18)}$$

The outer law is sensitive to pressure gradient effects and in particular to the evaluation of a boundary layer thickness δ. In compressible flow at high Mach number there may well be large discrepancies between δ_u and δ_p. It is usual to employ the δ_p thickness defined at the point where the impact pressure equals 0.99 of the freestream impact pressure. Fernholz (1969) has suggested a semi-empirical outer law which attempts to overcome the problem of evaluating δ by using the length scale Δ^*, originally proposed by Rotta (1950), where:

$$\Delta^* = \delta_p \int_0^1 \frac{\overline{U}_\delta^* - \overline{U}^*}{U_\tau} d(y/\delta_p) \qquad \text{(Eq. 2.19)}$$

The Fernholz relationship is valid for zero pressure gradient flows over isothermal walls:

$$\frac{\overline{U}_\delta^* - \overline{U}^*}{U_\tau} = -4.70 \ln (y/\Delta^*) - 6.74 \qquad \text{(Eq. 2.20)}$$

In this expression the constants were obtained from a correlation of data

as a function of T_w/T_{aw} and Re_{δ_2} .

2.4.7. Determination of Skin Friction and Heat Transfer

The determination of skin friction in the compressible turbulent boundary layer is of obvious importance to flight at hypersonic velocities, but the prediction of skin friction, even for the zero pressure gradient flow, has proved an intractable problem. The numerous theories so far presented show large discrepancies amongst themselves, and the available measurement methods, such as floating element gauges or indirect devices such as Preston tubes, have serious experimental or calibration difficulties. Determination of C_f from heat transfer is also of dubious value due to the uncertainty in the Reynolds analogy factor F. Most of the available C_f prediction theories are based on one of three approaches:

a) Intermediate Temperature Methods

This method relies on evaluating the boundary layer transport properties at an intermediate or reference temperature somewhere between the wall and freestream temperatures; this approach had shown success in evaluating compressible laminar boundary layers e.g. White (1974) p.590. Once the fluid properties such as density and viscosity have been evaluated at the reference temperature the skin friction can be evaluated from one of the constant density formulations e.g. Karman-Schoenherr formula (Schlichting p.602). Two of the best known reference temperatures are due to:

(i) Eckert (1955) $$\frac{T^*}{T_e} = 0.5 + 0.039\, M_e^2 + 0.5\, \frac{T_w}{T_e} \qquad \text{(Eq. 2.21)}$$

(ii) Sommer and Short (1955) $$\frac{T^*}{T_e} = 0.55 + 0.035\, M_e^2 + 0.45\, \frac{T_w}{T_e} \qquad \text{(Eq. 2.22)}$$

b) Methods based on transformation theories

If a transformation method can be found to map the compressible turbulent flow into the equivalent incompressible flow then it is also possible to determine the skin friction from the incompressible formulae, e.g. Schlicting (1968). The limitations of the available transformation methods have been discussed earlier, section 2.4.2, and the same comments are also applicable to the skin friction methods based on these methods. The Coles (1962) transformation has formed the basis of many of these formulae , e.g. Baronti and Libby (1966).

c) Methods based on the van Driest mixing length theory

The effective velocity method discussed in section 2.4.3 can be extended to provide a skin friction formula e.g. van Driest (1951). A second theory was later produced by van Driest (1956) which incorporated the von Karman mixing length formulation and is commonly known as van Driest(II). The von Karman mixing length is used in the Prandtl shear stress equation, and a temperature recovery factor, r = 0.89, was used in the Crocco temperature distribution thus enabling van Driest to calculate the density profile. The van Driest (II) formula is given by Hopkins and Keener (1972), using the notation of Spalding and Chi (1964), in terms of the incompressible skin friction coefficient, $\overline{C}_f$, and the incompressible momentum thickness Reynolds number $\overline{Re}_\theta$.

$$\overline{C}_f = (F_c)_{vd}\, C_f \qquad \text{(Eq. 2.23)}$$

$$\overline{Re}_\theta = (F_\theta)_{vd}\, Re_\theta \qquad \text{(Eq. 2.24)}$$

where vd stands for van Driest and,

$$(F_c)_{vd} = \frac{r(\gamma-1)}{2} M_e^2 \left(\sin^{-1}\alpha + \sin^{-1}\beta\right)^{-2}, \qquad (F_\theta)_{vd} = \mu_e/\mu_w .$$

$$\alpha = (2A^2 - B)/(4A^2 + B^2)^{\frac{1}{2}} \quad , \quad \beta = B/(4A^2 + B^2)^{\frac{1}{2}}$$

where,

$$A = \sqrt{\frac{r(\gamma-1)}{2} M_e^2 \frac{T_e}{T_w}} \quad , \quad B = \frac{T_e}{T_w} + A^2 - 1$$

This theory is recommended by Hopkins and Inouye (1971) on the basis of an evaluation of the available methods. Other theories have been based on the van Driest formula for instance the Spalding-Chi (1964) method which used empirically derived functions to account for heat transfer.

None of the available prediction methods have yet been able to accurately predict the observed values of skin friction over the wide range of Mach number and heat transfer conditions experienced in practice. The direct measurement of skin friction using the floating element balance is questionable due to the reliability and comparability of these devices. Indirect devices such as the Preston tube require a calibration which is often based on a comparison with floating element balance data. Although Winter (1976a) in his review of measurement techniques concluded that the Preston tube is probably the most reliable of the devices available to date but the choice of calibration in compressible flow is often arbitrary.

Winter (1976b) has comprehensively reviewed the measurement techniques for heat transfer in compressible boundary layer flow. The well known Reynolds analogy, section 2.4.1, is the method often used to predict the heat transfer rate or the equivalent non-dimensional Stanton number, where:

$$F = 2St/C_f \qquad \text{(Eq. 2.25)}$$

The accuracy of the Reynolds analogy factor, F , is inherently linked to the accuracy of the skin friction coefficient which, as described earlier,

has proved difficult to predict or measure with confidence. From simultaneous measurement of skin friction and heat transfer rate the range of F has been found to vary from 0.8 to 1.2 although a value of 1.16 is often used in practice at high Mach number.

2.4.8 Time-averaged Data

The early work in compressible boundary layers has been reviewed by Hornung (1966), Beckwith (1970), Coleman (1973) and Fernholz (in Bradshaw 1976a). A recent review paper by Bradshaw (1977) contains an overview of the topic, and a valuable source of data is the critical compilation of data by Fernholz and Finley (1977). More recently the same authors, Fernholz and Finley (1979), have produced an evaluation paper on the data.

An early investigation of an adiabatic boundary layer with zero pressure gradient was performed by Coles (1953) at a Mach number range from 2 to 4.5. He found that various types of transition device resulted in negligible differences in profile quantities e.g. velocity. A null balance technique was used to measure C_f which was subsequently used to verify the momentum-integral equation. Lobb, Winkler and Persh (1955) made an investigation of a hypersonic cold wall boundary layer; the nozzle wall boundary layer was studied at $5 < M_e < 8.2$, and profile measurements of total temperature and pitot pressure were made but C_f values were estimated from the velocity gradient at the wall. Hill (1959) investigated a cold wall axisymmetric boundary layer at $8 < M_e < 10$ and found a quadratic dependance of total temperature function (Θ_t)on velocity which has since proved typical of a nozzle wall flow. The properties of a flat plate boundary layer at $M_e = 5$ were measured by Winkler and Cha (1959). This boundary layer showed significant transitional characteristics; Walz (1964) and Fernholz and Finley (1979) have questioned the accuracy of the C_f measurements which were determined from the slope of the velocity profile at the wall. This comment

also applies to the earlier study by Lobb et al (1955).

Spalding and Chi (1964) extensively reviewed the available prediction formulae for skin friction. They produced a method based on the van Driest (1956) mixing length theory but including constants based on empirical data.

Cary and Bertram (1974) recommend the Spalding-Chi formula for general use at hypersonic speeds but prefer the Coles (1962) formula for very cold walls at high Mach number. Hopkins et al (1972) found that the Spalding-Chi underpredicted their data by more than 10%.

In a review of data, Bertram and Neal (1965) concluded that no single theory for skin friction could adequately describe the available data over a wide range of Mach number and heat transfer rate. Danberg (1964, 1967) investigated a transitional boundary layer at $M_e = 6.7$ under conditions of both heat and mass transfer. He found that the transformed velocity, using the van Driest method, was in reasonable agreement with the law of the wall, but in contrast to incompressible flow the constant terms are functions of the heat and mass transfer rate. Allen (1968) used the Baronti and Libby (1966) form of the Coles transformation to calculate skin friction from velocity profiles. A graphical interpolation technique, originated by Clauser (1954), was used to determine skin friction; Allen concluded that the method gave good results for adiabatic flow but did not predict the correct trend with heat transfer. Fernholz (1969) has proposed a semi-empirical relationship, using the van Driest transformation, for the velocity defect distribution in the outer layer. The author suggests that this method correlated the data better than previous methods such as those by Stalmach (1958) or Maise and McDonald (1968), which fall down on the evaluation of a representative boundary layer thickness in compressible flow.

In an extensive review of velocity profile data Johnson and Bushnell (1970) have presented a correlation for the exponent of the power law fit to the velocity profile in terms of Re_θ and T_w/T_{oe}. Hastings and Sawyer (1970) have reported measurements at $M_e = 4$ over a range of Re_θ including profiles which showed significant transitional and non-equilibrium effects. Estimates of the strength of the wake component confirmed a similar trend to that proposed by Coles (1962) for incompressible flow.

Hopkins and Inouye (1971) have reviewed the skin friction formulae and recommend the use of van Driest (II). In addition, they suggest that the same formula, in conjunction with a Reynolds analogy factor of 1.0, be used to determine heat transfer rate at high Mach number. Using a novel combined pitot and total temperature probe, Meier and Rotta (1971) have investigated a nozzle wall boundary layer at $1.5 < M_e < 3.0$. This data was used, in conjunction the results of a complementary study by Mabey, Sawyer and Meier (1974), to calculate the turbulent Prandtl number distribution through the boundary layer. They found that turbulent Prandtl number increased close to the wall indicating that the turbulent transport of heat decreased more rapidly towards the wall than the turbulent transport of momentum.

Hopkins et al (1972) made direct measurements of skin friction and determined velocity profiles for $M_e = 5.9$ to 7.8 at $T_w/T_{oe} = 0.3$ and 0.5. They found that van Driest (II), Coles and a finite difference method predicted the skin friction data to within $\pm$ 10%. It was also found that van Driest (II) gave the most satisfactory transformation of the compressible velocity profile data onto the law of the wall and velocity defect curves. Voisinet and Lee (1972) investigated a zero pressure gradient nozzle wall boundary layer at $M_e = 4.9$. This data is probably subject to considerable upstream history effects due to heat transfer in the nozzle region.

Horstman and Owen (1972) and Owen and Horstman (1972) present mean profile data obtained from a detailed investigation of the boundary layer on a cone-ogive-cylinder model at $M_e = 7.2$ and $T_w/T_{oe} = 0.5$. Using the similarity method based on the time averaged conservation equations of Bushnell and Morris (1971), they calculated the shear stress distribution which agreed well with incompressible results. The van Driest (1956) transformation gave the best agreement of their data with the incompressible law of the wall. The measured skin friction was found to be bracketed by the commonly used formulae i.e. Coles, van Driest (II) and Spalding-Chi. The finite difference method of Dwyer (1972) gave the most satisfactory agreement with the skin friction and heat transfer data.

Hopkins and Keener (1972) investigated a nozzle wall boundary layer with upstream history effects and contrasted the results with data from a reference flat-plate study in the same facility by Kenner and Hopkins (1972). They found that the flat plate data fitted the linear Crocco temperature-velocity relationship but the nozzle wall data was found to be closer to a quadratic dependance.

The use of Preston tubes in compressible flow was assessed by Allen (1973) who tested several calibrations against floating element balance measurements. Allen recommends the use of one of the log-law calibrations, e.g. Patel (1965), rather than one based on a power law, e.g. Hopkins and Keener (1972). A least squares calibration equation was also developed from the measured balance data which gave better accuracy than the others tested. Watson et al (1973) presented data on the development of a boundary layer through a transition region. Significant low Reynolds number effects were found and a correction scheme suggested which greatly improved the agreement between measured and predicted values. Bradshaw and Unsworth (1973) assessed the C_f data of Allen (1973) and presented a

revised calibration in terms of inner layer variables; the authors state that this calibration should be valid for boundary layers with significant pressure gradients. The Van Driest mixing length method was applied by Keener and Hopkins (1973) to the nozzle wall data of Hopkins and Keener (1972); it was found that by using a modified temperature velocity distribution in the Van Driest equations it was possible to predict velocity profiles with upstream history effects.

Meier, Voisinet and Gates (1974) extended the work of Meier and Rotta (1971) on the evaluation of the turbulent Prandtl number distribution through the boundary layer. Using Prandtl's mixing length concept a relationship was proposed for the increase in turbulent Prandtl number near the wall which gave good agreement with data from three different wind tunnels.

Detailed mean flow measurements were made by Laderman and Demetriades (1974) in their study of a cooled wall boundary layer at $M_e = 9.4$. The authors could not give a satisfactory explanation for the large normal pressure gradient detected across the layer. Non-dimensional total temperature showed a quadratic dependance on velocity in the outer layer but changed to a linear dependance close to the wall. This could be a result of the interpolation procedure used to determine the total temperature data close to the wall.

Cary and Bertram (1974) reviewed the available skin friction formulae and recommend the use of the Spalding-Chi formula of Mach numbers up to 9 but showed that the Coles (1962) formula gave better correlations at higher Mach number on cold walls. Mabey et al (1974) extended the adiabatic flat plate data of Hastings and Sawyer (1972). Fernholz and Finley (1979) considered this to be the most reliable zero pressure gradient, adiabatic wall data in its Mach number range.

A comprehensive review of the measurement techniques for heat transfer and skin friction has been published by Winter (1976a and 1976b). In the case of skin friction, Winter concludes that due to the lack of a reliable and reproducable floating element balance, the Preston tube remains the most repeatable device. Bradshaw (1976) has used the van Driest transformation to produce a skin friction formula in terms of wall variables, which he suggested in Bradshaw (1977) was one of the best methods for evaluating experimental data without the usual arbitrary assumptions.

A version of Coles' wall-wake velocity profile has been proposed by Sun and Childs (1976) for high Mach number flows with heat transfer. This method was found to give good agreement with experimental data over a wide range of Mach number and heat transfer rate. Whitfield and High (1977) have investigated the temperature-velocity relationships for non-unity Prandtl number and produced an analytic relationship which has shown good agreement with experimental data; earlier, Meier and Rotta (1974) achieved similar results using a numerical method of solution.

Watson (1977) has invesigated wall cooling effects on a transitional boundary layer at M = 11. He found the transition position little effected by heat transfer rate. Cold wall total temperature data followed the usual linear Crocco solution for flat plate data but adiabatic wall data showed similar departures from the linear solution as those reported by Mabey et al (1974).

In the light of revised floating element data, Allen (1977) re-evaluated the compressible flow Preston tube calibrations of Allen (1973). The general conclusions of the original paper remain unchanged but the author now recommends the use of either his own least squares fit calibration or the method of Bradshaw and Unsworth (1973). Fernholz and Finley (1977) assembled a comprehensive compilation of data from compressible turbulent boundary layers investigations which is a valuable source of experimental

detail and numerical data. Mean flow data have been reported by Laderman (1978) for various heat transfer rates in a $M_e = 3$ boundary layer. Using the van Driest transformation the velocity defect law incorporating a wake function correlated the non-adiabatic data successfully. The turbulent transport properties deduced from mean flow data were found to be in good agreement with previous adiabatic flow results. Acharya, Horstmann and Kussoy (1979) report mean profile measurements as part of a turbulence study at $M_e = 2.3$ in an adiabatic nozzle wall boundary layer. They found that using the van Driest transformation the profile data correlated well with the incompressible form of the law of the wall.

2.5 Fluctuating Properties of Turbulent Compressible Boundary Layers

2.5.1 Fluctuating quantities

In incompressible turbulent flow the velocity fluctuations give rise to the well known apparent or Reynolds stresses which are generally much larger than the viscous stresses. Compressible flow is complicated by the additional variation of mean density and the subsequent need for an equation of state to relate the pressure, density and temperature. Turbulent compressible flow is further complicated by the existence of density fluctuations:

$$\rho = \overline{\rho} + \rho' \qquad \text{(Eq. 2.26)}$$

If the density fluctuations are present, the equation of state automatically implies that temperature fluctuations must also exist,

$$T = \overline{T} + T' \qquad \text{(Eq. 2.27)}$$

Hence, in a compressible turbulent flow it is possible for velocity, density, temperature and pressure fluctuations to co-exist. The derivation of the two-dimensional, compressible boundary layer equations from the full Navier-Stokes equations requires the following assumptions:

$$\overline{V} \ll \overline{U} \quad , \quad \frac{\partial}{\partial x} \ll \frac{\partial}{\partial y} \quad , \quad \overline{W} = 0 \quad , \quad \frac{\partial}{\partial z} = 0 \quad .$$

The additional assumption that the fluctuations are small with respect to the mean value is also required, i.e.

$$Q' \ll \overline{Q} \qquad \text{for all } Q,$$

where $Q = u, T, p$ and ρ. One of the first applications of these assumptions to the compressible Navier-Stokes equations was by van Driest (1951); the form of the time-averaged boundary layer equations (two-dimensional, compressible

and turbulent) presented here is a development of van Driest's work by Rotta (1963):

Continuity: $$\frac{\partial}{\partial x}\left(\bar{\rho}\,\bar{U}\right) + \frac{\partial}{\partial y}\left(\overline{\rho V}\right) = 0 \qquad \text{(Eq. 2.28)}$$

X-Momemtum: $$\bar{\rho}\,\bar{U}\frac{\partial \bar{U}}{\partial x} + \overline{\rho V}\frac{\partial \bar{U}}{\partial y} = -\frac{d\bar{p}}{dx} + \frac{\partial \tau}{\partial y} \qquad \text{(Eq. 2.29)}$$

Y-Momemtum: $$\frac{\partial \bar{p}}{\partial y} + \frac{\partial}{\partial y}\left(\bar{\rho}\,\overline{v'v'}\right) = 0 \qquad \text{(Eq. 2.30)}$$

Energy: $$\bar{\rho}\,\bar{U}\,c_p\frac{\partial \bar{T}}{\partial x} + \overline{\rho V}\,c_p\frac{\partial \bar{T}}{\partial y} = \bar{U}\frac{d\bar{p}}{dx} + \frac{\partial q}{\partial x} + \tau\frac{\partial \bar{U}}{\partial y} \qquad \text{(Eq. 2.31)}$$

where, $$\tau = \frac{\partial \bar{U}}{\partial y} - \bar{\rho}\,\overline{u'v'} \quad \text{and} \quad q = k\frac{\partial \bar{T}}{\partial y} - \bar{\rho}\,\overline{v'T'}\,c_p \qquad \text{(Eq. 2.32)}$$

(A quantity with an overbar represents a time-averaged value and one with a prime represents a fluctuating quantity, e.g. $\bar{U}$ and u' respectively). These equations, together with the equation of state, describe the two-dimensional compressible boundary layer. In contrast to incompressible flow, the turbulent shear stress term, τ_t , and the turbulent heat flux term, q , become triple products as the mean density varies. The equations do not form a closed set thus cannot be solved without further knowledge of the turbulence structure, i.e. further simplifying assumptions.

The turbulence structure of the compressible boundary layer shows the same type of intermittency in the outer region as found in the constant density case. The intermittent structure is usually observed as a characteristic 'one-sided' signal obtained from a hot wire aneomometer, as first reported by Kovasznay (1953). This phenomenon is observed at both the interface between the thick laminar sublayer (thick compared to an incompressible layer at the same Re_θ) with the turbulent inner layer, and at the true

boundary layer edge with the inviscid freestream flow. In the case of a cold wall, usual at high Mach number, the hotter turbulent flow at the sublayer interface mixes with the colder laminar flow in the sublayer to form the intermittent signal. At the outer interface, the reverse process occurs with the hotter freestream flow intermingling with the slower colder turbulent flow in the boundary layer.

Morkovin (1962) has surveyed the available data to produce an hypothesis which states that, if the root-mean-square density fluctuation is small compared to the local mean density, then the turbulence structure of the boundary layer is similar to that of an equivalent incompressible flow. The validity of Morkovin's hypothesis has been discussed in detail by Bradshaw (1977), who concluded the hypothesis is proven for boundary layers up to a freestream Mach number of about 5. This implies that the turbulence modelling concepts successful in low speed flows can be used with confidence for compressible flow if the variation of mean density is taken into account up to $M < 5$. At Mach numbers higher than 5, density fluctuations become increasingly more important, and it is conventional to use the equivalent fluctuation modes of vorticity, entropy and sound (corresponding to velocity, total temperature and pressure fluctuations). Morkovin's hypothesis implies that the pressure fluctuations are negligible and that the sound mode can be ignored for $M < 5$, but at $M > 5$, the sound mode can be significant and interact with the other modes. This can lead to difficulty in analysing the output of the most common measuring technique, i.e. the hot wire aneomometer, which requires an assumption regarding the pressure fluctuations to close the controlling equations. Other techniques, such as the electron beam fluorescence probe or the laser doppler aneomometer, do not require such an assumption but are still in the development stage for use in high supersonic or hypersonic turbulent flows.

2.5.2 Turbulence Modelling

Many of the turbulence models used in the various calculation and prediction methods are based on the mixing length and eddy viscosity concepts which have proved valuable in incompressible flows, e.g. Schlichting (1968). The eddy viscosity, ξ , and the mixing length, ℓ , are defined by the following relationships:

$$\tau_t = \rho \ell^2 \frac{\partial U}{\partial y} \left| \frac{\partial U}{\partial y} \right| = \rho \xi \frac{\partial U}{\partial y} \qquad \text{(Eq. 2.32)}$$

where, τ_t is the turbulent shear stress.

These concepts have formed the basis for modelling the shear stress in most of the differential or finite difference calculation methods in incompressible flow. To apply these methods to compressible flow, it is necessary to modify the eddy viscosity or the mixing length hypothesis to allow for variable density. A compressibility transformation approach is often used to allow for the effects of variable density; a comprehensive review of the various turbulence modelling concepts is given by Bushnell et al (1977) or Frost and Moulden (1977).

2.5.3 Turbulence Properties from Time-averaged Conservation Equations

With the lack of turbulence measurements in compressible flow much effort has gone into obtaining the turbulent shear stress and heat flux terms in Eq. 2.31 from the mean flow profile data, using the time-averaged conservation equations and an assumption of similarity. The time-averaged conservation equations for the two-dimensional flat plate boundary layer are:

Continuity: $$\frac{\partial}{\partial x} (\overline{\rho}\, \overline{U}) + \frac{\partial}{\partial y} (\rho \overline{V}) = 0 \qquad \text{(Eq. 2.33)}$$

Momentum: $$\frac{\partial}{\partial x}\left(\bar{\rho}\,\bar{U}\,\bar{U}\right) + \frac{\partial}{\partial y}\left(\bar{\rho}\,\bar{U}\,\bar{V}\right) = -\frac{dp}{dx} + \frac{\partial \tau}{\partial y} \qquad \text{(Eq. 2.34)}$$

where, $$\tau = \tau_l + \tau_t = \frac{\partial U}{\partial y} - \left(\bar{\rho}\overline{v'u'}\right) \qquad \text{(Eq. 2.35)}$$

If the boundary layer is fully turbulent the profiles U/U_e, ρ/ρ_e and T/T_e are functions of y/δ only which allows the approximation, following Horstman and Owen (1972):

$$\frac{\partial Q}{\partial x} = (Q/Q_e)\frac{dQ_e}{dx}\,, \text{ where } Q = \rho U \text{ or } \rho U^2.$$

Eq. 2.33 can be integrated to give ρV which can be then substituted into Eq. 2.34 , which on integration with respect to y/δ gives:

$$\frac{\tau}{\rho_e U_e^2} = \frac{C_f}{2} + \left[\frac{\delta}{\rho_e U_e^2}\frac{d}{dx}\left(\rho_e U_e^2\right) + \frac{d\delta}{dx}\right]\left[\int_0^{y/\delta} \frac{\rho U}{\rho_e U_e^2}\, d(y/\delta)\right] - \left[\frac{\delta}{\rho_e U_e}\frac{d}{dx}\left(\rho_e U_e\right) + \frac{d\delta}{dx}\right]\left[\frac{U}{U_e}\int_0^{y/\delta} \frac{\rho U}{\rho_e U_e}\, d(y/\delta)\right] + \frac{\delta}{\rho_e U_e^2}\frac{y}{\delta}\frac{dp}{dx} \qquad \text{(Eq. 2.36)}$$

The x derivatives of δ , $\rho_e U_e$, $\rho_e U_e^2$ and p can be found from the profile data and the integrals evaluated numerically to determine the total shear stress distribution through the boundary layer. The miximg length or eddy viscosity can be found from the following equations:

$$\tau_t = \rho \ell^2 \frac{\partial U}{\partial y}\left|\frac{\partial U}{\partial y}\right| = \rho \xi \frac{\partial U}{\partial y} \qquad \text{(Eq. 2.37)}$$

The y derivatives are also determined from the profile data and to a good approximation $\tau \simeq \tau_t$. Sandborn (1974) has examined the available shear stress distributions obtained from meam flow data and has found that, for zero pressure gradient flows, the distributions correlate independently from Mach number. From this data review Sandborn formed a 'best estimate' dist-

ribution of supersonic shear stress data which agreed well with the incompressible data of Klebanoff (1955) and Zoric (1968).

2.5.4 Turbulence Measurements

It is essential to have direct measurements of turbulence properties, such as shear stress and the distributions of the various fluctuation modes, in order to test the validity of the turbulence models. The majority of data has been obtained with the HWA and a limited amount with the laser doppler aneomometer, which measures the velocity fluctuations directly without assumptions in the data reduction. As regards the pressure fluctuations, there is no acceptable method to measure these, except at the wall with a flush mounted microphone, since fluctuating pitot pressures do not yield static pressure without knowledge of the correlated velocity and density fluctuations. It is proposed to discuss the HWA as the majority of the data have been obtained with this technique.

2.5.4.1 Hot Wire Aneomometer (HWA)

Most fluctuation measurements in compressible flow have been made with the HWA, which is a fine electrically heated wire that responds to flow fluctuations. The HWA is usually operated in either a constant current or constant temperature mode; a full description of the HWA operation is given by Sandborn (1972). The analysis of the output signals is complex, especially in compressible flow in which significant fluctuations of U, T, ρ and p are possible. Kovasznay (1950) and Morkovin (1956) have developed the analysis of the HWA signals using a method of modal analysis in which the equivalent fluctuations of vorticity, entropy and sound (acoustic pressure) are used in place of velocity , temperature, density and pressure. They proposed a linearised analysis which is only valid for small fluctuation levels so that higher order terms in the response equation of the wire can be ignored. The HWA has been shown to respond principally to mass-flux (ρU) or total temperature (T_o) fluctuations; the output signal (e) can be represented by the equation,

in the notation of Morkovin (1956):

$$e' = S_{T_o}\frac{T_o'}{T_o} - S_{\rho U}\frac{(\rho U)'}{\rho U} \qquad \text{(Eq. 2.38)}$$

$$= S_{T_o} t - S_{\rho U} m$$

where, $t = T_o'/T_o$ and $m = (\rho U)'/\rho U$.

This expression can be re-written in terms of the experimentally determined mean square quantity:

$$\overline{e'}^2 = S_{\rho U}^2 m^2 + S_{T_o}^2 t^2 + 2S_{\rho U}S_{T_o} mt\, R_{mt} \qquad \text{(Eq. 2.39)}$$

where S_{T_o} and $S_{\rho U}$ are the HWA mass-flux and total temperature sensitivity coefficients, and R_{mt} is the correlation coefficient between the mass-flux and total temperature. The sensitivity coefficients are determined by calibration and the physical properties of the wire material. The HWA is operated at three wire overheat ratios to determine the three unknowns in the response equation, i.e. m, t and R_{mt}. In practice, the HWA is operated at a large number of overheat ratios, usually at least 10, and a method of least squares used to determine the unknown parameters. Using this method, it is possible to determine the distribution of mass-flux and total temperature fluctuation levels through the boundary layer.

To obtain the fluctuation levels of density, velocity, temperature or pressure from the mass-flux and total temperature data, it is necessary to expand the equations in the following way:

$$m^2 = \frac{\overline{\rho'}^2}{\rho^2} + \frac{\overline{u'}^2}{U^2} + 2\frac{\rho'u'}{\rho U} \qquad \text{(Eq. 2.40)}$$

$$t^2 = \alpha_1^2\frac{\overline{T'}^2}{T^2} + \beta_1^2\frac{\overline{u'}^2}{U^2} - 2\alpha_1\beta_1\frac{T'u'}{TU} \qquad \text{(Eq. 2.41)}$$

$$mt\ R_{mt} = \frac{\overline{u'^2}}{U^2} + \frac{\overline{T'\rho'}}{T\rho} + \frac{\overline{u'\rho'}}{U\rho} + \frac{\overline{T'u'}}{TU} \qquad \text{(Eq. 2.42)}$$

where $\alpha_1 = (1 + \frac{(\gamma-1)}{2}M_e^2)^{-1}$ and $\beta_1 = \frac{(\gamma-1)}{2}M_e^2$.

This set of three equations is underdetermined with six unknowns and it is necessary to make an assumption to simplify the equations. It is usual to assume that the pressure fluctuations are negligible:

$$\frac{p'}{p} << \frac{u'}{U} \ , \ \frac{\rho'}{\rho} \ , \ \frac{T'}{T} \ .$$

This assumption in conjunction with the equation of state gives:

$$\frac{p'}{p} = 0 = \frac{\rho'}{\rho} + \frac{T'}{T} \ .$$

Using this identity the equations form a closed set from which it is possible to determine the individual fluctuating components, e.g. u'/U, T'/T or ρ'/ρ. This assumption has been used by several investigators in their data analysis, see for example Kistler (1959), Owen et al (1975) and Laderman (1976). The validity of the assumption of negligible pressure fluctuations at Mach numbers above 5 is questionable. At higher Mach numbers the intensity of the pressure fluctuations increases, i.e. the sound mode becomes increasingly important; Laderman and Demetriades (1974) have attempted to allow for pressure fluctuations by assuming that the entropy and vorticity modes were out of phase but perfectly correlated. The data evaluated using this assumption was compared with the same data evaluated assuming zero pressure fluctuations and it was found that the difference was small.

2.5.5 Turbulence data

As mentioned in the previous sections, the HWA technique has been the method

most often used to investigate the turbulence properties of high speed boundary layer flows. Kovasznay (1950, 1953) and Morkovin (1956) laid the foundations of applying the HWA to compressible flow (section 2.5.4).

Kovasznay (1953) found that the peak fluctuation levels of velocity were similar to those expected from previous incompressible studies. Morkovin and Phinney (1958) made a limited survey of a boundary layer at $M_e = 1.77$ and concluded that the turbulence structure was similar to that of a constant density flow. Kistler (1959) made an extensive study of an adiabatic flat plate boundary layer including the effect of varying Mach number, $1.5<M_e<4.7$. Assuming negligible pressure fluctuations, Kistler found both the mass flow and total temperature fluctuation levels increased with increasing Mach number. The static temperature fluctuation levels were found to be proportional to the mean static temperature difference across the layer. Kistler proposed that this was due to the transport of the mean temperature field by the velocity fluctuations.

In a review of the limited available fluctuation data in compressible flow, Morkovin (1960) has discussed the problem of the interaction of the various fluctuation modes; this paper formed the foundation of Morkovin's hypothesis, Morkovin (1962, 1964). Wallace (1968) used the election beam fluorescence technique to measure mean density and RMS density fluctuation levels in a nozzle wall boundary layer at $M_e \simeq 8$. In addition measurements were made of fluctuating pitot pressure which were used in conjunction with the density data by Harvey, Bushnell and Beckwith (1969) to estimate the longitudinal velocity fluctuation levels. These results were compared with a simple mixing-length calculation method; the authors concluded that the mixing-length approach gave good estimates of the magnitude and trend of the measured fluctuation data.

Fischer et al (1971) in a HWA study of a nozzle wall boundary layer at $M_e \simeq 20$ found large mass flow fluctuations which were attributed to large density fluctuations near the wall. A detailed investigation of the turbulence structure of a cold wall, hypersonic boundary layer was reported by Owen and Horstman (1972). Extensive HWA auto and cross-correlation measurements were made in the layer formed on a cone-ogive-cylinder model at $M_e = 7.2$. A model for the turbulence production and growth was proposed which proved consistant with previous incompressible results.

Laderman (1974) studied the adiabatic boundary layer on a slender cone at $M_e=7$ and found that the static temperature fluctuations dominated the turbulence structure. Kistler's (1959) correlation of static temperature fluctuations for supersonic flow was found to be inadequate at hypersonic speeds. Distributions of velocity fluctuations were found to be similar to equivalent low speed data but showed a slow decrease in magnitude with increasing Mach number.

A laser doppler aneomometer was used by Yanta and Lee (1974) to study a $M_e=3$ boundary layer; turbulence quantities from LDA measurements agreed well with data obtained from conventional probes, and the distributions were similar in magnitude to previous incompressible data suggesting Mach number independence. Rose and Johnson (1974) have made shear stress measurements in a $M_e =2.9$ boundary layer using both conventional HWA equipment and a laser doppler aneomometer. The laser data agreed well with HWA measurements over the outer 60% of the layer but showed unexplained systematic differences nearer the wall.

Laderman and Demetriades (1974) examined the boundary layer formed on the nozzle wall of a continuous tunnel at $M_e = 9.4$ under conditions of significant heat transfer. The authors report detailed measurements of the mean flow field, turbulent fluctuations and intermittent structure;

a significant contribution from the sound mode was assumed in the data reduction scheme. This investigation showed that the turbulence was dominated by the high frequency pressure fluctuations. The static temperature fluctuations agreed with projections from adiabatic, supersonic data and the longitudinal velocity component fluctuations were small differing little from results at lower Mach number.

In his comprehensive review of turbulence measurements in compressible flow Sandborn (1974) has found that the majority of data at super and hypersonic speeds have been made in a zero pressure gradient, turbulent boundary layer. The majority of turbulent shear stress data was found to be similar to that measured in the equivalent incompressible flow especially in the outer regions. Intermittency measurements appear to show a pronounced difference from the incompressible case in that the intermittency extended over a much smaller percentage of the layer. Sandborn concluded that the shear stress could be estimated to within $\pm$ 15% and that the equivalent incompressible case was probably a good model up to M_e = 10 (the Mach number limit of the reviewed data). Owen, Horstman and Kussoy (1975) extended the measurements of Owen and Horstman (1972) by making a detailed investigation of the turbulence structure. The velocity fluctuation level was found to agree with the Mach number trend set by previous compressible data and the incompressible data of Klebanoff (1955). However, the measured hypersonic density fluctuation data did not follow the low Mach number trend and appeared to be independent of Mach number above $M_e \simeq 5$.

Smith and Driscoll (1975) used the electron beam fluorescence technique to simultaneously measure density and temperature fluctuations in a $M_e \simeq 16$ adiabatic wall boundary layer. The density and temperature fluctuations were observed to be much larger than expected in a supersonic boundary layer and asymmetrically distributed about the mean, thus preventing a linearised

analysis. Pressure fluctuations were also large and this could not be neglected in the data reduction. Similar results were obtained in two other studies at Mach number above 10, e.g. the studies by Kemp and Owen (1972) and Fischer et al (1971).

Unique direct measurements of the total heat flux were made by Mikulla and Horstman (1975) in a turbulent non-adiabatic boundary layer. This data agreed well with values obtained by integrating the energy equation. Statistical properties of the cross correlations were found to be similar to corresponding measurements at approximately the same momentum thickness Reynolds number. Mikulla and Horstman (1976) report turbulence intensity and Reynolds shear stress measurements for a shock wave boundary layer interaction region with and without separation. The authors conclude that the differences in turbulence liftimes for separated and attached flows were due to a coupling between the turbulence energy and separation bubble unsteadiness.

Laderman (1976) has made turbulence measurements in a hypersonic $M_e \simeq 7.1$ boundary layer over a sharp slender cone for both adiabatic and cold wall conditions. The results agreed with previous findings at $M_e = 9.4$ (Laderman and Demetriades (1974)) and showed that there was significant reduction in the Reynolds stress component with increasing Mach number; the Mach number effect dominated any effect due to heat transfer.

Acharya, Horstman and Kussoy (1979) have investigated the Reynolds number effects on the turbulence field of a compressible boundary layer at $M_e \simeq 3$. They found that the vertical and transverse velocity components (u and v) are approximately equal and independant of Reynolds number in contrast to the incompressible result. The streamwise velocity fluctuations correlated well with the previous compressible and incompressible data if scaled using the method originated by Morkovin (1964).

3.0 Experimental Detail

This section deals with the models and instrumentation used to obtain time-averaged boundary layer data but also includes a brief description of the No. 2 Gun Tunnel. Details of the electron beam system and associated instrumentation are included in the next chapter. Appendix A contains details of the design and construction of the Gun Tunnel Data Acquisition System and Appendix B describes the calibration procedure for the total temperature probes.

3.1 The Imperial College No. 2 Hypersonic Gun Tunnel

All the experiments described herein were performed in the Imperial College No. 2 Gun Tunnel. Full details of the design, construction and performance are given in Needham et al (1970), and only a brief description is included here.

As shown in fig. 3-1, the facility is a conventional intermittent blowdown tunnel with a contoured Mach 9 axisymmetric nozzle fed by a free piston compression heater. By virtue of the double diaphagm firing system excellent repeatability of test conditions is obtained at all pressures. Pure nitrogen is used as both the test gas and the driver gas. The 0.4m diameter nozzle exit plane enables a flat plate model of 0.2m span and 0.95m chord to be accommodated in the coreflow. Stagnation pressures of up to 104 MNm^{-2} are used to generate freestream unit Reynolds numbers ranging from 2×10^7 m^{-1} to 6×10^7 m^{-1} at a stagnation temperature of approximately $1060^{o}K$. The performance envelope for the Mach 9 contoured nozzle is shown in fig. 3-2, and a summary of the standard operating conditions is given in Table 1. The method outlined in Culotta and Richards (1970) was used to calculate real gas compressibility effects on the expansion from the reservoir to the test section.

3.2 Windtunnel Models

3.2.1 Large modular flat plate model

The model used for all the time-averaged boundary layer measurements was a sharp flat plate with leading edge thickness of 0.01mm (15^{o} included angle) and of 0.18m span by 0.76m chord. The model is shown in fig.3-3 fitted with hanging sideplates which were used as previous tests had shown these to be an effective way of preventing disturbances from the model underside interfering with the test flow. A surface slot, 0.10m x 0.65m, was machined in the flat plate into which various combinations of instrumentated modules could be fitted where required. The empty spaces were filled with flat, blank modules thus avoiding unwanted disturbances due to, for example, pressure tappings upstream of the measuring station. A high order of surface finish and fit was maintained between the modules and the model, the surface roughness being better than 15 microns in both cases. The model was mounted 10mm below the tunnel centreline in order to avoid any upstream flow disturbances that might focus on the nozzle axis.

3.2.2 Inclined flat plate

This model was used for the variable incidence tests required in the total temperature probe calibration described in Appendix B. A sharp flat plate (15^{o} included angle) of 0.13m span and 0.30m chord was used fitted with hanging sideplates. The model acn be inclined at various fixed angles of both positive and negative incidence by means of machined spacers. A probe holder was fitted to the trailing edge to allow up to four probes to be held in the flow region between the boundary layer edge and the leading edge shock. The probes were adjusted to be parallel to the model surface and the position checked by means of Schlieren photography for each angle.

3.2.3 Boundary layer transition trips

Boundary layer trips consisted of a single row of delta shaped vortex generators 1mm high and 3mm apart; the generators were inclined approximately 30^{o} to the flow direction. A single strip of vortex generators was fixed 10mm from the model leading edge and used to force transition at the lower Reynolds number running condition (Table 1). The type of trip and its application was identical to that described in an earlier study by Coleman(1973).

3.3 Instrumentation

The flat plate modules, described in section 3.2.1, were used to mount all the instrumentation required in the time-averaged boundary layer measurements. The probe displacement was measured with a micrometer screw gauge using an electrical buzzer circuit to indicate mechanical contact.

3.3.1 Digital data acquisition system

The majority of the data obtained from the instrumentation described herein was recorded on the digital acquisition system. This system was developed during the investigation with the aim of replacing the existing 'analogue' oscilloscope-camera recording equipment, and to enable time-resolved measurements to be made from the electron beam probe. These two functions imposed essentially different requirements. The oscilloscope recording equipment was used to make time-averaged measurements from conventional instrumentation . This type of measurement required the digitizing of many analogue input channels at modest conversion rates, typically 2×10^{4} to 6×10^{4} samples per sec. The electron beam function required the digitizing of one or two analogue channels at high conversion rates, e.g. 1×10^{6} to 4×10^{6} samples per sec. A system incorporating these requirements was developed utilising a local buffer memory to store the data until run

completion, when the data was transmitted to a remote minicomputer system for processing and subsequent permanent storage. Considerable Assembler programming was required to develop a Hypersonics Laboratory control program suite in addition to the many specific application programs or tasks for each type of measurement. Full details of the Hypersonics Laboratory Data Acquisition System are available in Bartlett, Davis and Harvey (1979), and further details are presented in Appendix A.

3.3.2 Transducers

The pressure transducers used were either of the unbonded strain gauge or of the piezoelectric type, i.e. Statham or Kistler respectively. All transducers were acceleration compensated types but as a further precaution flexible mountings were used for all tests. Tests were also made with blocked probes or pressure tappings in order to assess these precautions and no significant signal was detected. The transducers were usually mounted in a housing using soft rubber O-rings as vibration insulation, and silicone rubber tubing to connect the transducer to either the probe or the pressure tapping.

3.3.3 Preston tubes

Skin friction values were inferred from surface impact pressure distributions which were measured with three different diameter Preston tubes, i.e. 1.25mm, 2.07mm and 2.96mm. Each Preston tube was mounted on an instrumentation module with a surface pressure tapping provided either side of the tube inlet in order to simultaneously measure the static pressure at the wall. A wirewool plug was fitted in the probes to prevent spurious signals due to the 'hot' test gas reaching the transducer diaphragm. Piezoelectric transducers have been found to be especially sensitive to heating effects.

Iron or steelwool has been found to be one of the best materials to act as a heat sink in these circumstances, e.g. Harvey(1979).

3.3.4 Surface pressure

To measure surface pressure two instrumentation modules were manufactured with five surface tappings, one module with a chordwise distribution and the other with a spanwise distribution; the spacing between adjacent tappings was 20mm in the chordwise direction and 10mm in the spanwise direction. The tappings were made by cementing 1.5mm internal diameter copper tube through clearance holes in the modules and then machining the tube flush to the surface. Flexibly mounted piezoelectric pressure transducers were situated inside the model connected by the shortest possible pipe length to ensure good response. Flexible mounting was required to exclude the possibility of spurious signals due to the large accelerations occuring in the tunnel start-up processes.

3.3.5 Heat transfer

Heat transfer rates were measured with thin film gauges flush-mounted on a flat plate module in either spanwise or chordwise distributions. A detailed account of the fabrication and mounting of the gauges will be available in Edwards and Hillier(1980). In brief, the platinum gauges were made either by hand painting or by evaporation through an accurately machined mask onto 3mm diameter polished quartz substrates. The gauges were carefully mounted into the plate to within 0.03mm, as preliminary results had indicated that it was vital to ensure the gauges were accurately levelled with the model surface. The amplified gauge output, representing the surface temperature, was recorded on the digital data

acquisition system (Appendix A), and from thence transmitted to the College mainframe computer where a numerical integration program was used to calculate heat transfer rates. The conversion rate employed was such that 1024 points were taken on up to 16 channels in 25.6 msec. The numerical integration technique was based on the method outlined in Schultz and Jones (1968), and was a significant improvement over the previous method which used an electrical analogue circuit to produce an output directly proportional to heat transfer rate. The 'analogue' method required repeated calibration with the measurements being taken from oscilloscope photographs.

3.3.6 Survey probes

3.3.6.1 Pitot probes

As shown in fig. 3-4 a rake of four probes was used to measure the boundary layer pitot pressure profiles. The probes were made from stainless steel tubing honed and flattened to improve the spatial resolution. The probe outside diamensions were typically 0.5mm high by 2.0mm wide with a wall thickness of approximately 0.075mm. Smaller probes were tried but were found not to respond adequately during the steady run time of the Gun Tunnel. Pitot probe height was approximately 5% of the traversed boundary layer thickness. To avoid vibrations the probes were connected to the pressure transducer with small bore silicone rubber tubing. Pressures were either measured with either unbonded strain gauge or piezoelectric pressure transducers, which were flexibly mounted inside the flat plate model.

3.3.6.2 Total temperature probes

The total temperature probes used were of the minature vented shield thermocouple type; the sensor utilised 12.5 μm diameter chromel-alumel

thermocouple wire, with length to diameter ratio equal to 180, held between 100 μm diameter supporting prongs. A lengthy development programme was undertaken before finalising the design used in this study. Full details of the probe design and development are available in Bartlett,Edwards and Hillier (1979). Probe calibration is difficult and was not precisely effected for the probes.It covered the appropriate range of unit Reynolds number but did not cover the precise Mach number range. Full details of the calibration are presented in Appendix B, together with a description of probe construction and dimensions.

Briefly the calibration involved measuring the probe response over a range of Reynolds number comparable to that experienced in traversing the boundary layer. It was not possible to duplicate the boundary layer Mach number variation, although this was likely to be a second order effect; in addition the calibration was carried out at a fixed total temperature . The appropriate Reynolds number range was generated by use of a compression or expansion surface , with the probes fixed parallel to the surface. The probes showed a very efficient response achieving maximum recovery factors in excess of 0.98 in the highest Reynolds number flow, i.e. freestream conditions, falling to 0.88 at the lowest Reynolds number. Corrections applied to the reading lead to measured total temperatures accurate to ±5% of the average total temperature obtained in the boundary layer.

Spatial resolution was determined by the probe shield which was a flattened and honed pitot head with four vent holes sited well behind the thermocouple junction; the pitot to vent area ratio was 1.67. Intake dimensions were typically 0.875mm high by 1.50mm wide with an average wall thickness of approximately 0.075mm. If the intake height was reduced further the thermal boundary layers within the shield impinged on the bead resulting

in a fall of recovery factor.

3.3.7 Stagnation pressure measurement

The tunnel stagnation pressure, p_o, was measured with a Kistler piezoelectric transducer mounted in the nozzle block; the p_o value was used to normalize pressure data to correct for run to run variations in diaphagm burst pressure. It was estimated that p_o could be measured to better than ±2% using the digital data system.

3.3.8 Freestream total temperature measurement

The freestream total temperature was measured using boundary layer probes fitted with circular inlets. $T_{o\infty}$ was used to normalize total temperature data for run to run variations. The estimated accuracy was better than ±5% using the digital data acquisition.

3.4 Signal processing

All the signals derived from instrumentation (time-averaged data) were amplified, passed through a 1kHz low pass filter and in most cases recorded on the digital data system. The amplification was normally chosen to produce a near 2.50 volt input to the data system thereby ensuring maximum digitization accuracy. Early measurements not recorded digitally were recorded on the oscilloscope-Polaroid camera system.

3.5 Estimates of accuracy

Estimates have been made of the maximum measurement error in the three

profile variables, i.e. normal displacement (y), pitot pressure (p_t), and total temperature (T_o). The probe centre was positioned to within ±0.05% and no significant vibration or displacement was detected by either flow visualisation or post run measurement. Using the digital data system it has been estimated that the pitot pressure was measured to better than ±2% and the total temperature to better than ±5%. Also it was estimated that surface impact pressure could be measured to better than ±2% and heat transfer to better than ±8%. The digital system contribution to these errors was 0.25% after averaging.

4.0 Electron beam system

4.1 Introduction

The electron beam fluorescence technique (EBFT) is a well established method for probing high Mach number rarified flows ($n < 10^{16}$ cm^{-3}) e.g. Muntz (1968), Davis and Harvey (1976). The non-intrusive character of this optical technique make its application to higher density ($n > 10^{16}$ cm^{-3}) turbulent flow especially attractive. Of equal importance to the non-intrusive nature is the inherent high frequency response of the technique, typically greater than 1MHz, compared to the frequency response of a hot wire aneomometer (HWA) which is usually limited to approximately 250kHz, e.g. Owen et al (1975) or Laderman and Demetriades (1974).

The schematic, fig. 4-1, shows the equipment used to apply the EBFT to the Gun Tunnel. Briefly, the technique involves firing a highly collimated beam of high energy electrons into the test gas flow; the interaction of the electrons with the gas molecules gives rise to optical band radiation which can be analysed spectroscopically to obtain estimates of rotational temperature, vibrational temperature or the molecular number density of the excited species. In the case of the Gun Tunnel the electron beam was fired horizontally from the vertical flat plate and subsequently collected in a graphite cup on the far side of the nozzle flow. The fluorescence could be examined by an optical photomultiplier system mounted on the working section floor. The determination of density is based on the observed relationship, usually linear, between the fluorescent intensity of the band system and the molecular number density; this relationship is often obtained from a calibration, using the same optical arrangement , over a comparable range of gas number density and temperature. Although theoretical calibration schemes also exist there remain constants due to both the optical geometry and beam

accelerating voltage that have to be determined experimentally. Rotational and vibrational temperatures are determined by measuring the relative intensities of the rotational lines and vibrational bands. In this chapterthe historical background of the technique is presented with particular emphasis on the applications at high density in turbulent flows. A brief outline of the theoretical background is also included together with full details of the electron beam equipment, instrumentation and models. The calibration of the fluorescent intensity against density is described, and the application of the technique to boundary layer measurements is discussed with reference to the present experiment.

4.2 Historical

The electron beam fluorescence (EBF) technique has been extensively applied to probing high speed, rarefied flows for the last 15 years. Most of these studies have been made in low density ($n < 10^{16} cm^{-3}$) laminar flows, principally of nitrogen or helium, in which estimates have been made of density and rotational temperature. An excellent summary of the theory, development and application of the EBF technique to rarefied flows has been published by Muntz (1968); this reference also contains a comprehensive bibliography of papers published up to 1968. Butefisch and Vennemann (1974) have fully reviewed the application of the EBF technique to rarefied, hypersonic flows up to 1974. These two references provide an excellent background to the technique and its application at low density. For that reason this survey is restricted to discussing the limited applications of EBF to relatively, high density ($n = 10^{17}$ to 10^{18} cm^{-3}) turbulent flows.

The apparent difficulty in applying the EBF technique to turbulent flows is reflected in the paucity of previous studies. Boyer and Muntz (1967) first applied EBF to the measurement of turbulent fluctuations in the wake

of a sharp, slender cone. This investigation was carried out in an intermittent, hypersonic shock tunnel at M=12.6 using pure nitrogen as the test gas; observation times were limited to a few milliseconds. The optical system used an interference filter with a wide band width transmitting wavelengths from 390nm to 480nm. The static calibration extended up to a room temperature equivalent pressure of 5 torr ($n \simeq 10^{17}$ cm^{-3}) and showed little variation with temperature over the range of $80^{o}K$ to $210^{o}K$. The technique was used to measure turbulent density and temperature fluctuations, and to monitor their axial history in the wake of a sharp 10^{o} half angle cone model free flying in the M=12.6 flow. This study demonstrated that the EBF technique and a shock tunnel to be a useful combination in the study of turbulent, hypersonic flows. Dionne et al (1967) have also made measurements in the hypersonic wakes of spherical projectiles fired into air or nitrogen. The spectral window in the case was defined by an interference filter centered at 337.5nm with a 5.5nm band width which permitted the observation of the strongest band $\{0,0\}$ of the N_2 (2+) system. The calibration was performed up to a room temperature equivalent pressure of 10 torr ($n \simeq 2 \times 10^{17} cm^{-3}$) and showed a linear response over this range for nitrogen but showed significant quenching in the case of air. The authors attributed this to the higher quenching cross-section for oxygen in comparison to nitrogen. Measurements of mean density, rms density and power spectra were reported.

Camac (1967) has used the EBFT to make flight measurements of density in the boundary layer of a non-ablating slender, re-entry vehicle. In preparation for the flight measurements the author reports a comprehensive study of the excitation-emission processes and the pressure dependence of both the $N_2^{+}(1-)$ and $N_2(2^{+})$ systems. This study also included measurements of beam attentuation and spreading at high density. A linear response of fluorescent intensity with pressure was found for the $N_2(2+)$

{0, 0} band at 337.1 nm up to a room temperature equivalent (RTE) pressure of 60 torr ($n \simeq 2 \times 10^{18}$ cm^{-3}) At pressures below 2 torr RTE this band was shown to exhibit a quadratic dependence on pressure. Wallace (1968) reported EBF measurements at relatively high density ($n \simeq 10^{17} cm^{-3}$) in the cold wall boundary layer of a shock tunnel nozzle wall. This study was carried out in air at M=8 using the N_2^+(1-) system {0,0} band at 391.4 nm. Mean density and density fluctuation measurements were reported but no account was taken of temperature fluctations in the data reduction scheme, i.e. no separation of modes. A peak fluctuation intensity of 9% (rms to mean) was detected close to the wall. Measurements of fluctuating pitot pressure were also made which show large fluctuation levels (peak rms to mean value of 50%) close to the wall. Harvey, Bushnell and Beckwith (1969) subsequently analysed the Wallace data to estimate the intensity of velocity fluctuations.

In one of the most comprehensive studies to date Smith and Driscoll (1975) have reported EBFT measurements in a helium, hypersonic ($M \simeq 16$) boundary layer. These measurements were made in the adiabatic tunnel wall boundary layer with a freestream number density of 4.4×10^{17} cm^{-3}. This paper also reviews the problems in applying the technique to a turbulent, high density flow including the factors controlling frequency response, spatial resolution and sensitivity. Simultaneous measurements were made of number density and temperature by observing the emission from two Helium lines (396.5 nm and 501.6 nm). Mean densities were observed to agree with those deduced from conventional probe surveys but mean temperatures were found to be considerably higher. RMS density fluctuations were found to reach a peak value of almost 67% of the local mean value at $y/\delta = 0.4$.

McRonald (1975) has studied a cold wall boundary layer in a continuously running M=9.4 wind tunnel using air as the test gas ($n \simeq 3 \times 10^{17} cm^{-3}$). A 50kV electron beam probe was used and the total fluorescent light output used to determine number density. It was necessary to include an integral of the mean density to account for the significant beam attentuation effects at boundary layer thicknesses of up to 125mm. Mean density and temperature fluctuations were measured across the boundary layer at three values of tunnel stagnation pressure. This data was compared to mean data obtained with conventional instrumentation (static pressure, pitot pressure and total temperature); agreement was found to be poor. The fluorescent light output was found to contain contributions from local temperature fluctuations and integrated beam attentuation fluctuations in addition to that from local gas density fluctuations. The author describes this situation as analogous to the separation of modes problem in the interpretation of hot wire fluctuation measurements in which simplifying assumptions are required to close the controlling equations. The measured gas density fluctuations were found to reach a peak of 6% to 8% of the local mean density in the central part of the boundary layer and to fall to about 3% at the edge.

Harvey and Hunter (1975) have reported a study of a hypersonic turbulent free mixing layer at three stations downstream of a M=19 nozzle with a freestream number density of $3 \times 10^{16} cm^{-3}$. The data were obtained with a 28kV electron gun. Good agreement was obtained between electron beam and conventional probe measurements of local mean flow parameters.

The limited number of investigations using the EBF technique in turbulent flow is partly due to experimental difficulties, such as beam scattering and

attentuation, but mainly a result of the general lack of interest, hence funding, for hypersonic research in the last decade. From the historical survey, it is apparent that the EBF technique has proved a successful and economic diagnostic tool for rarefied laminar flows, but in the case of turbulent flow the technique requires further development before it becomes a routine diagnostic method. For nitrogen flows, the excitation-emission mechanisms are well understood over the density range of interest, i.e. n = 10^{15} to 10^{20} cm^{-3}, and the necessary optical detection and data acquisition techniques are widely available. However, from the studies cited earlier it is clear that in addition to a meticulous calibration further development is required in the design of the electron beam generation and injection equipment to minimize beam broadening, attenuation and flow interference effects.

4.3 Background theory

4.3.1 Excitation-emission mechanisms

Molecular nitrogen exhibits significant emissions from two band systems in the pressure range of interest. At low pressures, typically less than one torr, the N_2^+ 1st negative system (1-) is predominant but at higher pressures the N_2 2nd positive (2+) system becomes increasingly more intense. The excitation-emission mechanism for the two systems is different.

The N_2^+ (1-) system is excited chiefly by direct inelastic collisions with primary beam electrons (20-50kV), with a small contribution from scattered electrons with sufficient energy. In contrast, the N_2(2+) system is excited by low energy secondary electrons which result from inelastic collisions between primary electrons and gas molecules. The vibrational energy levels

of nitrogen are shown in the simplified diagram, fig. 4-2, from Camac (1967).

The mechanism for the direct excitation of N_2^+ (1-) by high energy primary electrons is well known and can be written:

$$N_2\ (X\ ^1\Sigma_g^+) + e \longrightarrow N_2^+\ (B^2\ \Sigma_u^+) + 2e \longrightarrow N_2^+\ (X^2\ \Sigma_g^+) + h\nu$$

Ground state N_2 molecule	High energy primary electron	Excited upper ionized state of N_2	Low energy secondaries	Stable ionized ground state	Photon

(Eq. 4.1)

The direct excitation results in an ionized molecule in an excited upper energy state which subsequently decays to the ionic ground state with the emission of a photon. The above analysis illustrates how the intensity of the fluorescence is directly proportional to the number density(n) of the ground state molecules. This is confrimed by the observed linear relationship of intensity against number density for this system. The most intense and thus commonly used system is the N_2^+ (1-) 0,0 band at 391.4 nm but at pressures greater than approximately 0.5 torr (at room temperature) quenching due to non-radiative collisions between excited ionic molecules and ambient gas molecules result in a fall off in sensitivity. For the N_2^+ (1-) system it has been found that oxygen accentuates the collision quenching effect and therefore it is desirable to use pure nitrogen rather than an oxygen-nitrogen mixture such as air.

The N_2 (2+) system becomes increasingly more important at pressures above 1 torr and dominates the total emission at higher pressures. The excitation mechanism of the N_2 (2+) system does not require ionisation as the upper transition level involving the neutral molecule lies well below the N_2 ionisation level. The excitation of the N_2 (2+) system can be written:

$$N_2\ (X\,^1\Sigma_g^+) + e \longrightarrow N_2\ (C\,^3\Pi_u) + e \longrightarrow N_2\ (B\,^3\Pi_g) + h\nu$$

Ground state N_2 molecule	Low energy secondary electron	Excited neutral state of N_2	Lower energy electron	Ground state	Photon

(Eq.4.2)

This excitation process has a small cross-section for the high energy primary electrons but has a large cross-section for the secondaries formed from the primary-ambient gas molecule collisions. The optimum accelerating voltage has been found experimentally, see for example Muntz (1968), to be approximately 50 kV for adequate penetration and secondary production. The secondary electron excitation mechanism should produce a quadratic dependence of intensity on number density as the cross-section also includes a number density term. The observed pressure dependence does in fact show a quadratic relationship up to around 2 to 3 torr (at room temperature), then almost a linear dependence at higher pressures. This is due to a quenching effect wherein the upper energy levels of the higher vibrational states are partially depopulated through non-radiative transfer to the lower energy levels, whilst the lower vibrational levels such as the (0,0) and the (0,1) bands are found to experience a cascading vibrational collision mechanism which populates the excited states. This cascade process is believed to be a major factor in the continued linear growth of the (0,0) band intensity with increasing pressure whereas the higher vibrational bands exhibit significant quenching.

For both systems, the N_2^+ (1-) and N_2 (2+), the collisional de-excitation rate of the excited states is temperature dependent which implies that any calibration of the fluorescent intensity against number density should be performed at a range of temperatures similar to those experienced in the wind tunnel tests.

4.3.2 Fluorescent intensity dependence

The fluorescent intensity of a spectral band can be related to the gas density and temperature by equating the production rate to the depletion rate of the upper level popualation of the observed molecular transition. Muntz (1968) has derived an equation for this intensity dependence which has the same form as a Stern-Volmer quenching equation; this relationship depends on the assumption of constant beam current and accelerating voltage and can be written, following the notation of Smith and Driscoll (1975):

$$I_{ul} = \frac{A\ n}{1 + B\ n\ Q(T)\ \{(8/\pi)\ RT\}^{\frac{1}{2}}} \qquad \text{(Eq. 4.3)}$$

The numerator of this equation represents the ratio of the excitation rate to the spontaneous decay rate for the excited level of the observed transition; in practice the constant, A, would also contain a dependence on the optical detection system, the beam current and the accelerating potential. The second term of the denominator represents the ratio of the rate of depopulation due to molecular collisions to the spontaneous decay rate for the excited level. The collision cross-section, Q, is assumed to be temperature dependent, and represents the cross-section for depopulation of the upper level by ground state molecules. If the average time between molecular collisions becomes comparable to the spontaneous lifetime of the excited molecules, typically 10^{-8} sec., collisional de-excitation drastically alters the observed fluorescence intensity. Under such conditions the second term of the denominator introduces a temperature dependence.

Equation 4.3 ignores the population of the upper excited levels by secondary electrons and if this effect is included the intensity dependence can be re-

written:

$$I_{ul} = \frac{A_1 + B_1 n^2}{1 + C_1 n Q(T) T^{\frac{1}{2}}} \qquad \text{(Eq. 4.4)}$$

This expression has been used by several investigators, e.g. Harvey and Hunter (1975) and McRonald (1975), to describe the intensity dependence of the fluorescence with number density; this expression can be re-written in a more compact form as:

$$I_n = \frac{A_2 + B_2 n^2}{1 + C_2 n T^D} \qquad \text{(Eq. 4.5)}$$

where, I_n is the measured ratio of photomultiplier output voltage to the collected beam current. At number densities below $\sim 5 \times 10^{17}$ cm^{-3}, it is possible to ignore the n^2 term of the numerator which is seldom greater than a few percent of the preceding term. In rarefied studies, typically number densities of 10^{15} to 10^{16} cm^{-3}, it is also possible to ignore the contribution of the second term of the denominator, see for example Muntz (1968). In this case, the observed fluorescence intensity will be directly proportional to number density. In the present study, number densities of around 10^{18} cm^{-3} occur and it is necessary to use the full relationship, i.e. Eq. 4.5.

4.3.3 Spatial resolution and frequency response

The spatial resolution and frequency response of the EBF technique are inherently linked by the intial beam diameter, d_o, which is defined by the final orifice diameter, i.e. the exit orifice in the model surface. The optical arrangement is shown in fig. 4-3; the spatial resolution is determined by the optical volume defined by the beam diameter and the slit spacing employed in the detection optics. In this case, the fluorescent cylinder formed by the passage of the beam is imaged onto a fibre-optic with a rect-

angular input section which effectively defined the slit width. Degradation of the spatial resolution is caused by beam spreading which occurs as a result of several processes:

a) Primary electrons are elastically scattered outside the initial beam diameter.

b) Secondary electrons are emitted at large angles to the primary beam direction.

c) Resonance radiation trapping occurs when the upper state of the observed transition has an optically allowed transition to the ground state, thus permitting radiation to be successively emitted and re-absorbed which results in the radiation being diffused.

d) Excited molecules could be convected out of the beam before the emission of a photon.

The first two factors are likely to produce the most significant beam broadening at high density; resonance radiation trapping is not significant for a diatomic gas such as nitrogen or air. Excited molecule lifetimes of $\sim 10^{-8}$ sec. also imply that molecules will not be convected out of the beam at the velocities considered in this investigation. The elastic scattering of primary electrons also results in beam current attentuation, i.e. the injected beam current does not necessarily pass through the optical volume under examination. It is possible to reduce these effects by increasing the accelerating voltage which reduces the cross-section for elastic scattering. This process also decreases the fluorescence intensity and it is generally accepted that 50kV is an optimum level. Above this voltage the cost, complexity and safety requirements of high voltage equipment rapidly increase.

Camac (1967) has proposed an empirical relationship by which it is possible to estimate the half intensity width of the beam, W_b, after it has traversed a length of gas, l_g, at a pressure, p, and temperature, T.

$$W_b = 0.044 \sqrt{\frac{p l_g^3 (300/T)}{V_a^2}} \qquad \text{(Eq. 4.6)}$$

where V_a is the accelerating voltage in units of 100kV. Assuming the worst possible conditions of a gas layer at the freestream density, temperature and of the local boundary layer thickness. These conditions give a half intensity width of 3mm at the boundary layer edge but obviously the beam broadening will be less under actual run conditions. Beam diameters of approximately 2 to 3 mm will reduce the maximum frequency response from 1.5 MHz to 0.5 - 1.0 MHz . Photodetectors with responses adequate to resolve disturbances in th is frequency range are widely available. Frequency response is ultimately limited by photomultiplier shot noise, which is the statistical error in measuring photons; in a time period corresponding to a fluctuation the detector must receive a sufficient photon flux to give good statistical accuracy. Unless the signal strength is sufficiently high, as the bandwidth increases, the higher frequencies appear as noise. This implies that a high beam current is necessary to result in adequate signal to noise ration and hence the ability to resolve the high frequency fluctuations. The smallest disturbance detectable is equal to the beam diameter hence the maximum frequency response is given by:

$$f_{max} = U_e/d_o \qquad \text{(Eq. 4.7)}$$

Typically, $U_e = 1450$ m sec^{-1} and $d_o = 1.0$ mm which gives:

$$f_{max} = 1.5\text{MHz}$$

This assumes that there is no appreciable beam spreading on transit through the boundary layer. If the beam diameter increases from 1mm to 2 to 3mm as calculated above, f_{max} will be reduced to 0.5 to 1MHz.

4.4 Equipment

The electron beam equipment is shown in the schematic fig. 4-1; the electron gun has been extensively used in the Hypersonics group at Imperial College for both rotational temperature and density measurements in the continuously running Nitrogen Tunnel, e.g. Lillicrap (1969), Davis and Harvey (1976) and Davis (1978). A brief description of the major system components is included in this section.

4.4.1 Model

The electron beam model is identical to the model described in section 3.2.1 in all respects apart from chord length, and is also similar to that used by Coleman (1973) in earlier tests at Imperial College. The model was a sharp flat plate with leading edge thickness 0.01mm and of 0.18m span by 0.91m chord. Hanging sideplates were used to prevent disturbances from the model underside interfering with the test flow. The plate was fixed to a faired aluminium alloy underbody which served as both a support for the model and provided a cavity, shielded from the flow, in which to house the differentially pumped section of the drift tube. Ports were machined into the base of the flat plate model at four centreline stations starting 460mm from the leading edge then at 50mm intervals. The pumped section of the drift tube assembly was located and locked into these ports using a trapped O-ring as the vacuum seal. A 1.0mm precision hole was drilled at each station to allow the passage of the electron beam normal to the model surface. At stations not in use the 1.0mm hole was fitted with a flush fitting plug to prevent any interference with the test flow.

4.4.2 Model support

In contrast to all previous Gun Tunnel studies it was not feasible to mount the model from the working section floor because the electron gun could not be fitted either above or below the working section without major tunnel modifications. To overcome this the flat plate was mounted by means of horizontal, faired supports onto a fabricated steel box section which replaced one of the existing Schlieren windows see fig. 4-1. The box section provided a good mounting surface 14" from the nozzle axis; two reinforced mild steel struts are used to support the aluminium alloy underbody of the flat plate. The upstream strut is faired to reduce loads and aluminium plates are fixed between the upstream and rear struts thus forming a void through which the draft tube passes. During all tests the working section door, onto which the model was mounted, was bolted to the working section to prevent movement during evacuation and subsequent venting to atmosphere.

4.4.3 Drift tube and differentially pumped block

The drift tube was a 22.0mm o.d. stainless steel tube extending from the electron gun through ports in the box section panel to the differential pumping block located in the model underbody. Four drift tube ports were machined in the box section panel corresponding to the four beam stations on the model: A differential pumping system was required to substain the pressure gradient between the low pressure gun (10^{-4} to 10^{-5} torr) and the relatively high pressure model surface (5 torr). The drift tube and pumping block are shown in fig. 4-4. High conductivity copper was used for all the pumping block ports that came into contact with the beam. A 22.0mm copper pipe was used to connect the pumping block to an external rotary vacuum pump (660 l/sec). A small pressure balancing chamber was incorporated into the pumped block to

prevent fluid suction/injection from the boundary layer. Pure nitrogen was supplied to the chamber through small bore tubing; a needle valve was used to control the nitrogen flow. The chamber pressure was monitored with a strain gauge pressure transducer.

4.4.4 Electron beam gun

A conventional three electrode gun was used in the tests described herein; full details of the electron gun and its operating characteristics are given in Lillicrap(1969). In brief, the gun is constructed from a commercial electron microscope gun with specially fabricated magnetic lenses and deflection coils. A vacuum of 10^{-4} to 10^{-5} torr is maintained in the gun chamber by an oil diffusion pump with a thermo-electrically cooled baffle. The gun is designed to operate at a maximum acceleration voltage of 30 kV with input beam currents of 2-3 mA.The power supply incorporated a commercial high voltage supply, 30kV at 3 mA, with additional circuitry to derive a bias voltage and a floating low voltage power supply to provide filament heating. Two magnetic lenses were used to focus the beam to a fine spot and three sets of deflection coils were used to steer the beam through the equipment to the model surface,where the series of coaxial holes in the differentially pumped section acted as a final collimation of the beam. High stability constant current power supplies were used to drive both deflection coils and magnetic lenses. The electron gun is shown in the photograph fig. 4-5.

4.4.5 Optical detectors.

The optical detection system is shown in the schematic, fig. 4-3, and in the photograph, fig. 4-6 . A maximum of three detectors were used as shown, rigidly mounted to the floor of the working section; the two primary detectors, D1 and D2, were mounted on precision optical traverse mechanisms operated by

micrometer screw gauges thus enabling the detectors to be traversed normally through the boundary layer. The third detector, D3, was fixed and used to monitor the beam fluorescence just outside the boundary layer edge. The arrangement of the detectors is shown in the inset diagram on fig. 4-3. A 40mm diameter quartz lens (f=125mm) was used in the primary detectors; the optical axis of the lens was inclined at 5^{o} to the vertical to remove the possibility of lens cut-off at points close to the model surface. A front surface mirror, with a coating chosen to give maximum reflectivity in the ultra-violet region, was used to turn the light path from the lens through 90^{o}. The quartz lens formed an image (m=0.93) on the rectangular input slit (1.00mm x 0.25mm) of a quartz fibre optic which could be replaced by a ground glass screen for initial focussing. The fibre optics were of the cross section transformer type with a rectangular input and a circular output section. Flexible vacuum connections were used to route the fibre optics to the photomultiplier tubes externally mounted to the working section. The photomultiplier housing contained a quartz relay lens and an interference filter (λ_c = 3 nm). EMI type 6526S photomultiplier tubes were used fitted with quartz windows.

4.4.6 Signal Processing and acquisition

Since photomultiplier tubes are current output devices, current to voltage amplifiers were required to amplify and condition the signal for recording on the digital data system. Two types of current amplifier were used in the investigation. The first was a commerically available current to voltage amplifier, Keithley model 427, which was a high precision instrument with facilities for variable time constant and gain. Although the bandwidth of this amplifier was not adequate for the proposed fluctuation measurements, i.e. - 3dB point at 100kHz, it was suitable for feasibility

studies and time averaged density measurements. The second type of amplifier used was designed and manufactured with the Department; the bandwidth was designed to extend from DC to 1MHz (-3dB point) with gains of up to 10^7 V/A.

The Gun Tunnel digital data acquisition system was designed with the possibility of making time resolved density measurements in mind; the high speed capability, one channel at 4MHz digitizing rate or two at 2MHz, is ideal for acquiring such data. Full details of the system are presented in Appendix A.

4.5 Calibration

As stated earlier, the relationship between the fluorescent intensity and the number density is usually determined by means of a calibration. Ideally the calibration should cover the exact density and temperature range experienced in the test flow. In addition the calibration should also be carried out in a flowing gas to prevent any possibility of heating the gas or the gradual increase of concentration of impurities, such as oxygen, which would quench the fluorescence. In the present case a quasi-static calibration was obtained only at one temperature.

4.5.1. Calibration equipment

To facilitate the calibration a cylinderical chamber was fixed to the model over the beam station. The beam was collected in a large graphite cap close to the exit orifice; pure nitrogen was injected into the chamber via a large pipe containing metal gauze and wirewool to ensure thorough mixing of the gas. A thermocouple was used to measure the temperature of the mixing chamber which was also assumed to be the gas temperature

as the gas velocities were very low. The gas flow was controlled with a high precision needle valve, and the gas pressure measured with a strain gauge transducer. The detector optics viewed the beam through narrow slits in the bottom surface of the chamber; these slits also formed the gas path into the working section which was maintained at a pressure slightly lower than the calibration chamber. The interior of the chamber was painted black to prevent reflections.

4.5.2. Calibration results.

The fluorescent intensity was represented by the voltage ouput from the photomultiplier detector system measured at the input to the data system; the beam current was measured as the voltage drop over a precision 10k ohm resistor. The fluorescent intensity, normalised by the beam current, is plotted against density for the three detectors in fig. 4-7 a, b and c. The figures show that the relationship is linear over a large proportion of the density range examined, but with a loss of sensitivity appearing at the higher densities. The calibration was limited to 26 torr RTE (room temperature equivalent pressure i.e. $293^{o}K$); this was due to the inability of the differential pumping system to maintain the gun pressure at 10^{-4} - 10^{-5} torr for greater densities. This problem prevented electron beam measurements being made at the HP running condition where the freestream density exceeded this level by a factor of four. It was decided to limit the investigation to the low pressure (LP) running condition but even so the freestream density level was 30 torr RTE. Re-design of the differential pumping system or an increase of pumping capacity was not practical at this stage, so it was necessary to extrapolate the calibration to 30 torr RTE. This was achieved by fitting the relationship, equation 4.5, to the data and using this relationship for further data reduction:

$$I_n = \frac{A_2 n + B_2 n^2}{1 + C_2 n T^D} \qquad \text{(Eq. 4.9)}$$

Without knowledge of the temperature dependence it must be assumed that D = 0 giving:

$$I_n = \frac{A_2 n + B_2 n^2}{1 + C_2 n} \qquad \text{(Eq. 4.10)}$$

The temperature dependence has been shown to be small and this assumption has been used by other investigators e.g. Harvey and Hunter (1975) and Wallace (1968). The calibration curves are shown in figs. 4-7a, b and c.

In order to assess the effects of quenching by oxygen, the calibration was repeated using air as the test gas; fig. 4-8 shows the quenching effect of oxygen emphasising the precautions that must be taken to limit the oxygen content of the test gas.

To assess the beam attenuation through a layer of high density nitrogen a series of tests were performed in the calibration chamber. The attentuation of an electron beam through a layer of gas is commonly modelled by:

$$i_y = i_o e^{-k^* y} \qquad \text{(Eq. 4.11)}$$

where k^* is a function of the beam voltage and Faraday cup construction. A mean value of $k^* = 0.00146$ was determined by varying the separation, y(mm), and the density (torr RTE); this value compares well with the recommendation of Smith and Driscoll (1977) of $k^* = 0.00167$.

4.6 Application to Boundary Layer measurements

The EBF system described in the earlier sections was used to make

preliminary measurements of mean and fluctuating density in the boundary layer formed on the model at the LP running condition, see Table 1. As described in the last section it became apparent during the calibration that it was not feasible to use the technique at the HP running condition as hoped. Therefore, it was decided to limit the investigation to the LP boundary layer using a boundary layer trip to ensure that the layer was fully turbulent at the EB station. Only one EB station, x = 560mm, was investigated due to time constraints. Conventional time-averaged measurements were made on the same model at identical conditions to provide data for comparison; these measurements included pitot pressure, total temperature, static pressure at the wall and Preston tube surveys. Heat transfer data was available from an earlier investigation, Coleman (1973), using an identical model.

Preliminary tests showed that the high bandwidth amplifiers were exhibiting high frequency response deficiencies; this was partly due to design faults and the moderate signal to noise ratio , which was a result of the low beam currents. These problems could not be solved quickly and the fluctuation data was obtained using the Keithley amplifiers which had a -3db bandwidth of 100kHz. At x = 560mm a profile was obtained by traversing one detector through the layer and using a second detector focussed at the boundary layer edge for normalisation. These data were acquired using the high speed data system at sampling rates of 1×10^6 to 4×10^6 samples per sec., with a maximum of 16384 samples. From the data it was also possible to calculate the root mean square value of the density fluctuations at several points through the layer. Correlation measurements were also made by fixing the location of one detector and traversing the other detector through the layer; a third detector was used to monitor the boundary layer edge for run to run variations.

4.7 Conclusions and recommendations

Applying the EBF technique to a high Reynolds number intermittent facility, such as the No 2 Gun Tunnel, imposes requirements additional to those necessary in a more rarefied continuous tunnel. Adequate penetration of the beam through the high density gas optimally requires accelerating voltages of approximately 50kV. In the present study, the accelerating voltage was limited by the design of the high voltage insulator within the gun to 30kV. It is hoped that a 50kV gun, at present under construction, will be available in the near future.

Fluorescent intensity is directly proportional to beam current therefore it is vital to maximise the injected beam current to ensure adequate signal to noise ratio. Significant losses were experienced in the 30kV gun with only 20-30% of the supplied current reaching the model surface; the design of the 50kV gun has been optimised for low current losses and would give a significant signal to noise improvement. Electron guns typically require pressures of about 10^{-5} torr to ensure reliable operation and long filament life. In contrast the wall static pressure levels are about 6 torr and 18 torr RTE for the LP and HP running conditions respectively. These pressure differences can be successfully maintained by the present differential pumping equipment but at the higher static pressure the gun pressure was marginal. The design of the differential pumping system could be significantly improved if it were possible to use larger diameter pipe to the main rotary pump which has its pumping speed limited by the present 22mm OD pipe. Alternatively a far smaller beam diameter, with a correspondingly smaller orifice in the model, would dramatically eliminate the pumping problems. It would also be advantageous to incorporate a rapid operation valve to isolate the gun from the working section after a run; this valve would have to be interlocked so as to switch off the gun power supply prior to closing.

Calibration at the higher densities also posed the identical problem of overloading the differential pumping system. It has been shown by Smith and Driscoll (1975) that dynamic calibration has significant advantages over a static calibration in which impurities may well quench the fluorescence. It is suggested that a better approach to calibration may be to use a free jet facility with a range of nozzles and to cover the temperature and density range of the test flow by varying the free jet supply conditions. Significant loads due to the high pressure levels are transmitted to the model especially during the tunnel starting processes, hence rigid mounting of both the model and associated electron beam equipment is required to prevent loss of delicate beam alignment. However, the gun and model mounting proved very successful with little or no re-alignment necessary between runs.

Detection optics proved adequate but larger aperture lenses and higher transmission interference filters could be employed to improve the signal to noise ratio by collecting more light. For the correlation measurements, it proved difficult to align and focus two separate detectors onto the same volume of the fluorescent light beam. It is suggested that one lens could be used to image the beam and use separate relay lenses to route the light to the detectors. The problems encountered with the broad band DC amplifiers have been solved by minor redesign and should enable the bandwidth of the fluctuation measurements to be raised to at least 500kHz. It is also suggested that it would be desirable to measure the beam broadening through the boundary layer to accurately determine the spatial degradation caused by this process.

The EBF system developed in this investigation have successfully been used to make preliminary measurements of mean and fluctuating density in a turbulent, hypersonic boundary layer.

5.0 Results and Discussion

The results described in this chapter were obtained in either the low pressure running condition boundary layer with forced transition or in the high pressure condition boundary layer with natural transition, see Table 1 for a summary of the Gun Tunnel conditions. For brevity, these flows will be referred to as the 'LP boundary layer" and the 'HP boundary layer' respectively in the discussion contained within this chapter. The results obtained from both the major experimental sections of the investigation, that is the mean or time-averaged measurements with conventional instrumentation and the fluctuating or time-resolved measurements using the electron beam probe, are presented in this chapter.

The time-averaged data obtained from conventional instrumentation, see section 3.0, can be divided into wall and profile measurements. At the wall, distributions of static pressure, heat transfer rate and skin friction (inferred from Preston tubes) were measured along the model centreline. Some spanwise wall distributions of static pressure and heat transfer rate were also measured to check the flowfield two-dimensionality and to determine the useful chord-length for testing. Transition position was also estimated from the centreline heat transfer and Preston tube distributions. Boundary layer profile measurements of pitot pressure and total temperature were taken at three stations in both the LP and HP boundary layers. From these, Mach number and velocity profiles were calculated in order to test the available velocity-temperature relationships and, after compressibility transformation, to compare with the well known incompressible results, such as the law of the wall and wake. The turbulent transport properties, such as mixing length or eddy viscosity, were calculated from the time-averaged velocity profile data using the time-averaged conservation equations with an assumption of similarity. The electron

beam fluorescence technique measurements were limited to the LP tripped boundary layer as discussed in section 4.6. Preliminary measurements were made of time-averaged and time-resolved density; the correlation between two points along the beam was measured for a range of separations. A fast Fourier transformation technique was used to obtain the coherence and the phase angle between the points along the beam, together with the power spectral density at each point.

The windtunnel running conditions are summarised in Table 1 and the parameters characterising the two boundary layers are presented in Table 2 and Table 3 for the LP and the HP flows respectively. The viscosity variation with temperature for the nitrogen test gas has been evaluated using the Sutherland law.

5.1 Flowfield two-dimensionality

To estimate the validity of the present data, it is important to assess the assumption that the boundary layer is two-dimensional at least over the region bounding the centreline of the flat plate. Inevitably, the finite span of the flat plate resulted in an outflow or spillage over the edges of the plate. Previous tests by Coleman (1973) have shown that hanging sideplates improved the flowfield two-dimensionality even though the sideplates introduced additional effects due to their own boundary layers. Hanging sideplates were used in all the present tests. Disturbances also emanated from the leading edge tips and these disturbances propagated along Mach lines eventually intersecting downstream on the model centreline and the flow within these Mach cones will be three-dimensional. Of course, disturbances can propogate across the boundary layer, either as mean variations or as turbulent disturbances, at angles greater than the Mach angle based on freestream conditions as the Mach number tended to zero at the bottom of the layer. However, such effects would be restricted to very thin layers.

5.2 Transition position

An estimate of the transition position for the HP running condition boundary layer can be obtained from the position of the peak heating rate or the peak surface impact pressure (Preston tube). From the centreline heat transfer rate distribution (section 5.4) the peak heating rate occurred at a position approximately 0.16m from the leading edge, corresponding to a Reynolds number, Re_x, of 8.82×10^6. This position agreed with the location of the peak surface impact pressure measurement obtained in the Preston tube-skin friction survey (section 5.5). At low speeds there is usually a strong correlation between the free stream turbulence level and transition, but at high Mach number one of the most significant factors influencing transition in a facility such as the Gun Tunnel is noise emanating from the nozzle wall boundary layer see, for example, Pate and Schueler (1969) and Wagner et al (1969). Obviously there are many other factors that can influence transition such as heat transfer, pressure gradient or surface roughness. Systematic studies can be performed to assess these effects, but if acoustic tripping is predominant as suspected at high Mach number, it can be difficult to compare data from different windtunnels.Assuming transition is influenced by noise, the transition position may well be sensitive to the model location relative to the nozzle. This was confirmed from the heat transfer tests of Coleman(1973) which showed a different transition position to the present tests, see section 5.4. For the tests described in in this report the model was always maintained at a strict position with respect to the nozzle such that the leading edge was 0.15m upstream from the nozzle exit plane.

For the LP condition boundary layer transition was initiated artificially by means of a boundary layer trip positioned 10mm from the leading edge,

see section 3.2.3. In this case, the model was positioned with the leading edge in the nozzle exit plane to be identical with the tests of Coleman (1973).

5.3 Surface Pressure

Surface pressure distributions were measured for both the LP and the HP boundary layers; the distributions were measured along the centreline with selected spanwise distributions to check flowfield two-dimensionality. The LP tripped boundary layer showed a slight favourable pressure gradient, see fig. 5-1, with an average variation of $(1/p)\ dp/dx = -3\%\ m^{-1}$. Also shown on this figure are the static pressure values in the freestream calculated from the measured stagnation and freestream pitot pressures. These values agreed well with the measured wall values. The HP natural transition boundary layer also showed a favourable pressure gradient, Bartlett et al (1979a), with an average value of $(1/p)\ dp/dx = -6\%\ m^{-1}$, see fig. 5-2. The calculated static pressures at the edge of the layer agreed well with the wall values. The pressure gradient for both flows has been shown to be close to zero and has been compared to data from zero pressure gradient studies in later sections. The measured pressure gradient has been used in the data reduction scheme in section 5.15 for the calculation of the turbulent transport properties.

5.4 Heat Transfer

The heat transfer rate has been measured along the centreline for the HP condition boundary layer, Bartlett et al (1979a), and is shown in fig. 5-3; the off centreline points shown correspond to spanwise distributions taken at several stations to test flow two-dimensionality. The peak heating rate is seen to occur at approximately 0.16m from the leading edge. This position is considerably different to that measured by Coleman (1973) in the No. 2 Gun Tunnel at almost identical flow conditions. He found

that the peak heating position occurred at approximately 0.32m from the leading edge; it is thought that this was due to the different model position relative to the nozzle exit plane. In the present study the leading edge was sited 0.15m upstream of the nozzle exit plane while Coleman positioned his model with the leading edge in the nozzle exit plane. If transition is triggered by acoustical disturbances emanating from the nozzle boundary layer it is likely that the peak heating position will depend on model position.

In the case of the LP condition boundary layer the heat transfer distribution was not measured but Coleman (1973) has reported measurements on a similar model at identical conditions in the same facility. An identical boundary layer trip was used in both studies (section 3.2.3) placed 10mm from the leading edge. The problem outlined above regarding transition dependance on the model position relative to the nozzle does not occur in this case as transition is forced close to the leading edge. Even so this model was maintained in a position such that the leading edge was in the nozzle exit plane. The heat transfer distribution measured by Coleman (1973) is shown in Fig. 5-4; this figure also includes data obtained with off centre-line gauges to check flowfield two-dimensionality.

5.5 Surface impact pressure

Surface impact pressure distributions along the model centreline were measured with the Preston tubes described earlier in section 3.3.3. The evaluation of skin friction from Preston tube data requires a calibration which is often based on floating element gauges that are questionable in both reliability and accuracy. The choice of calibration

is difficult with all compressible flow Preston tube data especially under cold wall conditions. Allen (1973) has made an extensive evaluation of the existing compressible calibrations and developed a calibration based on his results. Allen (1977) subsequently re-evaluated his results in the light of improved floating element gauge data. Bradshaw and Unsworth (1973) have also developed a calibration using Allen's compilation of data but based entirely on wall variables. A full assessment of the different calibrations has been made with the present data and some of the prediction methods, such as Spalding-Chi (1964) or van Driest(II) (1956), in Edwards and Hillier (1980b).

For the LP boundary layer, the surface impact pressure distribution is shown in fig. 5-5 and the corresponding range of skin friction, C_f, obtained from the various calibrations presented by Allen (1977), is shown in fig. 5-6. The calibrations give rise to a wide range of C_f values highlighting the inherent uncertainty in compressible flow calibrations, especially under cold wall conditions. Also shown in fig. 5-6 are the C_f values calculated from the faired heat transfer distributions assuming three values of Reynolds analogy factor, F, where:

$$F = \frac{2St}{C_f} \qquad \text{(Eq. 5.1)}$$

The traditional value of F is 1.0 for compressible flow, although a value of 1.16 was suggested by Chi and Spalding (1966) from a review of the available compressible data. Coleman (1973) in the present facility found F values of approximately 0.9, which represents the lower limit of the commonly accepted range of F. The C_f values obtained using these three F values, i.e. F = 0.9, 1.0 and 1.16, have been plotted in fig. 5-6, which shows that the range of C_f obtained from the six Preston tube calibrations considered herein appear to fall within these bounds with the exception

of the Fenter-Stalmach prediction.

The surface impact pressure distribution for the H.P. boundary layer, see Bartlett et al (1979a), is shown in fig. 5-7 where the peak pressure occurred at approximately 0.15 to 0.18m from the leading edge which agreed with the peak heat transfer rate (section 5.4). The range of C_f obtained from the six calibrations is shown in fig. 5-8 ; a similar trend to the LP data was obtained with the majority of data falling within the bounds of C_f obtained from a Reynolds analogy factor of F=0.9 to 1.16 using the faired heat transfer distributions. The Fenter-Stalmach calibration again overpredicts the trend of C_f obtained from the other calibrations; a similar effect when using this calibration was reported by Coleman (1973) on a cold wall study in the present facility.

The measurement of skin friction at high Mach number with appreciable heat transfer or pressure gradient is still an intractable problem. There remains considerable problems with both the reliability and the repeatability of the direct methods, in particular the floating element balance and as shown above the most commonly used indirect method, the Preston tube, relies on the choice from the wide range of calibrations. The Hopkins and Keener (1966) calibration appears to give 'the most consistent' agreement with floating element balance measurements made on a cold wall at high Mach number, see for example Keener and Hopkins (1969). This calibration collapsed the present Preston tube data from different tube diameters, e.g. Edwards and Hillier (1980b), and has been used to deduce C_f values for further data reduction described later in this report.

5.6 Pitot Pressure Profiles

Pitot pressure profiles were obtained using the honed and flattened probes described earlier in section 3.3.6.1 The boundary layer thickness, δ_p, was obtained from each profile at the point where $p_t/p_{te} = 0.99$. The δ_p values are presented in Tables 2 and 3 for the LP and HP condition boundary layers respectively. The profiles presented in this section are shown normalised against the measured freestream total pressure, p_o, to account for run-to-run variations, i.e. the expected scatter in the diaphagm burst pressure.

For the LP condition tripped boundary layer, pitot profiles were measured at three stations, i.e. x = 260, 360 and 560mm, from the leading edge. The profiles are shown in fig. 5-9 a, b and c; the profiles appear self-consistent amongst themselves and are typical of profiles obtained previously in the Gun Tunnel facility.

In the case of the HP condition natural transition boundary layer, profiles were measured at five stations, the first 360mm from the leading edge then at 50mm intervals. The profiles are shown in fig. 5-11 a to e, and in several of these there appears to be an increase in the scatter of the pressure points near the boundary layer edge, which made the evaluation of δ_p more difficult; the worst case observed was at the x = 460mm station with scatter of $\pm 3.5\%$ at $y/\delta_p > 1$. Re-evaluation of the original data traces provided no obvious reason to discount these points. It is very unlikely that intermittency could be responsible as the time-averaging period was relatively long, around 2 to 3 msec., and the fluid velocity high, around 1500 m/sec; no satisfactory explanation can be presented at this time. Another interesting effect was observed in the HP profile at x = 560mm , fig. 5-11e, which showed a 'pronounced kink' close to the model wall; an

effect that has been previously reported by Allen (1972). A separation region in front of the probe, caused by either probe and/or support interference was suspected. A series of further tests were undertaken to investigate the effects of varying probe and support geometry. A new pitot rake was constructed to form the basis of a variable geometry probe system; the first test involved increasing the pitot tube unsupported length by almost 90%. This modification proved very successful and further tests to investigate this phenomenon were not considered necessary at this time. The resulting profile is shown in fig. 5-11e compared to the original data; the new profile is very similar to those measured at upstream stations and both probe types agreed well for all the layer except the suspect region close to the wall. A composite profile utilising the data from both probe types was used for all further data reduction.

5.7 Mach Number Profiles

Mach number profiles were calculated for each pitot profile using the well known Rayleigh supersonic pitot formula, with the usual assumption of constant static pressure through the boundary layer:

$$\frac{P_t}{p_e} = \left[\frac{(\gamma-1)}{2} M^2\right]^{\frac{\gamma}{(\gamma-1)}} \left[\frac{(\gamma+1)}{2\gamma M^2 - (\gamma-1)}\right]^{\frac{1}{(\gamma-1)}} \qquad \text{(Eq. 5.2)}$$

For the test gas, nitrogen, $\gamma = 1.40$ and Eq. 5.2 reduces to:

$$\frac{p_t}{p_e} = \left[\frac{6}{5} M^2\right]^{7/2} \left[\frac{6}{7M^2 - 1)}\right]^{5/2} \qquad \text{(Eq. 5.3)}$$

Eq. 5.3 was solved for each point in the pitot profile; no displacement correction has been applied to these profiles due to the arbitrary and uncertain nature of these corrections at hypersonic Mach numbers. Mach number profiles are presented, normalised by the Mach number at the layer edge,

M_e. For the LP condition boundary layer the Mach number profiles are shown in fig. 5-10 a, b and c, and for the HP condition layer in fig. 5-12 a to e. The profiles for both conditions appear to be typical of a turbulent boundary layer and the scatter discussed earlier in some of the HP profiles is much reduced by virtue of the Mach number calculation procedure.

5.8 Total temperature profiles

The total temperature profiles were measured with a rake of four vented-shield miniature probes as described in section 3.3.6.2. An additional probe was fixed below the flat plate to monitor the freestream total temperature $T_{o\infty}$. It is difficult to construct a series of probes with identical geometric and physical characteristics hence it is desirable to calibrate individually each probe over a range of Mach and Reynolds number comparable to that experienced in traversing the boundary layer. The calibration of the probes is discussed in Appendix B and in detail by Bartlett, Edwards, Hillier (1979). To correct the measured total temperatures an iterative scheme was devised based on the variation of probe recovery factor (obtained from the calibration) with the local Reynolds number in the probe Re_{3d} each time with the new estimate of total temperature. The profiles were normalized against the total temperature at the boundary layer edge T_{oe}, and adjusted for run to run variations of $T_{o\infty}$.

For the LP condition total temperature profiles were measured at the three stations x= 260,360 and 560 mm. to be coincident with the Mach number profiles .The measured profiles are shown in fig. 5-13 a,b and c and the corrected profiles are shown in fig. 5-14 a,b and c .For the HP condition boundary layer total temperatures were measured at only three

of the five pitot pressure stations,i.e. at x= 360,460 and 560 mm. The measured profiles are shown in fig. 5-15 a-c and the corrected profiles in fig. 5-16 a, b and c.

In general the total temperature profiles tend to exhibit more scatter than the corresponding pitot profiles, reflecting the inherent difficulty in making total temperature measurements. The problem was compounded by the use of a rake of four probes, with individual responses, instead of a single probe traversing the layer. This is highlighted by the LP condition profiles, fig. 5-13 in which due to breakages only two probes were used as opposed to four for the HP condition tests, and the scatter appears reduced in the LP profiles. It is likely that both the pitot and total temperature measurements suffered from wall interference effects at the points closest to the surface, for which no adequate correction scheme exists.

5.9 Velocity profiles

Velocity profiles were calculated from the corrected total temperature profiles and the corresponding Mach number profiles using Eq. 5.4. In general, the y points through the boundary layer at which the pitot pressures and total temperatures were measured, were not coincident; it was necessary either to draw smoothed curves through both sets of data or to use the individual readings of one parameter with interpolated values of the other. The latter choice was made by retaining the total temperature data and taking interpolated Mach number values as this data required the least smoothing. The resulting velocity profiles are shown normalized by the velocity at the boundary layer edge.

$$\frac{U}{U_e} = \frac{M}{M_e}\frac{T}{T_e} = \frac{M}{M_e}\frac{T_o}{T_{oe}}\left[\frac{(1 + \frac{1}{2}(\gamma-1)M_e^2)}{(1 + \frac{1}{2}(\gamma-1)M^2)}\right] \qquad \text{(Eq. 5.4)}$$

The velocity profiles for the LP tripped condition are shown in fig. 5-17 a, b and c for x = 260, 360 and 560 mm from the leading edge, and for the HP layer the velocity profiles are shown in fig. 5-18 a, b and c for x = 360, 460 and 560 mm respectively. In both cases the profiles appear to be typical of a turbulent boundary layer. The values of the exponent, N , of the power law fit to the velocity profile were estimated, where N is defined from:

$$\frac{U}{U_e} = \left(\frac{y}{\delta_u}\right)^{1/N} \text{, where } \delta_u \text{ is defined as the point such that } U = 0.995U_e. \qquad \text{(Eq. 5.5)}$$

It was found that the velocity profile was best scaled by δ_u rather than δ_p in this case; values of N and δ_u are presented in Tables 2 and 3. Johnson and Bushnell (1970) have plotted the power law exponent variation with Re_θ for a large body of data, fig. 5-19. At low values of Re_θ , e.g. $2000 < Re_\theta < 5000$, an overshoot region was found where N reached values of up to 13. This region corresponds to the non-equilibrium turbulent boundary layer in which the velocity profiles are non-similar. At higher Re_θ typically above 10000 the exponent N exhibits a gradual increase, approximately scattering around the traditionally accepted value of 7. This is the region of the so-called equilibrium turbulent boundary layer although it must be emphasised that there is not a clear cut dividing line between non-equilibrium and equilibrium turbulent boundary layer flow. The present data is also plotted on the Johnson and Bushnell data, fig 5-19, together with some of the more recent published data, e.g. Owen et al (1975), Watson (1977) and Laderman (1978). The LP condition data follows the low Reynolds number trend of the Johnson and Bushnell data with N falling from 10 to 8.7 as Re_θ increased

from 2800 to 5600. The HP data also shows a decrease in N with increasing Re_θ although two of the points fall outside the shaded region, the present data does appear to follow the local trend of the Johnson and Bushnell data. It is apparent from fig. 5-19 that the exponent N is of limited value as a parameter from which to determine whether a boundary layer has reached equilibrium or not due to the inherent scatter of N with upstream history effects,heat transfer or Mach number.

5.10 Velocity-Temperature Correlations.

The measured profile data have been compared with several of the common velocity-temperature relationships,for example the non-unity Prandtl number Crocco solution as modified by van Driest,Eq.2-5,re-expressed here as:

$$\frac{T}{T_e} = \frac{T_w}{T_e} + \frac{(T_r - T_w)}{T_e}\frac{U}{U_e} - \frac{r(\gamma - 1)M_e^2}{2}\frac{U^2}{U_e^2} \qquad \text{(Eq. 5.6)}$$

This expression is valid for flows with zero pressure gradient, i.e. $dp/dx = 0$ and isothermal wall, T_w = const. The recovery factor for turbulent flow is usually taken as:

$$r = \sqrt[3]{Pr} \simeq 0.89 \qquad \text{(Eq. 5.7)}$$

The recovery temperature is defined as:

$$T_r = T_e(1 + r(\gamma - 1)/2\, M_e^2) \qquad \text{(Eq. 5.8)}$$

Thus, Eq. 5.6 can be re-written as:

$$\frac{T_o - T_w}{T_{oe} - T_w} = \psi \frac{U}{U_e} + (1 - \psi)\left[\frac{U}{U_e}\right]^2 \qquad \text{(Eq. 5.9)}$$

where, $$\psi = \frac{T_r - T_w}{T_{oe} - T_w}$$

As shown in section 2.4.1, if Pr = 1 then $T_r/T_{oe} = 1$ hence $\psi = 1$ and Eq. 5.9 reduces to the so-called 'linear Crocco' solution, i.e.

$$\frac{T_o - T_w}{T_{oe} - T_w} = \frac{U}{U_e} \qquad \text{(Eq. 5.10)}$$

In the case of an adiabatic wall, i.e. no heat transfer, $\psi = 0$ and Eq. 5.9 reduces to:

$$\frac{T_o - T_w}{T_{oe} - T_w} = \left[\frac{U}{U_e}\right]^2 \qquad \text{(Eq. 5.11)}$$

One of the common approaches in evaluating velocity-temperature data has been to plot the velocity data against the total temperature function Θ_t where,

$$\frac{T_o - T_w}{T_{oe} - T_w} = \Theta_t \qquad \text{(Eq. 5.12)}$$

This is the traditional 'Crocco plot' in which a comparison is made with the linear solution, Eq. 5.10, and the quadratic or Walz solution, Eq. 5.11. The linear solution has shown good agreement with zero pressure gradient, boundary layers under conditions of heat transfer, but the quadratic solution has been found to give close agreement with adiabatic flows with non-

zero pressure gradients in the stream direction and normal to the wall, e.g. nozzle wall boundary layers, see. Beckwith et al (1971). In the case of the present data, the LP boundary layer profiles are plotted in fig. 5-20 a, b and c and the points fall between the linear and quadratic solutions, although the data tends to show marginally better agreement with the linear solution. There also appears to be a Reynolds number trend with the higher Re_θ profiles falling closer to the linear solution. The HP boundary layer data shows an approximately linear behaviour, fig. 5-21a, b and c with the agreement again appearing to improve with increasing Re_θ, thus suggesting that the boundary layer is not yet fully developed.

Better agreement has been obtained with the non-unity Prandtl number Crocco relationship, Eq. 5,6, using a recovery factor r = 0.89. The experimental data are replotted in fig. 5-22 a, b and c and fig. 5-23 a, b and c for the LP and HP data respectively. The agreement is fair for the LP case and excellent for the HP case. This expression has shown good agreement with high Mach number cold wall data, with zero pressure gradient, see for example Bushnell et al (1969).

The non-unity Prandtl number Crocco relationship has not been successful in predicting the trend observed on adiabatic or near adiabatic walls in which case there is a pronounced overshoot in the distribution, e.g. Laderman (1978). Recently Whitfield and High (1977) have proposed a velocity-temperature relationship for non-unity Prandtl number by including approximate models for the turbulent shear stress distribution. This approach results in a 2nd order, non-linear ordinary differential equation which relates the specific enthalphy ratio h^* to the velocity

ratio ${}^{*}U$ where,

$$ {}^{*}h = \frac{h}{h_e} \quad \text{and} \quad {}^{*}U = \frac{U}{U_e} $$

Zeroth- and first-order perturbation solutions were obtained in terms of the small parameter ε ,where $\varepsilon = 1 - Pr$. The final expression for an isothermal wall read:

(Eq. 5.13)

$$ {}^{*}h({}^{*}U) = {}^{*}h_w + ({}^{*}H_\infty - {}^{*}h_w){}^{*}U - \frac{G}{2}{}^{*}U^2 + $$

$$ \varepsilon\left[\frac{4G{}^{*}U}{(\Omega+1)(\Omega+2)}(1-{}^{*}U^{\Omega+1}) - \frac{4({}^{*}H_\infty - {}^{*}h_w)}{(\Omega+1)}(1 - {}^{*}U){}^{*}U + \right. $$

$$ \left. \frac{G}{2}{}^{*}U(1 - {}^{*}U) + (1 - {}^{*}U)\, f(0) + {}^{*}U\, f(1) - f({}^{*}U) \right] $$

where,

$$ f({}^{*}U) = (\Delta/G)\left[(Z - \Delta)\ln|Z-G| - (Z + \Delta)\ln|Z+G| \right] $$

and

$$ \Delta = \left[2G{}^{*}h_w + ({}^{*}H_\infty - {}^{*}h_w)^2 \right]^{\frac{1}{2}}, \quad G = (\gamma-1)M_e^2 $$

$$ Z = ({}^{*}H_\infty - {}^{*}h_w - G{}^{*}U), \quad {}^{*}H_\infty = H_\infty/h_\infty = (1 + G/2) . $$

Also $\Omega = (5/2)N$, where N is the exponent from the power law representation of the velocity profiles, i.e.

$$ {}^{*}U = \frac{U}{U_e} = \left[\frac{y}{\delta} \right]^{1/N} $$

The Whitfield and High approach has shown good agreement over a range of T_w/T_{oe} values, e.g. Whitfield (1976), Laderman (1978) and Watson (1979), and has been evaluated for the two present cases to assess whether this more general approach will yield better correlations with cold wall ($T_w/T_{oe} \simeq 0.3$) data than Pr≠1 Crocco solution i.e. Eq. 5.6. The Whitfield and High solution is also shown in fig. 5-22 for the LP boundary layer and fig. 5-23 for the HP layer. In the LP case the theory gave slightly worse agreement than Eq. 5.6 but showed improved agreement for the HP case. The LP boundary layer profiles may well be suffering from the effects of transition, and/or low Reynolds number effects at all three stations, whereas the HP is much closer to a fully developed, equilibrium boundary layer. Although the Pr≠1 Crocco solution, Eq. 5.6, does not represent adiabatic wall data adequately, it has shown good agreement with the present and other cold wall data thus can be used as an accurate approximation for cold wall data in prediction or calculation methods.

5.11 Integral quantities

The following integral quantities have been calculated from the measured profile data:

Displacement thickness,	δ_1 (δ^*).
Momentum thickness,	δ_2 (θ).
Kinetic energy defect thickness,	δ_3
Total enthalpy defect thickness,	δ_4

The trapezium rule has been used for the evaluation of these integrals but the reliability of these quantities must be questioned due to the accentuation of experimental scatter in this type of computation. In

the case of the defect integrals the measured points did not extent close enough to the wall to detect the peak present in these quantities. The momentum thickness Reynolds number, Re_θ, and the Reynolds number $Re_{\delta 2}$ as recommended by Fernholz and Finley (1977) together with various shape factors defined below have been calculated and are presented in Tables 2 and 3 for the LP condition and HP condition boundary layers respectively, where,

$$Re_{\delta 2} = \frac{\rho_e U_e}{\mu_w} \delta_2 \quad \text{and} \quad Re_\theta = \frac{\rho_e U_e}{\mu_e} \delta_2 \ ,$$

$$H_{12} = \delta_1 / \delta_2 \ ; \ H_{32} = \delta_3 / \delta_2 \ ; \quad H_{42} = \delta_4 / \delta_2 \ .$$

5.12 Compressibility Transformation.

At present there is no rigorous mathematical basis to any of the available compressibility transformation methods as described in section 2.4.2, but these methods remain a useful tool in the comparison and evaluation of high speed data. The van Driest (1951) effective velocity method, although not strictly a whole layer transformation method, has been shown to give the best agreement with the well known incompressible expressions over a wide range of Mach number on both adiabatic and cooled walls, see for example Fernholz (1976).

Using the form of the van Driest transformation as given by Keener and Hopkins (1973) and incorporating a temperature distribution based on a recovery factor, r = 0.89. Eq. 2.11 is rewritten as:

$$\frac{\overline{U}^*}{U_\tau} = \frac{1}{A\sqrt{(C_f/2)(T_w/T_e)}} \left[\sin^{-1}\left[\frac{2A^2(U/U_e) - B}{\sqrt{(4A^2 + B^2}}\right] + \sin^{-1}\left[\frac{B}{\sqrt{(4A^2 + B^2}}\right] \right] \qquad \text{(Eq. 5.15)}$$

where, $A^2 = \frac{T_e}{T_w}\frac{(\gamma-1)}{2} M_e^2$ and $B = \frac{T_e}{T_w} + A^2 - 1$

Eq. 5.15 requires the skin friction coefficient at each station to be specified, but as discussed earlier in section 5.5 the evaluation of C_f from Preston tube measurements (in compressible flow on cold walls) presents serious difficulties due to the scatter in the various calibrations. The Hopkins and Keener (1966) calibration appears to give the most consistent agreement with skin friction balance measurements at high Mach number and cold wall conditions, see for example Keener and Hopkins (1969). This calibration has been used to determine C_f from the Preston tube data, section 5.5, and these C_f values subsequently used in the evaluation of the generalised velocity $\overline{U}^*$ from the velocity profile data. The 'transformed' velocity profiles , $\overline{U}^*/U_\tau$, have been calculated and the LP condition data are shown in fig. 5-24 and the HP condition data in fig. 5-25, both plotted against yU_τ/ν_w. These profiles appear typical of high Mach number, cold wall boundary layers although with a relatively short log-law region.

5.12.1 Law of the Wall

Also shown in fig. 5-24 and 5-25 is the law of the wall, i.e.

$$\frac{\overline{U}^*}{U_\tau} = \frac{1}{k} \ln \frac{yU_\tau}{\nu_w} + C \qquad \text{(Eq. 5.16)}$$

where, $k = 0.40$ and $C = 5.10$.

In the case of the LP condition data, there is good agreement with the law of the wall at all three stations, hence the compressible profiles are satisfactorily reduced to the incompressible relationship. For the HP condition, the agreement between the transformed data and the law of the wall is shown to be good at the two rear stations x = 460 and 560mm in Fig. 5-25, but the data falls below the incompressible relationship at x = 360mm. This could be due to the skin friction being overestimated at the first station or the effects of an uncompleted transition process.

In general the van Driest transformed profiles agreed well with the law of the wall confirming the agreement found previously for zero pressure gradient, cold wall boundary layers, e.g. Laderman (1978) and Watson (1979).

5.13 Outer Law

Maise and McDonald (1968) have suggested an outer or velocity defect law for compressible, turbulent boundary layers of the form:

$$\frac{\bar{U}_\delta^* - \bar{U}^*}{U_\tau} = -\frac{1}{k} \ln (y/\delta) + \frac{1}{k} f(y/\delta) \qquad \text{(Eq. 5.17)}$$

where $f(y/\delta) = 2-W$

and $W = 1 - \cos(\pi y/\delta)$.

A value of k = 0.4 was recommended by the authors; the wake component was taken to be equal to 0.5, a value typical of a fully developed, incompressible boundary layer, see for example Coles (1953). Using these values gives,

$$\frac{\bar{U}^*_\delta - \bar{U}^*}{U_\tau} = -2.5 \ln (y/\delta)_p + 1.25(2 - W) \qquad \text{(Eq. 5.18)}$$

Maise and McDonald achieved good agreement with adiabatic wall data using this expression over a range of Mach number from $1.5 < M_e < 5$. The present data has been compared with Eq. 5-18 as shown in fig.5-26 for the LP condition boundary layer and in fig. 5-27 for the HP layer respectively. Not suprisingly the correlation was poor; the Maise and McDonald form of the outer law contains a fully developed wake component term which is not the case for the present data. In addition the relationship is highly dependent on the evaluation of a boundary layer thickness, in this case δ_p has been used,which as can be seen in figs. 5-9 and 5-11 is difficult due to the scatter in the pitot pressure points at the edge of the layer.

Fernholz(1976) has criticised such relationships as Eq. 5.18 on the basis of the evaluation of a representative boundary layer thickness in compressible flow. For example, Laderman(1978) has found good agreement with Eq. 5.18 in a Mach 3 layer over a range of heat transfer conditions by using δ_p as the reference length, although at this relatively low Mach number $\delta_p \simeq \delta_u$. At higher Mach number the velocity field can be much smaller than the pitot pressure (density) field, i.e. $\delta_p > \delta_u$. Horstman and Owen(1972) found good agreement with Eq. 5.18 at $M_e = 7$ by using δ_u as the reference length but δ_u was found to be only 87% of δ_p . The present data at the LP running condition has been replotted in fig. 5-26 using y/δ_u as the abcissa and re-evaluating $\bar{U}^*_\delta / U_\tau$; the correlation is improved but, as stated earlier, Eq. 5.18 contains a fully developed wake component term which is generally not the case for the present data, see section 5.14. The agreement would improve with

with a representative wake term in Eq. 5.18.

The use of δ_u as a reference length has been criticised by Fernholz (1976) who suggested that as U/U_e rapidly asymptotes to its freestream value the evaluation of δ_u is liable to 'personal touch'. To overcome this Fernholz has produced a semi-empirical relationship for the outer region which he states collapses high Mach number data onto Klebanoff's velocity defect profile for incompressible, zero pressure gradient boundary layers. This relationship is only valid for flows with isothermal walls and zero pressure gradient. To alleviate the problem of evaluating a representative thickness in compressible flow, a new length scale, Δ^*, was used as first suggested by Rotta(1950). Fernholz's semi-empirical relationship read:

$$\frac{\bar{U}^*_\delta - \bar{U}^*}{U_\tau} = -4.70 \ln (y/\Delta^*) - 6.74 \qquad \text{(Eq. 5.19)}$$

where $$\Delta^* = \int_0^{\delta_p} \frac{\bar{U}^*_\delta - \bar{U}^*}{U_\tau} \, dy \, .$$

The constant terms were obtained from a correlation of experimental data as a function of T_w/T_{aw} and $Re_{\delta 2}$. The velocity profiles were 'transformed' using the van Driest method, as descibed in section 5.12. The use of Eq. 5.19 for the outer law was suggested by Fernholz as a good method for distinguishing profiles suffering from low Reynolds number effects. Low Reynolds number effects occur in the region between transition and the fully developed, equilibrium turbulent boundary layer. Townsend(1961) defined the equilibrium turbulent boundary layer as one in which "the turbulence production and dissapation

terms nearly balance and similarity is maintained in the outer wake-like portion of the velocity profile". In the region between transition and the fully developed equilibrium layer, the flow although turbulent has not reached equilibrium hence the outer profiles are not similar. The turbulence quantities in this region, such as mixing length or eddy viscosity, are functions of the local Reynolds number. This phenomenon is well known in incompressible flows, for example see Coles(1953) , but at high Mach number the situation is further complicated by increased lengths of transitional flow due to the increase of the transition Reynolds number Re_{CR} with Mach number. In this case it is often difficult to isolate the effects of an uncompleted transition process from the low Reynolds number effects. Fernholz and Finley (1979) have suggested a criterion to distinguish between transitional and the low Reynolds number turbulent profiles. The authors limit the validity of the criterion to zero pressure gradient flows on adiabatic or isothermal walls. They suggest that the compressible boundary layer can only be considered as fully turbulent if the velocity profile (transformed by the van Driest method, see section 5.12) agrees with both the law of the wall (Eq. 5.16) and the outer law proposed by Fernholz (Eq. 5.19). The authors have assessed many profiles using this criterion and found that low Reynolds number profiles generally show fair agreement with the log-law relationship, Eq. 5.16, but transitional profiles disagree. In the case of the outer law, the low Reynolds number profiles agree only for a short region with Eq. 5.19 while transitional profiles disagree markedly.

The investigation by Watson et al (1973) is considered to be one of the most comprehensive by Fernholz and Finley (1979) in that it

included transitional, low Reynolds number and turbulent profiles. The data of Watson et al is shown in fig. 5-28 plotted in the outer law format of Eq. 5.19 (reproduced from Fernholz and Finley (1979)). This data exhibits the features outlined above for transitional and low Reynolds number profiles. The present data has been compared to the Fernholz outer law in fig. 5-29 and fig. 5-30 for the LP and the HP condition boundary layers respectively. The LP data shows the characteristics typical of profiles suffering from low Reynolds number effects, i.e. the same type of behaviour as the data of Watson et al. These results suggest that the LP profiles are turbulent but not as yet fully developed into an equilibrium turbulent boundary layer. Fernholz and Finley (1979) also suggested that a useful parameter to assess the state of a boundary layer at low Reynolds numbers was the kinematic shape factor, H_{12K}, which is defined as:

$$H_{12K} = \frac{\delta_{1K}}{\delta_{2K}}$$

where,

$$\delta_{1K} = \int_o^{\delta_p} (1 - U/U_e) \, dy$$

and

$$\delta_{2K} = \int_o^{\delta_p} U/U_e (1 - U/U_e) \, dy \, ,$$

i.e. the ratio of the displacement to the momentum thickness assuming that the density remains constant. A typical value of H_{12K} for a laminar subsonic boundary layer with zero pressure gradient is 5.20, and for a turbulent layer $H_{12K} \simeq 1.40$. The values of H_{12K} for the LP condition profiles have been calculated and are presented in Table 2; the shape factor decreases from $H_{12K} = 1.60$ at the $x \simeq 260$mm station to $H_{12K} = 1.50$

at the x = 560mm station. Those values are typical of profiles suffering from the low Reynolds number effects as described by Fernholz and Finley (1979).

In contrast to the LP boundary layer profile data, the HP condition profile data shows good agreement with the Fernholz form of the outer law Eq. 5.19 as shown in fig. 5-30. Taking account of the scatter the agreement appears good over the whole profile for all three stations. These profiles had previously shown good agreement with the law of the wall, see fig. 5-25, thus fulfil the requirements suggested by Fernholz and Finley (1979) for zero pressure gradient boundary layers with no upstream history effects, i.e. obey the law of the wall and outer law.

5.14 Wake Component

An estimate of the wake component strength can be obtained from the maximum 'overshoot' or difference between the transformed velocity profile and the logarithmic inner region; the method of obtaining the strength, $\Delta(\overline{U}^*/U_\tau)$, is illustrated in fig. 5-31. This approach was originated by Coles (1952) in his study of incompressible boundary layer profiles. This method is obviously prone to 'personal interpretation' and to the selection of the constant terms, k and C, in the logarithmic law of the wall (Eq. 5.16); the recommendation of Fernholz and Finley (1979) is followed hence,

$$k = 0.4 \qquad \text{and} \qquad C = 5.10$$

A comparison between the present velocity profiles transformed using the van Driest ' effective velocity method' and the law of the wall,

Eq. 5.6, was presented in section 5.12. Estimates of the wake component strength were made from this comparison using the method outlined above and are presented for the LP and HP running conditions in Tables 2 and 3 respectively. In both cases, the profiles show an increase of $\Delta(\bar{U}^*/U_\tau)$ with Reynolds number Re_θ or $Re_{\delta 2}$ which indicates that the boundary layer is still developing. Coles (1962) found that the strength of the wake component was zero at $Re_\theta \simeq 500$ increasing to a maximum value of 2.8 at $Re_\theta \simeq 5000$. Fernholz and Finley (1979) have shown that $\Delta(\bar{U}^*/U_\tau)$ is best correlated with the subsonic data of Coles (1952) if plotted against $Re_{\delta 2}$ rather than Re_θ. The present data is shown in Fig. 5-32 a and b plotted against the correlations of adiabatic and isothermal wall data respectively obtained by Fernholz and Finley (1979) for zero pressure gradient flows with a defined origin i.e. flat plate boundary layers. The adiabatic data plot is included due to the paucity of data from boundary layers with heat transfer. Also shown in both fig. 5-32 a and b is the Coles (1962) correlation of $\Delta(U^*/U_\tau)$ for incompressible flows.

The present data shows a well defined increase with $Re_{\delta 2}$ falling below the Coles correlation although the trend is very similar. In comparison with the adiabatic wall data, fig. 5-32a, the present data shows lower values of $\Delta(\bar{U}^*/U_\tau)$ than the majority of the other data. For the cold wall case the available data is limited, fig. 5-32b and no trend with heat transfer can be detected, although the present data does agree well with the data of Keener and Hopkins (1972) which was obtained at $M = 6.5$ with a T_w/T_{oe} value similar to that of the present tests. It is apparent from these comparisons that the available data is very scattered with apparently no systematic Mach number variation although the overriding trend is similar to that found by Coles in

incompressible flow with $\Delta(\bar{U}^*/U_\tau)$ tending to zero at $Re_{\delta_2} \simeq 500$ and reaching a maximum value at $Re_{\delta 2} \simeq 6000$. Mabey(1974,1979) has reported a local maximum value of $\Delta(\bar{U}^*/U_\tau) = 3.6$ at $Re_{\delta 2} \simeq 5000$ falling back to the Coles value at higher Reynolds number. He suggested that the turbulence structure or upstream influences may be responsible,possibly due to small local pressure gradients near the leading edge of the flat plate model. Fernholz and Finley(1979) concluded that the wake component strength followed the Coles correlation with a scatter of about $\pm$20% when plotted against $Re_{\delta 2}$. The present data appears to confirm this conclusion but until more data is available it is not possible to identify any trend of $\Delta(\bar{U}^*/U_\tau)$ with either T_w/T_{oe} or Mach number. The conclusions regarding the wake component strength are consistent with the findings of section 5.13 in which a comparison was made with the outer law. This comparison showed that the LP condition profiles, in particular, were not fully developed.

5.15 Turbulent Transport Properties

Boundary layer calculation methods almost always require accurate models to describe the turbulent transport of energy and momentum in order to close the controlling time-averaged equations. At high Mach number it becomes increasingly difficult to measure the turbulence quantities directly, for instance with either a hot wire or laser doppler aneomometer. Consequently, this has resulted in limited data from which to assess the structure of the turbulent motion and the effects of Mach number, Reynolds number, heat transfer or pressure gradient on the turbulence structure. In the absence of direct turbulence measurements, turbulence transport properties can be calculated from the experimental mean flow data using the time-averaged conservation equations for a zero pressure gradient, two-dimensional boundary layer.

To solve the time-averaged conservation equations, an assumption of local similarity is often made, i.e. profiles of U/U_e, p/p_e, ρ/ρ_e and H/H_e are functions of y/δ only; this assumption was first introduced by Meier and Rotta (1970). Of course, exact similarity can only occur if the shear stress at the wall is constant with x. The method presented herein is valid for a two-dimensional flat plate flow with the usual assumption of constant static pressure through the boundary layer. The final equation for the total shear, see section 2.5.3, is:

$$\frac{\tau}{\rho_e U_e^2} = \frac{C_f}{2} + \left[\frac{\delta}{\rho_e U_e^2}\frac{d}{dx}(\rho_e U_e^2) + \frac{d\delta}{dx}\right]\left[\int_o^{y/\delta}\frac{\rho U^2}{\rho_e U_e^2}\,d(y/\delta)\right] - \left[\frac{\delta}{\rho_e U_e^2}\frac{d}{dx}(\rho_e U_e) + \frac{d\delta}{dx}\right]\left[\frac{U}{U_e}\int_o^{y/\delta}\frac{\rho U}{\rho_e U_e}\,d(y/\delta)\right] + \frac{\delta}{\rho_e U_e^2}\frac{y}{\delta}\frac{dp}{dx}, \quad \text{(Eq. 5.20)}$$

where the total shear, τ, is: $\tau = \tau_l + \tau_t = \mu\partial U/\partial y - \overline{\rho' u'}$.

The equations presented above are identical to those derived by Bushnell and Morris (1971), subsequently presented by Horstman and Owen (1972) and Laderman (1978). Evaluation of Eq. 5.20 was limited to the HP condition profiles as the LP condition data appeared to suffer from low Reynolds number effects, and the profiles were not measured at sufficiently close intervals to ensure local similarity under these circumstances. The HP data evaluation was further limited to the profile at the middle station, i.e. x = 460mm, so that the x-derivatives of $\rho_e U_e$, $\rho_e U_e^2$ and p could be determined by a simple differencing scheme from the upstream and downstream stations at x = 360mm and x = 560mm. Also as found in section 5.13, there is a difficulty of selecting a representative boundary layer thickness in compressible flow, in which the thicknesses derived from pitot pressure and velocity profiles do not coincide, in general, at hypersonic Mach numbers. Thus, there is some difficulty in knowing which is the correct one to use as the similarity parameter in the evaluation of Eq. 5.20.

However, in order to make comparisons with the majority of the other data, the approach of Horstman and Owen (1972) was followed and δ_p was used as the similarity thickness parameter in Eq. 5-20. The gradient, dp/dx, was found by plotting δ_p as a function of x then fairing a curve through the points; five pitot pressure profiles were available for the evaluation, see section 5.6. The skin friction was again derived from the Preston tube surveys using the Hopkins and Keener calibration, section 5.5, which was found to give good agreement when used in conjunction with the van Driest transformation for comparison with the law of the wall.

Using the approach outlined above in conjunction with Eq. 5-20 the total shear stress distribution at x = 460mm for the HP condition boundary layer was calculated and is shown in fig. 5-33. The small negative shear stress at $y/\delta_p = 1.0$ could be due to either errors in determining the position of the boundary layer edge or in deriving the streamwise derivatives in Eq. 5-20. Similar small negative shear stresses have been also reported by Horstman and Owen (1972) and Laderman (1978). Sandborn (1974) has reviewed the available turbulence measurements in compressible boundary layers up to $M_e \simeq 7$ and derived a 'best estimate' shear stress distribution. The present data is also shown in fig. 5-33 compared to this 'best estimate' distribution and two of the most notable recent investigations using the similarity approach, namely Horstman and Owen (1972) and Laderman (1978). The present data shows good agreement with both the Sandborn distribution and the other data. With regard to the sensitivity of the total shear stress distribution to either Mach or Reynolds number, Sandborn (1974) found no consistent trend in his extensive review of the data; the limited data presented in fig. 5-33

supports this conclusion. Both Watson (1977) and Laderman (1978) have investigated the effects of wall cooling on the shear stress distribution, but no detectable sensitivity to wall temperature was found. Both Sandborn (1974) and Bradshaw (1975) have suggested that as the boundary conditions are fixed, i.e. $\tau/\tau_w = 1$ at $y/\delta = 0$ and $\tau/\tau_w = 0$ at $y/\delta = 1$, the shear stress distribution is a geometric property thus large discrepancies are unlikely using the similarity approach. In conclusion it appears that the shear stress distribution obtained with cold wall conditions at $M_e = 9.26$ appears to be in good agreement with previous compressible data obtained on both cooled and adiabatic walls.

If the total shear stress is assumed to be equal to the turbulent shear stress, i.e. $\tau \simeq \tau_t$, the mixing length and eddy viscosity distributions can be calculated from the following:

$$\tau_t = \rho \ell^2 \left|\frac{\partial U}{\partial y}\right| \frac{\partial U}{\partial y} = \rho \xi \frac{\partial U}{\partial y} \qquad \text{(Eq. 5.21)}$$

The assumption of $\tau_t \simeq \tau$ is valid as τ_l is less than 2% of τ at $y/\delta=0.1$. Following the approach of Laderman(1978), to obtain the mixing length Eq. 5.21 can be re-expressed as:

$$\frac{\ell}{\delta_p} = \left[\frac{(\tau_t/\rho_e U_e^2)}{\rho/\rho_e \{\partial(U/U_e)/\partial(y/\delta)\}^2}\right]^{\frac{1}{2}} \qquad \text{(Eq. 5.22)}$$

The values of $\partial(U/U_e)/\partial(y/\delta)$ were determined from a faired line through the normalised velocity distribution. The mixing length distribution calculated from Eq. 5.22 is shown in fig. 5-34; ℓ/δ reaches a maximum value of 0.08 at $y/\delta \simeq 0.5$. Maise and McDonald(1968) have calculated mixing

length distributions based on their correlation of adiabatic wall data up to $M_e = 5$, over a Reynolds number range of $10^3 < Re_\theta < 10^5$. Maise and McDonald found that the effects of Mach number and Reynolds number variations on the computed mixing length were small and within the experimental uncertainty of ℓ/δ. They concluded that the incompressible mixing length distribution was a satisfactory model thus confirming Morkovin's hypothesis. The present M_e=9.26 cold wall data is shown in fig. 5.34, also shown is the Bushnell et al (1970) correlation which predicts a constant value of $\ell/\delta \simeq 0.07$ for $y/\delta > 0.3$. The present data falls below the Maise and McDonald curve although showing fair agreement for $y/\delta > 0.2$; the Bushnell correlation is in closer agreement with the present data at $y/\delta < 0.2$ than the Maise and McDonald correlation.

In fig. 5-35 the present data is compared with mixing length distributions obtained from studies using the similarity method under conditions of significant heat transfer. The present data, with the exception of the point at y/δ=0.2, shows good agreement with the main body of data especially the cold wall data of Laderman (1978) at $y/\delta > 0.2$. The Laderman data is of particular interest in that the experiment was performed at three heat transfer conditions, i.e. $T_w/T_{oe} \simeq$ 0.54, 0.71 and 0.94, for almost constant Mach and Reynolds number, M_e=3 and $Re_\theta \simeq 3500$. This data appears to show a small increase of ℓ/δ with decreasing T_w/T_{oe}, i.e. increasing heat transfer. Watson (1977) calculated mixing length distributions for increasing Reynolds number at M_e=11 with nominally constant heat transfer conditions such that T_w/T_{oe} varied from 0.46 to 0.51. He found significant increases in ℓ/δ in the outer region of the boundary layer as Re_θ decreased from 18000 to 11000. These profiles were typical of those suffering from low Reynolds number effects, see section 5.13; under low Reynolds number conditions such increases in mixing length are to be expected in this region, see for example Bushnell, Cary

and Holley (1975). Overall the limited data shown in fig. 5-35 shows no discernable trend of ℓ/δ with Mach number, but it is apparent that the mixing length distribution is sensitive to other parameters such as heat transfer, Reynolds number or pressure gradient, hence it is difficult to isolate the effects of any one parameter.

The eddy viscosity can also be obtained from Eq. 5.21 which can be re-expressed to give:

$$\frac{\xi}{U_e \delta_i^*} = \frac{(\tau_t/\rho_e U_e^2)}{(\rho/\rho_e)\{\partial(U/U_e)/\partial(y/\delta)\}\ (\delta_i^*/\delta)} \qquad \text{(Eq. 5.23)}$$

where,

$$\delta_i^* = \int_0^\delta (1 - U/U_e)dy \qquad \text{(Eq. 5.24)}$$

The eddy viscosity ξ is normalised by $U_e \delta_i^*$ which has been shown by Maise and McDonald (1968) to collapse eddy viscosity distributions obtained at different Mach numbers and Reynolds numbers. Maise and McDonald also derived an eddy viscosity correlation from the same data, M_e=5 and $Re_\theta = 10^4$, used to obtain the mixing length distribution discussed earlier. The present data is shown compared to the correlation in fig. 5-36, and in general the data falls below the Maise and McDonald curve although the position of the maximum value, ξ =0.02 at y/δ=0.35, is in fair agreement with the correlation maximum. The Maise and McDonald correlation has been found to overpredict the derived distributions of $\xi/U_e\delta_i^*$; see for example Horstman and Owen (1972) and Sandborn (1974). The present data have also been compared with some of the available data. As shown in fig. 5-37 the agreement was found to be good especially with the Laderman (1978) data, which again showed a slight, but definite, trend of $\xi/U_e\delta_i^*$ increasing with T_w/T_{oe}. The

agreement with the Watson(1977) data is good although the Watson data does exhibit higher peak values of eddy viscosity. The data of Horstman and Owen(1972) and the data of Owen et al(1975) showed eddy viscosity distributions significantly lower than the other data or the Maise and McDonald correlation. These two investigations were performed on an axisymmetric model at $M_e = 7$ and it is possible that the difference is due to transverse curvature effects.

The solution of the boundary layer equations in compressible flow requires accurate models of the turbulent transport properties and in the absence of experimental turbulence measurements at hypersonic Mach numbers, the data obtained from the mean flow profiles using the time-averaged conservation equations are most valuable to supplement the direct measurements. Most compressible flow calculation methods make the assumption that the mixing length or eddy viscosity distributions are independant of Mach number, see for example Bradshaw(1976). If Morkovin's hypothesis is accepted, the turbulence structure for a zero pressure gradient boundary layer is almost the same as that in an incompressible flow at least for $M_e < 5$. Sandborn(1974) concurred with this conclusion in his extensive review of turbulence data in compressible flow. At $M_e > 5$ the Mach number independance of the turbulent transport properties, such as eddy viscosity or mixing length, has yet to be established. The present $M_e = 9.26$ data agrees well with the Maise and McDonald(1968) correlations for mixing length and eddy viscosity which were based on data up to $M_e = 5$. However, it is difficult to isolate the effects of Mach number from the effects of Reynolds number, heat transfer or pressure gradient on these quantities without further systematic experiments.

5.16 Electron beam density measurements

A major objective of the present study has been to test the feasibility of using the electron beam fluorescence technique at high number density in turbulent flow, $n > 10^{18} cm^{-1}$. This aspect of the feasibility study proved successful and is discussed in detail in section 4.0. As a result of the feasibility study some preliminary time-averaged and time-resolved density data were obtained and are presented in this section. The reported studies containing fluctuating data in hypersonic turbulent boundary layers are scarce and made almost exclusively made with the hot wire aneomometer technique, see for example the well known studies of Laderman and Demetriades(1974) and Owen et al(1975). The present data, although preliminary, are nevertheless valuable because of the paucity of fluctuating data which are required to develop the turbulence models for the numerical prediction methods. The present data were obtained with a non-intrusive technique with an inherent high frequency response and do not suffer from probe interference effects. Techniques such as the electron beam fluorescence technique and the laser doppler aneomometer are required to supplement the hot wire aneomometer at high Mach number in compressible flow.

Due to time and equipment constraints, see section 4.0, the time-averaged and time-resolved density measurements were limited to the x=560mm station in the tripped boundary layer at the LP tunnel running condition.Conventional wall and profile measurements were also made at this station and are presented earlier in this chapter. Freesteam properties at the x=560mm station were $M_e=8.93$, $T_e=58.9^{o}K$ and $p_e=760\ Nm^{-2}$; the Reynolds number based on distance from the leading edge was $Re_x=8.40x10^{6}$ and the momentum thickness Reynolds number, $Re_\theta=5600$. Wall temperature remained constant at $T_w=293^{o}K$ for the test series.

5.16.1 Time-averaged density profile

The variation of time-averaged fluorescent light intensity, suitably normalised by the beam current at the wall, is shown in fig. 5-38 for a traverse through the LP boundary layer at x = 560mm. These data were corrected for run-to-run variations using the signal from the monitor detector focused just outside the boundary layer in the freestream; the edge of the layer was determined from the pitot pressure survey. The fluorescent light intensity profile appears to be reasonably smooth with an approximately linear variation through the layer. Using the calibration equation for the traversing photo-multiplier detector, Eq. 4.10, and incorporating the term for beam current degradation , Eq. 4.11, the density was inferred at each point in the profile by iteration. The measured values of k and the fitted values of A_2, B_2 and C_2 were used in Eq. 4.5, see section 4.5.2. The time-averaged density, ρ_{eb}, is shown in fig. 5-39 normalised by the freestream density, ρ_e.

5.16.2 Comparison with time-averaged density from conventional probes

For comparison with the electron beam data the time-averaged density has been calculated from the velocity profile and Mach number profile, see section 5.9 and 5.7 respectively, using the isentropic relationships with the usual assumption of constant static pressure through the layer . For a perfect gas,

$$\frac{U}{U_e} = \frac{M}{M_e}\left[\frac{T}{T_e}\right]^{-\frac{1}{2}} = \frac{M}{M_e}\left[\frac{\rho_e}{\rho}\right]^{\frac{1}{2}} \qquad \text{(Eq. 5.25)}$$

The comparison is shown in fig. 5-40 and the agreement appears to be good except in the region close to the wall. This good agreement with the results obtained from conventional instrumentation, although limited to one boundary layer station, validates the use of the electron beam fluorescence technique in the present turbulent flow. The density ratio, ρ_w/ρ_e , is also shown in fig. 5-40, as calculated from the measured wall and freestream static

temperature. Both the electron beam and the conventional probe measurement techniques are liable to errors close to the wall. In the case of the electron beam extraneous reflections from the semi-bright model wall could cause anomolous results. In future the extent of wall reflections could be estimated by measuring the fluorescent light intensity profile without flow thus obtaining an instrument profile. The model surface could also be blackened to minimize the possibility of such reflections. In the case of the conventional probes, the pitot and the total temperature probes may well give rise to wall interference effects close to the model surface. The presence of the probe also gives rise to streamline displacement effects, but the magnitude of displacement corrections are subject to uncertainty at hypersonic Mach numbers hence no correction has been made to the profiles obtained in this investigation. The static temperature profiles obtained from both techniques are compared in fig. 5-41; the data plotted in this way emphasise the differences close to the wall.

5.16.3 Fluctuating density

In comparison to the extensive data available at low speeds, there are few studies of compressible turbulent boundary layers containing turbulence measurements. Direct turbulence measurements are especially scarce at hypersonic Mach numbers on cold walls, and of the limited data available much has been obtained in nozzle wall boundary layers possibly suffering from significant upstream history effects. Thus there remains a need for fluctuating data from flows of known origin,such as a flat plate, at hypersonic Mach numbers in order to develop the turbulence models essential to the calculation methods. At high supersonic Mach numbers the fluctuations of velocity tend to decrease in importance whereas the density and temperature fluctuations grow in significance.

The flowfield is further complicated by the onset of pressure fluctuations and, of course, their interactions with the other fluctuation modes. With pressure fluctuations present the analysis of the HWA output signal, the most common measurement technique, becomes intractable without simplifying assumptions. It is common to assume zero or negligible pressure fluctuations, for example Kistler(1959) or Owen et al(1975), although Laderman and Demetriades(1974) made more complex assumptions it was conceded that this approach made only a small difference to the velocity fluctuation levels.

The electron beam technique does not require the zero pressure fluctuation level assumption but does require calibration over the density and temperature range to be investigated. In the present study due to time constraints the temperature dependence term in the fluorescent light - density calibration was neglected although previous studies,see section 4.3.2 , suggest that this would be a minor correction. This was confirmed by the good agreement of the electron beam derived density profile with that obtained from conventional instrumentation, fig. 5-40 . In addition to the density fluctuations the fluorescent light signal also contained contributions from the local static temperature fluctuations and from variations in the beam current arising from the attentuation of the electron beam as it passed through the test gas. The sensitivity to mean temperature was minor hence the sensitivity to temperature fluctuations was also liable to be small. Beam current variations were due to electron scattering by collisions with ambient gas molecules; this was an integrated effect depending on the instantaneous values of density along the beam path. The scattering resulted in the electrons being deflected beyond the region from which observations were made, a nett loss, or the electrons suffered small angle deflections thus remained within the limits of the optical observation region. Such secondary electrons that remained within

the limits of the beam might as a consequence of their reduced velocity have had either an enhanced cross-section, which resulted in an increase of the fluorescent light intensity, or were too slow to cause a radiative transition, i.e. emission of a photon.

5.16.3.1 Fluctuating Density Profile

At each point in the electron beam traverse through the boundary layer at x = 560mm, the root mean square (rms) value of the fluctuating density signal, $\langle\rho'\rangle$, was calculated from the digital data file using the relationship:

$$\frac{\langle\rho'\rangle}{\rho} = \sqrt{\frac{1}{n}\Sigma_1^n (\rho_n - \rho)^2}/\rho \quad , \qquad \text{(Eq. 5.26)}$$

where n is the number of data points.

The rms density is normalised by the local mean density in Eq. 5.26, and the usual number of data points, n , in a typical data file used for this calculation was 4096. The variation of the rms density, i.e. $\langle\rho'\rangle/\rho$, for the traverse through the layer at the x = 560mm station is shown in fig. 5-42. The distribution shows maximum of approximately $\langle\rho'\rangle/\rho = 0.09$ close to the wall at $y/\delta \simeq 0.1$ to 0.15, falling off to a level of $\langle\rho'\rangle/\rho = 0.02$ in the freestream.

5.16.3.2 Comparison with the available fluctuating density data

The fluctuating density distributions from three hot wire aneomometer(HWA) investigations Kistler(1959), Laderman and Demetriades(1974) and Owen et al(1975) have been compared to the present electron beam data in fig. 5-43. This figure shows that the maximum fluctuation level varied from $\langle\rho'\rangle/\rho \simeq 0.09$ to 0.12 falling off to 0.03 in the freestream with the present data peaking closer to the wall than the other distributions. The Kistler (1959) data were obtained in an adiabatic wall boundary layer whereas the other studies were performed on a cold wall. Kistler found that both the mass-flux and the total temperature fluctuation levels (the basic outputs of a HWA operated at high and low overheat ratios) increased with Mach number over the range $1.72 < M_e < 4.67$, whereas both Laderman and Demetriades and Owen et al found the mass-flux fluctuations appeared independent of Mach number above $M_e \simeq 5$ and the total temperature fluctuation level decreased with increasing Mach number. This suggests that the effect of wall cooling was to reduce the level of the total temperature fluctuations. For the Kistler data the density fluctuations showed an increase with increasing Mach number but the cold wall data of Laderman and Demetriades, Owen et al and the present study appear to be independent of Mach number with a peak density fluctuation level of $\langle\rho'\rangle/\rho \simeq 0.10$.

The longitudinal velocity fluctuation levels obtained from the three HWA investigations show the expected trend of a decreasing level with increasing Mach number. Owen et al(1975) plotted the longitudinal velocity fluctuations against the density stretching co-ordinate suggested by Morkovin(1961), and the high Mach number data did not collapse onto the well known Klebanoff incompressible curve whereas the Kistler(1959) data, $M_e > 5$, agreed well with the incompressible curve.

The 'strong Reynolds analogy' , i.e. $T'/T = (\gamma-1)M^2\, u'/U$, has been proved valid on adiabatic walls at M_e=4.7 by Kistler(1959) and at M_e=7 by Laderman (1974). On cold walls at hypersonic Mach numbers the strong Reynolds analogy breaks down hence density and temperature fluctuations are suppressed and the magnitude of these fluctuations is liable to be dependent on wall temperature. Both the density and the longitudinal velocity fluctuations on cooled walls at hypersonic Mach numbers, $M_e > 5$ say, appear not to follow the trend of the lower Mach number data.

A comparison has also been made with the fluctuating density data obtained from the limited electron beam fluorescence studies in turbulent boundary layer flow, fig. 5-44. The Wallace(1968) data were obtained in a shock tunnel at M_e =8.5 and was one of the earliest applications of the fluorescence technique to turbulent flow. This data, which spanned a Reynolds number range of $3750 < Re_\theta < 9600$, showed a large variation in peak fluctuation intensity but without any systematic dependance on Re_θ . The present data agreed well with the maximum and freestream levels of the Wallace data but did not show the minimum at $y/\delta_p \simeq 0.2$ to 0.5 found by Wallace in both the fluctuating density and fluctuating pitot pressure profiles. It is possible that the Wallace data, which was obtained in a nozzle wall boundary layer, was suffering from upstream history effects thus was not typical of a zero pressure gradient flow. The McRonald(1975) data was obtained at identical conditions and in the same facility as the well known Laderman and Demetriades(1972) HWA investigation, i.e. fig. 5-43. The peak fluctuation level of the McRonald distribution, curve C in fig. 5-44, was approximately half that of the corresponding Laderman and Demetriades data using the HWA technique. McRonald suggested that this discrepancy was probably due to the assumptions required in the analysis of the HWA signal to allow for pressure fluctuations. It is

apparent that the HWA data of Laderman and Demetriades agreed well with the majority of the other published data shown in fig. 5-43. McRonald was unable to make electron beam density measurements beyond $y/\delta_p = 0.4$ at the two higher density conditions, i.e. curves B and C in fig. 5-44, due to calibration and attenuation difficulties hence the data must be cosidered doubtful until these problems are resolved.

From these results it is apparent that the turbulence structure at $M_e > 5$, say, is different from the structure at lower Mach supersonic Mach numbers, which has been shown to be similar to that found at low speeds, see for example Bradshaw (1976). Pressure fluctuations also begin to increase in significance at hypersonic Mach numbers and may well interact with the other fluctuation modes to influence the turbulence structure. At present, there is not a satisfactory method of measuring pressure fluctuations except perhaps at the wall with a microphone. The intensity of the density fluctuations obtained in the present study agree well with the limited data available at $M_e > 5$, under conditions of moderate to severe heat transfer.

5.16.3.3 Power spectral density

At several locations in the LP boundary layer, estimates have been made of the power spectral density function, which describes the distribution of power over the constituent frequencies of the density fluctuations. In turbulent shear flow, the power spectra of the various fluctuation modes have a characteristically 'broad spectrum' usually smooth without discrete frequency peaks except perhaps in the transition region between laminar and turbulent flow, see for example Hinze (1973). A spectral analysis program, Powerspec (Davis (1974)), has been used to calculate the power spectrum of a single channel of data using a discrete fast Fourier transformation technique. At the electron beam station, x = 560mm, power spectra have been measured at six locations in the layer, i.e. $y/\delta_p = 0.1$,

0.2, 0.3, 0.6, 0.8 and 1.0 as shown in fig. 5-45 a to f respectively. The power spectral density function, P(f), is defined as:

$$P(f) = \overline{\rho'(f)}^2 \; / \; \overline{\rho'}^2 \qquad \text{(Eq. 5.27)}$$

The spectra are valid up to the Keithley amplifier 'cut-off' frequency at 100kHz, above which the noise spectrum of the amplifier becomes predominant. In general, it is difficult to assess the accuracy of a spectral estimate but Davis (1974) recommended at least 40,000 samples (40 x 1024 blocks) to ensure good statistical accuracy with the Powerspec program. He estimated that for turbulence spectra, which are expected to be smooth, the standard deviation was about 6% with frequency averaging. In the present feasibility study, the number of samples was limited by the local buffer memory size to a maximum of 16384 which resulted in a reduction of accuracy.

Nevertheless, the present data, although preliminary, are of value due to the scarcity of fluctuating data, especially spectra, in turbulent boundary layers at hypersonic Mach numbers. The power spectra, fig. 5.45 a to f, appear typical of turbulent flow with the characteristic broad spectrum, while the lack of smoothness is probably a result of the limited sample size. The overall level of fluctuation energy increases with distance from the wall reaching a maximum at $y/\delta_p = 0.6$, levelling off at $y/\delta_p = 0.8$ and decreasing significantly at $y/\delta_p = 1.0$. In this case the relevant boundary layer thickness may well be δ_u in which case the maximum fluctuation energy occurs at $y/\delta_u = 0.8$ to 1.0. This agrees with the longitudinal velocity data of Horstman and Owen (1972) who found that the maximum fluctuation energy occurred near the edge of the boundary layer at $y/\delta_p \simeq 0.75$ ($y/\delta_u \simeq 0.86$). Also plotted on fig. 5-45 a to f is the well known - 5/3 power law which has been shown to be valid in the inertial subrange region of the spectrum, see for example Bradshaw (1971). In this region the power spectral density is proportional to

$f^{-5/3}$ and the transfer of energy from the 'energy-containing eddies' is dominated by interial forces thereby almost independent of viscosity. The lack of smoothness of the present data makes a comparison with the line of - 5/3 slope difficult but it appears that there is a larger region of agreement towards the edge of the layer. This tendency towards the inertial subrange as the distance from the wall increases is due to the consequential rise in the turbulence Reynolds number with y. Most of the limited number of studies containing turbulence data at hypersonic Mach numbers have used the HWA aneomometer technique, in which case it is usual to measure the power spectrum of either the longtudinal velocity or mass-flux fluctuations. It is often difficult to compare spectra due to the many different ways of scaling and plotting such data. However, Sandborn (1974) has compared a power spectrum from incompressible flow with spectra from two of the best known investigations in compressible flow, i.e. the longitudinal velocity spectra of Laderman and Demetriades (1974) and the mass-flux fluctuations of Owen and Horstman (unpublished data, private communication to Sandborn (1974)). Two examples of the present spectra are shown in fig. 5-46 compared to the Sandborn data, plotted in terms of the wavenumber, k, and the power spectral density function f(k):

$$F(k) = (U/2\pi)\, P(f) \qquad \text{(Eq. 5.28)}$$

where, $$k = 2\pi f/U$$

and U is the local mean velocity (for convenience the units employed by Sandborn are retained in this figure). The present spectra appear to follow the trend of the data when plotted on the wavenumber basis. The rapid fall-off of the power spectrum at high wavenumber is probably a result of the frequency limitation of the amplifier.

5.16.3.4 Correlation Measurements

In addition to the power spectral density measurements, correlations have been made between the fluctuating density signal from two points along the electron beam. This was achieved by means of a fixed detector and one focused at several locations through the layer. Lateral space-time correlations between two points along the beam would indicate the degree of turbulent mixing in the lateral direction. A second spectral analysis program, Cophase (Davis (1974)), was used to compute the cross-spectral power density function for two simultaneous input channels, using a discrete fast Fourier transformation technique. The main outputs of the program are the Coherence, which describes the fraction of the total energy at frequency f that is contained in the correlated parts of the two input fluctuating density signals, and the Phase Angle between the correlated parts of the two signals.

To validate the technique, both detectors were focused at the reference point, $y/\delta_p = 0.1$, where the coherence should be unity and the phase angle zero degrees, i.e. perfect correlation, although it was not expected that perfect correlation would be acheived due to the limited sample size and optical differences in the two detector systems. In practice, as shown in fig. 5-47 a and b, the correlation showed serious departures from the expected values, for example the correlation was always less than 0.5 except at the low frequencies, f < 5kHz, where the tunnel run time becomes significant hence the correlation is high. The phase angle also showed large excursions from zero degrees at the higher frequencies. From these results, it was apparent that the optical alignment of the two detectors was not as precise as hoped, i.e. the detectors were not focused on the same optical volume of the beam. Unfortunately, the spectral analysis was performed some time after the test series and it was not possible to repeat

the tests with re-aligned detectors because of the inevitable time constraints. This misalignment throws considerable uncertainty on the correlations and for that reason, and because the main aim of the study was to test the feasibility of using the electron beam technique at high density, it is not proposed to discuss the present data in depth. However, for completeness an example of the correlation between $y/\delta_p = 0.1$ and $y/\delta_p = 0.6$ is shown in fig. 5-48 a and b. This shows a significant reduction in the coherence and a more erratic behaviour of the phase angle with the increased lateral separation.

In conclusion, the electron beam fluorescence technique has been shown to be viable in a turbulent compressible flow at least up to the number density level of the LP condition boundary layer. The technique has the advantage of being non-intrusive with inherent high frequency response, and is capable of further refinement particularly in the area of spatial resolution by means of smaller diameter electron beams. The optical alignment problem could be due to either mechanical vibration occuring during the tunnel firing or due to the difficulty in aligning and focusing two separate detectors on the same small volume in space. With the experience of designing rigid model mountings obtained previously in the facility, and the excellent retention of the delicate electron beam alignment with the series of orifices in the model, it is thought that the misalignment is not a result of vibration. Even with the considerable care exercised, it is suspected that the detectors were not precisely focused on the same optical volume. To overcome this problem, it is recommended that only one lens is used to image the beam with a short focus relay lens arrangement to direct the light from different sections of the beam into the photodetectors.

6.0 Concluding Remarks

A detailed investigation of the mean and fluctuating properties of a zero pressure gradient hypersonic turbulent boundary layer has been made in the Imperial College No. 2 Gun Tunnel at a freestream Mach number of 9. Accurate mean profile data are needed over a wide range of conditions, such as M_e, Re_θ, T_w/T_{oe} and dp/dx, to form a reliable database for design purposes and for the validation of the numerical prediction methods for turbulent compressible boundary layers.

The objective of the first phase was to obtain sets of reliable mean profiles and wall data at several streamwise locations for a turbulent flat plate boundary layer, thereby extending the range of the existing data to include a combination of Mach number, Reynolds number and wall temperature ratio not covered previously, namely $8.96<M_e<9.26$, $2800<Re_\theta<12000$ and $T_w/T_{oe} = 0.28$. The boundary layer was studied at two wind tunnel operating points. At the low pressure (LP) operating point, transition had to be forced and the boundary layer was found to be typical of one exhibiting the so called 'low Reynolds number effects'. At the high pressure (HP) operating point, transition occured naturally and the boundary layer approached a fully developed equilibrium flow.

The objective of the second phase was to develop the electron beam fluorescence technique for use in turbulent flow at relatively high molecular number density of the order of $10^{18} cm^{-3}$, and to use it to make preliminary measurements of mean and fluctuating density in the $M_e=9$ boundary layer flow. The development of the technique is valuable as it provides an independent check on the results obtained using techniques such as the hot

wire or laser doppler aneomometers, assessing also the calibration and data reduction methods used with these techniques. Reliable fluctuating data are especially important for an improved understanding of the structure of the turbulent compressible boundary layer, particularly at high Mach number.

In the first phase of the study, extensive mean measurements of heat transfer, surface pressure, surface impact pressure and surveys of pitot pressure and total temperature have been made in the flat plate boundary layer flow at two freestream unit Reynolds numbers: at the LP tunnel condition with forced transition and at the HP condition with natural transition. In summary, the main conclusions from the first phase were as follows:-

1. From the surface pressure measurements along the model centreline, the longtitudinal pressure gradient was found to be slightly favourable for both the LP and HP condition boundary layers. In the HP natural transition case, the position of transition (taken to be the position of the peak heat transfer rate) was found to be around 0.15m from the leading edge, giving $Re_{x,\ transition}$ as 8.3×10^6.

2. The precise measurement of skin friction in a high Mach number turbulent boundary layer with appreciable heat transfer remains a severe experimental problem. In the present study, the use of a Preston tube, a convenient and commonly used indirect method of determining C_f, relies heavily on the arbitrary choice from a wide range of Preston tube calibrations which have been shown by the

present study to have a large inherent variations amongst themselves. Development of a reliable calibration for compressible flow requires accurate data from a direct method, such as the floating element balance, but there remains considerable uncertainty attached to the reliability and repeatibility of the available balance data especially on severely cooled walls as in the present study. The Hopkins and Keener (1969) calibration has been used in the present investigation. This calibration has been found to give consistant agreement with floating element balance measurements on a cold wall at high Mach number, see for example Keener and Hopkins (1969).

3. Velocity profiles have been derived from the measured pitot pressure and total temperature profiles for both the LP and HP condition boundary layers. Fair agreement has been found for the present velocity data with the well known linear Crocco total temperature velocity relationship. Much turbulent flat plate data follows the linear relation but better agreement has been obtained in the present case with the non-unity Prandtl number form of the Crocco relationship, which has been shown to hold for a wide range of compressible turbulent boundary layer data on isothermal walls with moderate to severe wall cooling by Fernholz and Finley (1969). It is concluded from the present and other cold wall data that the non-unity Prandtl number form of the Crocco relationship can be used as a satisfactory approximation for the mean

temperature profile in calculation and prediction methods for hypersonic flows over isothermal walls with zero pressure gradient.

4. After compressibility transformation by the method of Van Driest (1951), the present velocity profiles for both boundary layers conditions showed good agreement with the well known incompressible logarithmic law of the wall, thereby confirming the adequacy of the van Driest transformation method for zero pressure gradient flows on cooled walls (with a defined flow origin) as previously reported by Owen and Horstman (1972), Owen et al (1975) and by Fernholz and Finley (1979) in their recent critical evaluation of the data. There is still uncertainty attached to the best choice of the constants associated with the law of the wall. The values of $k = 0.40$ and $C = 5.1$, recommended by Fenter and Stalmach (1957) and later by Fernholz and Finley (1979), have been used in this study.

5. Fernholz (1976) has extended the van Driest transformation method to the outer boundary layer with a semi-empirical velocity defect relationship, using an integral thickness to avoid the difficulty of evaluating a representative boundary layer thickness in compressible flow. The LP condition velocity profiles, in which transition was forced, showed the limited agreement with the Fernholz outer law typical of a flow

suffering from low Reynolds number effects. In the early stages of tuburlent flow, turbulent length scales are functions of the local Reynolds number, both for incompressible and compressible flow. It can be difficult to distinguish between a transitional boundary layer and a flow suffering from low Reynolds number effects. The mechanism of transition in high Mach number compressible flow is not fully understood. Both theoretical and experimental studies of transition under these conditions are scarce and the experimental studies are also confused by the influence on the flow of high intensity wind tunnel noise emanating from the nozzle wall boundary layer. In hypersonic laminar boundary layers, there appears to be a critical layer of high fluctuation-energy concentration situated in the outer layer which moves closer to the boundary layer edge with increasing Mach number. Disturbances or turbulent bursts in the laminar boundary layer originate close to this critical layer and spread toward the wall at a shallow angle, taking longer to reach the inner region of the boundary layer than at low speeds, thereby resulting in a longer region of transitional flow at high Mach number. Forcing of transition, as in the present study, may not result in the same critical fluctuation level as would occur in the natural transition case until some distance from the transition device or trip.

If the Fernholz and Finley (1979) criterion is used to distinguish between transitional and low Reynolds

number profiles, i.e. the profiles agree with the law of the wall and show limited agreement with the outer law, the present LP profiles do not show the characteristics of a transitional flow but appear to suffer from low Reynolds number effects. The extent of the region of agreement with the outer law grows with increasing Re_θ as the boundary layer tends toward an equilibrium flow. In contrast, the HP condition profiles showed the excellent agreement with the Fernholz relationship typical of a boundary layer at or near equilibrium and free from upstream history influences or effects.

6. The strength of the wake component can be used to characterize the development of the boundary layer. In incompressible flow, the strength of the wake components shows a well defined dependence on Reynolds number varying from zero at $Re_\theta \simeq 500$ to a limiting value at $Re_\theta \simeq 5000$ of about 2.8, typical of a fully developed layer. In compressible flow, the trend is similar although the data shows a better collapse onto the incompressible curve if plotted against the momentum thickness Reynolds number, Re_{δ_2}, in which the viscosity is evaluated at the wall temperature. Estimates of the strength of the wake component for the LP condition profiles show the low values typical of a flow in the non-equilibrium flow region in which low Reynolds number effects are expected. For the HP condition profiles, the wake component strength did not quite reach the values expected of a fully developed equilibrium boundary layer. The present wake component

data, at both conditions, followed the trend of the available data from both isothermal and adiabatic wall studies when plotted against Re_{δ_2}, although the considerable scatter in the available data prevents the identification of any trend due to Reynolds number, heat transfer rate or other effects.

7. Using the time-average conservation equations with an assumption of local profile similarity, the mean flow profile data at the HP condition were analysed to extract the turbulent transport terms, such as the shear stress, mixing length and eddy viscosity distributions. The calculated shear stress distribution showed good agreement with the 'best estimate' distribution compiled by Sandborn (1974) and the limited available hypersonic cold wall data. The geometric nature of the shear stress profile, forced by the boundary conditions, makes unlikely the identification of any consistent trend with either Mach number or Reynolds number. Such effects will be small and liable to be obscured by the uncertainties of the current measurement techniques. The mixing length and eddy viscosity distribution agreed favourably with the Maise and McDonald (1965) correlation which was based on data up to $M_e = 5$. The present data agreed well with the cold wall distributions of Laderman (1978) and Watson (1977), but both the mixing length and eddy viscosity distributions were significantly higher than those of Owen and Horstman (1972) and Owen et al (1975)

both of which may have been suffering from transverse curvature effects.

The stated objective of the second phase of the study was to develop the electron beam system in order to test the feasibility of using the technique in turbulent flow at high Mach number and high molecular number density, $n \simeq 10^{18} cm^{-3}$. This aspect of the study proved successful for the LP condition boundary layer flow, although equipment limitations prevented testing at the HP condition. It is concluded that the non-intrusive elctron beam fluorescence technique, with its inherent high frequency response and good spatial resolution, is a viable method for high Mach number turbulent flows. Further studies are recommended involving the use of the electron beam fluorescence technique in turbulent flow. There is considerable scope for increasing the spatial resolution and frequency response of the technique by the use of higher accelerating voltages in the electron gun, around 50 kV, in conjunction with smaller beam diameters of around $\frac{1}{4}$mm to $\frac{1}{2}$ mm. Studies are also required to determine the maximum level of number density at which the technique is still viable in turbulent flow. Detailed conclusions and recommendations regarding the equipment and use of the technique in turbulent flow are presented in section 4.9. In summary, the main conclusions drawn from the density measurements obtained in the second phase of the study were as follows:

1. The boundary layer survey of mean density showed very good agreement with the density profile inferred from the conventional Mach number and total temperature surveys, except close to the wall where both techniques may have deficiences.

2. The profile of the rms density fluctuations reached a maximum of about $\langle\rho'\rangle/\rho \simeq 0.90$ at $y/\delta_p \simeq 0.15$ and was similar to profiles obtained from other studies using both the electron beam and hot wire aneomometer techniques in hypersonic cold wall boundary layers. At lower Mach numbers, $M_e \lesssim 5$, the density fluctuations have been shown to increase with increasing Mach number, for example the adiabatic wall data of Kistler (1959). The density fluctuations in the boundary layer on cooled walls at hypersonic Mach numbers, $M_e \gtrsim 5$ say, do not follow this trend with a maximum value of $\langle\rho'\rangle/\rho \simeq 0.10$. With wall cooling, Morkovin's 'strong Rynolds analogy', i.e. the assumption of negligible total temperature fluctuations, begins to break down resulting in a supression of the density and temperature fluctuations. The magnitude of the fluctuations is liable to be dependent on wall temperature. At hypersonic Mach numbers with wall cooling, it is possible that the validity of Morkovin's hypothesis, i.e. $\langle\rho'\rangle/\rho$ is small, may extend beyond the present limit of $M_e \simeq 5$ but further experimental evidence is required to substantiate this. With the onset of significant pressure fluctuations, possibly at Mach numbers of around 8, the effects of all the fluctuation modes, i.e. temperature, density, pressure and velocity, and their mutual interactions on the turbulence structure may have to be taken into account.

3. The power spectra of the fluctuating density signal appear typical of turbulent flow and follow the trend of the

incompressible spectra and the limited spectra available from high Mach number turbulent flows, when plotted on a wavenumber basis.

The mean and fluctuating measurements presented herein provide a thorough documentation of a hypersonic turbulent flat plate boundary layer under conditions of severe heat transfer at the wall. The utility of the electron beam fluorescence technique has been demonstrated in high Mach number turbulent flow at high molecular number density conditions. However, the use of the Gun Tunnel for this study with its short running time and the effort that had to be put into the development of the electron beam equipment imposed a serious limitation on the quantity of fluctuating density data that could be obtained in the time available and further work is needed to complete the study.

APPENDIX A

A1:0 Digital Data Acquisition System

The Gun Tunnel has a general requirement to gather data within the very short steady run time, typically 5 msec., and a specific need to make time-resolved measurements, with an upper frequency limit of around 1MHz, for the electron beam fluctuating density study. To these ends, a versatile digital data acquisition system was commissioned which enabled direct replacement of the existing analogue equipment for the time-averaged measurements, and also provided the opportunity of making very fast time-resolved measurements with an upper conversion rate of 4×10^6 samples per sec. This acquisition system was incorporated into the Hypersonics Laboratory Data System which was designed to handle all the data acquisition, storage and routine processing from the two hypersonic wind tunnels at Imperial College. The requirements of each wind tunnel are inherently different but as they share major compressor and vacuum plant, thus making it impossible for the tunnels to run simultaneously, it was possible to envisage a common computer control system combining the data storage and processing needs of both. This was the approach taken within the Hypersonics group to link both the Gun and Nitrogen Tunnels to a time-shared minicomputer system.

This approach has entailed the development of an extensive software package, written by the author in conjunction with Dr. J. Davis, to serve the needs of both facilities. This software package combined a common control program with application tasks specific to each tunnel. Full details of the Hypersonics Data System are available in Bartlett, Davis and Harvey (1979) and Davis (1978). A description of the elements of the Hypersonics Data System specific to the Gun Tunnel is presented herein.

A2.0 Minicomputer System

A time-shared minicomputer system was available within the Aeronautics Department. The system had three main functions:

a) Remote Job Entry (RJE) service to the Imperial College mainframe computers.

b) Local copying, graphics and disk management functions.

c) Background assembly language task processing.

The major function of the system was to provide a RJE service and this function had the highest priority of system resources. The minicomputer operated under a time-sharing operating system, MOS, which provided the facilities to perform the functions listed above. At present the Hypersonics group are the sole users of the background assembly task processing function which had been implemented to provide an on-line data acquisition and processing service. Minicomputer system control was by means of a console VDU from which all the functions had to be initiated including background task processing, although after initialisation the background users, e.g. Hypersonics group, operated entirely remotely. All system input-output devices and local storage devices, e.g. disk or magnetic tape, were available to all users i.e. RJE, local copying or background. MOS did not support a high level language compiler such as FORTRAN IV hence all background tasks had to be written in the "Basic Data General Assembler" {Data General (1976)}. As the minicomputer and main peripherals were sited in an air-conditioned room some distance from the Hypersonics Laboratory, communication was by means of twisted pair lines driven by asychronous line units at a maximum rate of 9600 baud. System configuration is shown in fig. A1 .

A 2.1. Minicomputer

The minicomputer system was based on a 32k word Data General Nova which was the maximum possible memory size for a 16 bit machine without a hardware memory management unit. Local mass data and program storage devices were disk and magnetic tape; a disk controller and two drives were interfaced to the Nova, each drive capable of accepting a removable disk cartridge with a capacity of 1.25×10^6 16 bit words. Four magnetic tape drives (two seven track and two nine track) were interfaced to the system although only two drives could be used simultaneously. The main input-output devices were a card-reader and a line-printer respectively. Although these devices were almost exclusively used for the RJE service they were available to local and background users. Paper tape reader and punch were available with the option of various tape formats; the punch was not a MOS supported device and was run under control of the Hypersonics control program. Incremental graph plotters were supported by the system to allow inspection or hardcopy of local plot-files created by the remote mainframe. The plot-files were stored on the Nova disk as part of a normal RJE output sequence; quick visual inspection of the plot was by means of a cathode ray tube storage oscilloscope and subsequent hardcopy by means of a revolving drum paper plotter. To interface non-system devices and, of course, background system peripherals a 16 port asynchronous line drive unit was incorporated and these lines were used to connect to the Hypersonics Laboratory as shown in fig.A1.

A 2.2 MOS Operating System

Only a brief outline of the main features of the MOS operating system is presented here but full details are available in Task Terminals (1976). The MOS system was entirely core resident and operated in a fore/background processing configuration such that RJE processing occurred in the foreground

with the highest priority of CPU resource allocation. User programs, i.e. Hypersonics control program and application tasks, together with local operations were run in the background. The MOS system resided in the lower part of the memory approximately occupying 23 k words of the available 32 k words. A large proportion of MOS was taken up by the device driver subroutines and their associated input-output buffers for all the system peripherals. In addition various mainframe RJE programs, known as emulators, were available for communication with computers such as CDC6400, IBM360 or CDC7600. All emulators were stored as object code disk files and copied into a reserved system 'core slot' as required to 'talk to' a specific mainframe. The RJE system was versatile in that various types of card format could be used using code conversion routines; the RJE link could also make use of magnetic tape or disk for data or program input-output. This feature was especially useful for driving the incremental plotters in which case a data plot file could be stored on disk as part of a normal RJE output sequence. The plot file was later copied to the required incremental plotter although MOS performed a considerable amount of post-processing on a plot file in order to drive the plotters. Multiple local copying processes and comprehensive disk maintenance/housekeeping facilities were also supported by MOS.

Users programs were run in the remaining 9k words of memory, including two service programs, an editor and an assembler, which were supplied with the system to facilitate the creation of further user programs. The NOVA architecture provided a limited number of locations, known as PAGE ZERO, which could be directly addressed from any memory location. These locations were available to background users to provide communication with MOS and to provide user access to the major MOS subroutines. MOS operated on an activity stack or queue basis such that control was passed to the program or task at the queue head until that program terminated or paused for input-output.

User programs could insert or remove tasks from the queue by means of the entry points provided in PAGE ZERO. Also other PAGE ZERO locations enabled users to access all the system devices and peripherals but in the case of non-system devices the user had to provide an interrupt handler subroutine to service input data.

A3.0 Hypersonics Control Program

A core resident control program linked the peripheral devices in the Hypersonics Laboratory to the MOS operating system described earlier. It provided the capability to access and run user tasks for the wind tunnels, and also permitted user tasks to access MOS system hardware and software. A brief description is given here of the Hypersonics peripherals (hardware) and the control program (software) while application tasks specific to the Gun Tunnel are presented in a later section; some of these application tasks were shared with the Nitrogen tunnel.

A3.1 Hardware

Control of the Hypersonics programs was through two console devices, a Tektronix 4010 graphics VDU and a Texas Instruments "Silent 700" teletype, subsequently to be referred to as VDU and TTY.

In the VDU alphanumeric mode, command sequences were fed to the minicomputer in the form of numeric or letter strings. Alternatively the results of computations were displayed in a graphical form using the plot mode of the terminal. The screen was divided into a grid of 1024 by 767 points and graphs were drawn by the generation of light or dark vectors between grid points. Alphanumeric anotations could be generated in software or locally at the 4010

by periodic reversion to the alphanumeric mode. A cross-wire cursor facility was provided to enable co-ordinate information to be returned to the computer from graphical displays. The cursor was initialised and manually set to the point of interest on the graph, and on striking a key, the co-ordinates of the chosen point were returned to the computer.

The Silent 700 teletype was a quite terminal running at up to 300 baud; the full ASCII character set was available. The TTY was a useful hardcopy device and a back-up control device if the VDU was out of service.

A 3.2 Software

The Hypersonics' control program provided the framework for the execution of data handling programs written specifically for the wind tunnels. The location of the main subroutines is shown in the Core Map fig. A2 . In brief, the control program performed four main functions:

A 3.2.1 Initialisation Functions

At the beginning of an acquisition of processing session by the Hypersonics group, initialisation functions were performed by a series of subroutines to enable the background user to communicate with and use the features of MOS. Some of these initialisation subroutines operated only once and then were overwritten to provide additional memory. As stated earlier the time-sharing aspect of MOS was controlled by means of an activity queue into which the initialisation subroutines placed the addresses of the major sub-programs of the Hypersonics control program. These sub-programs included the interrupt handlers for the non-system devices used in the Laboratory and a set of routines which continuously monitored the output buffers of each device for data requiring transmission.

A 3.2.2 Input-Output Functions

Output to the Hypersonics' peripherals and devices was controlled by two types of subroutine, one of which was designed for message string output (i.e. multiple character strings) and the other for single character output. By means of device address table these two routines would store the character or characters for transmission into the relevant output buffer, from which it would be transferred to the device by the continuously running routines described in section A3.2.1 above. For input under interrupt control, the usual case, MOS transferred control to the subroutine address supplied on initialisation provided that no interrupt of higher priority was operating. Input characters were stored in a buffer for subsequent processing by an application task see section 4.2.0. An exception was for a hardware interrupt from the VDU or TTY in which case a Master Task, see section A3.2.4 below, was inserted into the activity queue. Disk input-output used a series of MOS supplied routines which were accessed by a set of corresponding Hypersonics control program routines. These routines assembled data in the correct format then entered the MOS disk routines and when the disk operation was completed returned control to the calling task.

A 3.2.3 Floating Point Arithmetic

As the MOS system did not provide for floating point arithmetic a version of the Data General Floating Point Interpreter was obtained and included as a permanent part of the Hypersonics control program. The Floating Point Interpreter, Data General (1977), provided all the usual arithmetic, trigonometric and logarithmic functions in addition to comprehensive numeric input-output options. Base conversion routines were incorporated by the Hypersonics group to permit conversion between binary, octal and decimal integers.

A 3.2.4 Master Console Tasks

Input from either TTY or VDU was monitored by two identical Master tasks as illustrated by the flow diagram fig. A3. These tasks were responsible for entering specific application tasks into the activity queue, loading the task from disk into the memory slot and the eventual termination of the task on operator request.

A 4.0 Gun Tunnel Data System

The Gun Tunnel data acquisition system performed two main functions which were the digitising of many analogue channels at modest conversion rates, 2×10^4 to 6×10^4 samples/sec, or the acquisition of one or two channels at high conversion rates, 1×10^6 to 4×10^6 samples/sec. A local buffer memory was used to store the data until run completion as the high data rates precluded direct transmission to the minicomputer for storage and processing. A system incorporating the above requirements was successfully linked to a minicomputer to provide an on-line data acquisition and processing service. The description of the system will be divided into the hardware aspects and the specific application programs or tasks of the Gun Tunnel.

A 4.1 Acquisition System

The main features of the data acquisition system are shown in fig. A4; the system was custom made to Imperial College specification by VF Instruments of Gloucester. Full details of the construction and design are available in the system manual, VF Instruments (1977), and only a brief description of the system philosophy is included here.

The design philosophy of the system was based on using four existing Ampex RF1 corestores to provide the primary data-buffer memory, i.e. 4 x 4k bytes. All the critical components shown in fig. A4, e.g. high speed analogue to digital convertors (ADC), analogue multiplexers (MPX) and high speed amplifiers, were manufactured in the USA by DDC Inc. to whom VF Instruments were the UK Agents*. The main data acquisition sub-system accommodated inputs for a maximum of 24 analogue inputs which were scanned by a twin level analogue multiplexer unit. Only the number of channels pre-set on the system controls would be scanned by this unit; the MPX output was fed, via a unity gain buffer amplifier, to the main ADC which was capable of digitising bipolar signals of up to ± 2.5V. The maximum conversion rate was 6.4×10^6 samples/sec to 8 bit resolution, but in order to be compatible with the Ampex primary memory units, which have a maximum address rate of 1×10^6 samples/sec, the ADC was limited to 4×10^6 samples/sec. Successive conversions from the ADC were sequentially stored in the four Ampex corestores by means of an output, digital multiplexer. Slower conversion rates were obtained by means of the sampling interval control which was calibrated in units of 1/4 μsec, i.e. the time for one conversion. The sampling interval was variable up to a maximum of 10^8 units but must always be greater than or equal to the number of channels in use, see fig. A5. By use of this control it was possible to achieve delays between successive channel sweeps of up to 25 sec, thus providing an extremely large range of conversion rates.

One of the major parameters of interest during a Gun Tunnel run was the tunnel stagnation pressure, p_o, which was used to determine when the nozzle flow had reached a steady condition, e.g. fig. A6 . It was usual to make

*At present DDC Ltd., 128, High Street, Hungerford, Berks, RG17 ODL

measurements of aerodynamic parameters of interest only during the steady run time, thus it was required to monitor the stagnation pressure, p_o, for the whole Gun Tunnel run, i.e. approximately 30 msec, but only to use the main digitising channels (described above) to gather data during the steady run time, typically 5msec. A system requirement was therefore to be able to trigger the main digitising unit from a set point (or pressure) on the p_o channel. To accomplish this, a separate data acquisition sub-system was used to digitise the p_o channel at a maximum rate of 10^4 samples/sec to 11 bit accuracy (for bipolar signals of up to 10V). It was possible to slow down the p_o conversion rate by a factor of two or four if required to give 5×10^3 or 2.5×10^3 samples/second respectively. The p_o data was stored in an internal 256 word x 11 bit semiconductor memory.

Comprehensive delay and triggering facilities were also provided to start the storage of data in the memory. The main ADC ran continuously although the data was only stored if the correct trigger signal had been received to initiate storage. The trigger operated either from a digital or an analogue signal; the analogue trigger could be derived either from the p_o channel or an auxiliary input. A variable delay option with a maximum setting of 999 msec. was also available.

The run was considered complete when the main and p_o data memories were both full, i.e. 16384 and 256 conversions respectively. After conversion the data was transferred to the mincomputer in inverse offset binary code via an asychronous line interface at 4800 band. On computer command any of the five data memories could be transmitted in serial form to the minicomputer. Each data word, either 8 or 11 bit, was split into two bytes for transmission in order to allow for the inclusion of a parity check bit. The data was read non-destructively from the memories and could be retransmitted in the event of errors.

A 4.2 Gun Tunnel Tasks

A series of assembly language tasks, or application programs, have been written to store the data from the acquisition system on minicomputer disk and to subsequently process the data for analysis and display. Those tasks were ran as sub-programs in the Hypersonics control program described in section A.3.2. Only a brief description is included here of the main tasks listed below:

Task G - Calibration data update task

Task P - Tunnel run data and p_o examination task.

Task Q - Data transmission and disk storage task.

Task F - Plot and calculation task.

Other tasks were produced for hardware debugging, data dumps and other development functions.

A 4.2.1 Task G

Every analogue channel in use during a Gun Tunnel run had a transducer connected to it, for example pressure transducer, heat transfer gauge or thermocouple, An amplifier, perhaps with some form of signal conditioning (i.e. filtering), was also used to boost the low voltage output of the transducer to the 2 volts required for optimum digitisation accuracy. The calibration data for each channel, i.e. gain and transducer sensitivity, were stored on a disk file known as GUNCAL. The disk file occupied one disk section which accommodated 510 characters hence each of the maximum 25 channels had 20 characters allocated to it. The first two characters were the channel number, e.g. 01 to 25; the p_o channel was always taken to be channel 25. The next character

was a type identifier used to indicate the physical quantity digitised e.g. pressure = P, temperature = T and heat transfer rate = Q. The amplifier gain was encoded by the following four characters and the remaining thirteen were used to encode two transducer calibration constants. On entry to the task the current calibration file was displayed in tabular format on the control device and if required the data could be updated channel by channel. If the disk file, GUNCAL, did not exist perhaps due to accidental purging it was automatically created by the task with zero data for all channels and the current data could then be entered as normal. The form of a typical set of channel calibration data is shown in fig. A7.

A 4.2.2 Task P

This task received and stored all the run information, e.g. number of channels used, sampling rate etc., required in the main data processing and calculation, see the flow diagram for the task fig. A8. The information required by the task is shown below and the order is the same as required by the task:

a) Run number: Four digit identifier corresponding to the total number of Gun Tunnel runs.

b) No. of channels: A two digit number corresponding to the number of channels required for the main digitising unit, i.e. 01 to 24.

c) Sampling Interval: The interval between successive channel sweeps as set on data system. Units of $\frac{1}{4}$ μsec - 3 digits.

d) Exponent of c: One digit exponent. Power of 10 to which sampling interval setting above is multiplied.

e) P_o frequency: P_o channel conversion rate either 10.0, 05.0 or 02.5 K samples/sec. - 4 digits.

All above inputs were in 'fixed format', i.e. leading and trailing zeros were required; after this information had been correctly entered, the p_o channel was automatically unloaded to the minicomputer and plotted on the graphics terminal. The p_o channel was visually inspected for irregularities and, if satisfactory, the cross-wire cursor was used to input co-ordinates corresponding to the steady run period.

A 4.2.3 Task Q

Task Q created a composite disk file containing the run information from Task P, calibration data from GUNCAL, p_o channel data and finally up to 24 channels of data from the main digitising unit memory. The flow diagram of the task is shown in fig. A9; the task unloaded each of the five memories to obtain the data although if only four channels (say) were required it was possible to arrange that all these channels were contained in one main memory unit. Each data word, either 8 bit or 11 bit, was reassembled from the two bytes used in transmission and converted to a four digit decimal integer. The data diskfile created by Task Q was formatted in 80 column card image style for subsequent input to a mainframe computer. The form of the disk file is shown in fig. A10.

A 4.2.4 Task F

This task accessed a chosen data disk file and plotted a channel on to the graphics terminal ; the channel for analysis could be selected at random but the p_o channel was usually evaluated first. The steady run time as determined in Task P was superimposed on the channel plot in the form of two vertical lines. The task could calculate a mean value of the data points in the region but quite often, due to different transducer response times that occurred with varying instrumentation setups, the steady run period obtained

from the p_o trace did not correspond to the most suitable region on any specific data channel. In these circumstances the cross-wire cursor could be used to input a more suitable averaging period. In simple circumstances the transducer sensitivity and amplifier gain was used to calculate the time-averaged value of the physical quantity in question, e.g. pressure or temperature. The flow chart of Task F is shown in fig. A11. Time resolved data analysis such as electron beam fluctuating density surveys or when considerable calculation was required, e.g. heat transfer rates, the data file could be transmitted via the RJE service to the mainframe computer for processing.

APPENDIX B: TOTAL TEMPERATURE PROBE CALIBRATION

B1.0 Total Temperature Probes

In studies of hypersonic boundary layers, the accurate determination of total temperature profiles has proved to be one of the most difficult measurements, particularly in the short duration or intermittent facilities. In the present investigation, this measurement proved difficult due to the high freestream total temperature, $T_{o\infty} = 1060^{o}K$, short steady run time, t_r = 5 to 7 msec., and the requirement of high spatial resolution in the relatively thin boundary layer, $\delta_p \simeq 10mm$. The problem of total temperature measurement under these rigorous conditions has been fully discussed in Bartlett, Edwards and Hillier (1979), hence it is proposed to discuss only the calibration of the boundary layer survey probes, described in section 3.3.6.2, in this appendix. These probes were the result of an extensive development programme by A. J. Edwards, to whom I am indebted for this work and the early wall distributions of heat transfer, static pressure and surface impact pressure. The construction of a survey total temperature probe is shown in fig. B1. This type of probe was used for all the boundary layer surveys reported herein, but it was apparent during the use of these so called 'inverted V probes' that the performance degraded with repeated testing as the thermocouple bead migrated from the plane of the supports into the influence of the shield boundary layer. This flexing of the sensor wire also led to early failure at the weld between the thermocouple sensor wire and the support prong. Therefore, the opportunity was taken to develop and assess two further probe designs in the calibration programme for the survey probes. The new probe designs incorporated a rigid sensor wire arrangement as can be seen in fig. B1, thereby avoiding the wire flexing problem of the inverted V probe.

B2.0 Probe calibration

The possibility of calculating the heat losses from the probe sensor was investigated in Bartlett, Edwards and Hillier(1979) but after an assessment of the available theoretical models it was found that they were too idealised to provide a reliable correction scheme. The obvious alternative was to calibrate the probes through a range of Mach number, Reynolds number and total temperature similar to that experienced within the boundary layer. Due to facility limitations and time constaints, the present calibration was limited to Reynolds number variations only, i.e. correctly simulating the Reynolds number behind the probe normal shock. The sensitivity to Mach number is believed to be a second order correction as the sensor response is primarily controlled by the subsonic flow within the flow. For $M_e > 4$, the subsonic Mach number behind the probe normal shock is relatively insensitive to the upstream Mach number. Although in the present study the Mach number fell to approximately two close to the wall, it has been estimated that the Mach number effect remained small.

The calibration was performed at only one total temperature but radiation losses are function of the absolute temperature hence a calibration at a fixed total temperature of $1000^{o}K$ might well overestimate the losses near the wall where the total temperature fell to around $700^{o}K$. Estimates in Bartlett, Edwards and Hillier (1979) have shown that the radiation losses would be overestimated by a factor of three by a calibration at $1000^{o}K$, but as radiation losses are small compared to the conduction losses, this would typically still only lead to an error of less than two per cent. Thermal conductivity is primarily a function of temperature difference and not of absolute temperature except for second order variations of sensor material and gas properties.

The Reynolds number variation for the calibration was achieved by using an inclined flat plate model as either an expansion or a compression surface, section 3.2.2. The freestream total temperature $T_{o\infty}$ is invarient to these flow processes. The probes to be calibrated were fixed parallel to the flat plate upstream of the trailing edge and the probe position confirmed to be midway between the plate boundary layer and the model leading edge shock at each incidence angle by Schlieren photography. The variation of probe Reynolds number, Re_{3d}, with plate incidence is shown in fig. B2 for the two standard tunnel running conditions, see Table 1. Re_{3d} was based on the conditions behind the probe normal shock, the sensor wire diameter and the gas viscosity evaluated at stagnation conditions. The total temperature at both the standard tunnel conditions has been estimated previously from stagnation point heat transfer measurements, Needham et al (1970). These measurements gave a freestream total temperature, $T_{o\infty} = 1070^{o}K$, for both conditions. In the present study total temperature has been estimated from the asymptotic behaviour of the data at high Reynolds number which resulted in $T_{o\infty} = 1064^{o}K$ for the HP condition and $T_{o\infty} = 998^{o}K$ for the LP condition. The total temperature at the HP condition agreed very well with the value inferred from stagnation point heat transfer. In the case of the LP condition, the driver-barrel pressure ration, P_{41}, has been slightly reduced since the earlier stagnation point heat transfer measurements which accounted for a lower total temperature in the present calibration. In the freestream where the calibration was at its most precise it has been estimated that $T_{o\infty}$ was measured to better than $\pm 2\%$.

In addition to the boundary layer survey probes two further types with a more rigid sensor wire design were calibrated in the present study; the

construction of the probes is shown in fig. B1 . The chromel-alumel sensor wire diameter was 12.5 μm, the smallest commercially available, and the support prong diameter equal to 0.1mm for all three probe types. As stated earlier the survey probes with the 'V' sensor wire were found to suffer, admittedly after repeated testing, from a reduction in performance due to the thermocouple bead migrating from the plate of the supports and perhaps entering the influence of the shield boundary layer. This flexing of the sensor wire also led to early failure at the support prong/ sensor wire weld.

The three probe types exhibit a significant Reynolds dependence as shown in fig. B3 a, b and c. It is difficult to draw clear conclusions from these results as the pairs of probes with nominally the design show markedly different Reynolds number dependence. The 'V' survey probe and the inclined wire probe showed a similar performance which could be expected as the wire inclination angle and sensor wire length to diameter ratio were similar. The normal wire probe showed a more rapid response than the inclined wire probe which can be predicted from theory, e.g. Bartlett, Edwards and Hillier (1979). All three probe types had a sufficiently rapid response to reach equilibrium even at the lowest Reynolds numbers experienced in the boundary layer flows investigated; this was confirmed from the temperature traces obtained in the boundary layer surveys i.e. a plateau was reached in the traces. The present results from the calibration have been compared with a simple idealised model for the heat losses, Equation 3(d) in Bartlett, Edwards and Hillier (1979), which is reproduced here:

$$\frac{T_r - T_b}{T_r - T_i} = \psi_1 + \xi_1 - \psi_1 \xi_1 \qquad \text{(Eq. A1)}$$

where $\psi_1 = 1/\cosh\sqrt{\lambda}$

$$\lambda = Nu_o (k_{go}/k_w) (L/d)^2 (1+\delta) ,$$

and

$$\xi_1 = \frac{\sigma \xi_w d}{Nu_o k_{go}} \left[\frac{T_r^4}{(T_r - T_i)} \right]$$

This relationship is valid if the support temperature remains constant throughout the process at T_i, the initial temperature of the whole probe. Equation B1 has been rearranged to give the probe recovery factor Γ :

$$\Gamma = (T_b - T_i)/(T_r - T_i)$$

A comparison with the steady state solution, Eq. B1, is shown in fig. B3 for all three probe types; the agreement is not satisfactory with Eq. B1 underpredicting the Reynolds number effect. This could occur if the steady state was not reached, but from the original data traces it appeared that the probes achieved a plateau region. It is also possible that the evaluation of a Nusselt number behind the normal shock was not sufficiently representative of the conditions at the sensor wire. This may be due to the diffusing effect of the probe shield or more significantly to the development of the shield boundary layer which will obviously be larger at the lower Reynolds numbers, thereby reducing the sensor Reynolds number and its effective length, hence the averaged total temperature. This is consistent with the probe to probe variations within a probe type where small internal geometric differences may cause more or less interaction with the shield boundary layer.

It is possible that the design of the shield may well be improved to overcome those effects but the use of the present shield was justified as tests had proved, over a considerable range of Reynolds number, that a much higher recovery factor was achieved with a shield as opposed to

operation without a shield. From the calibration data shown in fig. B3 a, b and c, it is apparent that small geometric and physical differences, e.g. position of sensor bead relative to the shield in nominally identical probes or shields resulted in varying performance. As a rake of four probes was used to measure the boundary layer profiles, section 5.8, it would have been desirable to calibrate each probe individually to account for the performance differences highlighted in the calibration. Due to limited probe life and, of course, inevitable time constraints this did not prove possible. Therefore, to correct the measured total temperature profile data, a simple fit to the results from the calibration from the 'V' survey probes and the similar inclined wire probe were used to determine the Reynolds number dependence. This provided a calibration to within better than $\pm 3\%$ of Γ for most probes. The uncorrected total temperature data was used in conjunction with the Mach number data to calculate a first estimate of Re_{3d}, the Reynolds number within the probe. From the calibration, it was possible to correct the measured total temperature for Reynolds number effects and then using this 'corrected' total temperature it was possible to re-calculate a new estimate of Re_{3d}. This process was repeated until convergence, which generally occured within three or so iterations.

References

Acharya,M,; Horstman,C.C. and Kussoy,M.I.: 'Reynolds Number Effects on the Turbulence Field in Compressible Boundary Layers'. AIAA Journal, vol. 17, p. 380, 1979.

Allen,J.M.: 'Use of the Baronti-Libby Transformation and Preston Tube Calibrations to Determine Skin Friction from Turbulent Velocity Profiles'. NASA TN D-4853, 1968.

Allen,J.M.: 'Pitot Probe Displacement in a Supersonic Turbulent Boundary Layer'. NASA TN D-6759, 1972.

Allen,J.M.: 'Evaluation of Compressible Flow Preston Tube Calibrations'. NASA TN D-7190, 1973.

Allen,J.M.: 'Re-Evaluation of Compressible Flow Preston Tube Calibrations'. NASA TM X-3488, 1977.

Baronti,P.O. and Libby,P.A.: 'Velocity Profiles in Turbulent Compressible Boundary Layers'. AIAA Journal, vol.4, p.193, 1966.

Bartlett,R.P.; Edwards,A.J.; Harvey,J.K. and Hillier,R.: 'Pitot Pressure and Total Temperature Profile Measurements in a Hypersonic Turbulent Boundary Layer at M=9'. Imperial College Aero Report No.79-01, 1979.

Bartlett,R.P.; Edwards,A.J. and Hillier,R.: 'Development and Calibration of a Total Temperature Probe for the Imperial College Aeronautics Dept. Gun Tunnel'. Imperial College Aero Report No. 79-02, 1979.

Bartlett,R.P.; Davis,J. and Harvey,J.K.: 'Data Acquisition Systems for the Hypersonics Gun and Nitrogen Wind Tunnels'. Imperial College Aero Report No. 79-03, 1979.

Bartlett,R.P. and Harvey,J.K.: 'Electron Beam Measurements of the Density in a Hypersonic Tubrulent Boundary Layer at M=9'. Imperial College Aero Report No. 80-01, 1980.

Beckwith,I.E.: 'Recent Advances in Research on Compressible Turbulent Boundary Layers'. NASA SP-228, 1970.

Beckwith I.E.; Harvey,W.D. and Clark, F.L.: 'Comparisons of Turbulent Boundary Layer Measurements at M=19.5 with Theory and an Assessment of Probe Errors', NASA TN D-6192, 1971.

Bertram,M.H. and Neal,L.N,Jr.: 'Recent Experiments in Hypersonic Turbulent Boundary Layers', NASA TM X-56335, 1965.

Boyer,A.G. and Muntz,E.P.: 'Experimental Studies of Turbulence Characteristics in the Hypersonic Wake of a Sharp Slender Cone', AGARD CP 19, 1967.

Bradshaw,P.: 'An Introduction to Turbulence and its Measurement', Pergamon Press, 1971.

Bradshaw,P. and Unsworth,K.: 'A Note on Preston Tube Calibrations in Compressible Flow', Imperial College Aero Report 73-07,1973.

Bradshaw,P.: 'Compressible Turbulent Shear Layers', Imperial College Aero Report 75-102, 1975.

Bradshaw,P.(Editor): 'Topics in Applied Physics:- Turbulence', Springer, Heidelberg, 1976a.

Bradshaw,P: 'A Skin Friction Law for Compressible Turbulent Boundary Layers based on the full Van Driest Transformation', Imperial College Aero Report 76-02, 1976.

Bradshaw,P: 'Compressible Turbulent Shear Layers', Annual Review of Fluid Mechanics Vol.9, 1977.

Busemann,A: 'Gasdynamik', Handbuch der Experimentalphysik, Vol. 14, p. 366,

Akademischer Verlag, Leipzig, 1931.

Bushnell,D.M.; Johnson,C.B.; Harvey,W.D. and Feller,W.V.: 'Comparison of Prediction Methods and Studies of Relaxation in Hypersonic Turbulent Nozzle Wall Boundary Layers', NASA TN D-5433, 1969.

Bushnell,D.M. and Morris,D.J.: 'Shear Stress, Eddy Viscosity and Mixing Length Distributions in Hypersonic Turbulent Boundary Layers', NASA TM-X 2310, 1971.

Bushnell,D.M. and Beckwith,I.E.: 'Calculation of Non-Equilibrium Hypersonic Turbulent Boundary Layers and Comparison with Experimental Data', AIAA Journal, Vol.8, p.1402, 1970.

Bushnell,D.M.; Cary,A.M. and Holley,B.B.: 'Mixing Length in Low Reynolds Number Compressible Turbulent Boundary Layers',AIAA Journal Vol.13, p.1119, 1975.

Bushnell,D.M.; Cary,A.M. and Harris,J.E.: 'Calculation Methods for Compressible Turbulent Boundary Layers", NASA SP-422, 1977.

Butefisch,K.A. and Vennemann,D.: 'The Electron Beam Technique in Hypersonic Rarefied Gas Dynamics'. Progress in Aerospace Sciences, vol.15, ed D. Kuchemann Pergamon Press, 1974.

Camac,M: 'Boundary Layer Measurements with an Electron Beam', AVCO Everett Research Report 275, 1967.

Cary,A.M. and Bertram,M.H.: 'Engineering Prediction of Turbulent Skin Friction and Heat Transfer in High Speed Flow', NASA TN-D 7507, 1974.

Cebeci,T. and Smith,A.M.O.: 'A Finite Difference Method for Calculating Compressible Laminar and Turbulent Boundary Layers'. ASME Paper 70-FE-A, 1970.

Cebeci,T. and Smith,A.M.O.: 'Analysis of Turbulent Boundary Layers', Academic Press, New York, 1974.

Clauser,F.H.: 'Turbulent Boundary Layers in Adverse Pressure Gradients'. Journal of Aerospace Science, Vol.21, p.91, 1964.

Coleman,G.T.: 'Hypersonic Turbulent Boundary Layer Studies'. University of London, Phd Thesis, 1973.

Coles,D.E.: 'Measurements in the Boundary Layer on a Flat Plate in Supersonic Flow'. Jet Propulsion Lab., Technical Reports 20-69, 20-70 and 20-71, 1953.

Coles,D.E.: 'The Law of the Wake in the Turbulent Boundary Layer'. Journal of Fluid Mechanics, Vol.1, p.191, 1956.

Coles,D.E.: 'The Turbulent Boundary Layer in a Compressible Fluid'. Rand Corporation, R-403-PR, 1963.(also ARC 24497, 1963).

Crocco,L.: 'Sulle Transmissione del Calore da una Lamina Piana a un Fluid Scorrenta ad alta Velocita'. L'Aerotechnica Vol.12, p.181, 1932.

Crocco,L.: 'Transformation of the Compressible Turbulent Boundary Layer with Heat Transfer'. AIAA Journal, Vol.1, p.2723, 1963.

Culotta,S. and Richards,B.E.: 'Methods for Determining Conditions in Real Nitrogen Expanding Flows'. Von Karman Institute, TN 58, 1970.

Danberg,J.E.: 'Characteristics of the Turbulent Boundary Layer with Heat and Mass Transfer at M = 6.7'. Naval Ordnance Laboratory, NOLTR 64-99,1964.

Danberg,J.E.: 'Characteristics of the Turbulent Boundary Layer with Heat and Mass Transfer at M = 6.7 - Data Tabulation'. Naval Ordnance Laboratory, NOLTR 67-6, 1967.

Data General : 'Assembler Language Reference Manual', Data General Corp., Southboro, Mass., USA, 1976.

Data General : 'Floating Point Interpreter Users Manual', Publication No. 093-000019-04, Data General Corp., Southboro, Mass., USA, 1977.

Davis,J. and Harvey,J.K.: 'A Comparison between Experiment and Direct Simulation Calculations of the Hypersonic Rarefied Flow Field over a Flat Plate with and without a Forward Facing Step'. Imperial College Aero Report 76-05, 1976.

Davis,J.: 'An Experimental Study to Evaluate and Develop the Direct Simulation Method as Applied to Rarefied Hypersonic Flow Fields'. University of London, Phd Thesis, 1978.

Davis,M.E.: 'Spectral Analysis Programs POWERSPEC and COPHASE'. Imperial College Aero Report 74-103, 1974.

Demetriades,A.: 'Hypersonic Viscous Flow over a Slender Cone: Part III Laminar Instability and Transition'. AIAA Paper 74-535, 1974.

Dione,J.G.; Sadowski,C.M.; Tardif,L. and Vanoverschelde,J.: 'Mean Density Measurements in Hypersonic Wakes'. AGARD Conference Procedings No. 19,1967.

Dwyer,H.A.: see Hopkins,E.J.; Keener,E.R.; Polek,T.E. and Dwyer,H.A.,1972.

Eckert,E.R.G.: 'Engineering Relations for Skin Friction and Heat Transfer for Surfaces in High Velocity Flow'. Journal of Aero. Science, Vol.22, p.585, 1955.

Edwards,A.J. and Hillier,R.: Private Communication, 1980a. (To Be Published as Imperial College Aero Report).

Edwards,A.J. and Hillier,R.: Private Communication, 1980b. (To Be Published as Imperial College Aero Report).

Fenter,F.W. and Stalmach,C.J.: 'The Measurement of Local Turbulent Skin Friction at Supersonic Speeds by means of Surface Impact Pressure Probes'. University of Texas, Report No. DRL-392, 1957.

Fernholz,H.H.: 'Geschwindigkeitsprofile und Halbempiriche Gesetze in Kompressiblem Turbulenten Grenzschichten bei Konstantem Druck'. Ing. Arch., Vol.38, p.311, 1969.

Fernholz,H.H.: 'Compressible Turbulent Boundary Layers'. In Von Karman Institute Lecture Series No. 86, 1976.

Fernholz,H.H. and Finley,P.J.: 'A Critical Compilation of Compressible Turbulent Boundary Layer Data'. AGARD Advisory Group Report AG-223, 1977.

Fernholz,H.H. and Finley,P.J.: Private Communication, 1979. Published as, 'A Critical Commentary on Mean Flow Data for Two-Dimensional Compressible Turbulent Boundary Layers'. AGARD Advisory Group Report No. AG-253, 1980.

Fischer,M.C.;Maddalon,D.V.; Wienstein,L.M. and Wagner,R.D.: 'Boundary Layer Pitot and Hot Wire Surveys at M = 20'. AIAA Journal, Vol.9, p.826, 1971.

Frost,W. and Moulden,D.V.: 'Handbook of Turbulence'. Plenum Press, 1977.

Gran,R.L.; Lewis,J.E. and Kubota,T.: 'The Effect of Wall Cooling on a Compressible Turbulent Boundary Layer'. Journal of Fluid Mechanics, Vol. 66, p.507, 1974.

Harvey,J.K.: Private Communication, 1979.

Harvey,W.D.; Bushnell,D.M. and Beckwith,I.E.: 'Fluctuating Properties of Turbulent Boundary Layers for Mach Numbers up to M = 9'. NASA TN D-5496, 1969.

Harvey,W.D. and Hunter,W.W.: 'Experimental Study of a Free Shear Flow at MAch 19 with Electron Beam and Conventional Probes'. NASA TN D-7981, 1975.

Hastings,R.C. and Sawyer,W.G.: 'The Turbulent Boundary Layer on a Large Flat Plate at M = 4'. Aeronautical Research Council, R&M 3678, 1970.

Hill,F.K.: 'Boundary Layer Measurements in Hypersonic Flow'. Journal of Aero. Sciences, Vol.23, p.35, 1956.

Hill,F.K.: 'Turbulent Boundary Layer Measurements at Mach Numbers from 8 to 10'. Physics of Fluids, Vol.2, p.778, 1959.

Hinze,J.O.: 'Turbulence'. McGraw-Hill, New York, 1959.

Hopkins,E.J. and Keener,E.R.: 'Study of Surface Pitot Tubes for Measuring Turbulent Skin Friction at Supersonic Mach Numbers-Adiabatic Wall'. NASA TN D-3478, 1966.

Hopkins,E.J. and Inouye,M.: 'An Evaluation of Theories for Predicting Turbulent Skin Friction and Heat Transfer on Flat Plates at Supersonic and Hypersonic Mach Numbers'. AIAA Journal, Vol.9, p.993, 1971.

Hopkins,E.J.; Keener,E.R.; Polek,T.E. and Dwyer,H.A.: 'Hypersonic Turbulent Skin Friction and Boundary Layer Profiles on Non-Adiabatic Flat Plates'. AIAA Journal, Vol.10, p.40, 1972.

Hopkins,E.J. and Keener,E.R.: 'Pressure Gradient Effects on Hypersonic Turbulent Skin Friction and Boundary Layer Profiles'. AIAA Journal, Vol. 9, p.1141, 1972.

Hornung,H.G.: 'A Survey of Compressible Flow Boundary Layers- Theory and Experiment'. Australian Aeronautical Research Council, Report ACA 67, 1966.

Horstman,C.C. and Owen,F.K.: 'Turbulent Properties of a Compressible Boundary Layer'. AIAA Journal, Vol.10, p.1418, 1972.

Illingworth,C.R.: 'The Laminar Boundary Layer associated with Retarded Flow of a Compressible Fluid'. ARC R&M 2590, 1946.

Johnson,C.B. and Bushnell,D.M.: 'Power Law Velocity Profile Exponent Variations with Reynolds Number, Wall Cooling and Mach Number in a Turbulent Boundary Layer'. NASA TN D-5753, 1970.

Kuster,H.J.: 'Fin Integral Verfahren zur Berechnung Zweidimensionaler Incompressibiler Turbulenter Grentschlichten mit Druckgradient und Warmeubergang auf der Basis einer Kompressibilitatstransformation'. Dr.-Ing. Thesis, Technical University of Berlin, 1972.

Keener,E.R. and Hopkins,E.J.: 'The Use of Preston Tubes for Measuring Hypersonic Turbulent Skin Friction'. AIAA Paper 69-345, 1969.

Keener,E.R. and Hopkins,E.J.: 'Turbulent Boundary Layer Velocity Profiles on a Non-Adiabatic Flat Plate at M = 6.5'. NASA TN D-6907, 1972.

Keener,E.R. and Hopkins,E.J.: 'Van Driest Generalistion Applied to Turbulent Skin Friction and Velocity Profiles Measured on the Walls of a M = 7.4 Wind Tunnel'. AIAA Journal, Vol.12, p.1784, 1973.

Kemp,J.H. and Owen,F.K.: 'Experimental Study of a Nozzle Wall Boundary Layer at Mach Numbers 20 to 47'. NASA TN D-6965, 1972.

Kendall,J.M.: 'Wind Tunnel Experiments Relating to Supersonic and Hypersonic Boundary Layer Transition'. AIAA Paper No. 74-133, 1974.

Kistler,A.L.: 'Fluctuation Measurements in a Supersonic Turbulent Boundary Layer'. Physics of Fluids, Vol.2, p.290, 1959.

Klebanoff,P.S.: 'Characteristics of Turbulence in a Boundary Layer with Zero Pressure Gradient'. NACA Report 1247, 1955.

Kovasznay,L.S.G.: 'The Hot Wire Aneomometer in Supersonic Flow'. Journal of Aero. Science, Vol.17, p.565, 1950.

Kovasznay,L.S.G.: 'Turbulence in Supersonic Flow'. Journal of Aero. Science, Vol.20, p.657, 1953.

Laderman,A.J.: 'Hypersonic Viscous Flow over a Slender Cone: Part II Turbulence STracture of the Boundary Layer'. AIAA Paper No. 74-534, 1974.

Laderman,A.J.: 'New Measurements of Turbulent Shear Stresses in Hypersonic Boundary Layers'. AIAA Journal, Vol.14, p.1286, 1976.

Laderman,A.J.: 'Effect of Wall Temperature on a Supersonic Turbulent Boundary Layer'. AIAA Journal, Vol.16, p.723, 1978.

Laderman,A.J. and Demetriades,A.: 'Mean and Fluctuating Flow Measurements in the Hypersonic Boundary Layer over a Cooled Wall'. Journal of Fluid Mechanics, Vol.63, p.121, 1974.

Laderman,A.J. and Demetriades,A.: 'Turbulent Fluctuations in the Hypersonic Boundary Layer over an Adiabatic Slender Cone'. Physics of Fluids, Vol. 19, p.359, 1976.

Lewis,J.E.; Kubota,T. and Webb,W.J.: 'Transformation Theory for the Adiabatic Compressible Turbulent Boundary Layer with Pressure Gradient'. AIAA Journal, Vol.8, p.1644, 1970.

Lewis,J.E.; Gran,R.L. and Kubota,T.: 'An Experiment on the Adiabatic Compressible Turbulent Boundary Layer in Adverse and Favourable Pressure Gradients'. Journal of Fluid Mechanics, Vol.51, p.657, 1972.

Li,T.Y. and Nagamatsu,H.T.: 'Similar Solutions of the Compressible

Boundary Layer Equations'. Journal of Aero. Science, Vol.20, p.653, 1953.

Li,T.Y. and Nagamatsu,H.T.: 'Similar Solutions of the Compressible

Boundary Layer Equations'. Journal of Aero. Science, Vol.22, p. 607, 1955.

Lillicrap,D.C.: ' A Study of Rarefied Flows using an Electron Beam'. University of London, Phd Thesis, 1969.

Lobb,R.K.; Winkler,E.M. and Persch,J.: 'Experimental Investigation of Turbulent Boundary Layers in Supersonic Flow'. Naval Ordnance Laboratory, NAVORD Report 3880, 1955.

Mabey,D.G.: 'Some Observations on the Wake Component of the Velocity Profiles of Turbulent Boundary Layers at Subsonic and Supersonic Speeds'. Royal Aircraft Establishment TR 77-004, 1977. (Also Aero Quarterly, Nov. 1979, p.590, 1979).

Mabey,D.G.; Meier,H.U. and Sawyer,W.G.: 'Experimental and Theoretical Studies of the Boundary Layer on a Flat Plate at Mach Numbers from 2.5 to 4.5'. Royal Aircraft Establishment, TR 74-127, 1974.

Mabey,D.G. and Sawyer,W.G.; 'Experimental Studies of the Boundary Layer on a Flat Plate at Mach numbers from 2.5 to 4.5'. Aeronautical Research Council R & M 3784, 1976.

Mack,L.M.: 'Boundary Layer Stability Theory'. Jet Propulsion Lab., Doeument 900-177, 1969. (Also available in the AIAA Professional Study Series).

Mack,L.M.: 'Linear Stability Theory and the Problem of Supersonic Boundary Layer Transition'. AIAA Journal Vol.13, p.278, 1975.

Maise,G. and McDonald H.: 'Mixing Length and Kinematic Eddy Viscosity in a Compressible Boundary Layer'. AIAA Journal Vol. 6, p.73, 1968.

Mager,A.: 'Transformation of the Compressible Boundary Layer Equations'.

Journal of Aero. Science, Vol.25, p.305, 1958.

Marvin,J.G.: 'Turbulence Modelling for Compressible Flows'. NASA TM X - 73188, 1977.

McRonald,A.D.: 'Measurements of Density and Temperature in a Hypersonic Turbulent Boundary Layer using the Electron Beam Fluorescence Technique', Univ. of S. California, P.hd Thesis, 1975.

Meier,H.U.. and Rotta,R.C.: 'Experimental and Theoretical Investigations of Temperature Distributions in Supersonic Boundary Layers'. AIAA Paper No. 70-744, 1970.

Meier,H.U. and Rotta,R.C.: 'Temperature Distributions in Supersonic Turbulent Boundary Layers'. AIAA Journal Vol.9, p.2149, 1971.

Meier,H.U.; Voisinet,R.L.P. and Gates,D.F.: 'Temperature Distributions using the Law of the Wall for Compressible Flows with Variable Turbulent Prandtl Numbers'. AIAA Paper No. 74-596, 1974.

Mikulla,V. and Horstman,C.C.: 'The Measurement of Shear Stress and Total Heat Flux in a Non-Adiabatic Turbulent Hypersonic Boundary Layer'. AIAA Paper No. 74-119, 1975.

Mikulla,V. and Horstman,C.C.: 'Turbulence Measurements in Hypersonic Shock Wave-Boundary Layer Interaction Flows'. AIAA Paper No. 76-162, 1976.

Morkovin,M.V.: 'Fluctuations and Hot Wire Aneomometry in Compressible Flows'. AGARDOGRAPH No. 24, 1956.

Morkovin,M.V. and Phinney,R.E.: 'Extended Applications of Hot Wire Aneomometry to High Speed Turbulent Boundary Layers'. John Hopkins University, Dept. of Aeronautics, AFOSR TN-58-469, 1958.

Morkovin,M.V.: 'The Structure of Supersonic Turbulent Boundary Layers.' AGARD Wind Tunnel and Model Testing Panel, 1960.

Morkovin,M.V.: 'Effects of Compressibility on Turbulent Flows'. Mechanique de la Turbulence, Colloq. Int CNRS, Paris, 1962. (Also in 'The Mechanics of Turbulence', Favre, A (Ed.) Gordon-Beech, New York, 1964).

Morkovin,M.G.: 'Critical Evaluation of Transition from Laminar to Turbulent Shear Layers with Emphasis on Hypersonically Travelling Bodies'. Wright-Patterson AFB Ohio AFFDL TR 68-149, 1969.

Muntz,E.P.: 'The Electron Beam Fluorescence Technique'. AGARDOGRAPH 132, 1968.

Needham,D.A.; Elfstrom,G.M. and Stollery,J.L.: 'Design and Operation of Imperial College No. 2 Hypersonic Gun Tunnel'. Imperial College Aero Report 70-04, 1970. (Also available as ARC 32,569).

Owen,F.K. and Horstman,C.C.: 'On the Structure of Hypersonic Turbulent Boundary Layers'. Journal of Fluid Mechanics, Vol.53, p.611, 1972.

Owen,F.K.; Horstman,C.C. and Kussoy,M.I.: 'Mean and Fluctuating Flow Measurements of a Fully Developed, Non-Adiabatic Hypersonic Boundary Layer'. Journal of Fluid Mechanics, Vol.70, p.393, 1975.

Pate,S.R. and Schueler,C.J.: 'Radiated Aerodynamic Noise Effects on Boundary Layer Transition in Supersonic and Hypersonic Wind Tunnels'. AIAA Journal, Vol.7, p.450, 1969.

Patel,V.C.: 'Calibration of the Preston Tube and Limitations on its Use in Pressure Cradients'. Journal of Fluid Mechanics, Vol.23, p.185, 1965.

Reshotko,E.: 'A Programme for Transition Research', AIAA Journal Vol.13, p.261, 1975.

Rose,W.C. and Johnson,D.A.: 'Turbulence in a Shock-Wave Boundary Layer Interaction'. AIAA Journal Vol.13, p.884, 1975.

Rotta, J.C.: 'Ober die Theorie der Turbulenten Grenzschichten'. Mitt. M.P.I. f. Stromungsforschung, Gottingen, 1950. (Also NACA TM 1344 (1953)).

Rotta,J.C.: ' Bemerkung zum Einfluss der Dichteschwankungen in Turbulenten Grenzschlichten bie Kompressibler Stromung'. Ing. Arch. 32, p.187-190, 1963.

Rubesin,M.W.;Crisalli,A.J.;Horstman,C.C. and Acharya,M.: 'A Critique of Some Recent Second Order Closure Models for Compressible Boundary Layers'. AIAA Paper 77-128, 1977.

Sandborn,V.A.: 'Resistance Temperature Transducers'. Metrology Press, Colorado, 1972.

Sandborn,V.A.: 'A Review of Turbulence Measurements in Compressible Flow'. NASA TM X-62-337, 1974.

Schlicting,H.: 'Boundary Layer Theory' 6th Edition McGraw-Hill, 1968.

Sigalla,A.: 'Calibration of Preston Tubes in Supersonic Flow'. AIAA Journal, Vol.3, p1531, 1965.

Smith,J.A. and Driscoll,J.F.: 'The Electron Beam Fluorescence Technique for Measurements in Hypersonic Turbulent Flows', Journal of Fluid Mechanics, Vol.72, p.695, 1975.

Sommer,S.C. and Short,B.J.: 'Free-Flight Measurements of Turbulent Boundary Layer Skin Friction in the Presence of Severe Aerodynamic Heating at Mach Numbers from 2.8 to 7.0'. NACA TN D-3381, 1955.

Spalding,D.B. and Chi,S.W.: 'The Drag of a Compressible Turbulent Boundary Layer on a Flat Plate With and Without Heat Transfer'. Journal of Fluid Mechanics, Vol.18, p.117, 1964.

Stalmach,C.J.: 'Experimental Investigation of the Surface Impact Pressure Probe Method of Measuring Skin Friction at Supersonic Speeds'. University of Texas, DRL-410, 1958.

Stewartson,K.: 'Correlated Incompressible and Compressible Boundary Layers',

Proc. Royal Society, London, Vol.200, p.84, 1949.

Stewartson,K.: 'The Theory of Laminar Boundary Layers in Compressible Flow'. Oxford University Press,1964.

Sturek,W.B. and Danberg,J.E.: 'The Supersonic Turbulent Boundary Layer in an Adverse Pressure Gradient- Experiment and Data Tabulation'. AGARD Conference Procedings No. 93,1976.

Sun,C.C. and Childs,M.E.: 'Wall-Wake Velocity Profiles for Compressible Non-Adiabatic flows'. AIAA Journal, Vol.14, p.820, 1976.

Task Terminals: 'MOS System Manual- Unitech Corporation'. Task Terminals Ltd., London, 1975.

Townsend,A.A.: 'Equilibrium Layers and Wall Turbulence'. Journal of Fluid Mechanics, Vol.11, p.87, 1961.

van Driest,E.R.: 'Turbulent Boundary Layer in Compressible Fluids'. Journal of Aero. Science, Vol.18, p.145, 1951.

van Driest,E.R.: 'The Problem of Aerodynamic Heating'. Aeronautical Eng. Review, Vol.15, p.26, 1956.

Voisinet,R.L.P. and Lee,R.E.: 'Measurements of a Mach 4.9 Zero Pressure Gradient Boundary Layer with Heat Transfer'. Naval Ordnance Laboratory, Technical Report 72-232, 1972.

VF Instruments: 'High Speed Data Acquisition System Manual'. VF Instruments Ltd., Northgate Mansions, Gloucester, 1977.

von Karman,T.: 'The Problem of Resistance in Compressible Fluids'. Proc. of the 5th Volta Conference, Rome, 1935.

Wagner,R.D.; Maddalon,D.V.; Weinstein,L.M. and Henderson,A.: 'Influence of Measured Free-Stream Disturbances on Hypersonic Boundary Layer Transition'. AIAA Paper 69-704, 1969.

Wallace,J.E.: 'Hypersonic Turbulent Boundary Layer Measurements using an Electron Beam'. Cornell Aeronautical Laboratory, Report CAL No. AN-2112-Y-1, 1968.

Walz,A.: 'Compressible Turbulent Boundary Layers'. In Mechanics of Turbulence, Favre,A (editor), Gordon-Beech, New York, 1964.

Walz,A.: 'Boundary Layers of Flow and Temperature'. M.I.T. Press, Mass., 1969.

Watson,R.D.; Harris,J.E. and Anders,J.B.: 'Measurements in a Transitional/Turbulent Mach 10 Boundary Layer at High Reynolds Number'. AIAA Paper No. 73-165, 1973.

Watson,R.D.: 'Wall Cooling Effects On Hypersonic Transitional/Turbulent Boundary Layers at High Reynolds Numbers'. AIAA Journal, Vol.15, p.1455, 1977.

Watson,R.D.: 'Characteristics of Mach 10 Transitional and Turbulent Boundary Layers'. NASA Technical Paper, TP 1243, 1979.

White,F.M.: 'Viscous Fluid Flow'. McGraw-Hill, New York, 1974.

Whitfield,D.L.: 'Analytical, Numerical and Experimental Results on Turbulent Boundary Layers'. ARO Inc., Arnold Air Force Station, Tenn., AEDC-TR-76-62, 1976.

Whitfield,D.L. and High,M.D.: 'Velocity-Temperature Relationships in Turbulent Boundary Layers with Non-Unity Prandtl Numbers'. AIAA Journal, Vol.15, p.431, 1977.

Winkler,E.M. and Cha,M.H.: 'Investigation of Flat Plate Hypersonic Turbulent Boundary Layers with Heat Transfer at M = 5.2'. Naval Ordnance Laboratory, NAVORD Report 6631, 1959.

Winter,K.G.: 'An Outline of the Techniques Available for the Measurement of Skin Friction in Turbulent Boundary Layers'. Royal Aircraft Establishment, Technical Memo Aero 1656, 1975.

Winter,K.G.: 'Notes on the Measurement of Aerodynamic Heat Transfer in Model Testing Facilities'. Royal Aircraft Establishment, Technical Memo Aero 1657, 1976.

Yanta,W.J. and Lee,R.E.: 'Determination of Turbulence Transport Properties with the Laser Doppler Aneomometer and Conventional Time-Averaged Mean Flow Measurements at M = 3'. AIAA Paper No. 74-575, 1974.

Young,G.B.W. and Janssen,E.:'The Compressible Boundary Layer'. RAND Corp., Report P-214, 1951.

Zoric,D.L.:'Approach of Turbulent Boundary Layer to Similarity'. Colorado State University, Colorado, Report CER 68-69DLZ9, 1968.

		HP RUNNING CONDITION		LP RUNNING CONDITION	
Stagnation pressure,	p_o	6.667×10^7	Nm^{-2}	1.520×10^7	Nm^{-2}
Stagnation temperature,	$T_{o\infty}$	1064	^oK	997	^oK
Freestream Mach number,	M_∞	9.26		8.93	
Freestream static pressure,	p_∞	2.620×10^3	Nm^{-2}	7.583×10^2	Nm^{-2}
Freestream static temperature,	T_∞	58.62	^oK	58.85	^oK
Freestream unit Reynolds number,	Re_∞	5.51×10^7	m^{-1}	1.53×10^7	m^{-1}

TABLE 1 NO 2 GUN TUNNEL STANDARD OPERATING CONDITIONS

x	260	360	560	$\times 10^{-3}$ m
Re_x	3.978×10^6	5.508×10^6	8.568×10^6	
Re_θ	2962	3494	5617	
Re_{δ_2}	702	829	1333	
δ_p	7.75	9.75	13.00	$\times 10^{-3}$ m
δ_u	6.47	8.19	11.11	$\times 10^{-3}$ m
$\delta_1(\delta^*)$	3.2457	4.0316	6.0070	$\times 10^{-3}$ m
$\delta_2(\theta)$	0.1936	0.2284	0.3671	$\times 10^{-3}$ m
δ_3	0.3340	0.4041	0.5232	$\times 10^{-3}$ m
δ_4	0.1862	0.2130	0.3422	$\times 10^{-3}$ m
H_{12}	16.76	17.65	16.36	
H_{32}	1.725	1.769	1.425	
H_{42}	0.9618	0.9326	0.9224	
H_{12K}	1.60	1.58	1.52	
$\Delta \frac{\overline{U}^*}{U_\tau}$	0.1	0.7	1.1	
Δ^*	23.51	28.25	42.99	$\times 10^{-3}$ m
N	10.2	9.75	8.80	

TABLE 2 LP CONDITION TRIPPED BOUNDARY LAYER PROPERTIES ($T_w = 293^oK$)

x	360	460	560	$\times 10^{-3}$ m
Re_x	1.984×10^7	2.535×10^7	3.086×10^7	
Re_θ	9163	10220	12028	
Re_{δ_2}	2174	2425	2854	
δ_p	7.20	8.25	9.25	$\times 10^{-3}$ m
δ_u	6.34	6.85	7.68	$\times 10^{-3}$ m
$\delta_1 (\delta^*)$	2.9999	3.5687	4.5431	$\times 10^{-3}$ m
$\delta_2(\theta)$	0.1663	0.1855	0.2183	$\times 10^{-3}$ m
δ_3	0.2308	0.2409	0.2608	$\times 10^{-3}$ m
δ_4	0.1687	0.1731	0.1897	$\times 10^{-3}$ m
H_{12}	18.04	19.24	20.81	
H_{32}	1.388	1.299	1.195	
H_{42}	1.008	0.9676	0.8689	
H_{12K}	-	-	-	
$\Delta\frac{\overline{U}^*}{U_\tau}$	1.5	1.8	2.2	
Δ^*	23.79	30.66	36.26	$\times 10^{-3}$ mm
N	8.8	8.6	7.7	

TABLE 3 HP CONDITION BOUNDARY LAYER PROPERTIES ($T_w = 293^oK$)

FIGURES

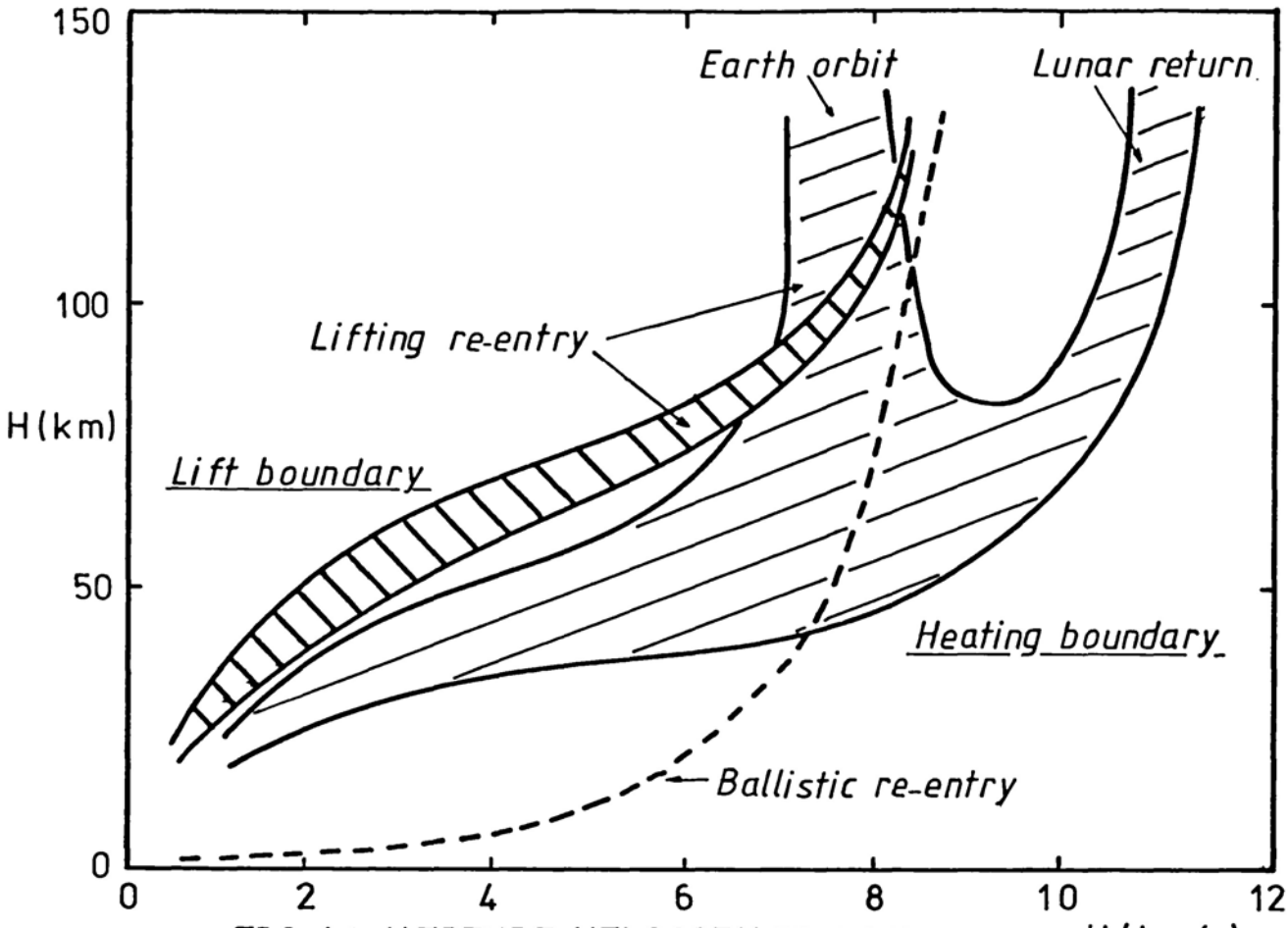


FIG. 1-1 ALTITUDE-VELOCITY TRAJECTORIES

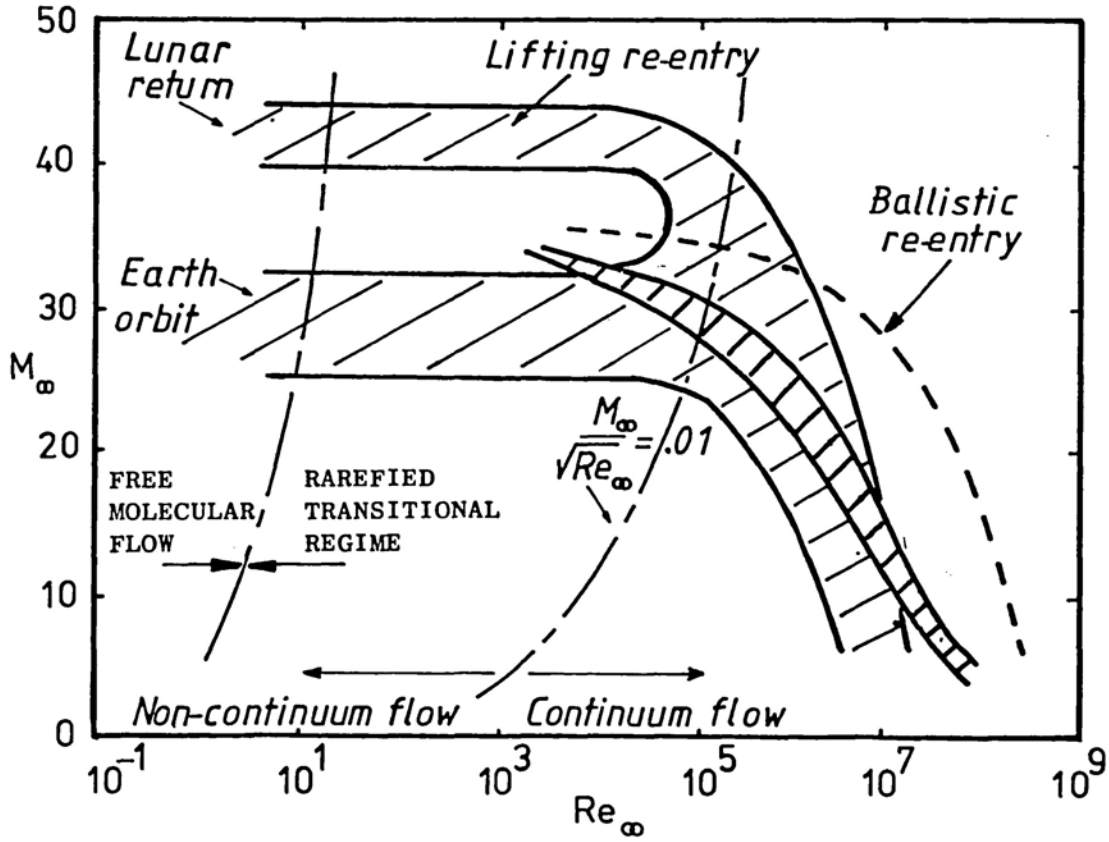


FIG. 1-2 MACH-REYNOLDS NO. TRAJECTORIES

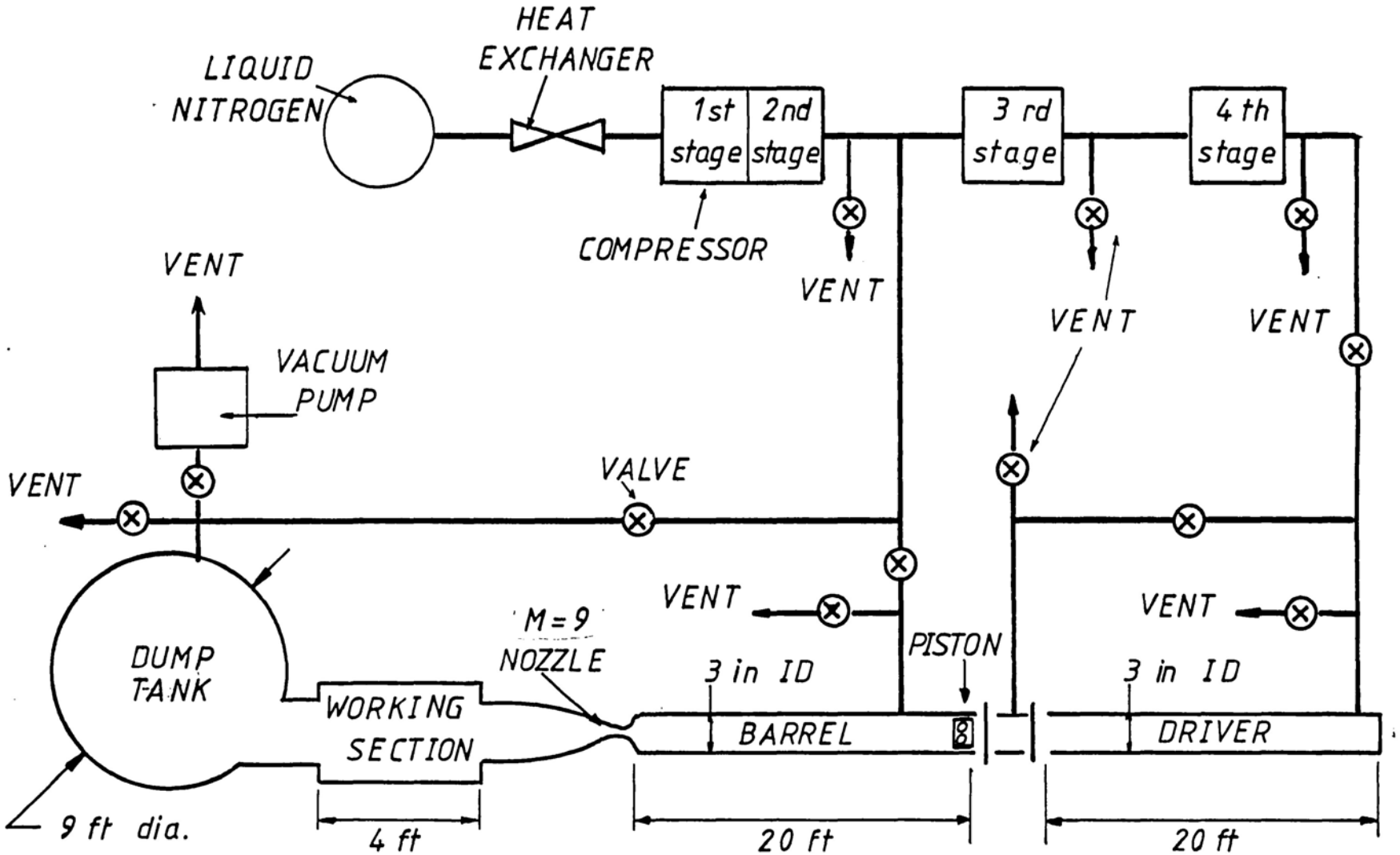


FIG. 3-1 SCHEMATIC OF GUN TUNNEL

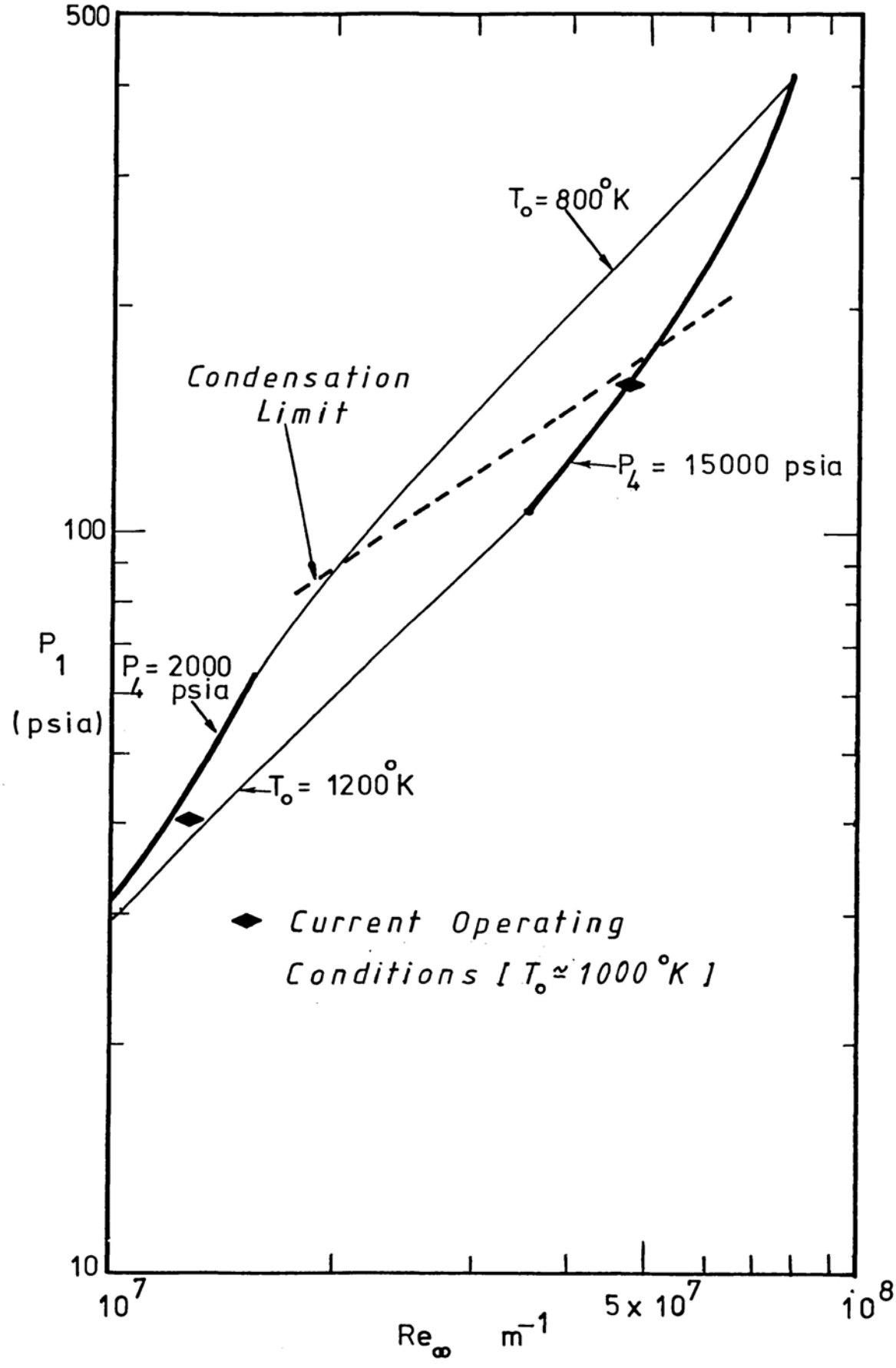


FIG. 3-2 PERFORMANCE ENVELOPE OF THE NO. 2 GUN TUNNEL

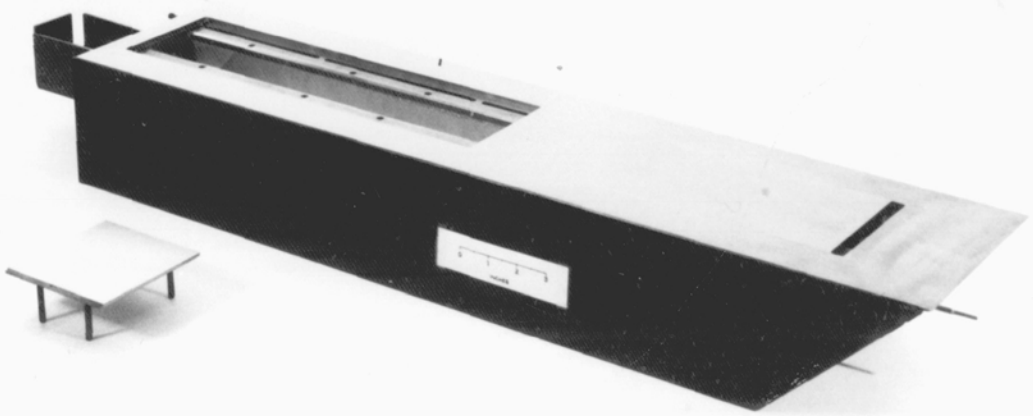


FIG. 3.3: MODULAR FLAT PLATE MODEL

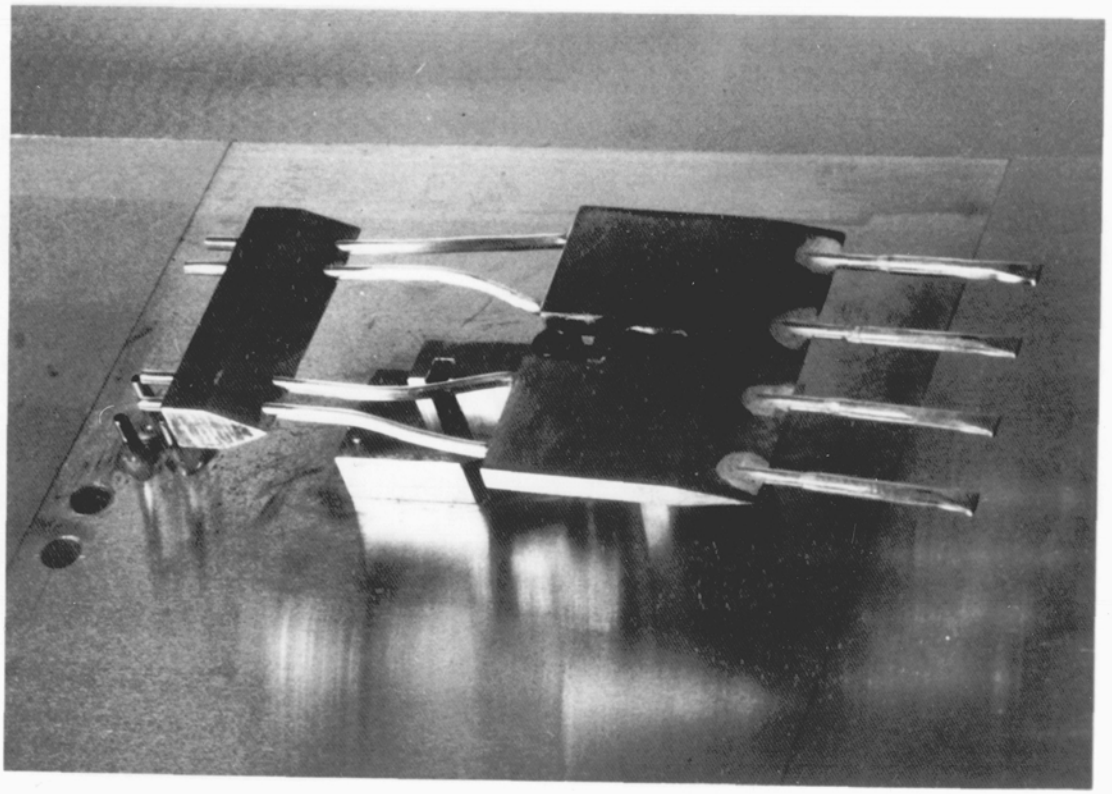


FIG. 3.4: PITOT TUBE RAKE

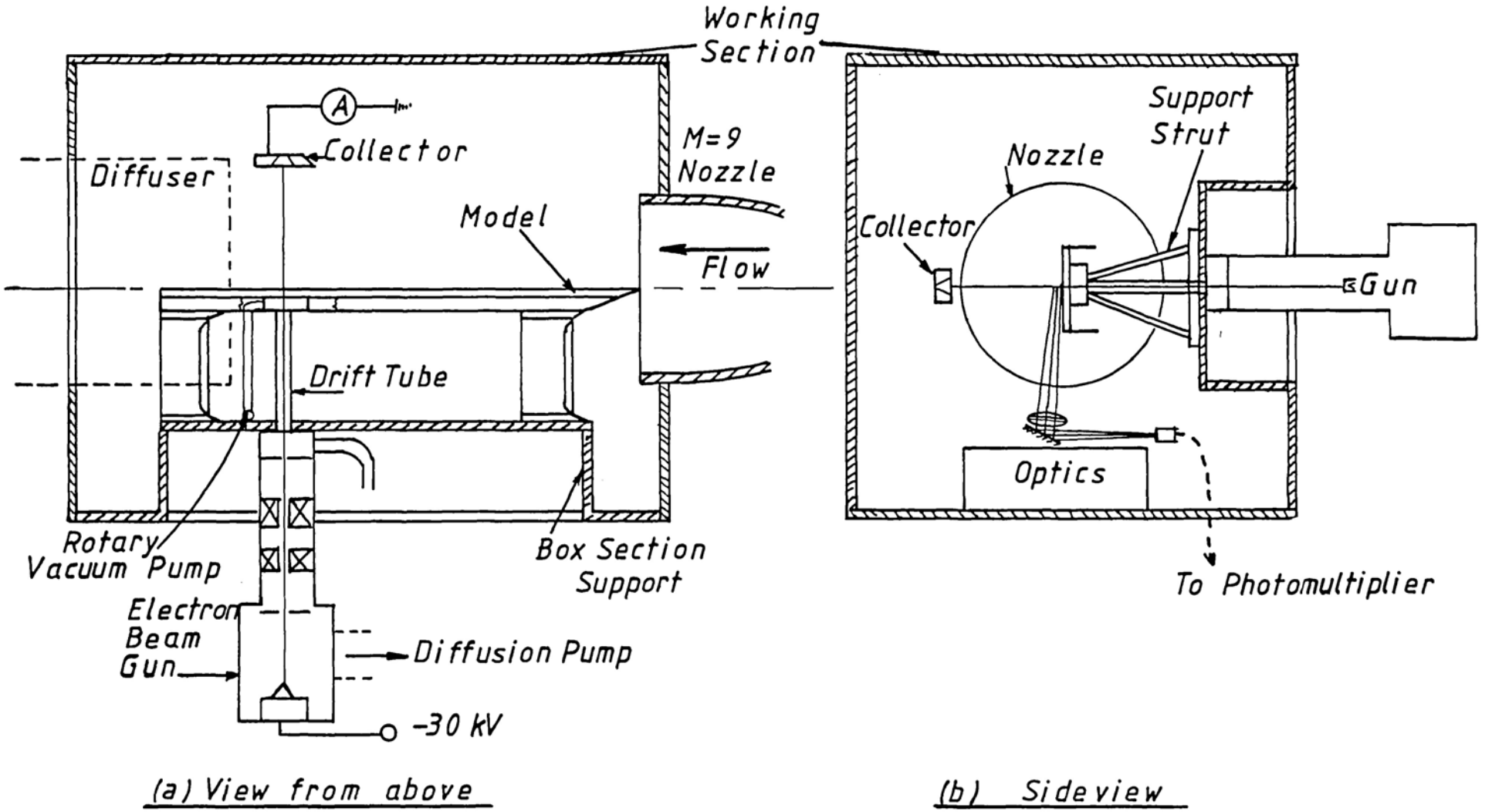


FIG. 4-1 SCHEMATIC OF THE EXPERIMENTAL ARRANGEMENT OF THE EQUIPMENT USED TO OBTAIN THE ELECTRON BEAM FLUORESCENCE DATA.

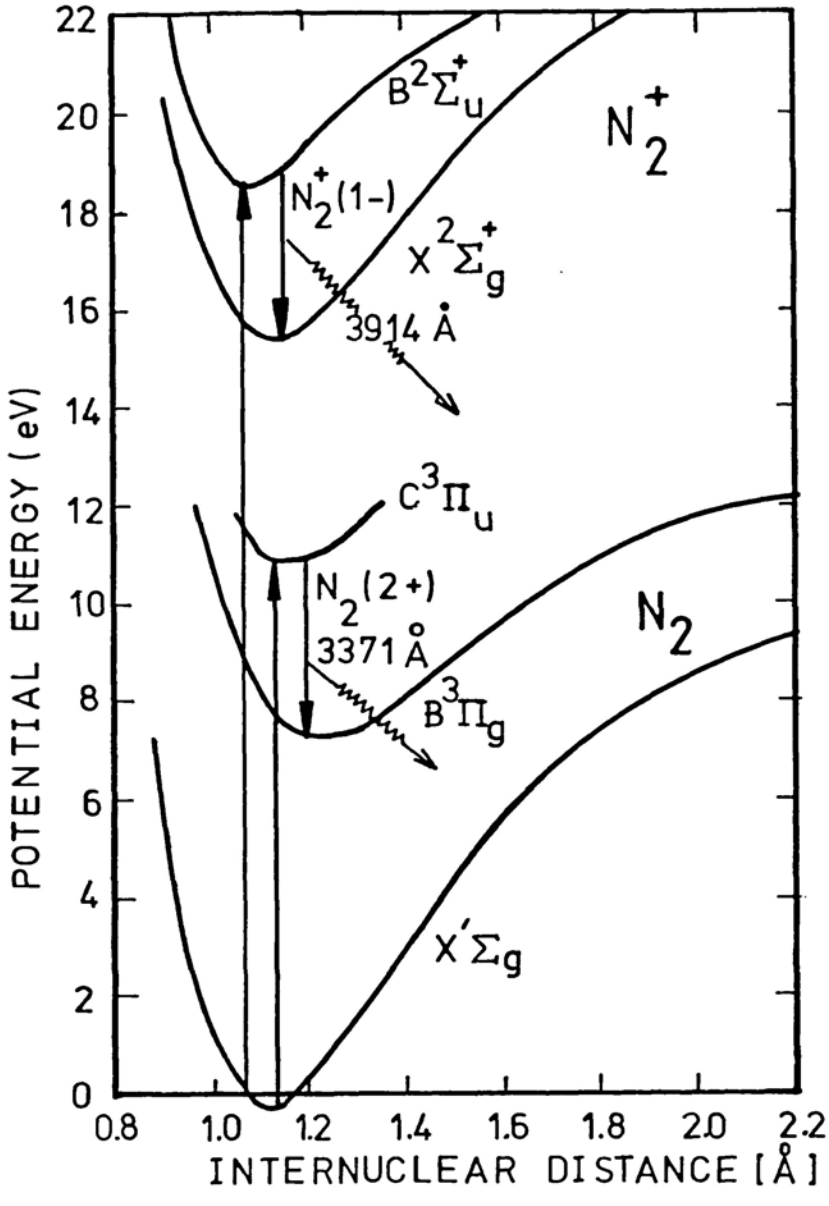


FIG. 4-2 SIMPLIFIED POTENTIAL ENERGY DIAGRAM FOR N_2 SHOWING ELECTRON EXCITATION AND RADIATION FROM THE $N_2^+(1-)$ AND $N_2(2+)$ BANDS.

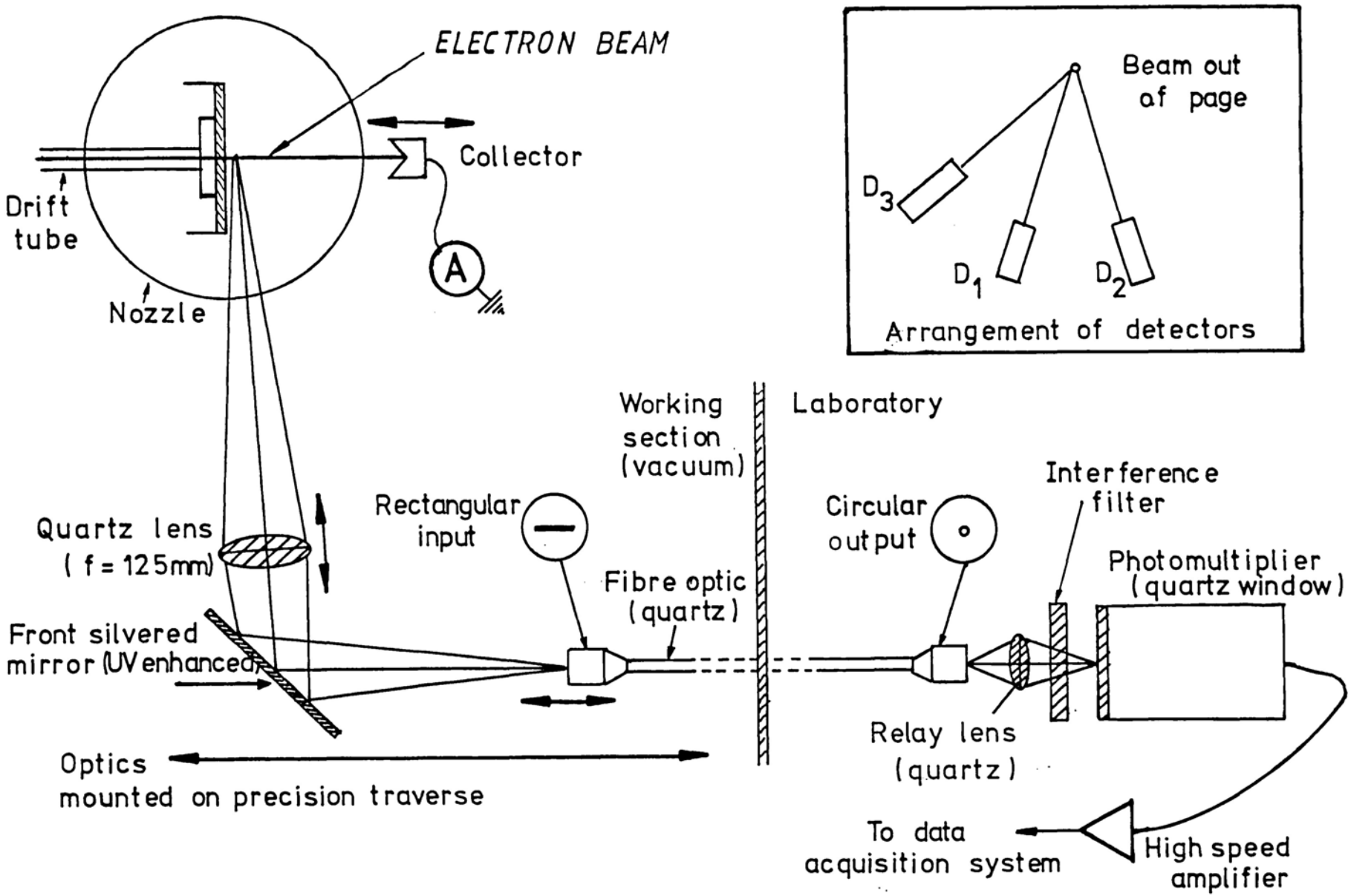


FIG. 4-3 SCHEMATIC OF THE OPTICAL SYSTEM.

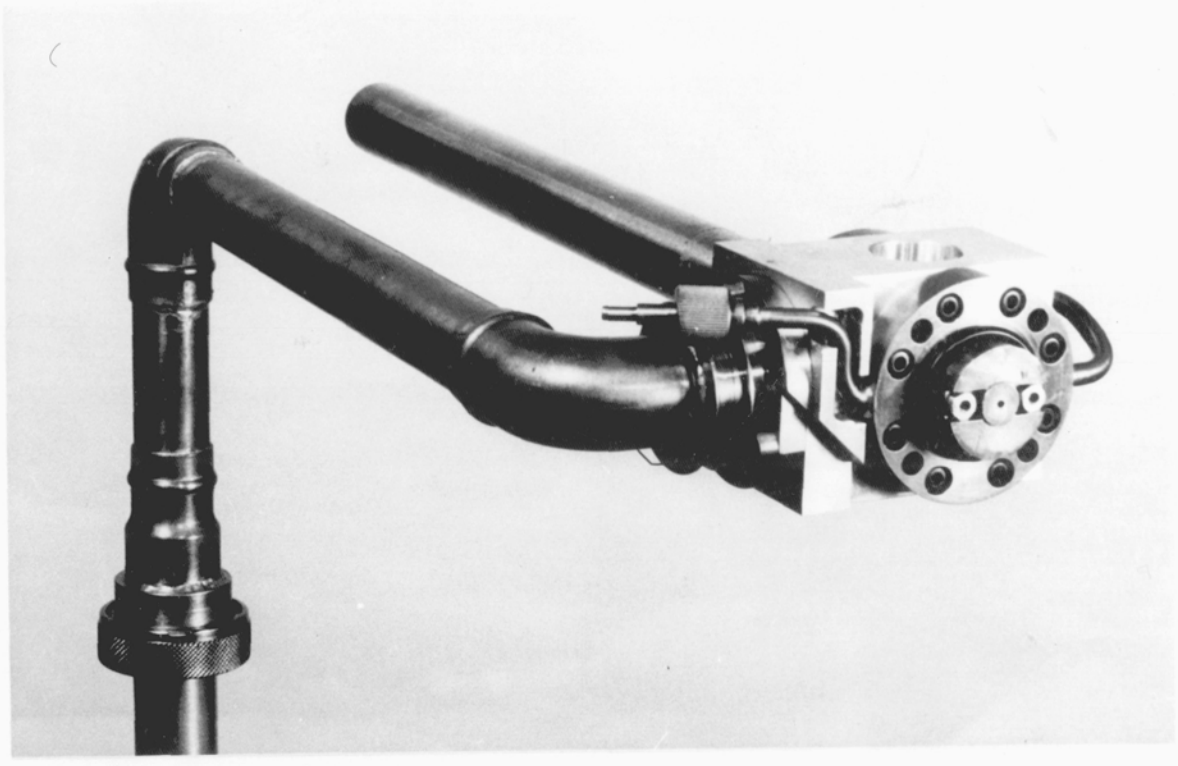


FIG. 4.4: DRIFT TUBE ASSEMBLY

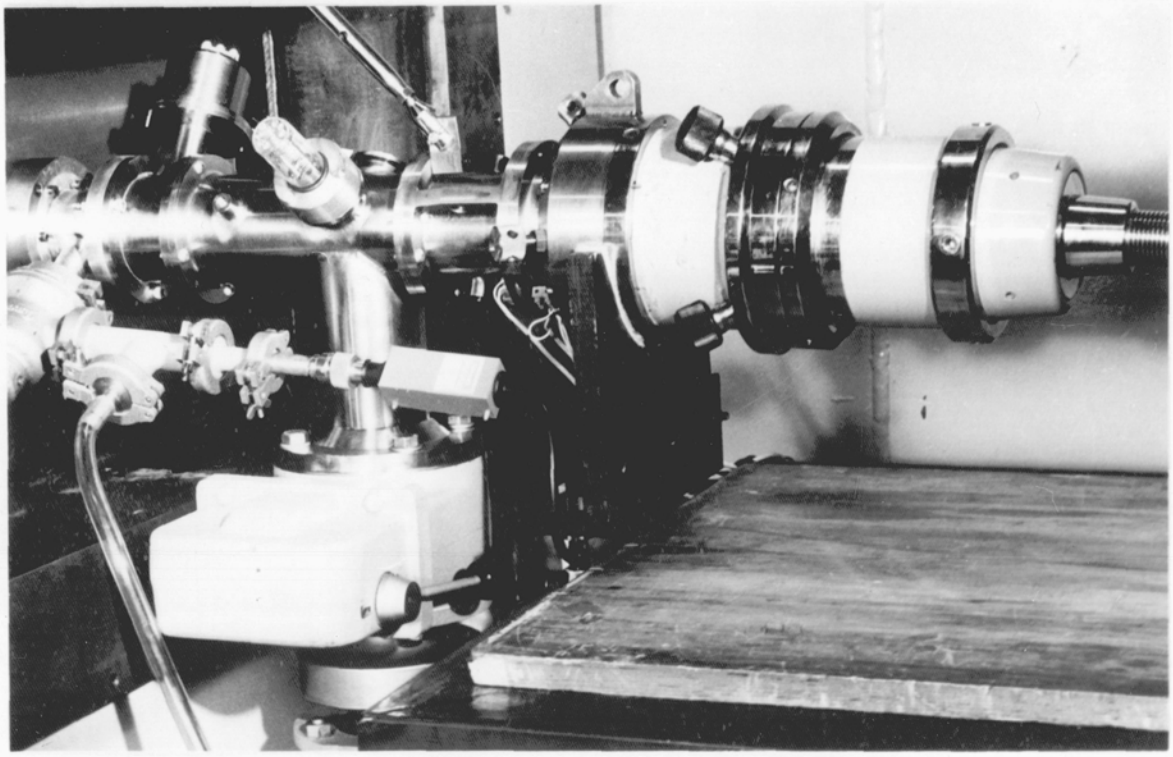


FIG. 4.5: ELECTRON BEAM GUN

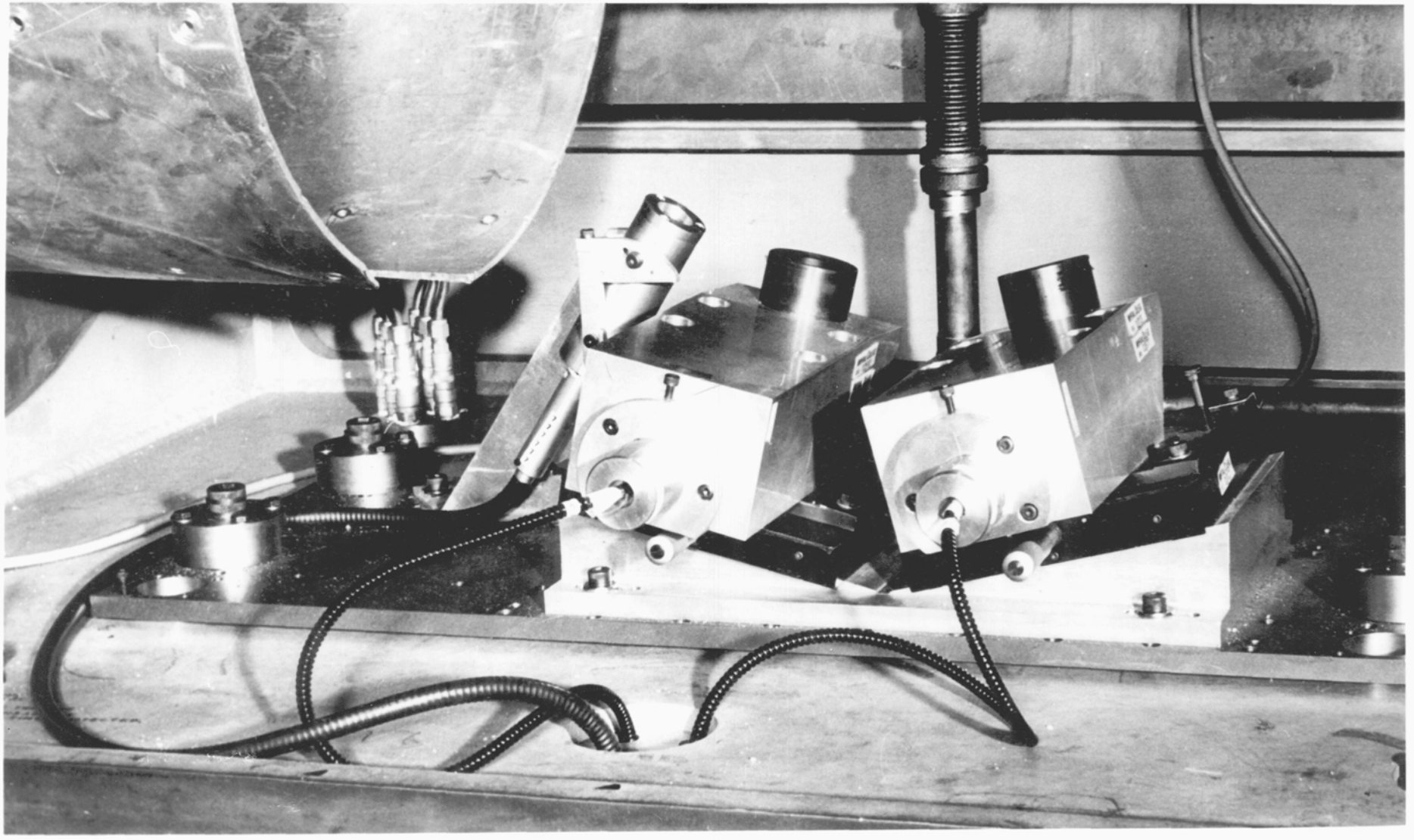


FIG. 4.6: OPTICAL DETECTORS

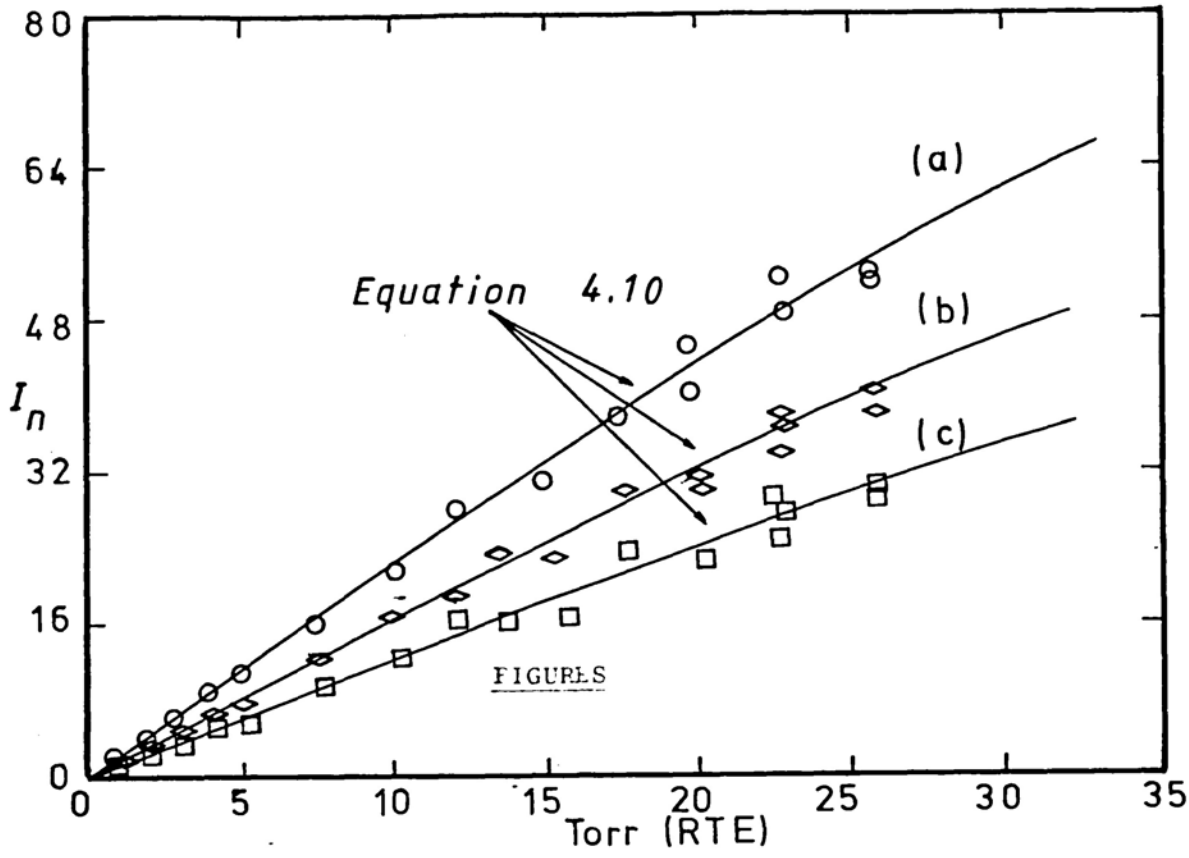


FIG. 4-7 DEPENDENCE OF FLUORESCENT LIGHT INTENSITY ON DENSITY FOR THE THREE BOUNDARY LAYER DETECTORS

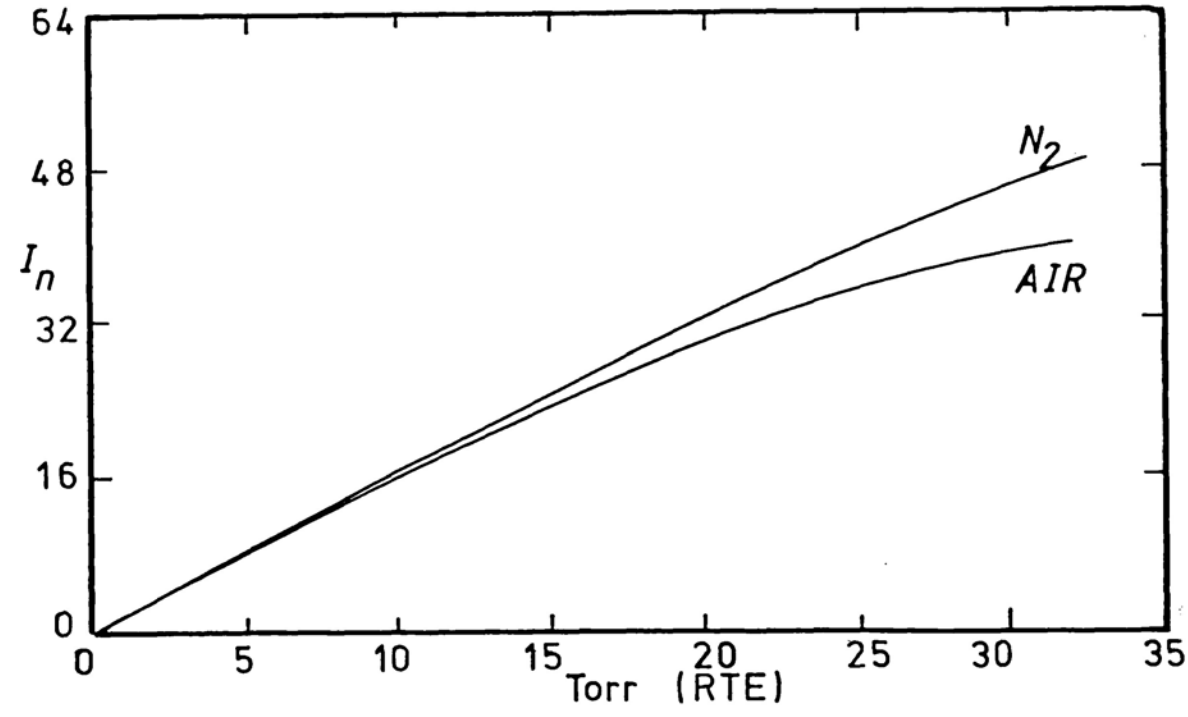


FIG. 4-8 QUENCHING EFFECT OF OXYGEN ON FLUORESCENT LIGHT INTENSITY

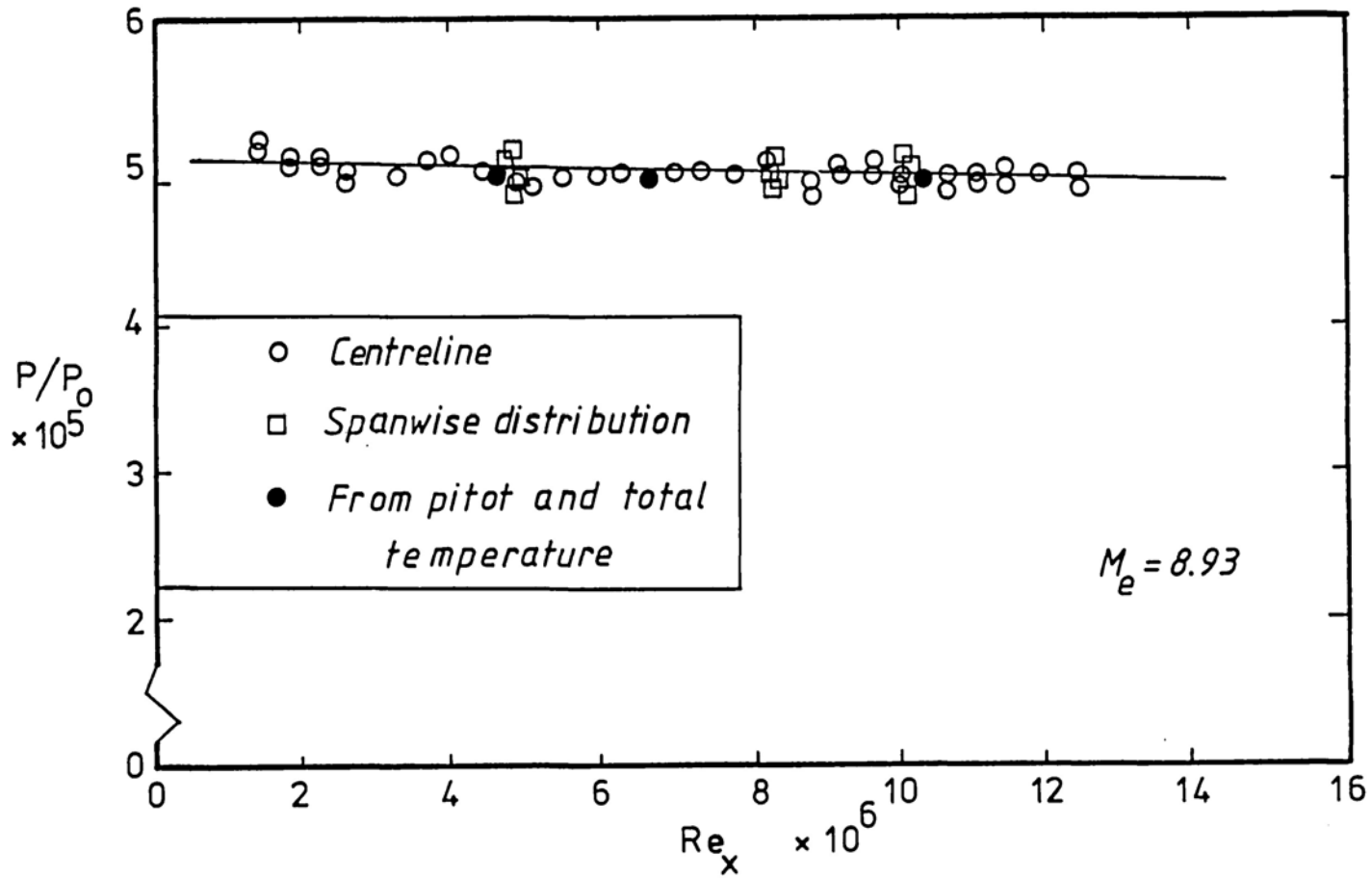


FIG. 5-1 LP CONDITION: SURFACE PRESSURE DISTRIBUTION

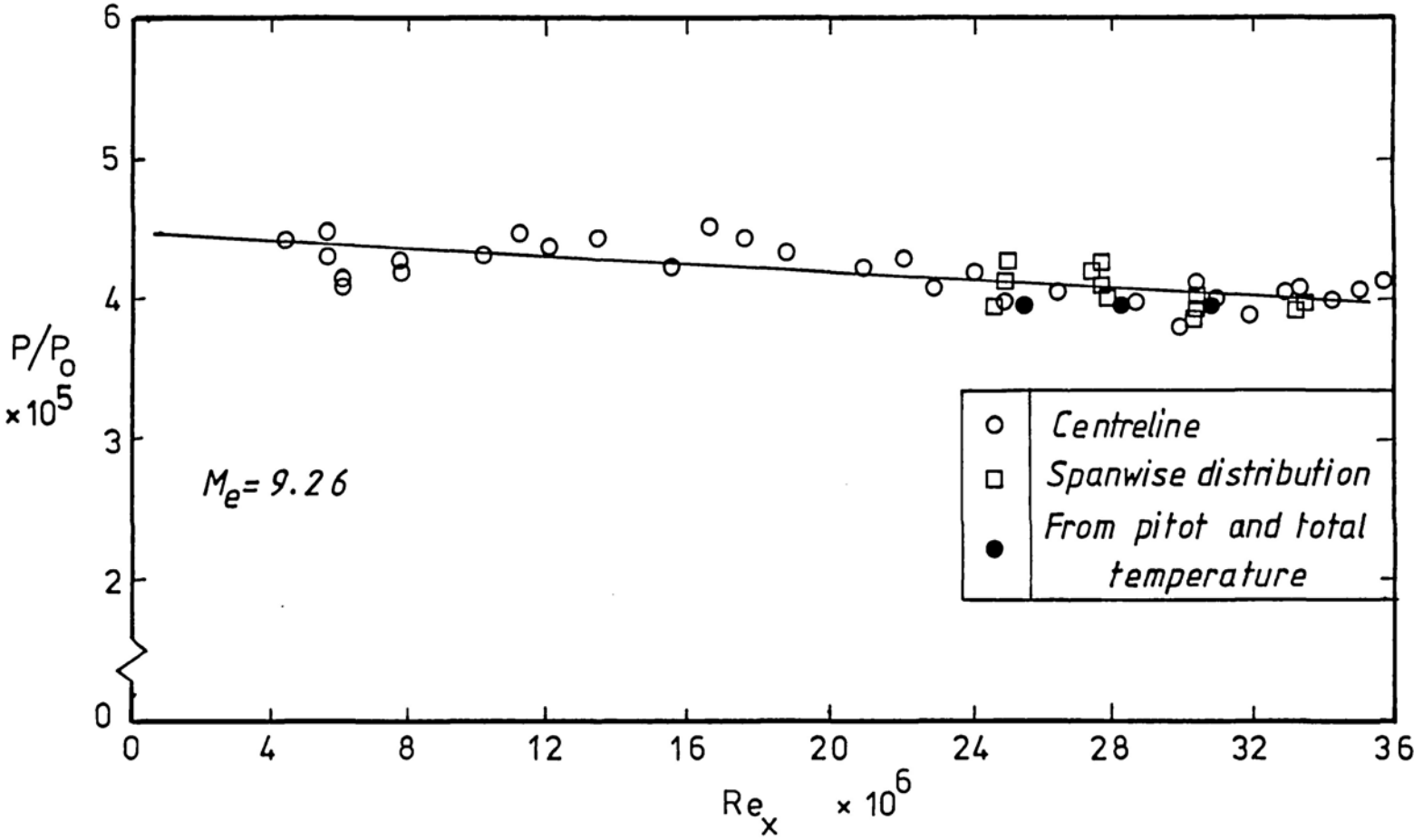


FIG. 5-2 HP CONDITION: SURFACE PRESSURE DISTRIBUTION

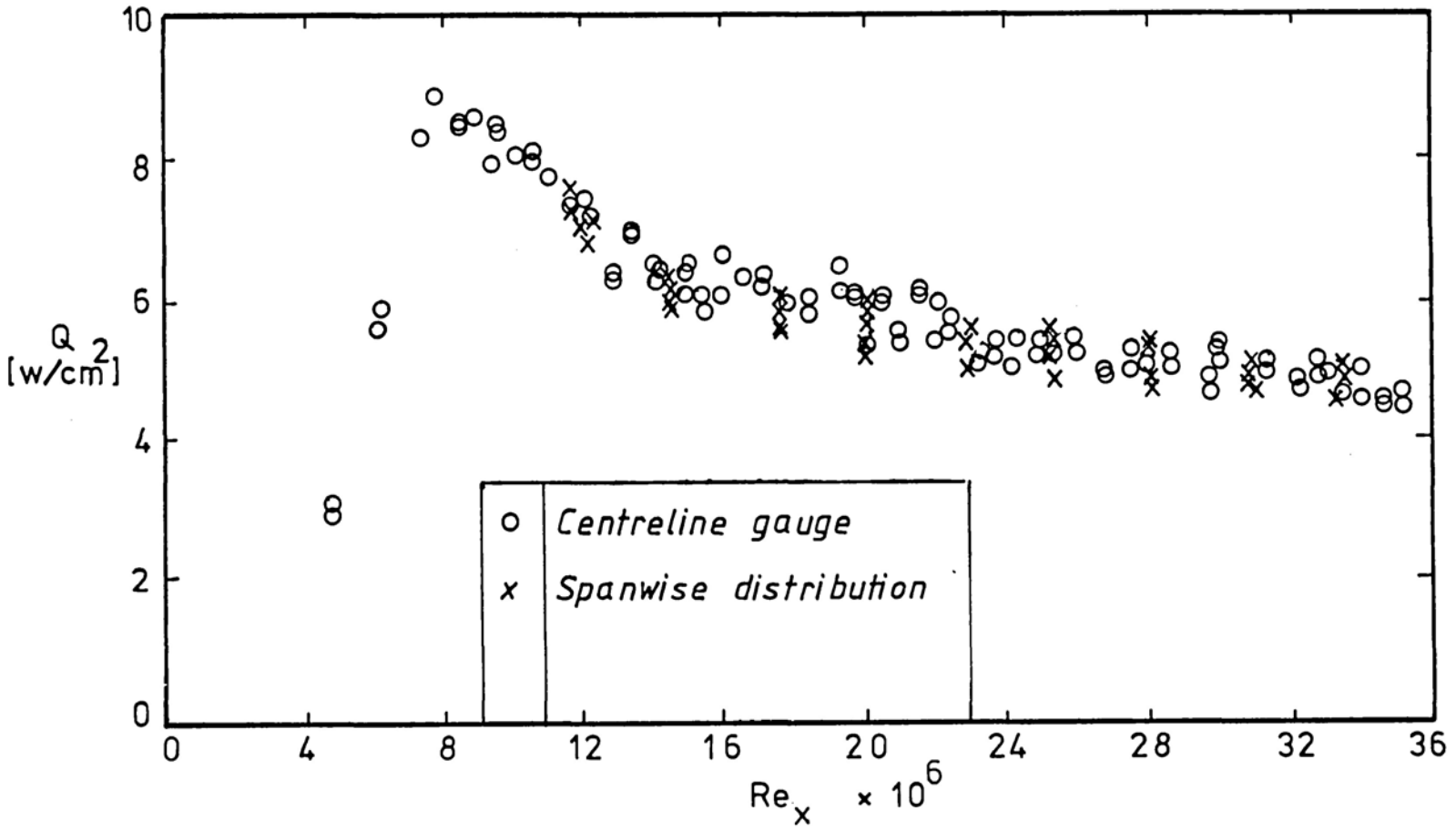


FIG. 5-3 HP CONDITION: HEAT TRANSFER DISTRIBUTION

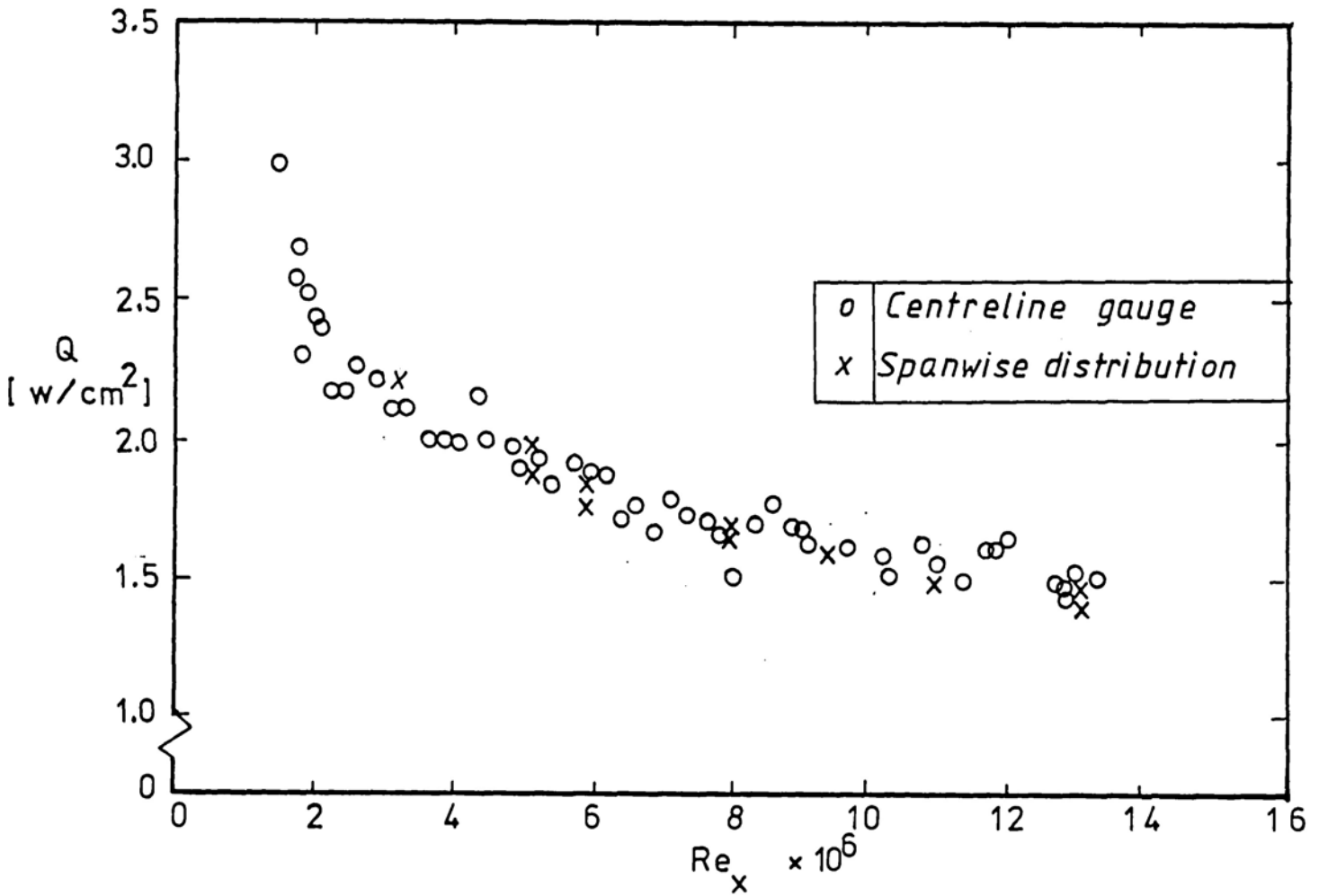


FIG. 5-4 LP CONDITION: HEAT TRANSFER DISTRIBUTION (AFTER COLEMAN(1973))

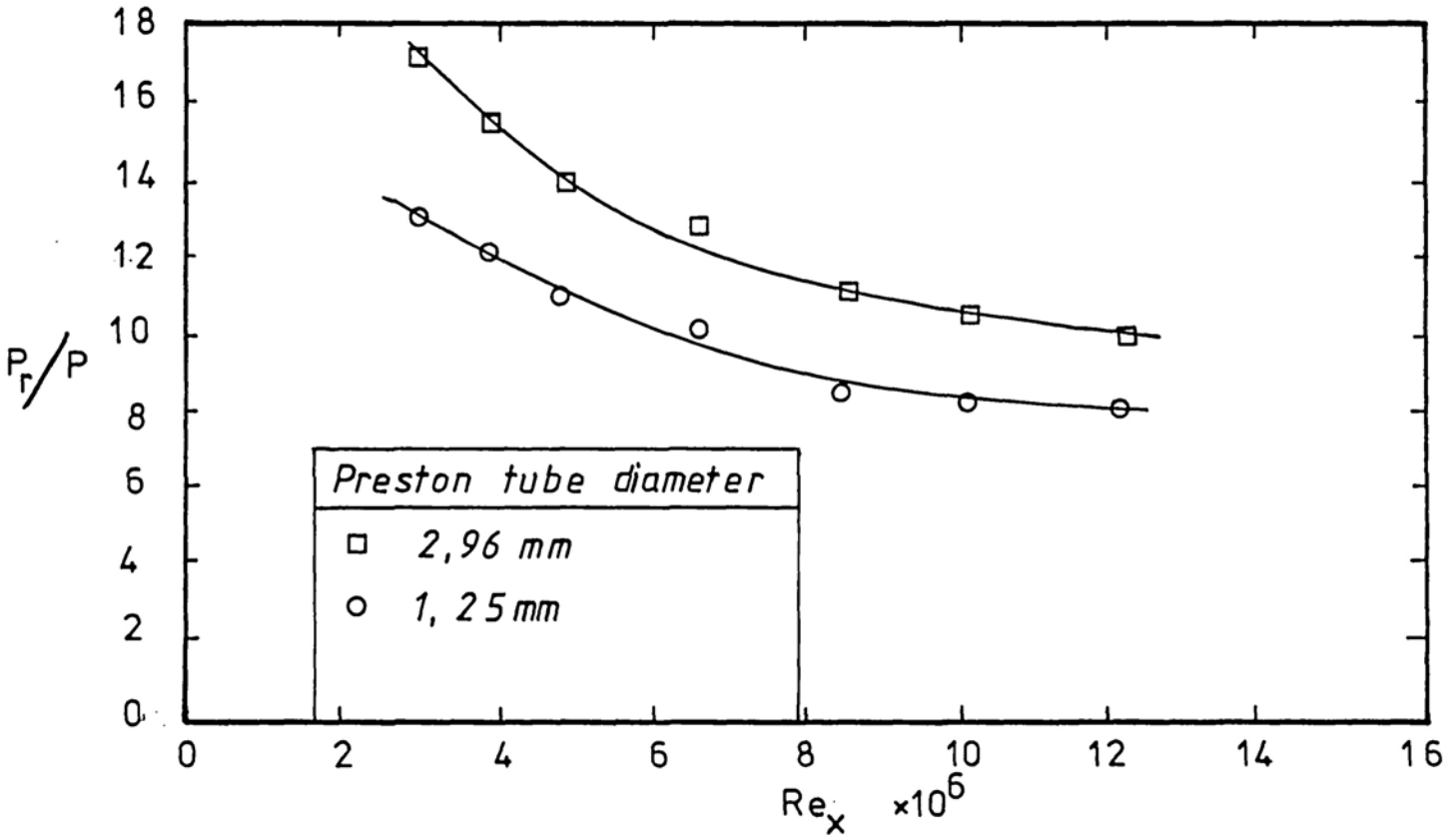


FIG. 5-5 LP CONDITION: SURFACE IMPACT PRESSURE DISTRIBUTION

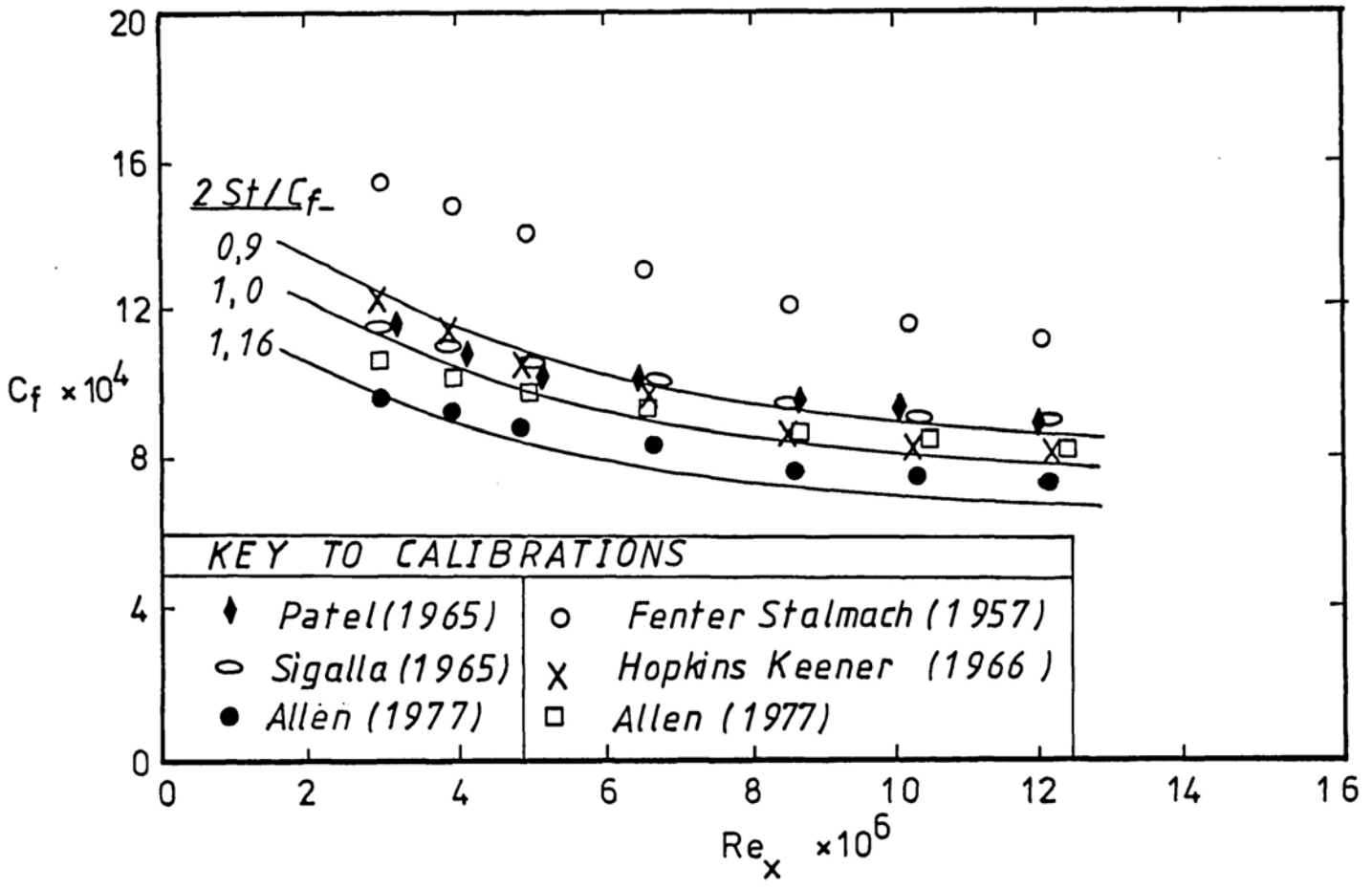


FIG. 5-6 LP CONDITION: C_f FROM PRESTON TUBE CALIBRATIONS

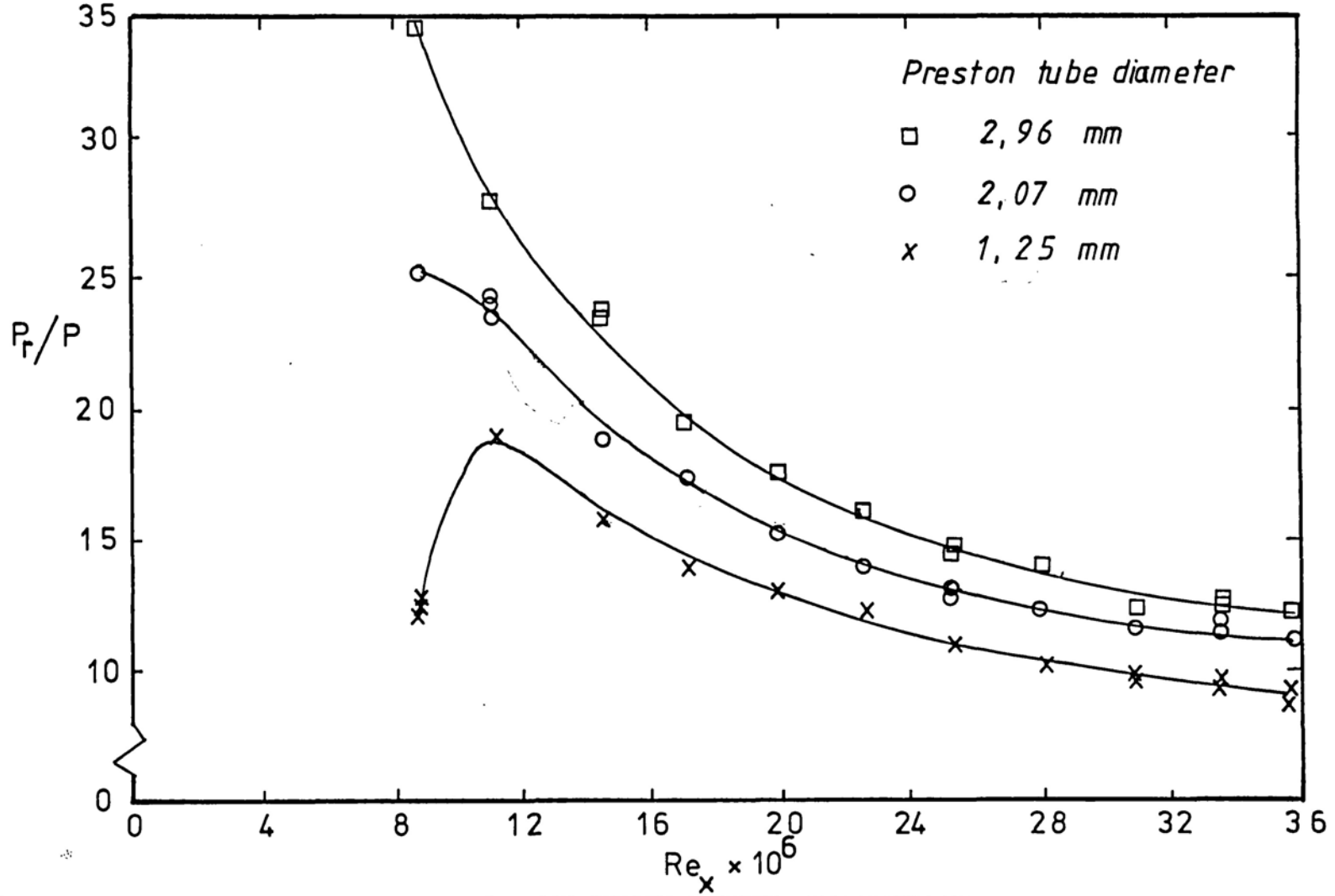


FIG. 5-7 HP CONDITION: SURFACE IMPACT PRESSURE DISTRIBUTION

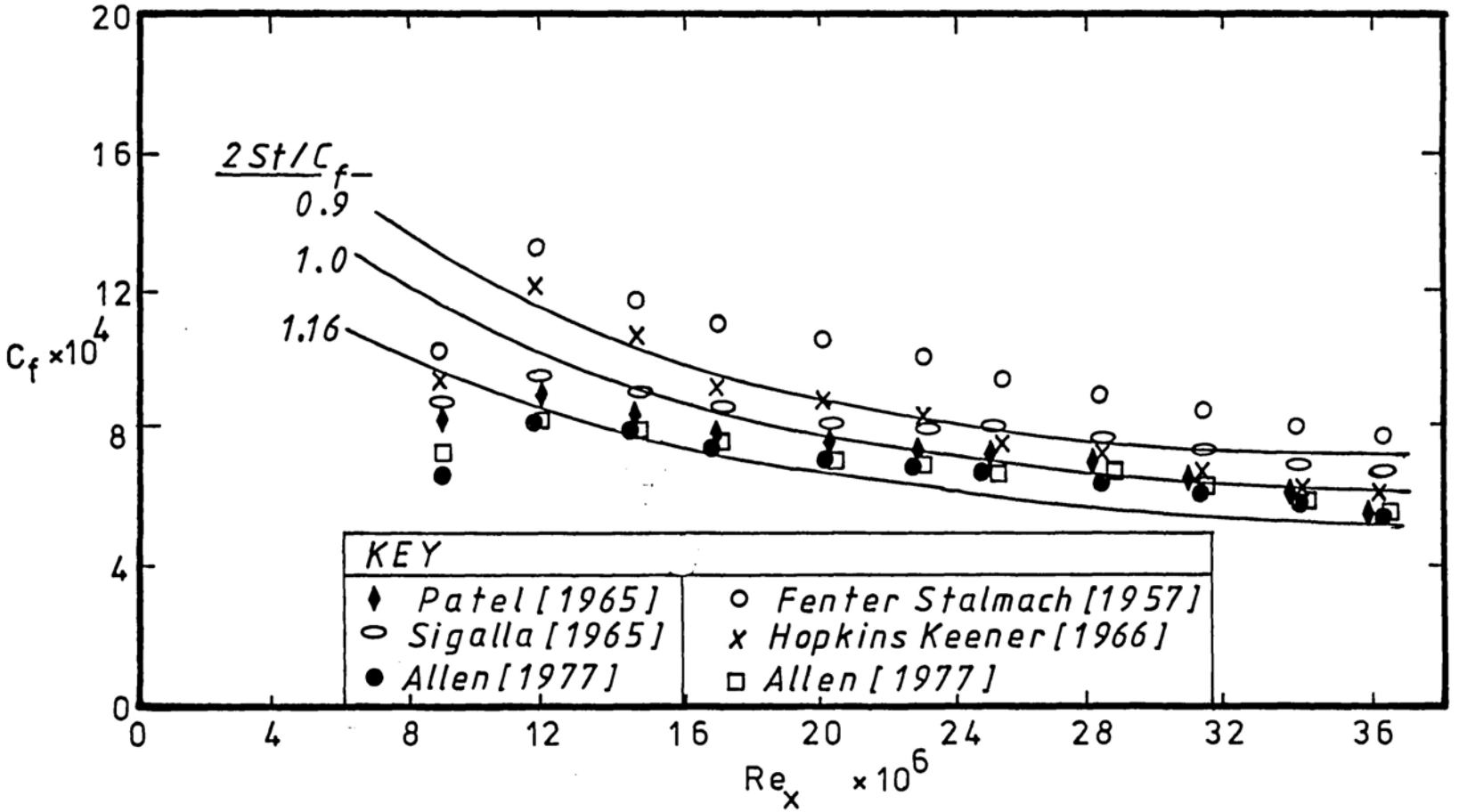


FIG. 5-8 HP CONDITION: C_f FROM PRESTON TUBE CALIBRATIONS

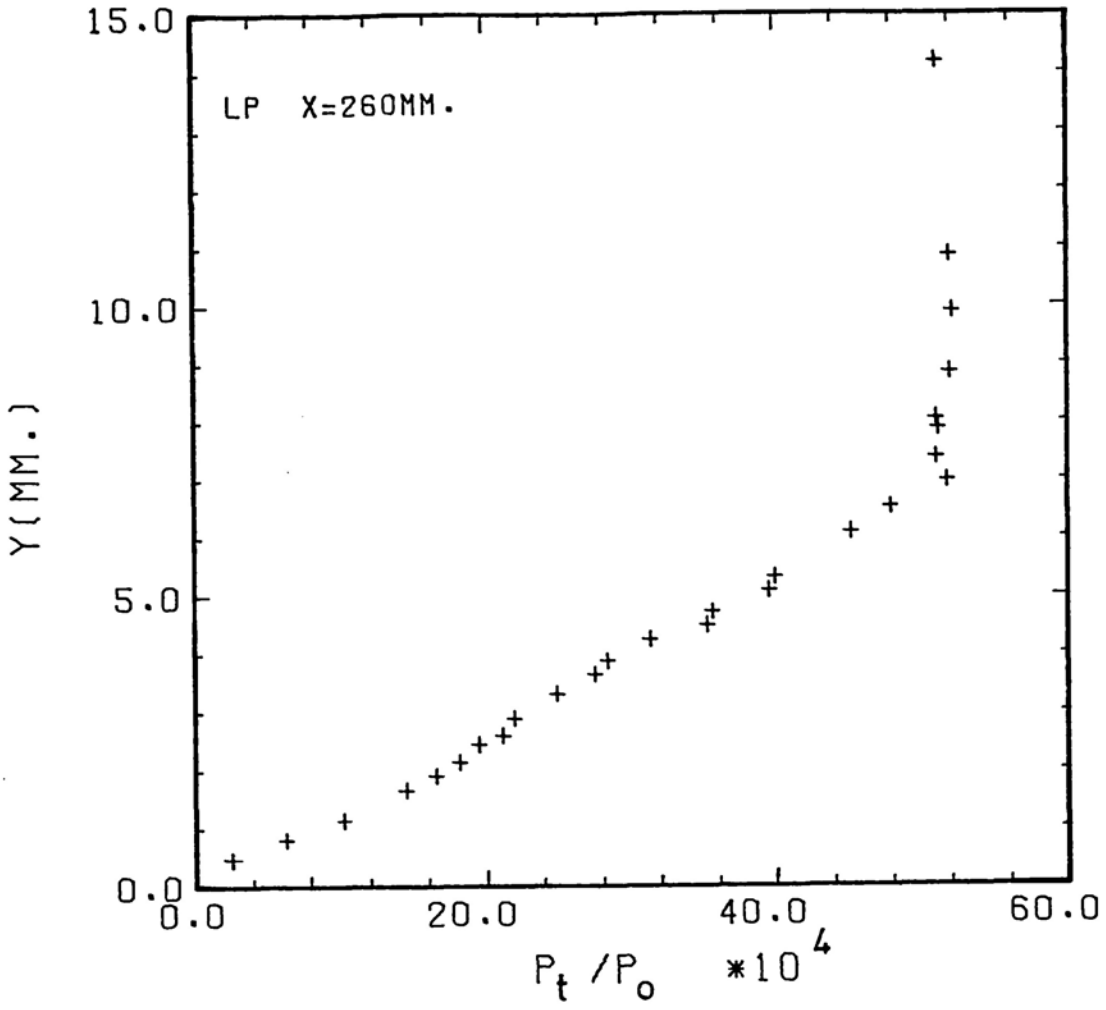


FIG. 5-9a LP CONDITION: PITOT PRESSURE PROFILE x = 260mm

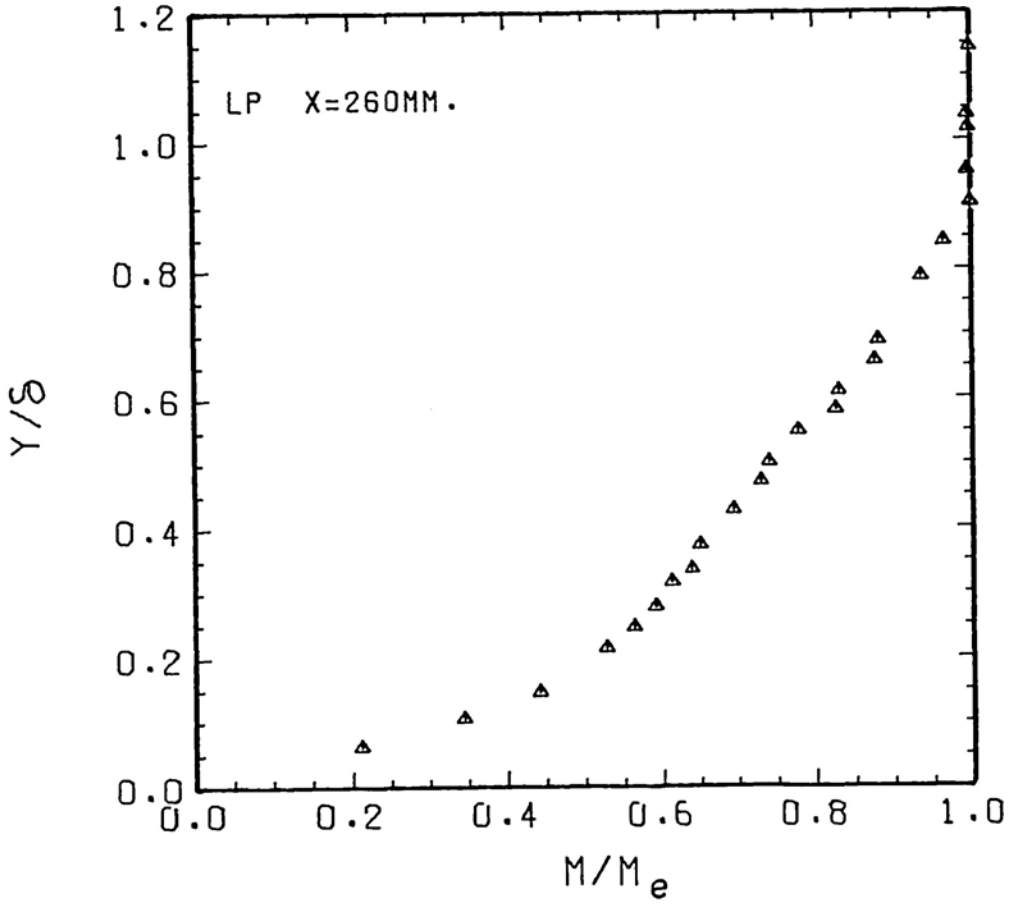


FIG. 5-10a LP CONDITION: MACH NUMBER PROFILE x = 260mm

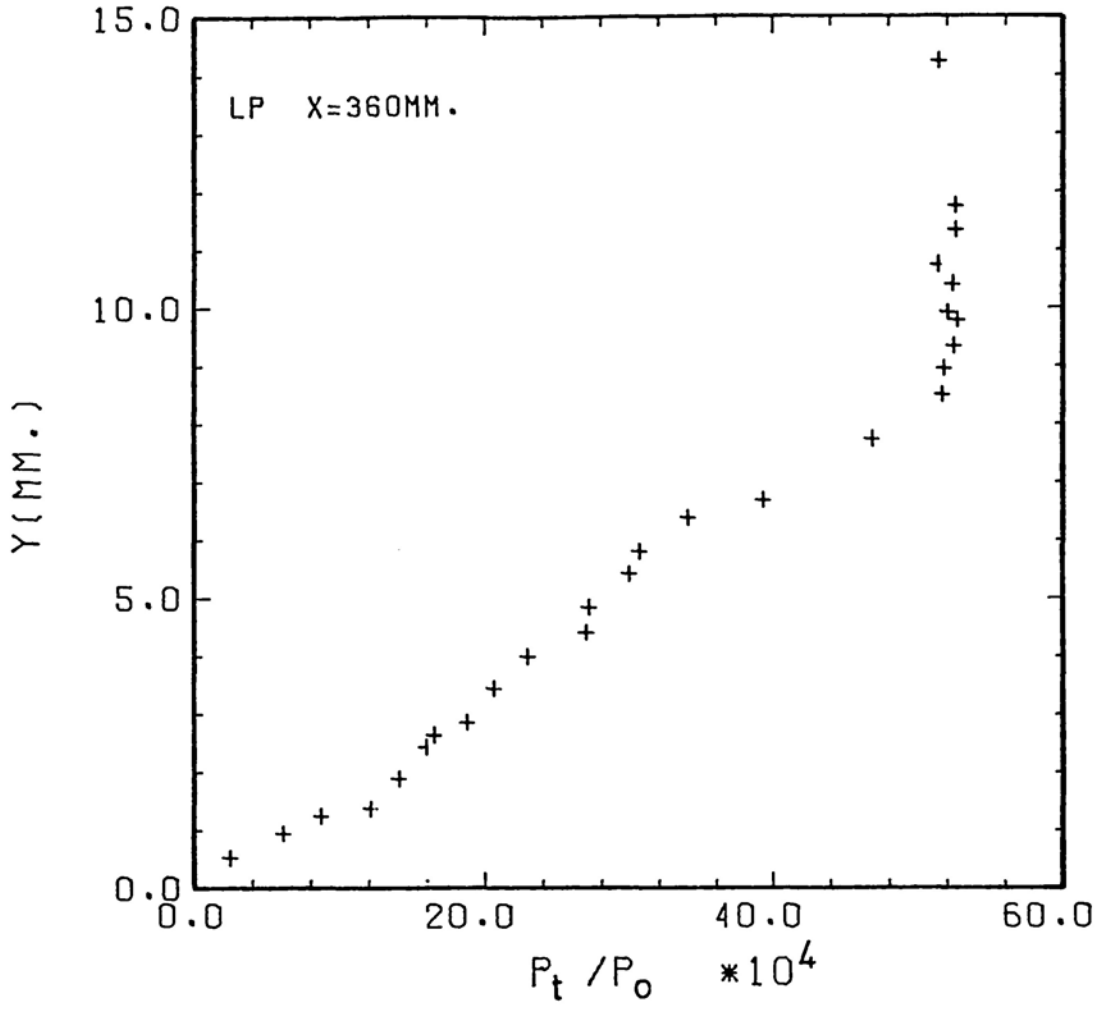


FIG. 5-9b LP CONDITION: PITOT PRESSURE PROFILE x = 360mm

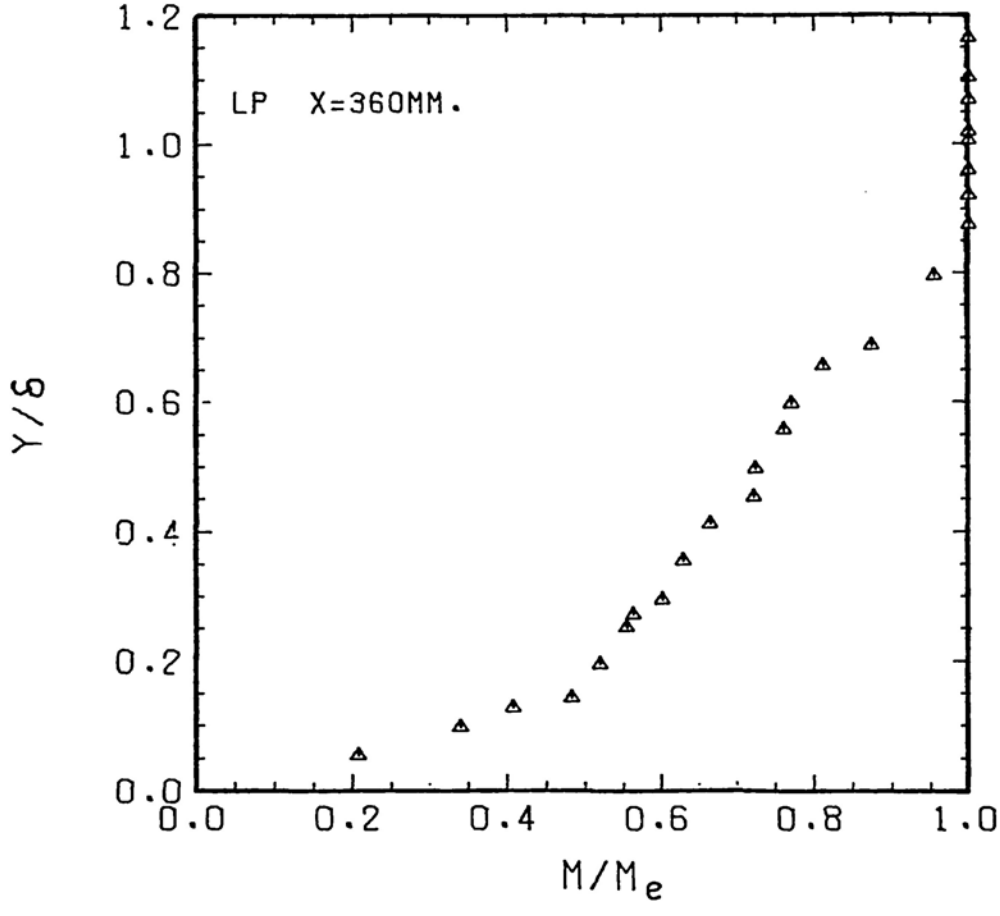


FIG. 5-10b LP CONDITION: MACH NUMBER PROFILE x = 360mm

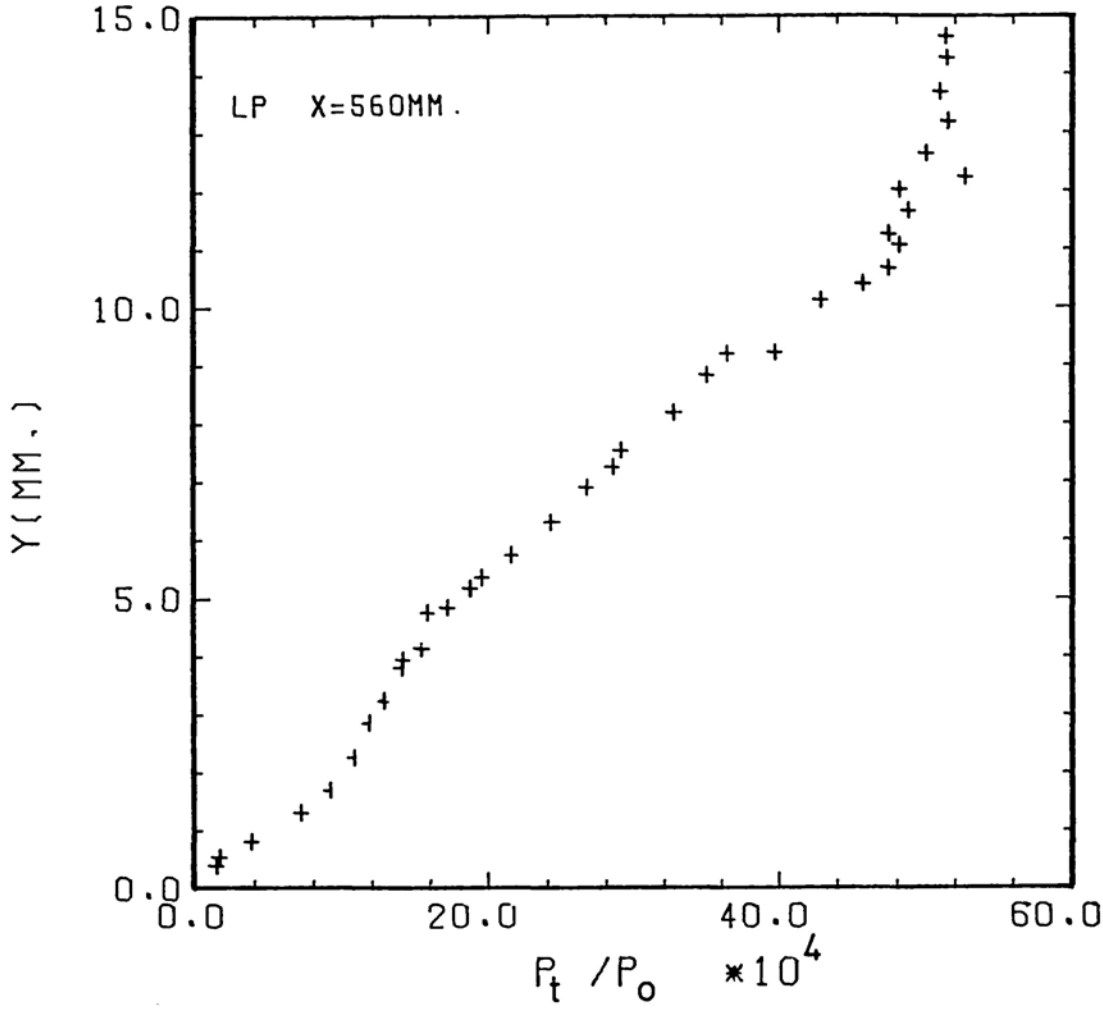


FIG. 5-9c LP CONDITION: PITOT PRESSURE PROFILE x = 560mm

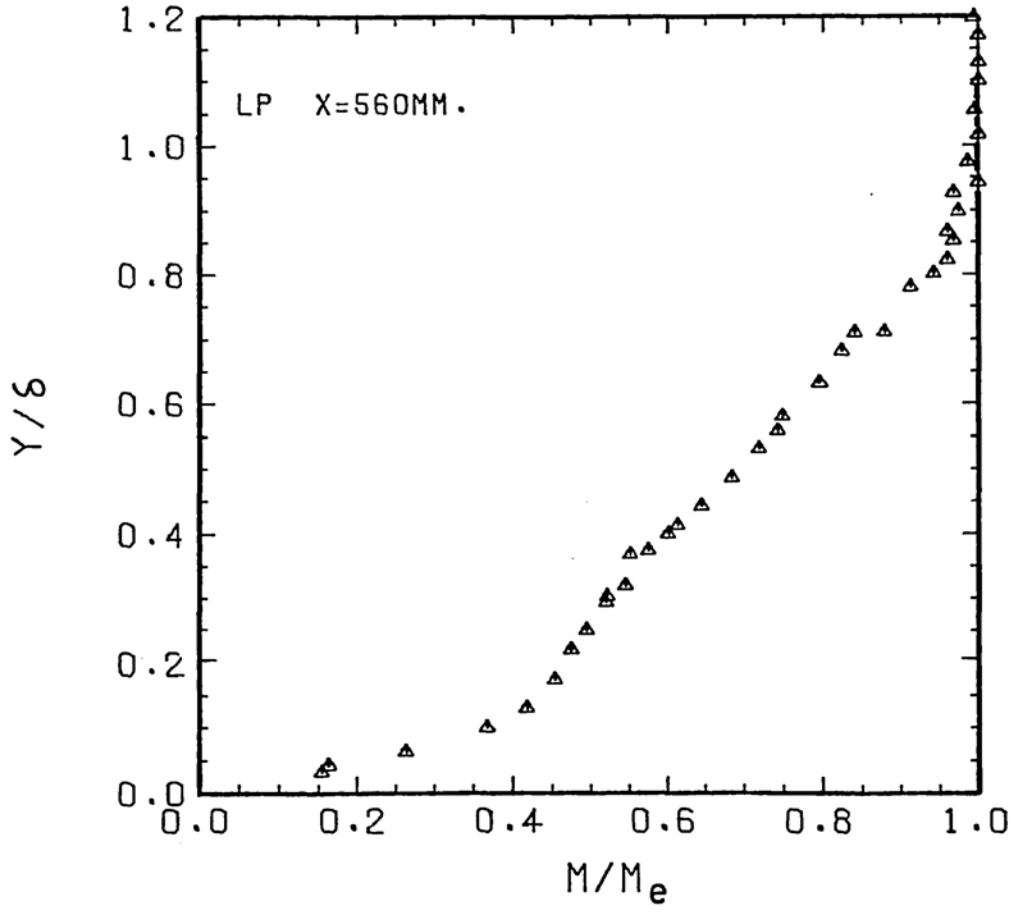


FIG. 5-10c LP CONDITION: MACH NUMBER PROFILE x = 560mm

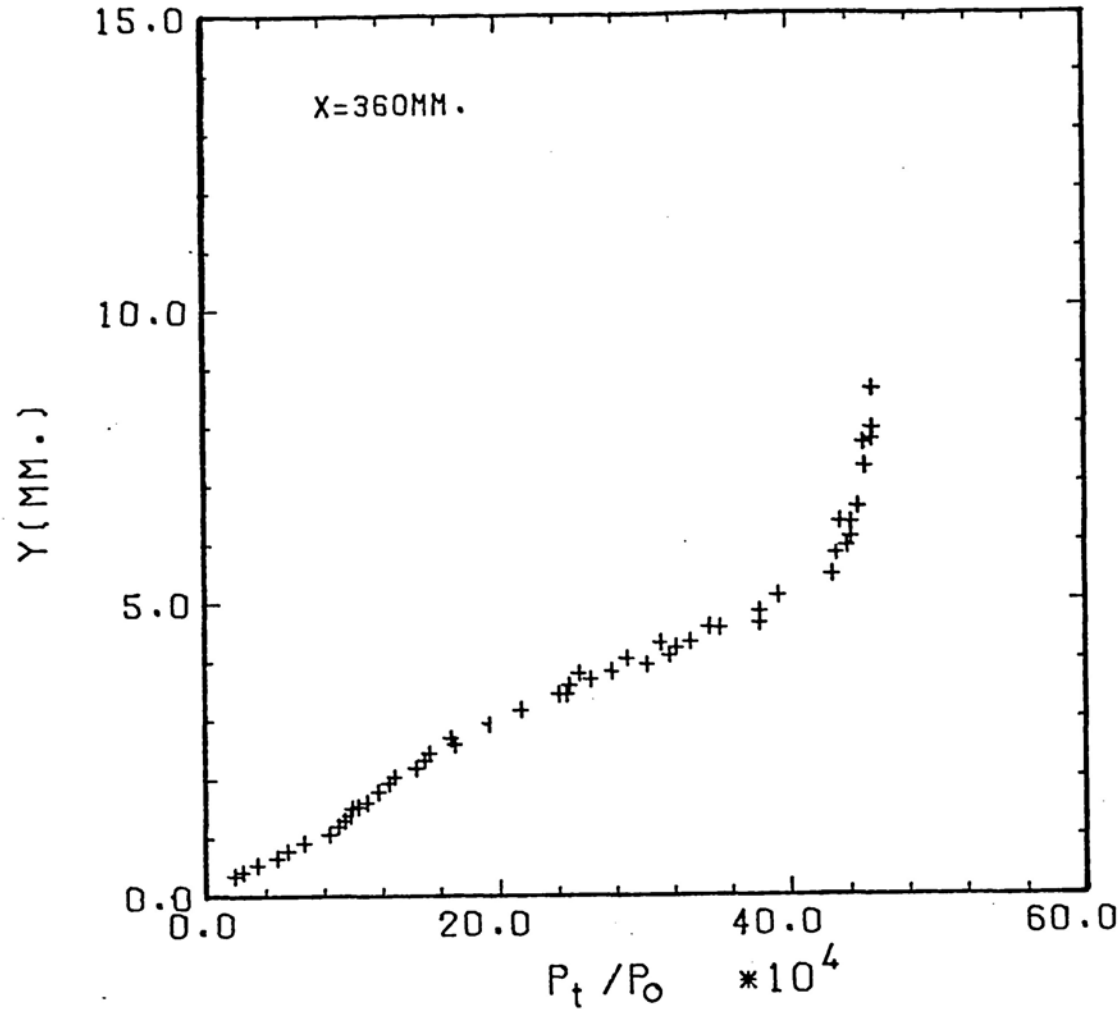


FIG. 5-11a HP CONDITION: PITOT PRESSURE PROFILE x = 360mm

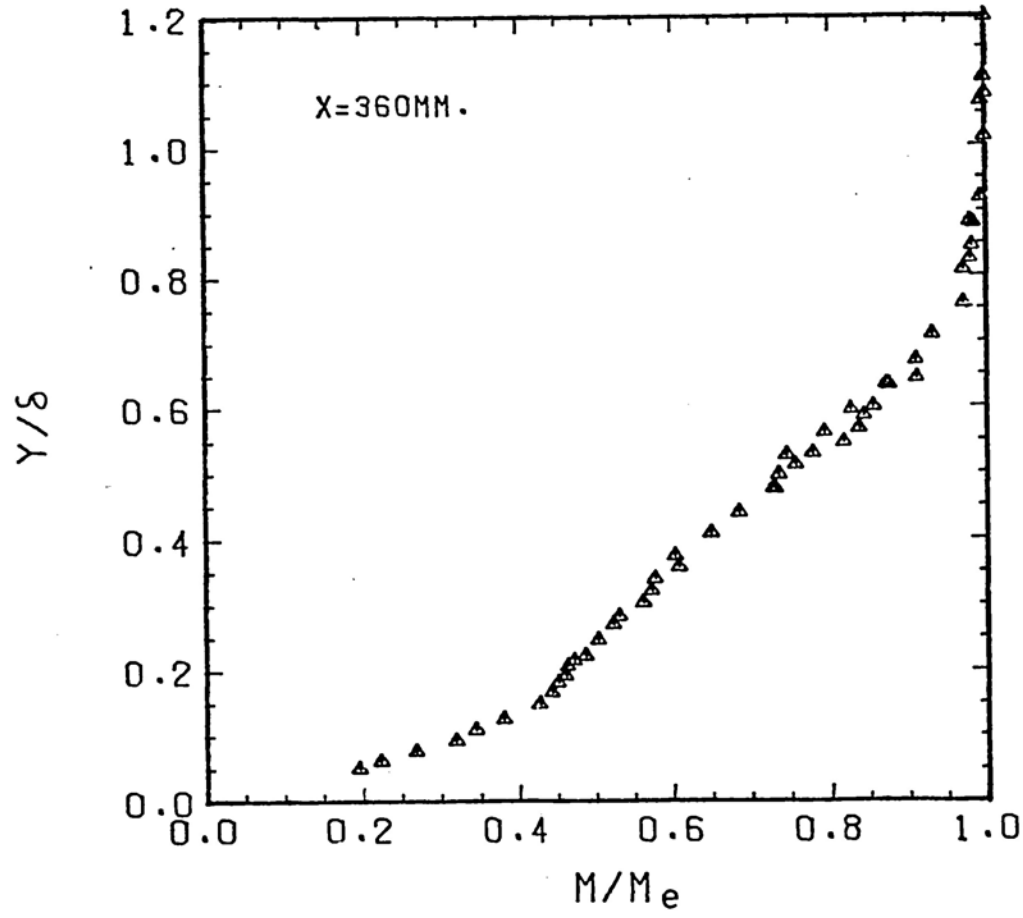


FIG. 5-12a HP CONDITION: MACH NUMBER PROFILE x = 360mm

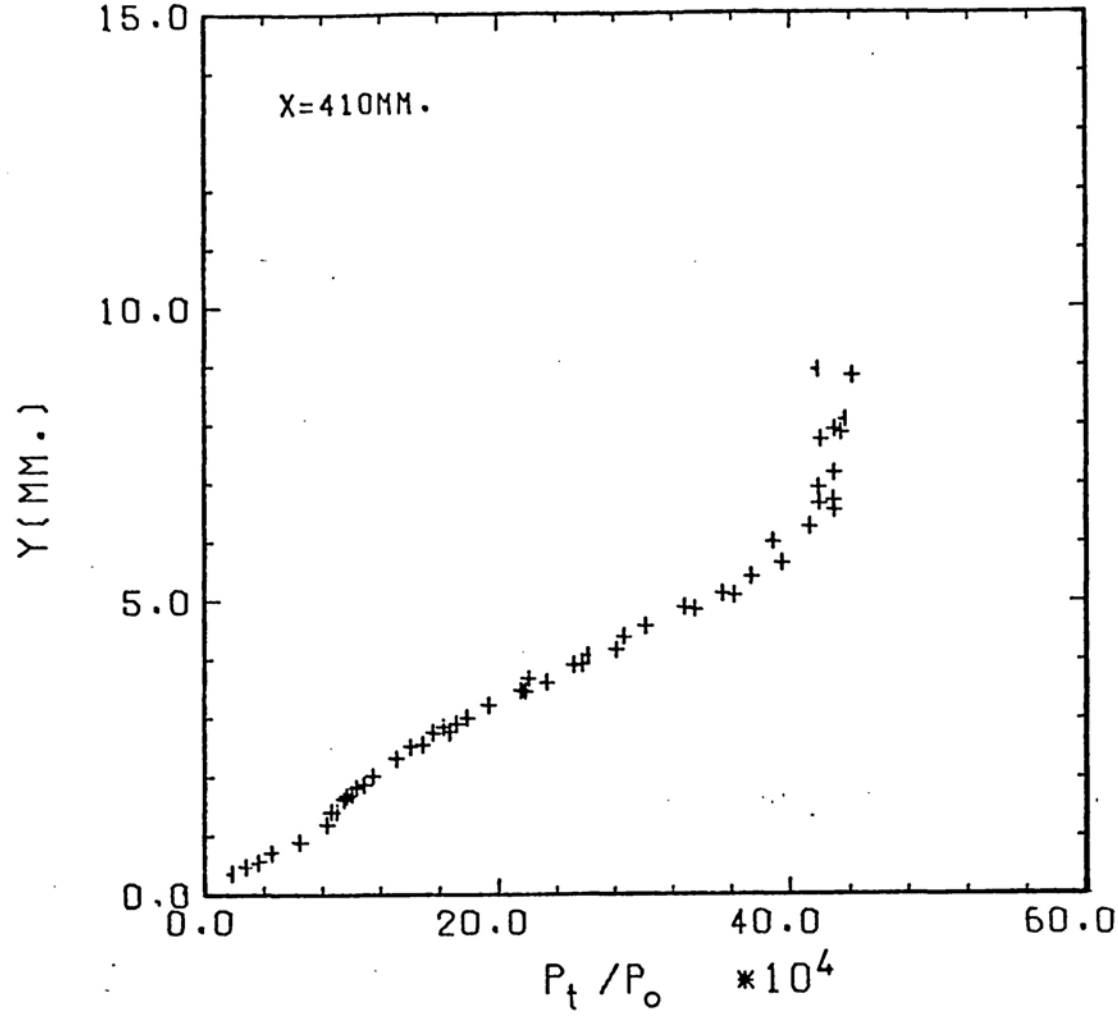


FIG. 5-11b HP CONDITION: PITOT PRESSURE PROFILE x = 410mm

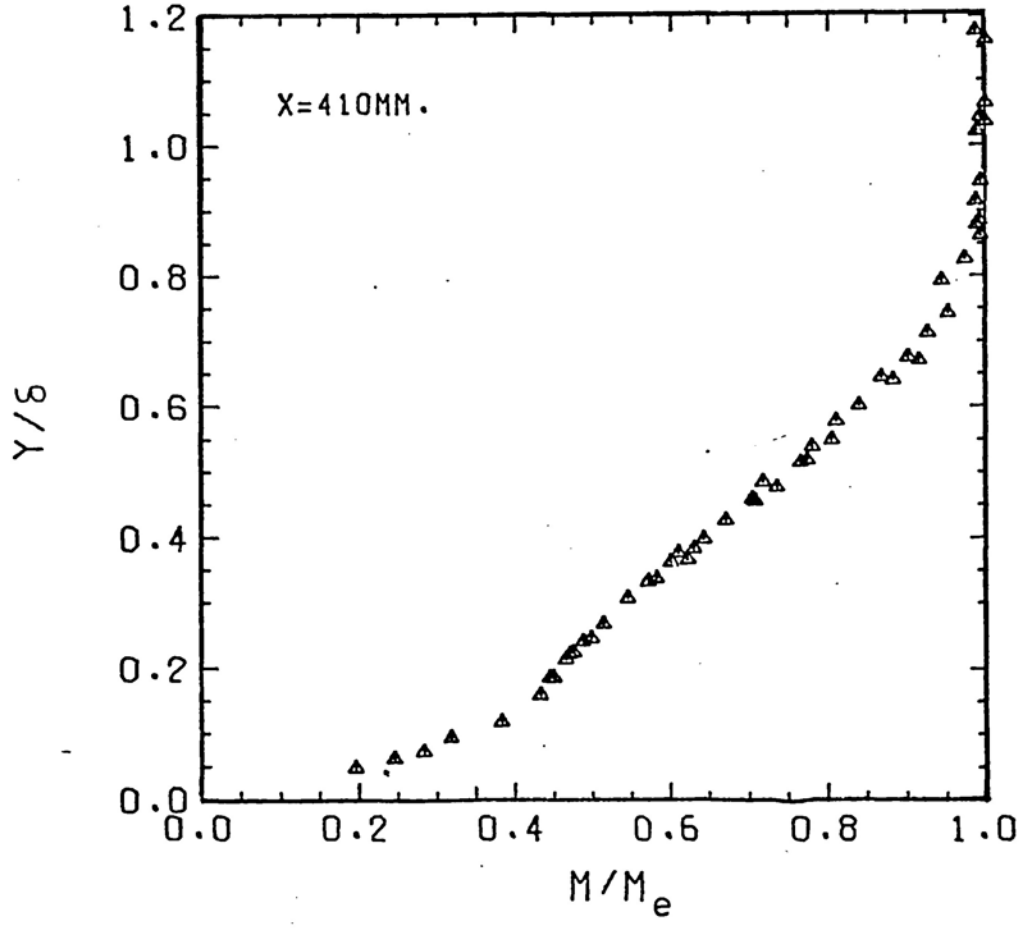


FIG. 5-12b HP CONDITION: MACH NUMBER PROFILE x = 410mm

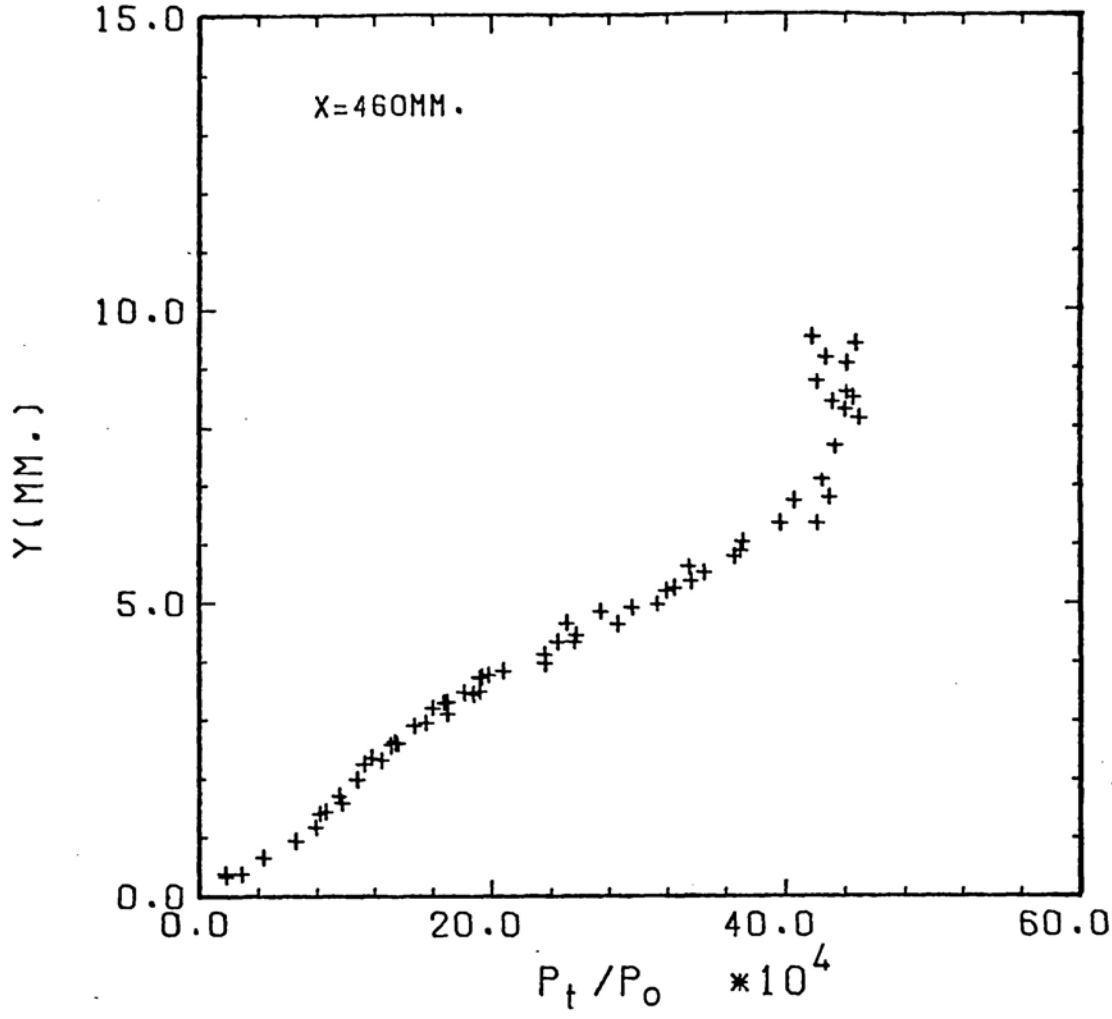


FIG. 5-11c HP CONDITION: PITOT PRESSURE PROFILE x = 460mm

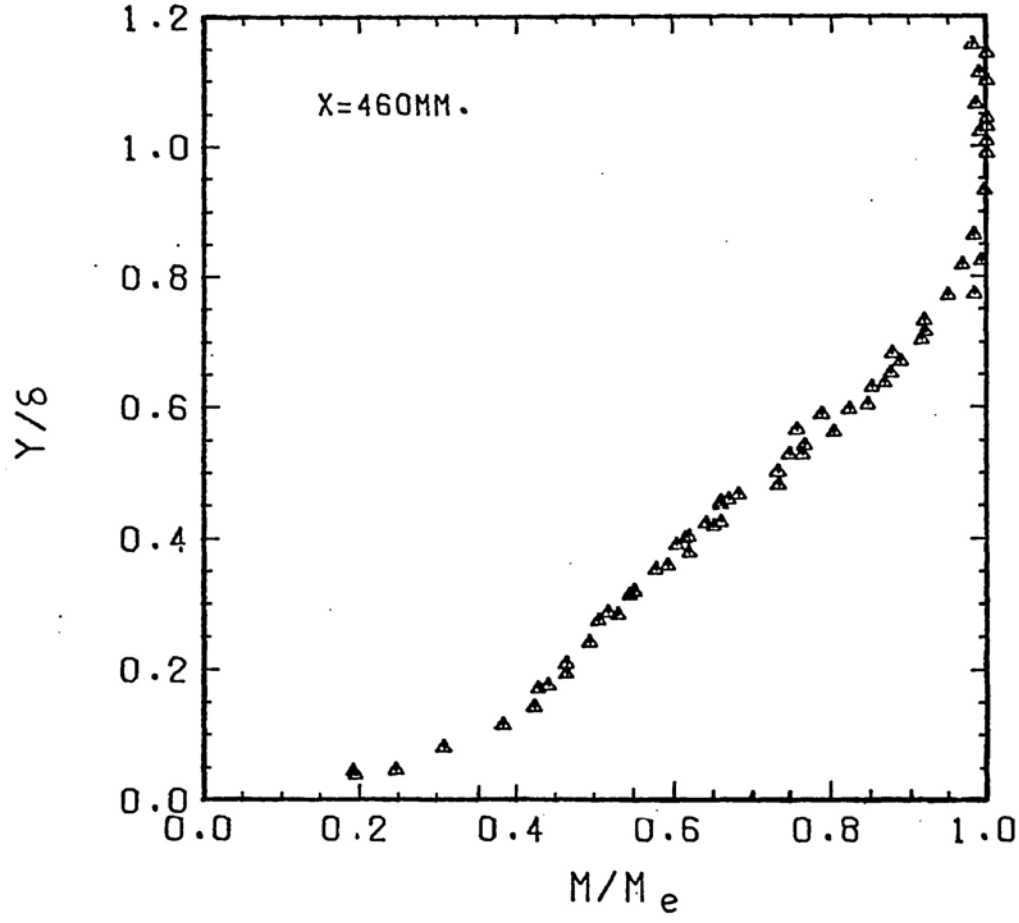


FIG. 5-12c HP CONDITION: MACH NUMBER PROFILE x = 460mm

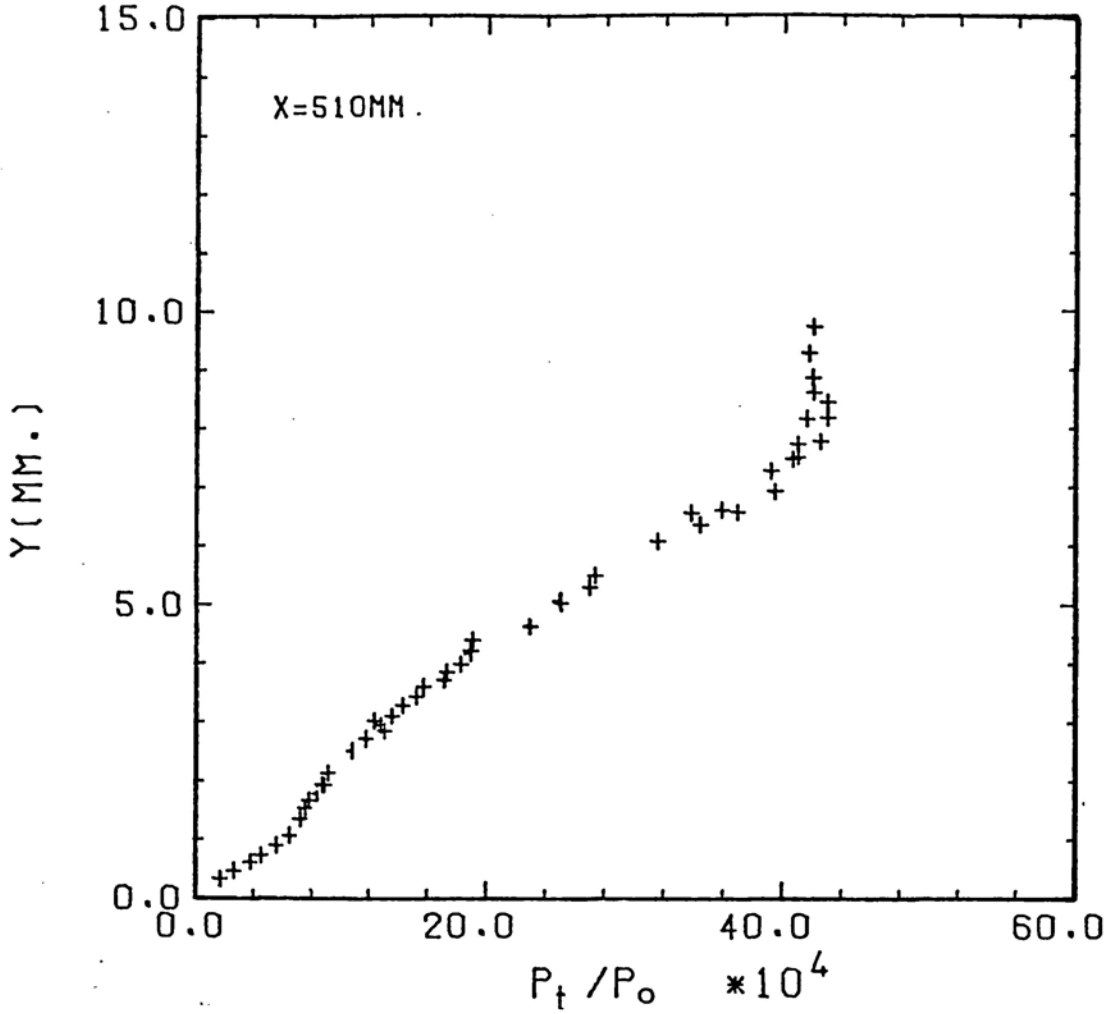


FIG. 5-11d HP CONDITION: PITOT PRESSURE PROFILE x = 510mm

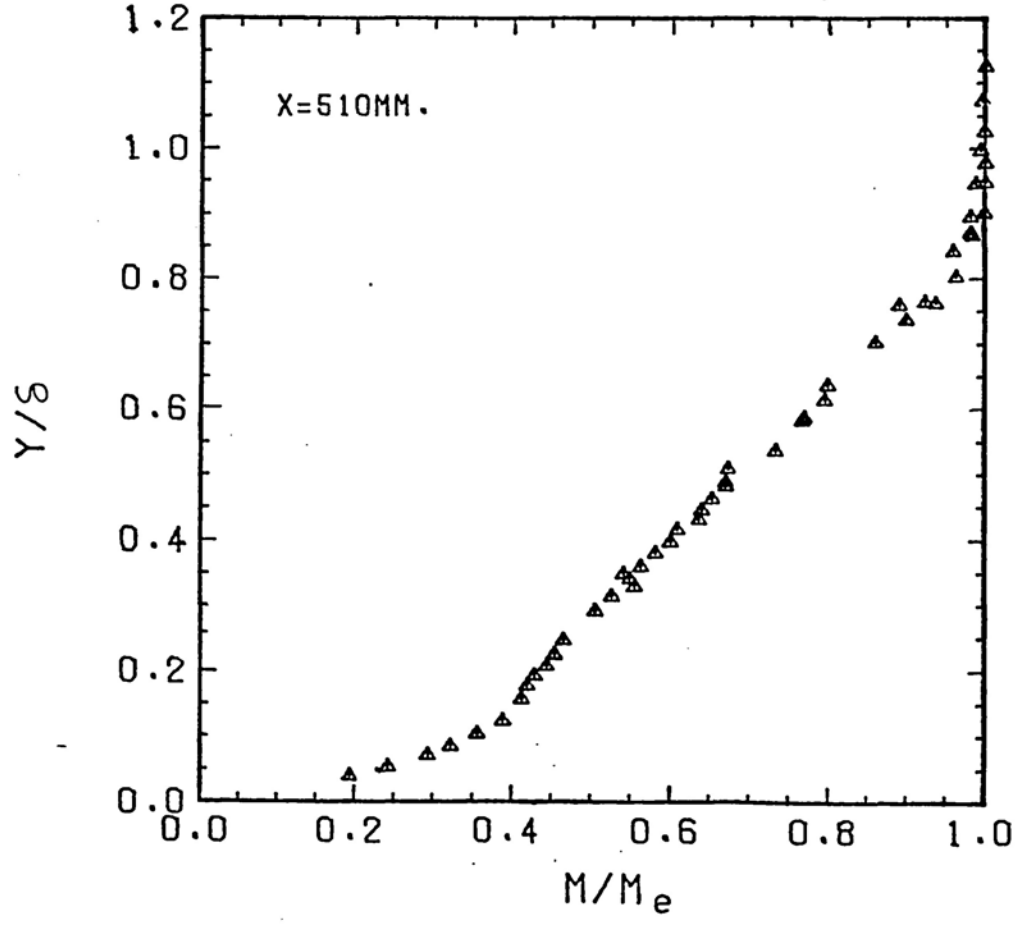


FIG. 5-12d HP CONDITION: MACH NUMBER PROFILE x = 510mm

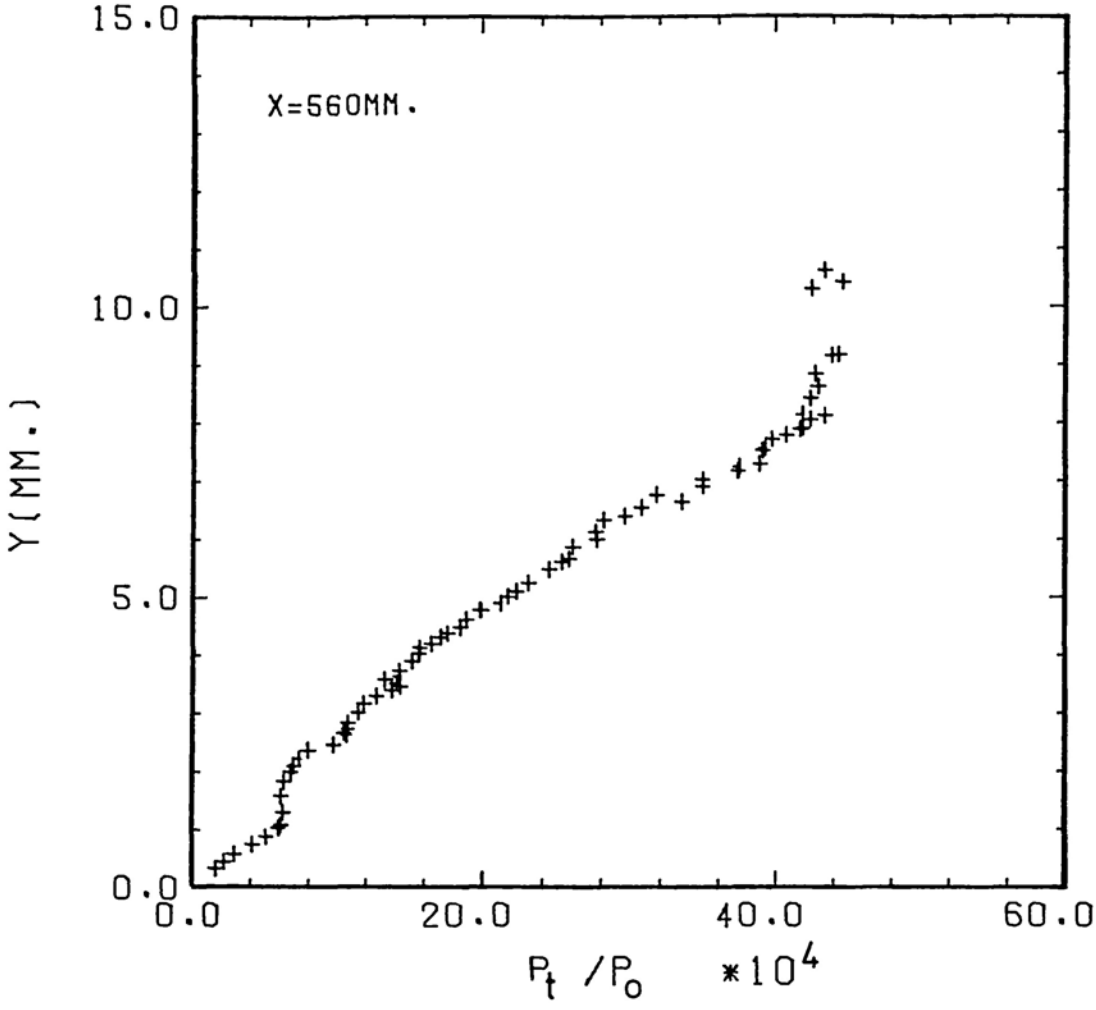


FIG. 5-11e HP CONDITION: PITOT PRESSURE PROFILE x = 560mm

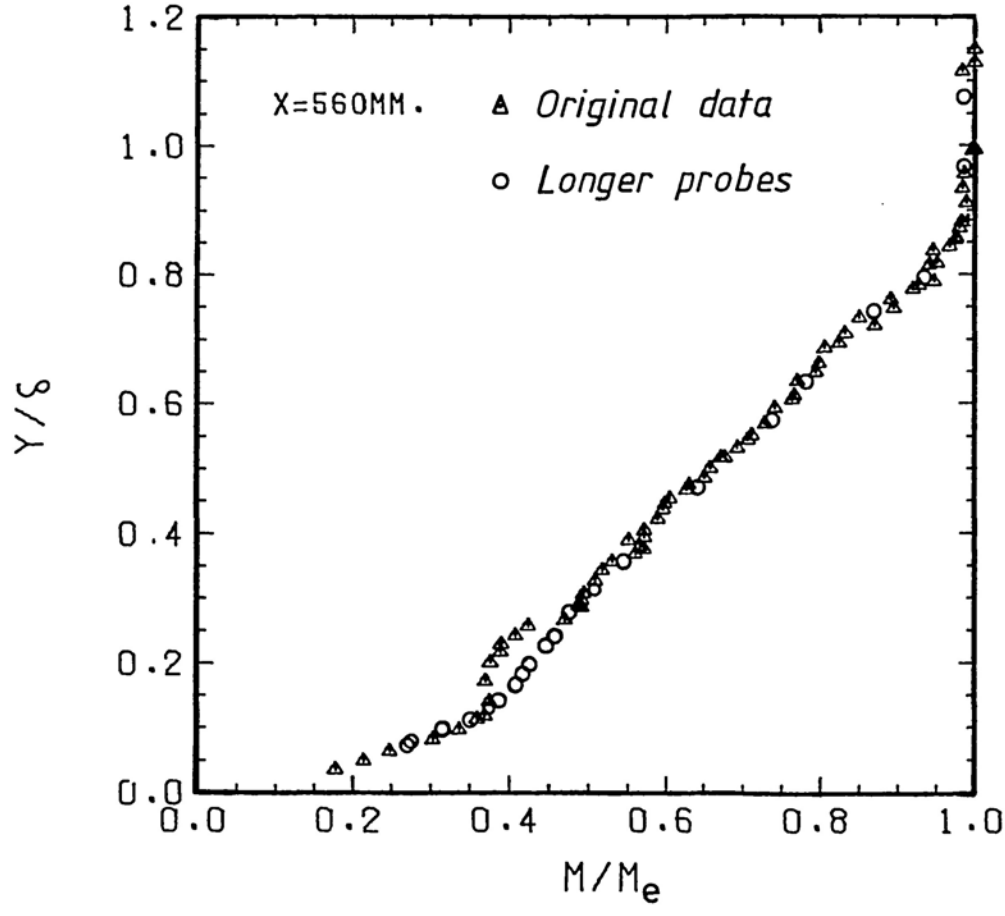


FIG. 5-12e HP CONDITION: MACH NUMBER PROFILE x = 560mm

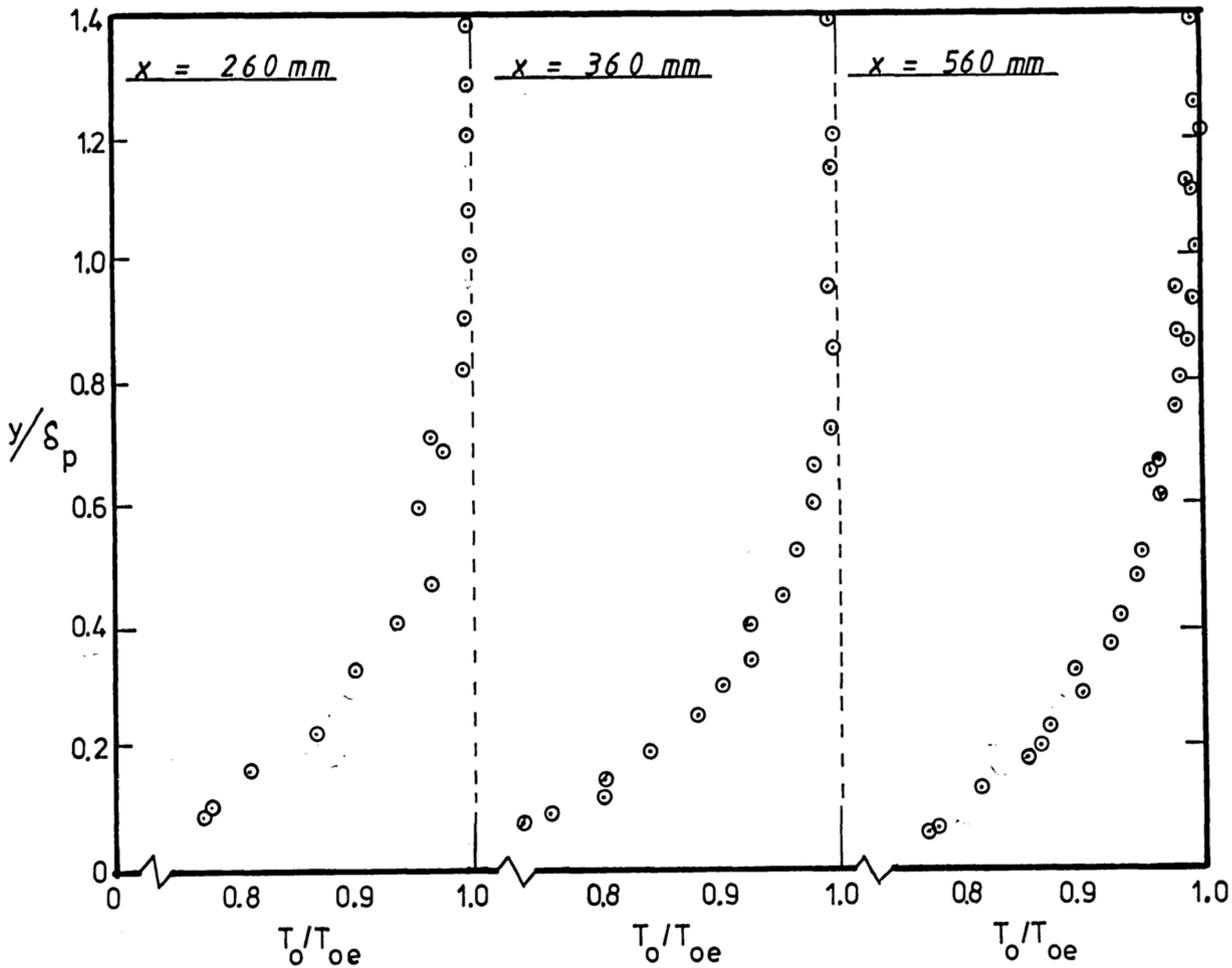


FIG. 5-13 LP CONDITION: TOTAL TEMPERATURE PROFILES (MEASURED)

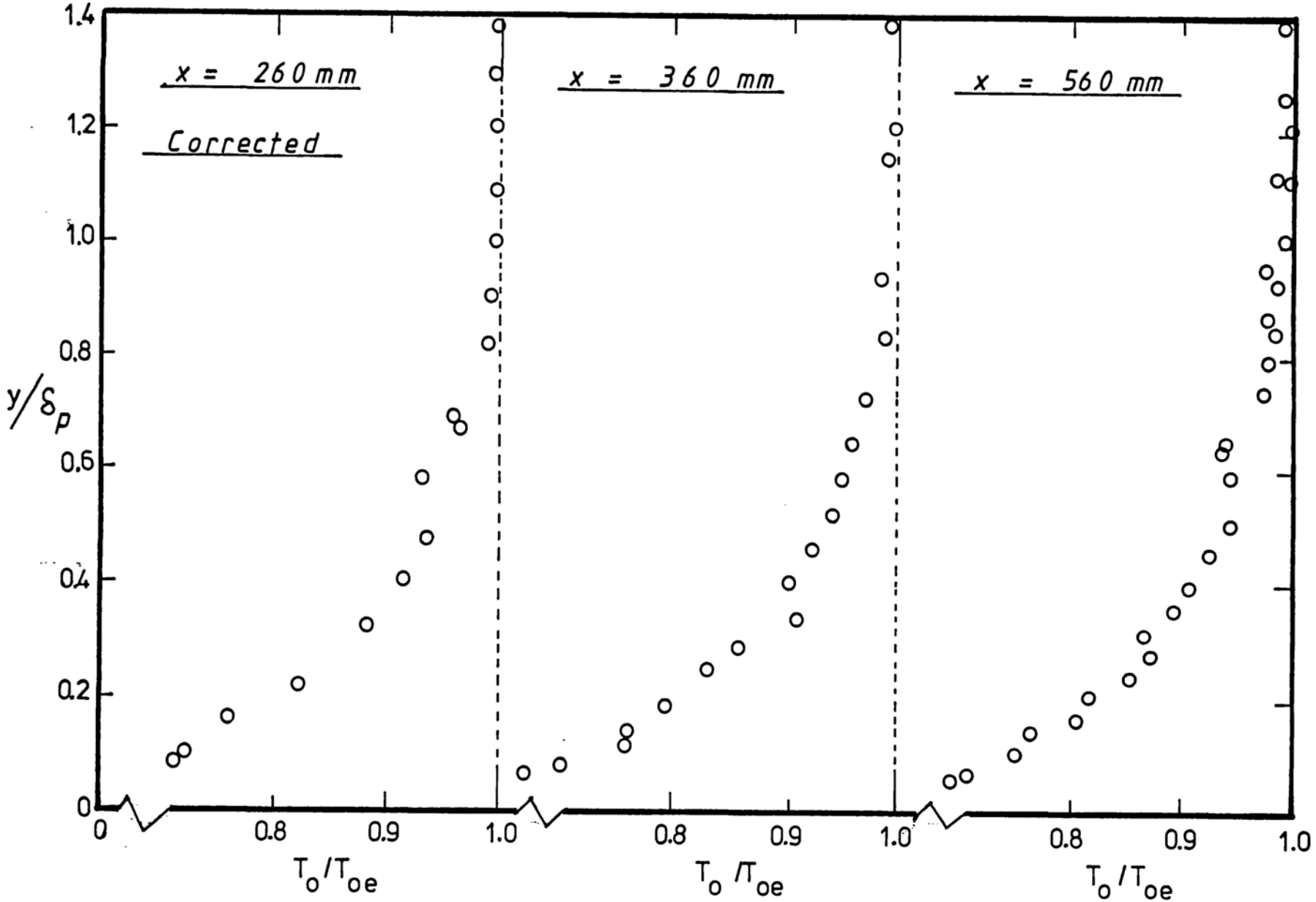


FIG. 5-14 LP CONDITION: TOTAL TEMPERATURE PROFILES (CORRECTED)

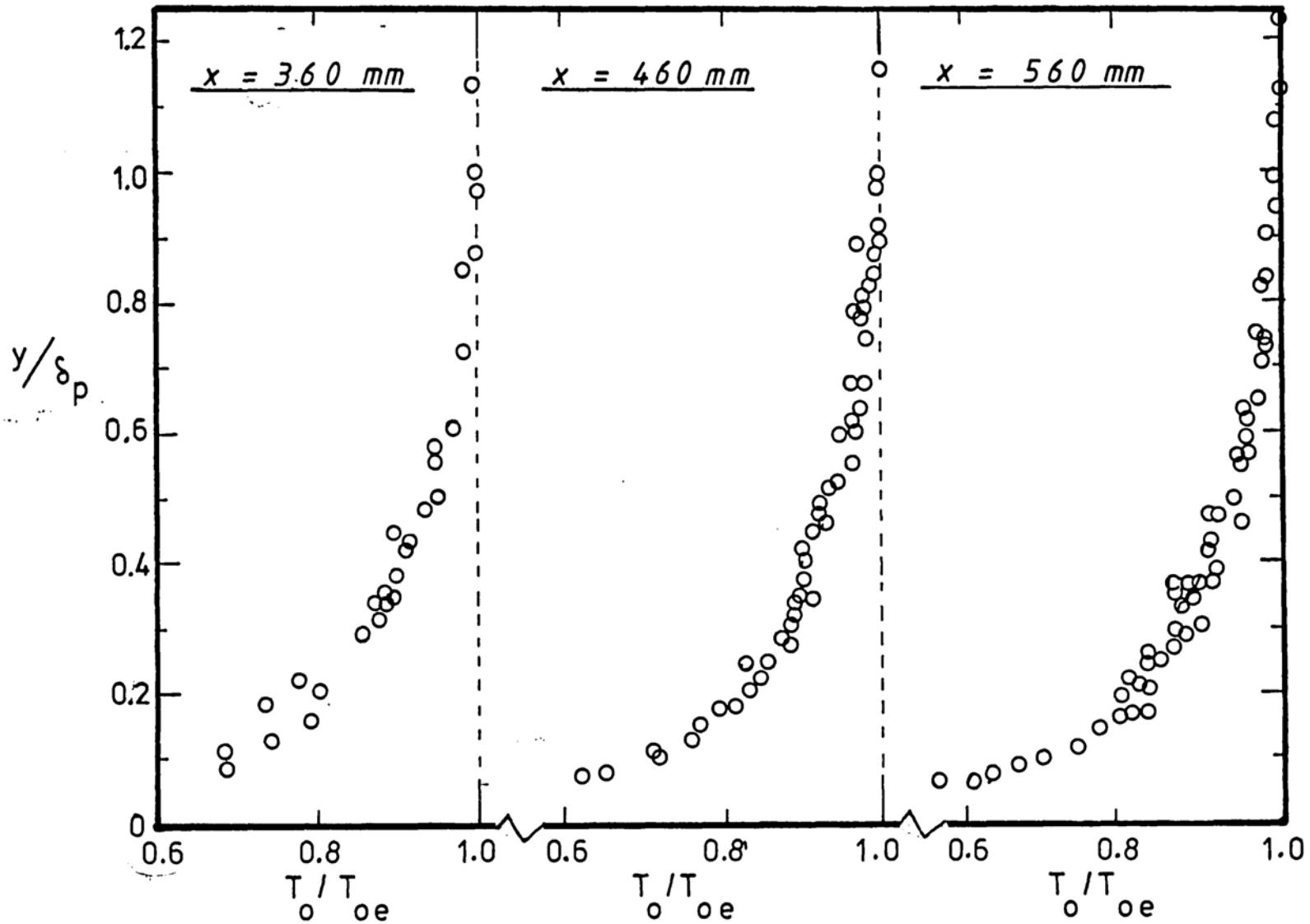


FIG. 5-15 HP CONDITION: TOTAL TEMPERATURE PROFILES (MEASURED)

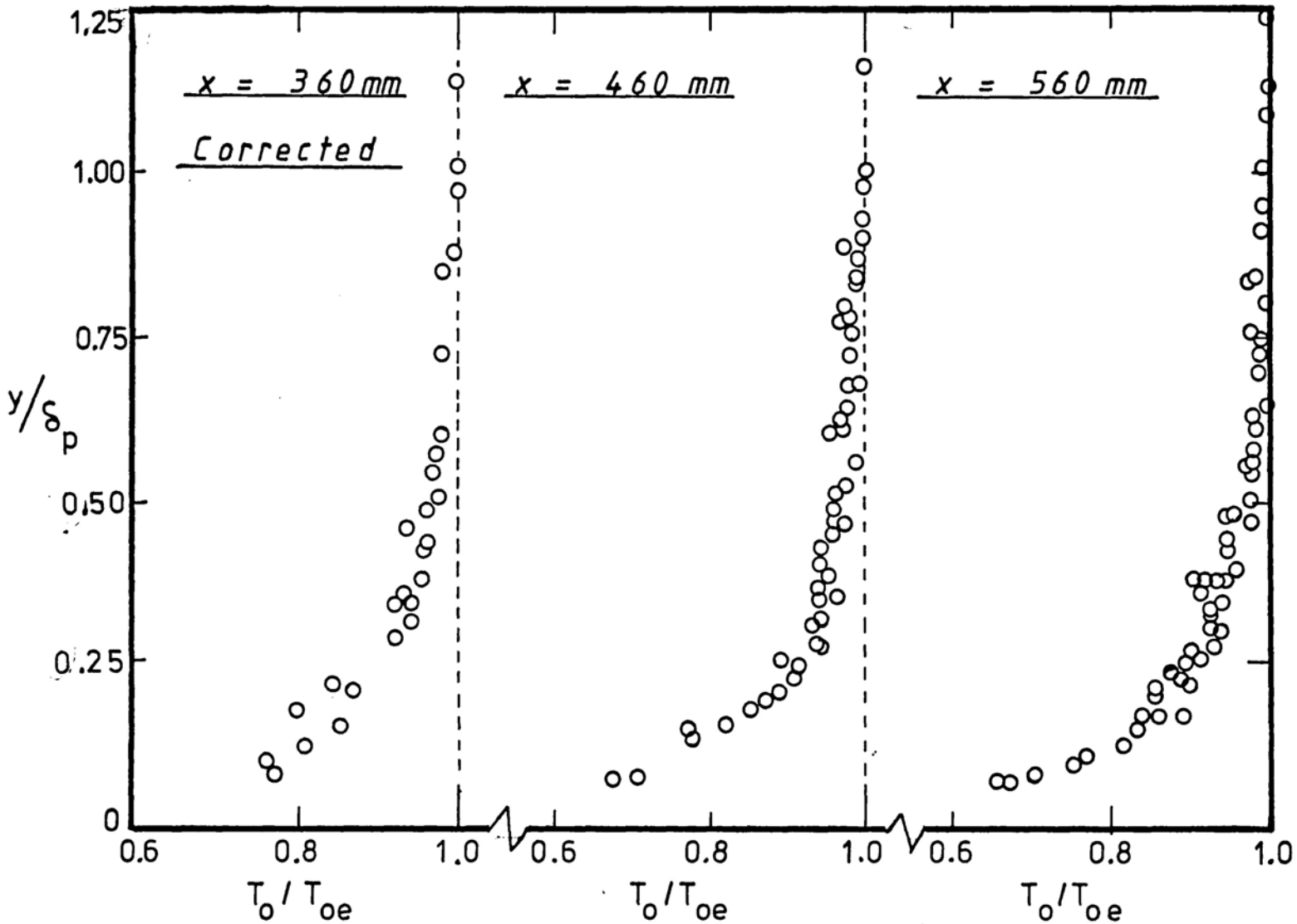


FIG. 5-16 HP CONDITION: TOTAL TEMPERATURE PROFILES (CORRECTED)

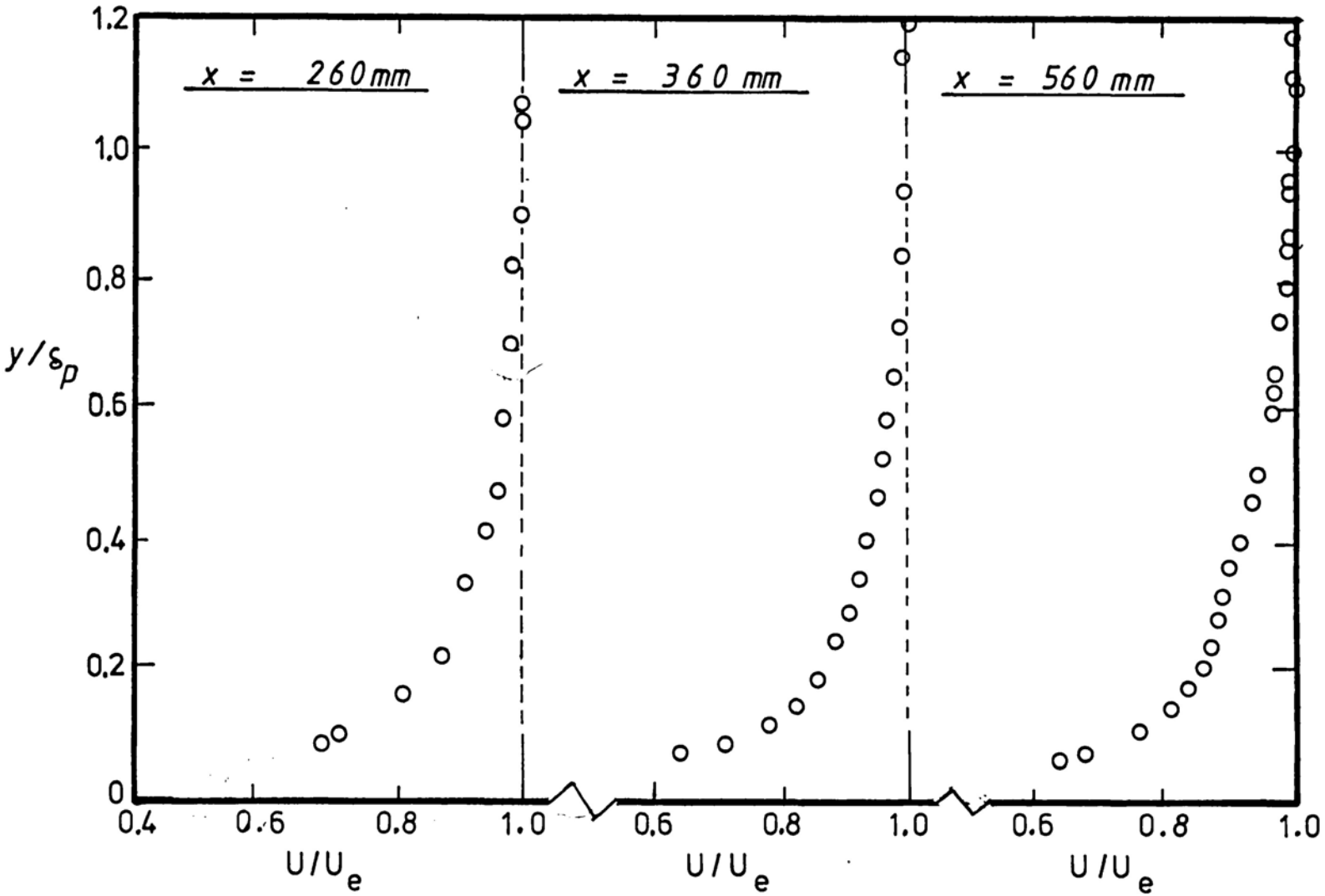


FIG. 5-17 LP CONDITION: VELOCITY PROFILES

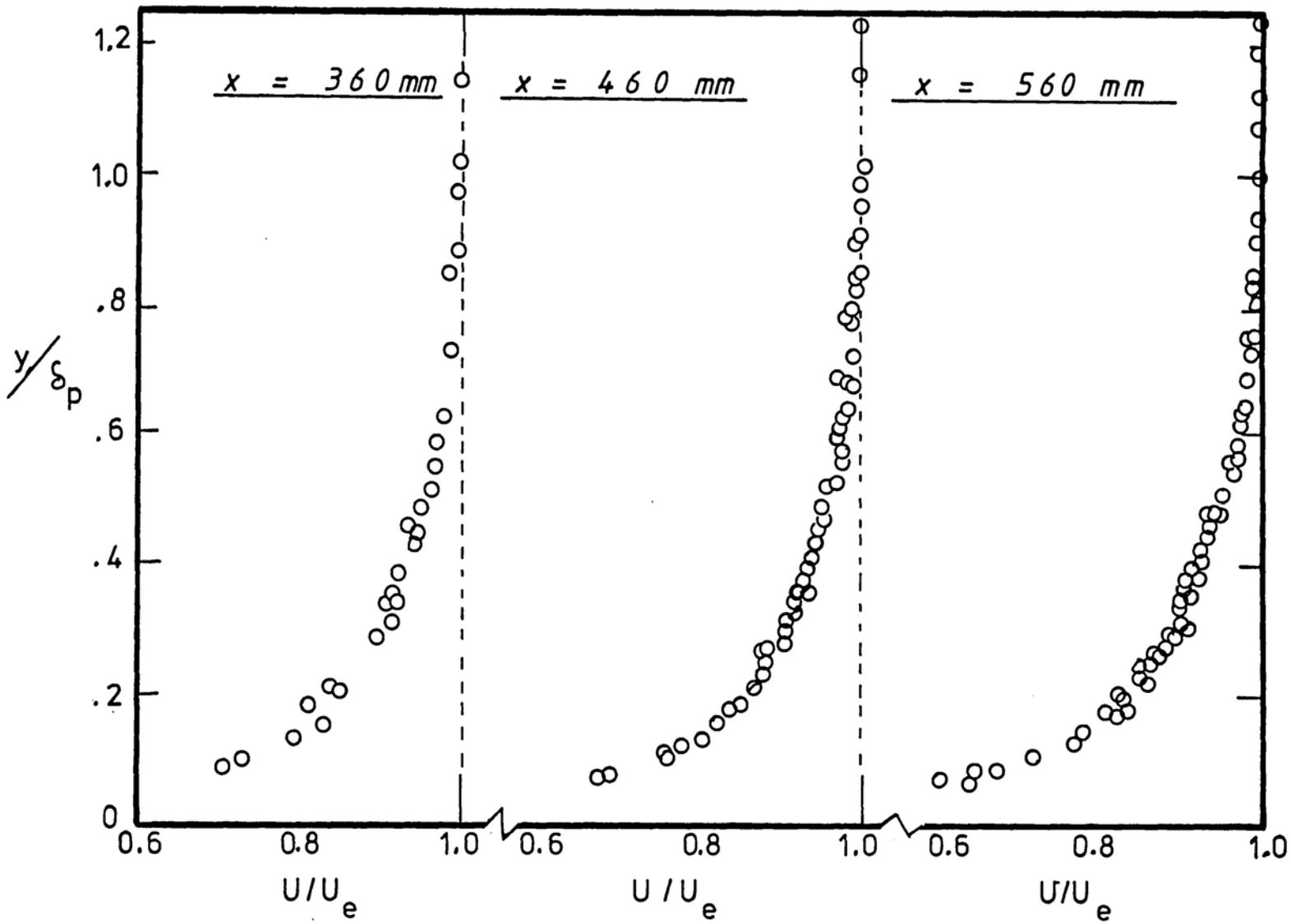


FIG. 5-18 HP CONDITION: VELOCITY PROFILES

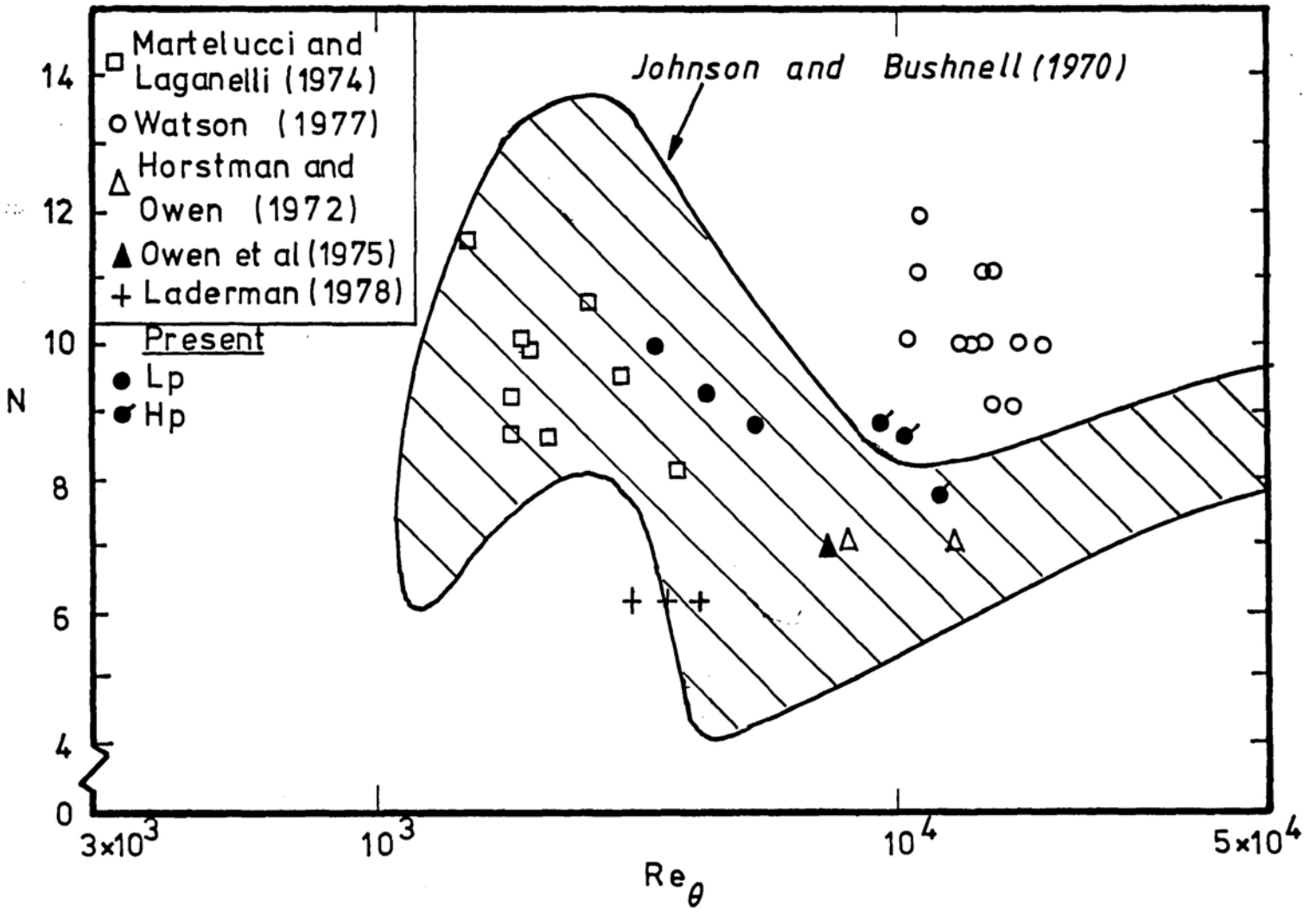


FIG. 5-19 VARIATION OF POWER LAW EXPONENT(N) WITH Re_θ

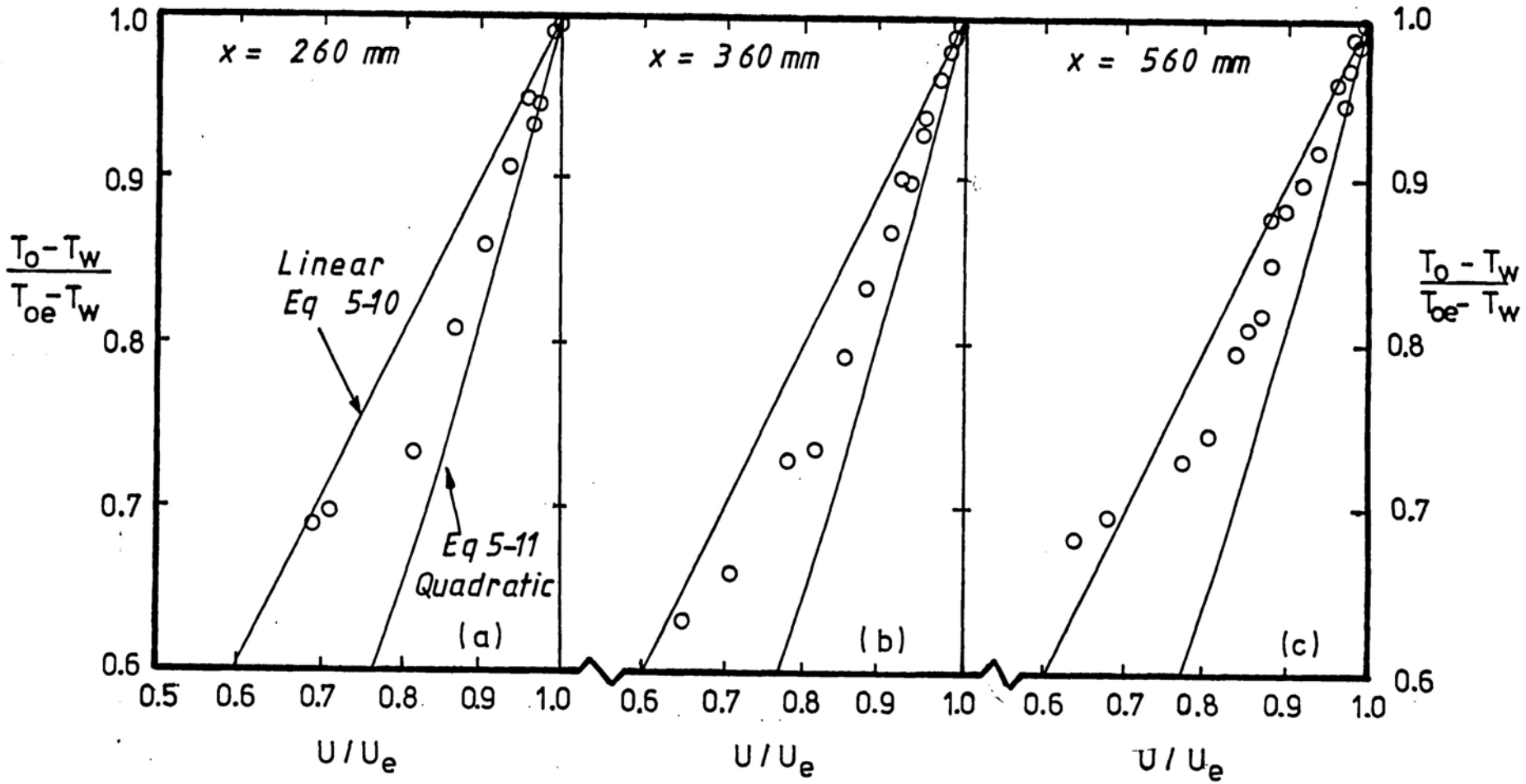


FIG. 5-20 LP CONDITION: COMPARISON WITH THE LINEAR AND QUADRATIC SOLUTIONS

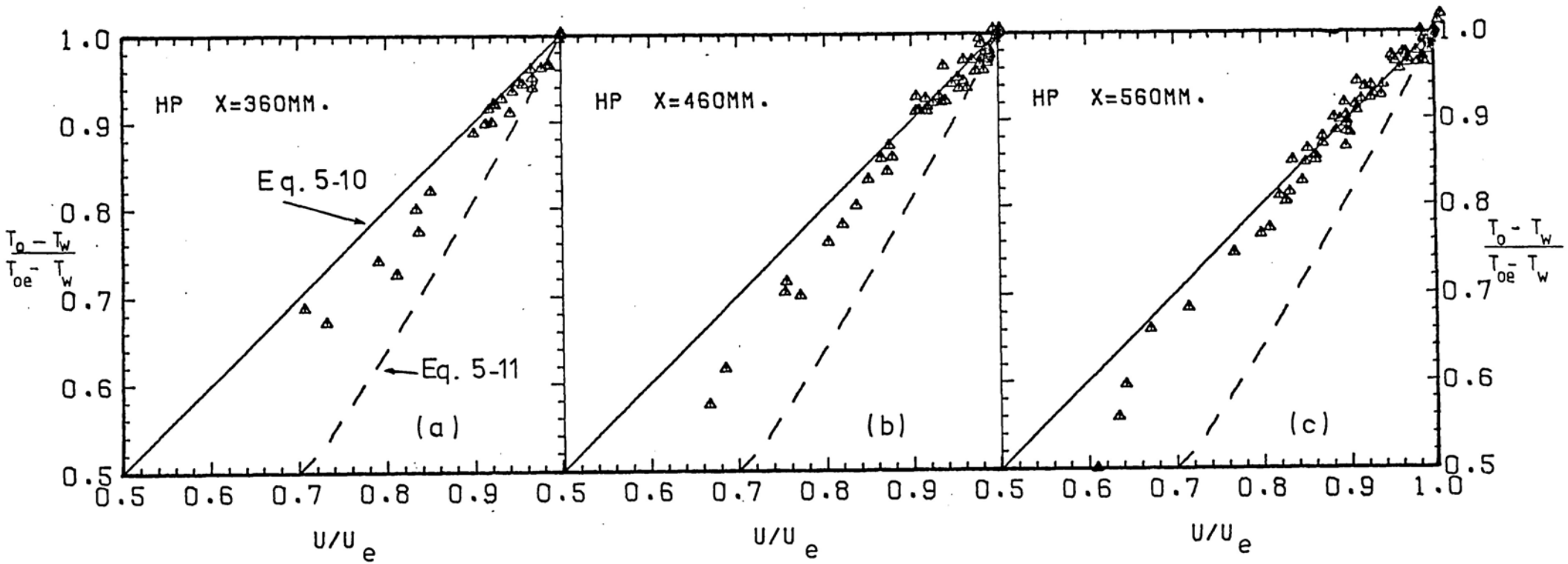


FIG. 5-21 HP CONDITIONS: COMPARISON WITH THE LINEAR AND QUADRATIC SOLUTIONS

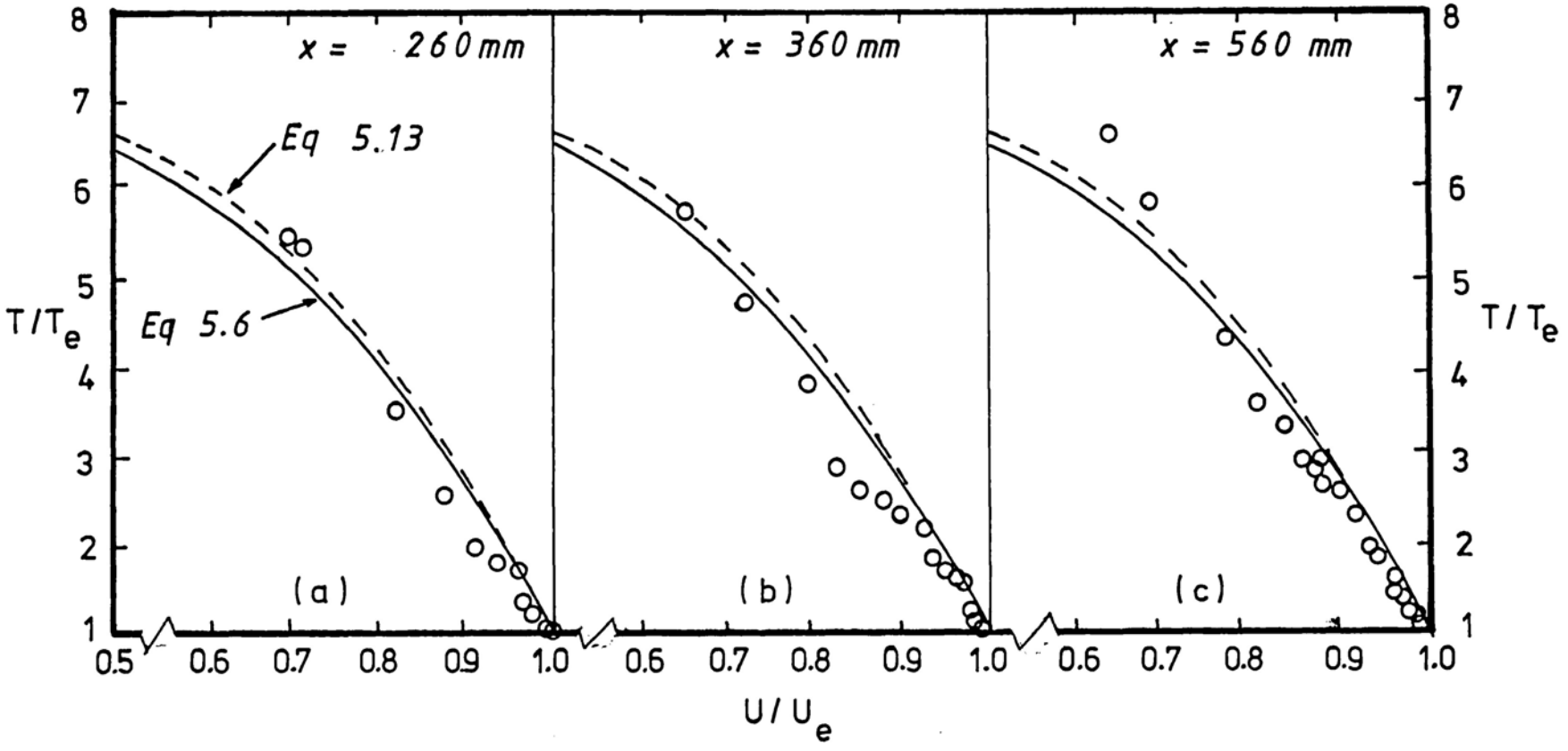


FIG. 5-22 LP CONDITION: VELOCITY- TEMPERATURE RELATIONSHIPS

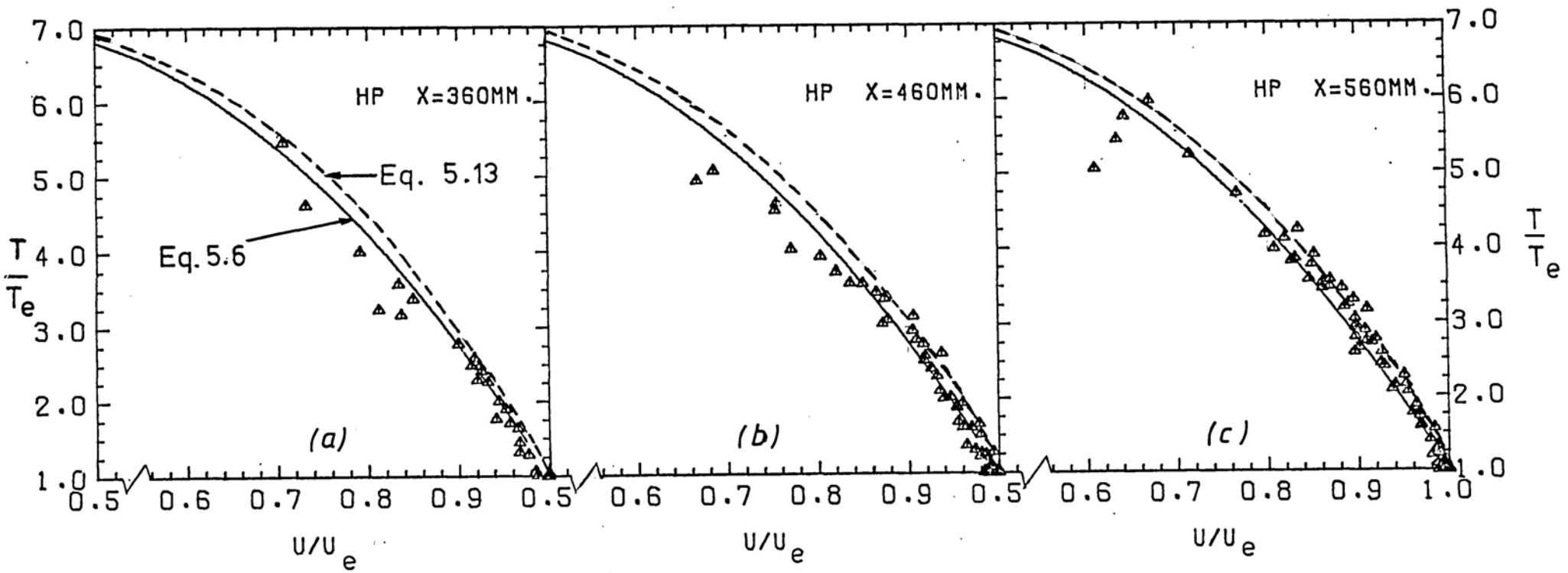


FIG. 5-23 HP CONDITION: VELOCITY-TEMPERATURE RELATIONSHIPS

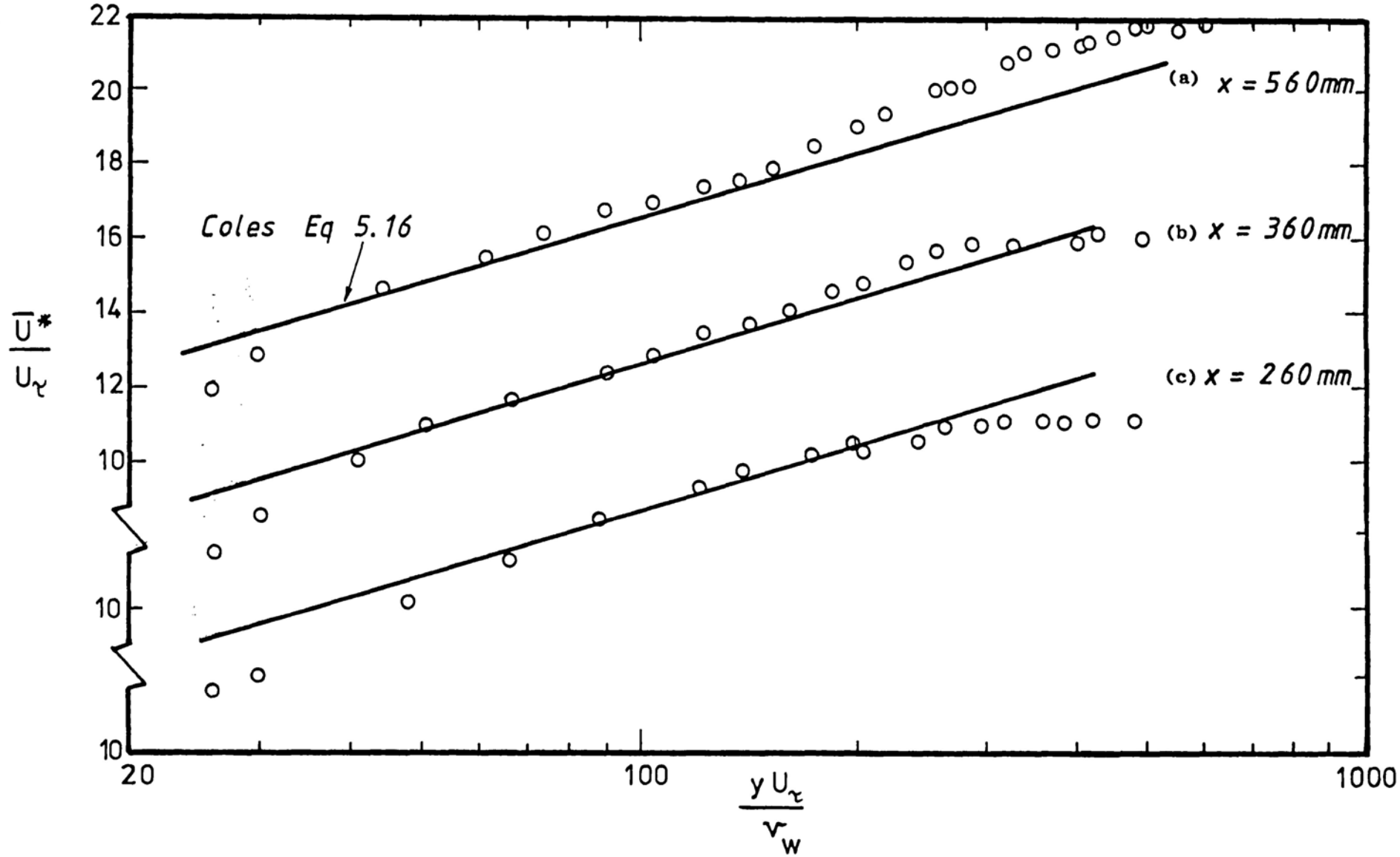


FIG. 5-24 LP CONDITION: TRANSFORMED VELOCITY PROFILES

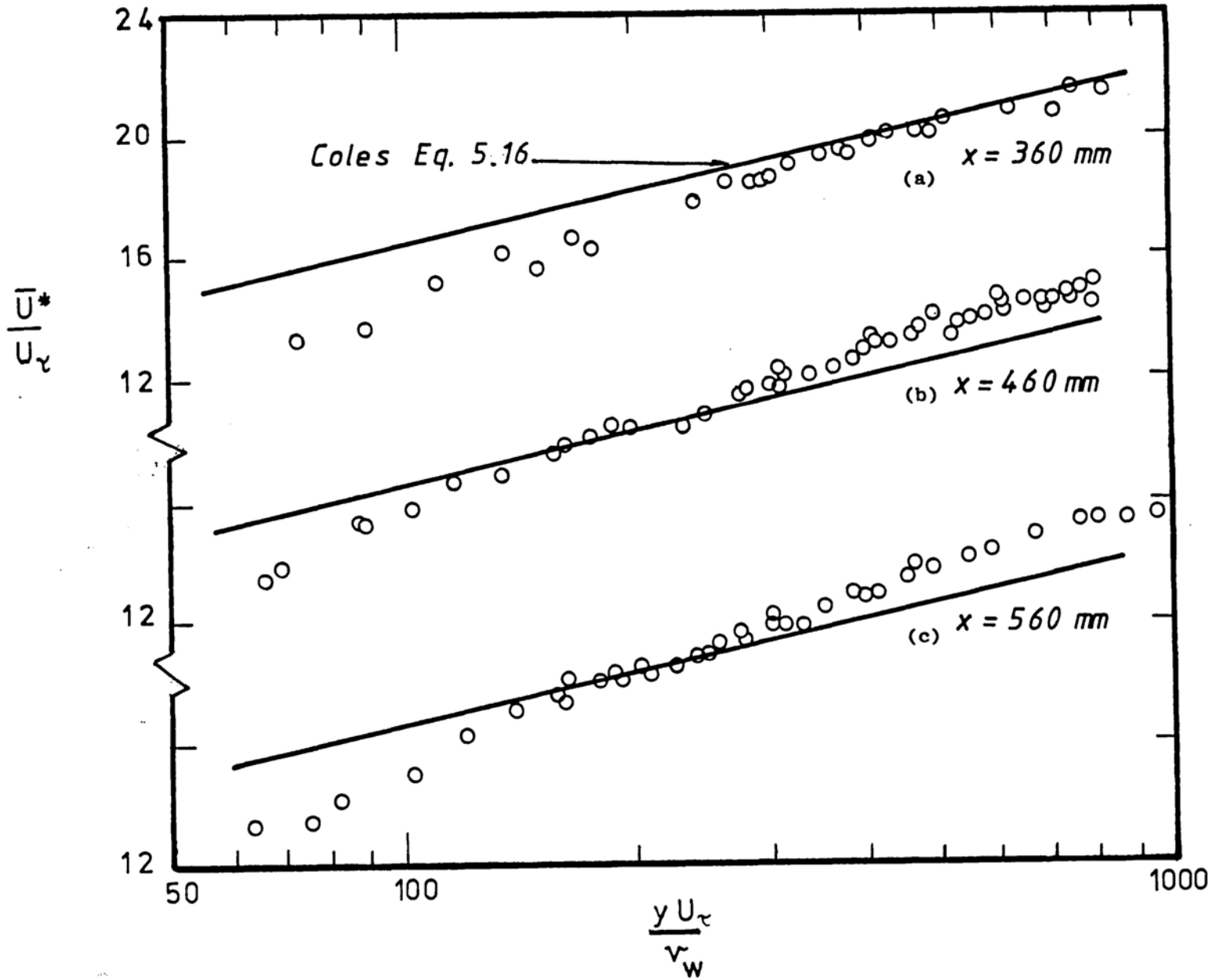


FIG. 5-25 HP CONDITION: TRANSFORMED VELOCITY PROFILES

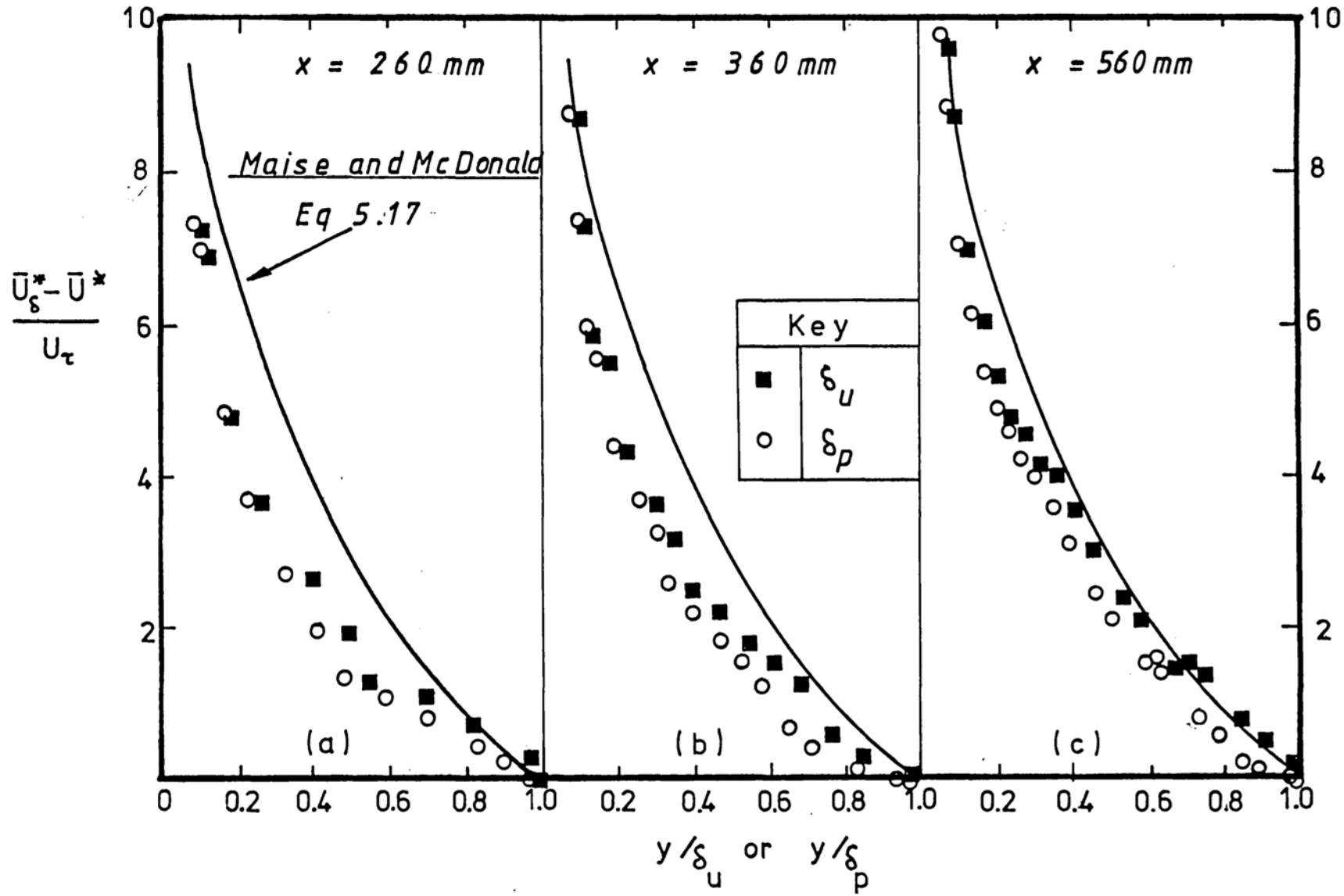


FIG. 5-26 LP CONDITION: OUTER LAW - COMPARISON WITH MAISE AND McDONALD(1968) CORRELATION

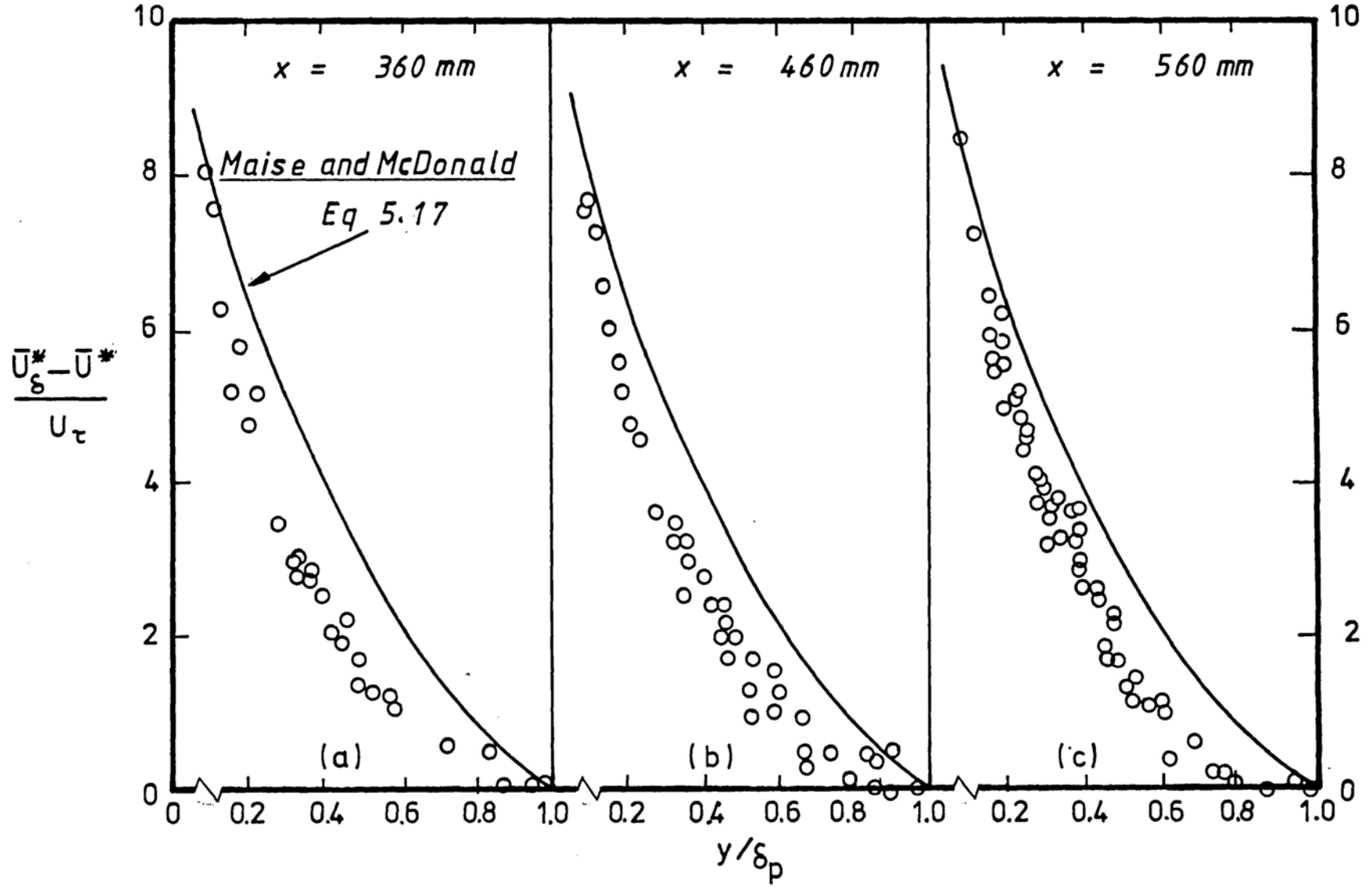


FIG. 5-27 HP CONDITION: OUTER LAW - COMPARISON WITH MAISE AND McDONALD(1968) CORRELATION

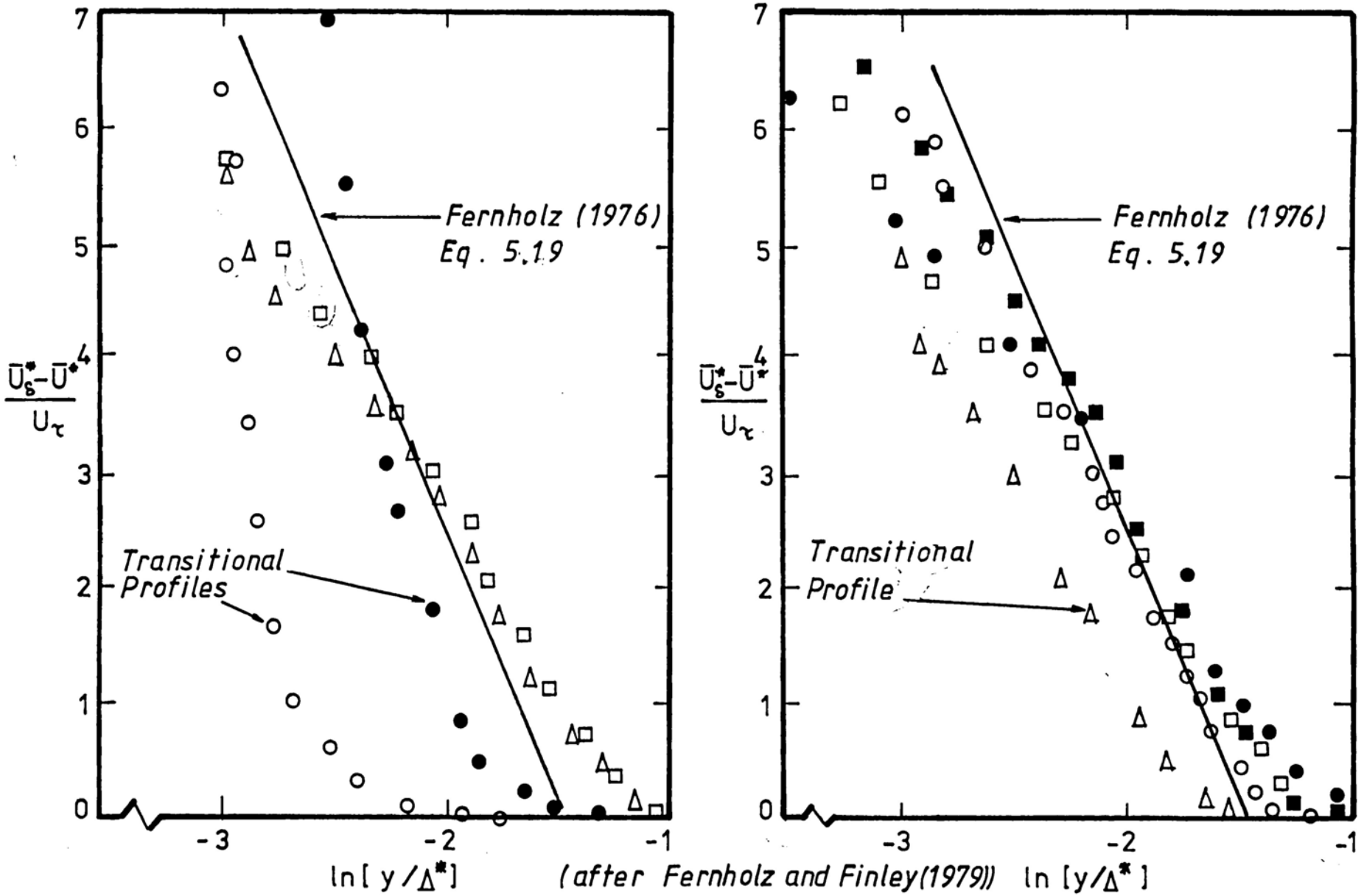


FIG. 5-28 OUTER LAW - DATA OF WATSON ET AL (1973)

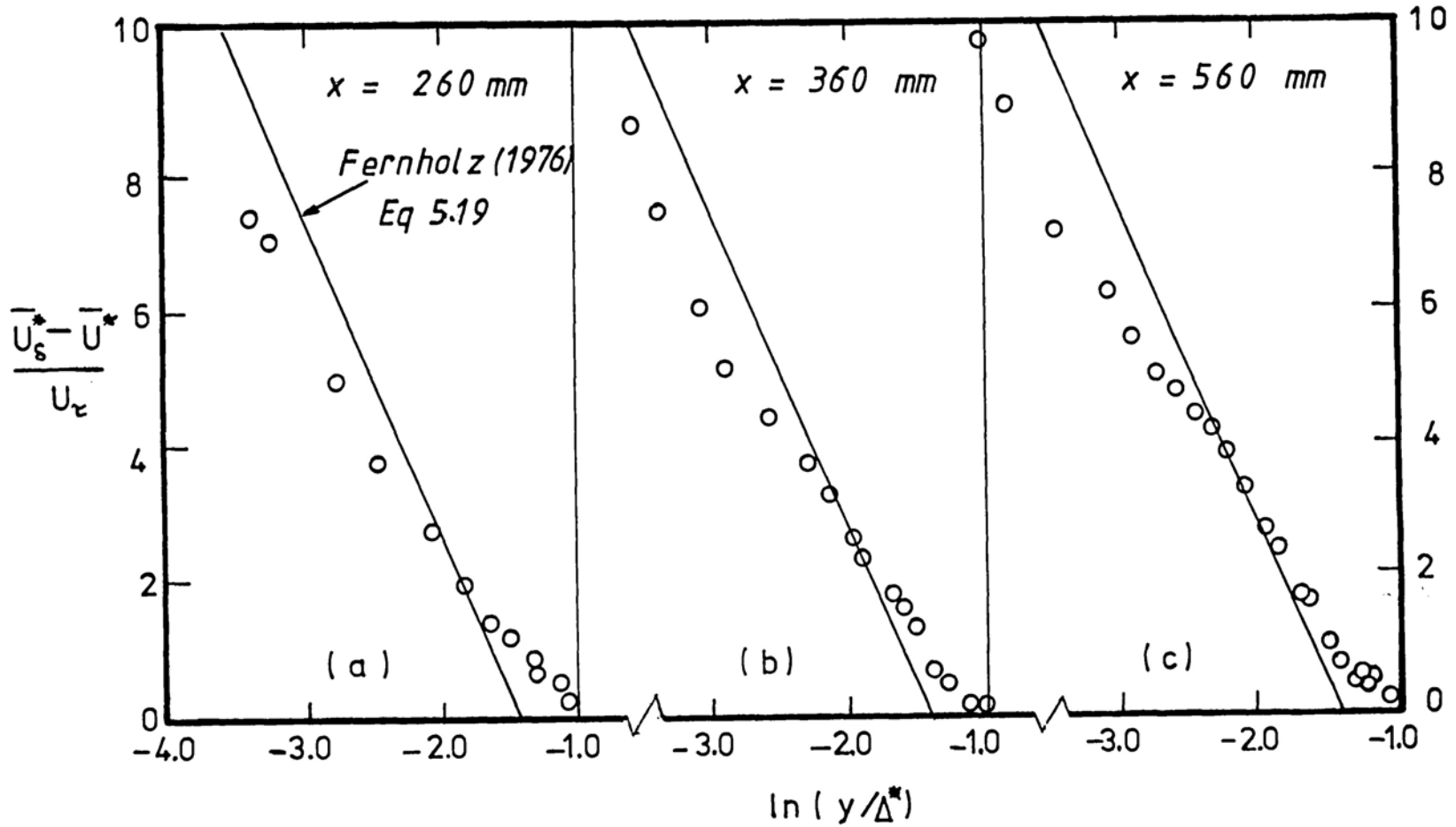


FIG. 5-29 LP CONDITION: OUTER LAW - COMPARISON WITH FERNHOLZ(1976) CORRELATION

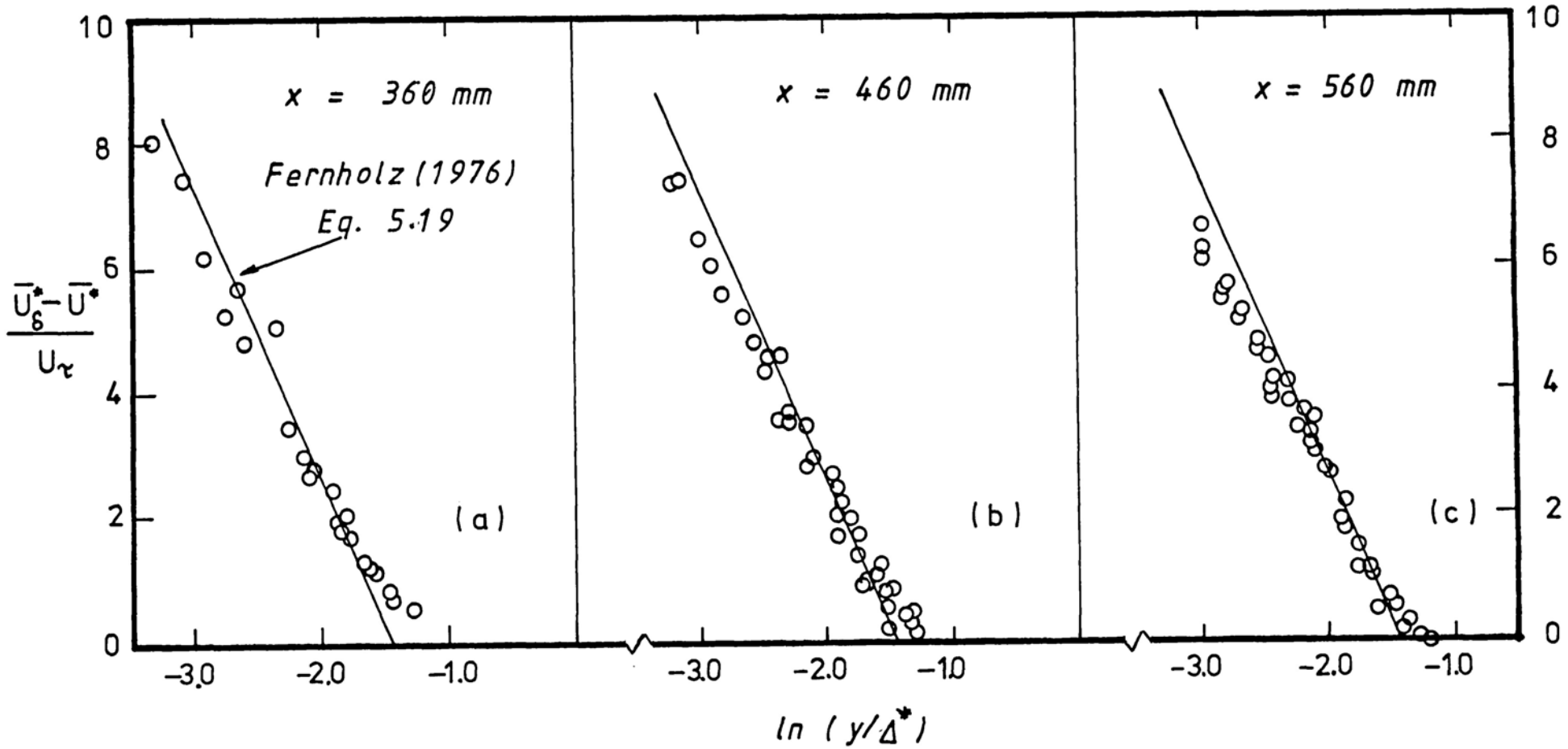


FIG. 5-30 HP CONDITION: OUTER LAW - COMPARISON WITH FERNHOLZ(1976) CORRELATION

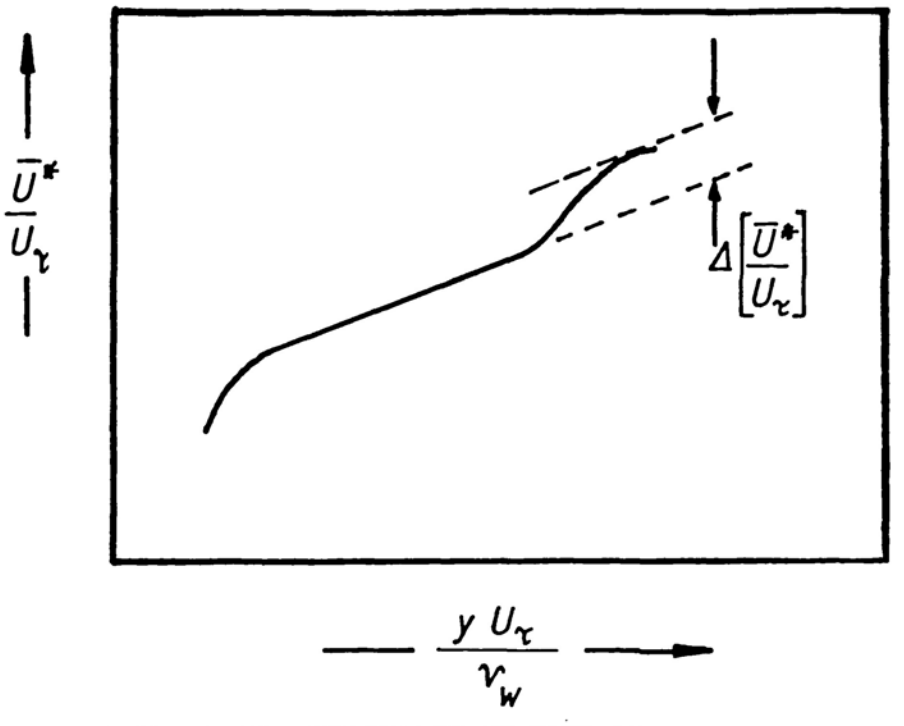
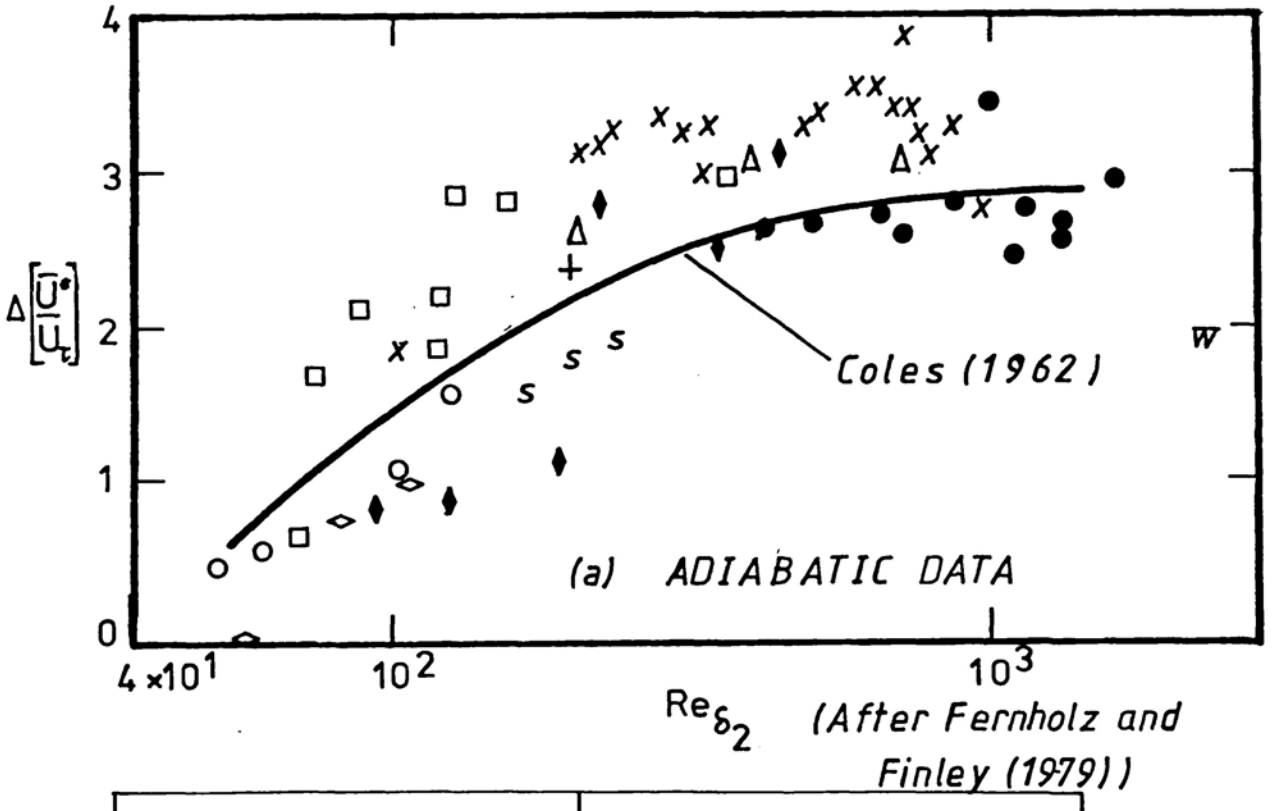
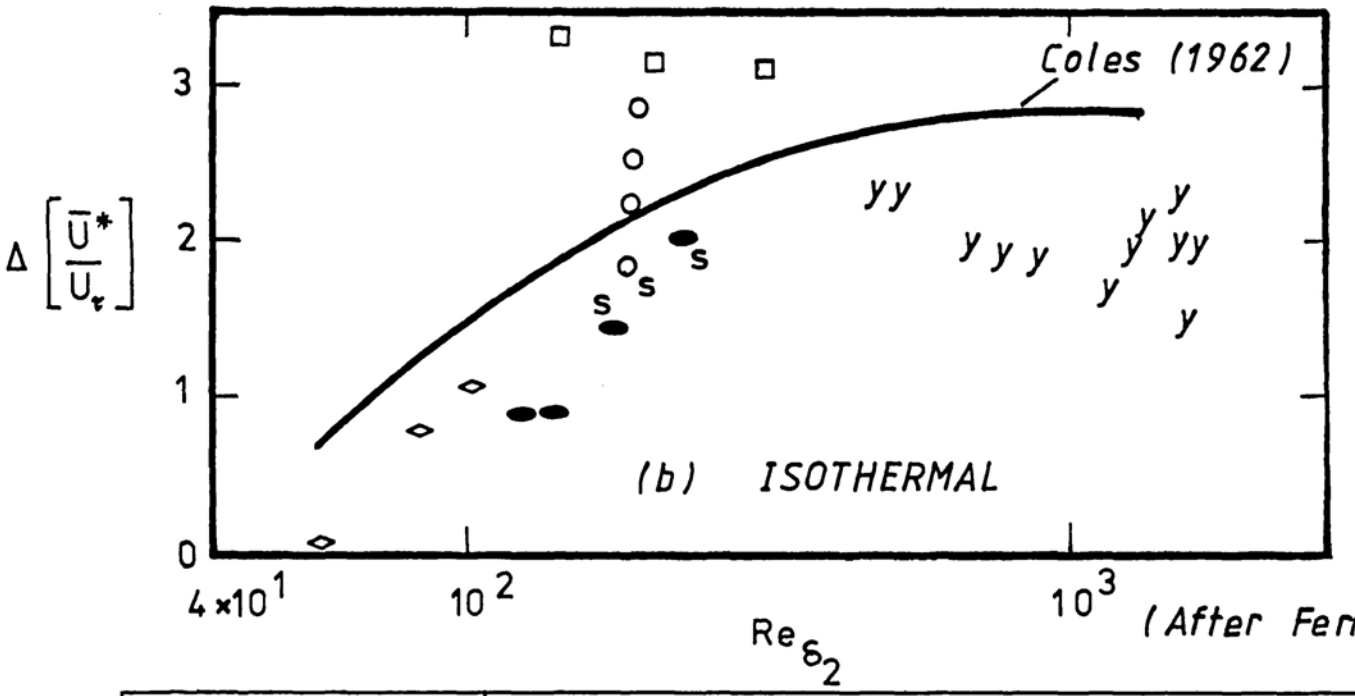


FIG. 5-31 ESTIMATION OF WAKE COMPONENT STRENGTH $\Delta(\bar{U}^*/U_\tau)$



PRESENT DATA	● SHUTTS ET AL (1955)
S HP CONDITION	▽ MOORE AND HARKNESS (1965)
◇ LP CONDITION	+ YOUNG (1965)
□ COLES (1953)	Δ HASTINGS AND SAWYER (1970)
X ♦ MABEY (1974) AND (1977)	○ WATSON ET AL (1973)

FIG. 5-32a WAKE COMPONENT STRENGTH ON ADIABATIC WALLS



(After Femholz and Finley (1979))

PRESENT DATA			
s	HP CONDITION	O YOUNG (1965)	□ HORSTMAN AND OWEN (1972)
◇	LP CONDITION	● KEENER AND HOPKINS (1972)	
		y HOPKINS AND KEENER (1972)	

FIG. 5-32b WAKE COMPONENT STRENGTH ON ISOTHERMAL WALLS

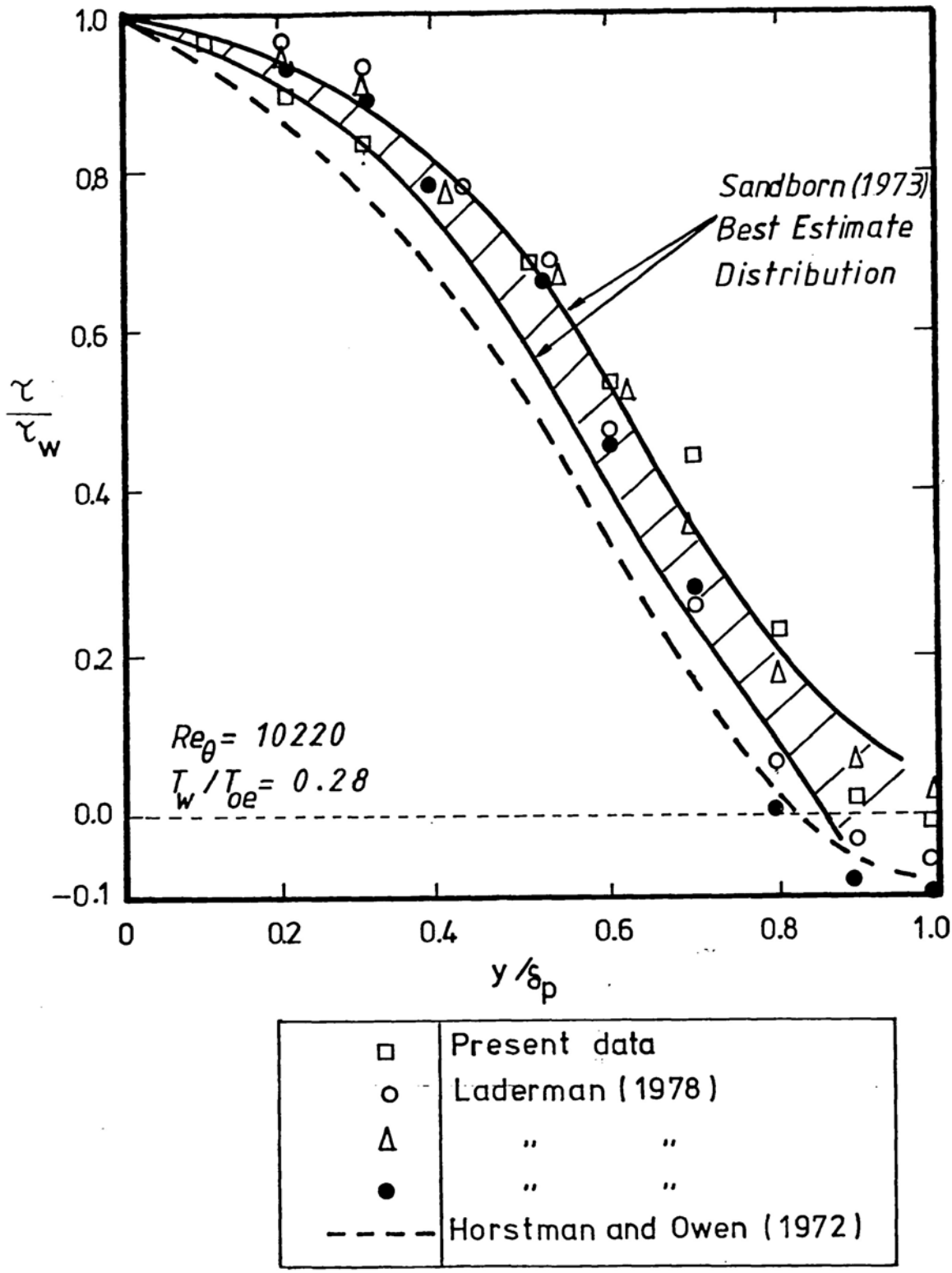


FIG. 5-33 TOTAL SHEAR STRESS DISTRIBUTION x = 460mm

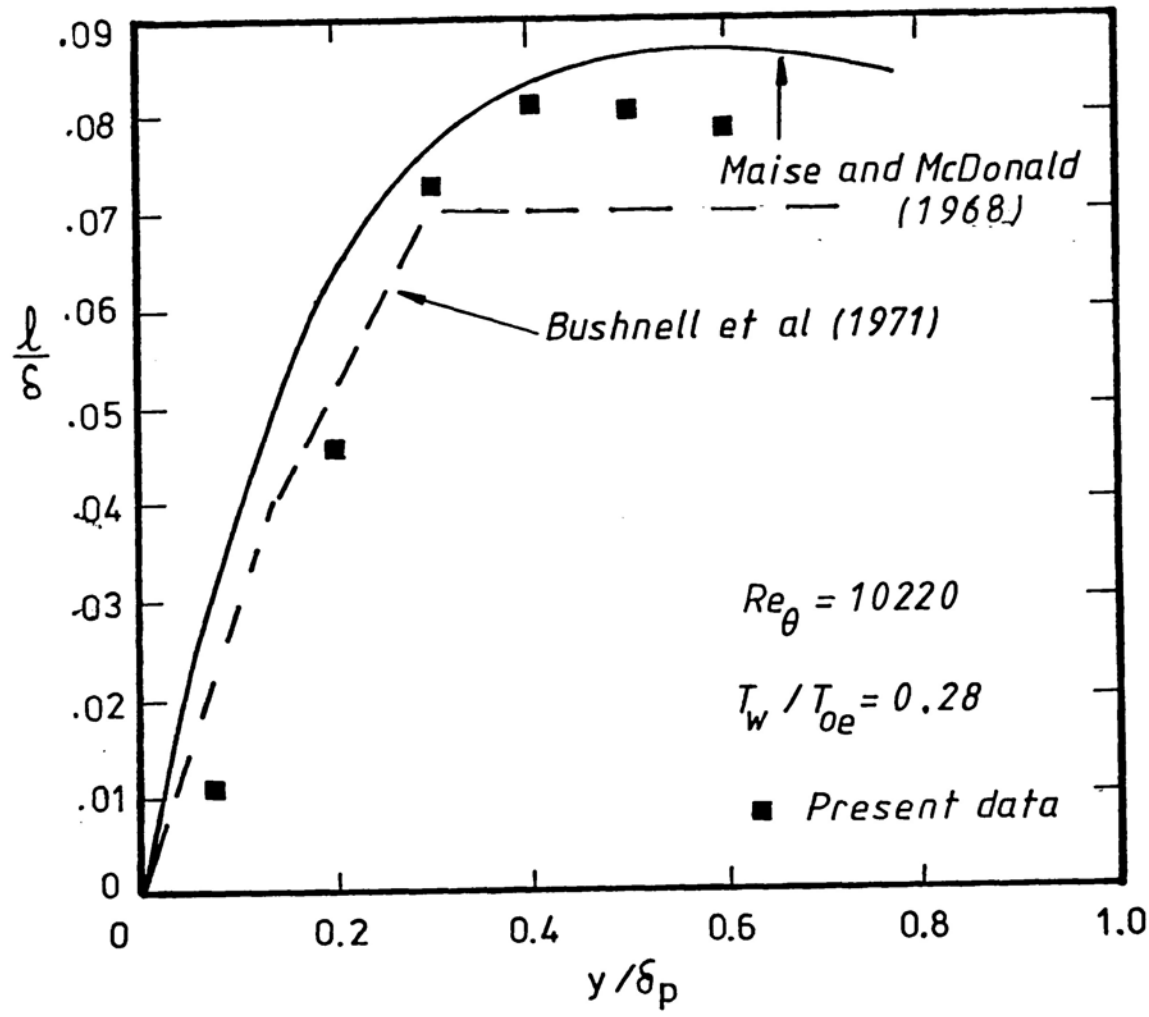
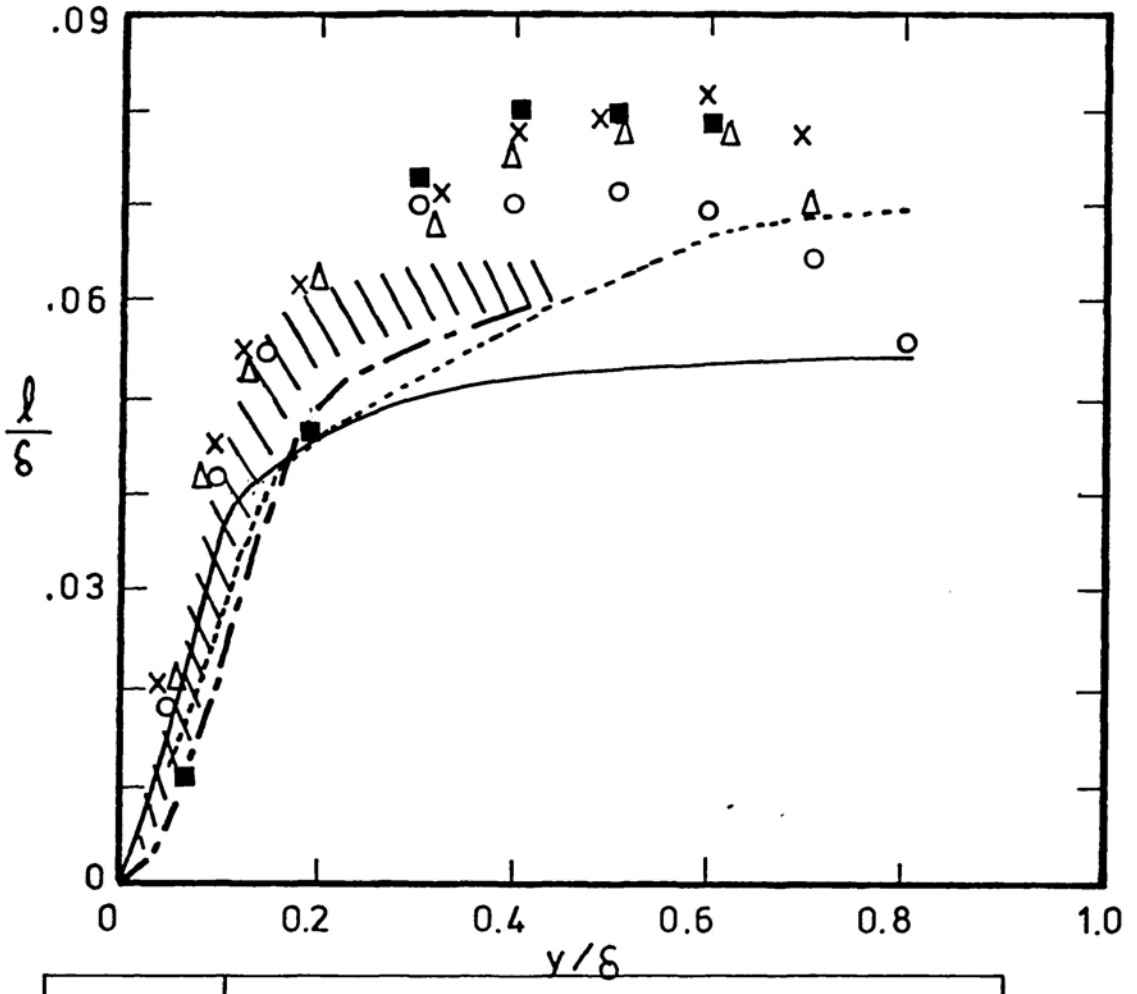


FIG. 5-34 MIXING LENGTH DISTRIBUTION x = 460mm



		M_e	T_w/T_{oe}
○	LADERMAN (1978)	3	0.94
△	" "	3	0.71
+	" "	3	0.54
■	PRESENT DATA	9	0.28
– – –	OWEN ET AL (1975)	7	0.43
\\\	HORSTMAN AND OWEN (1972)	7	0.46
———	WATSON (1977)	11	0.46
-------	" "	11	0.49

FIG. 5-35 COMPARISON OF MIXING LENGTH WITH AVAILABLE DATA

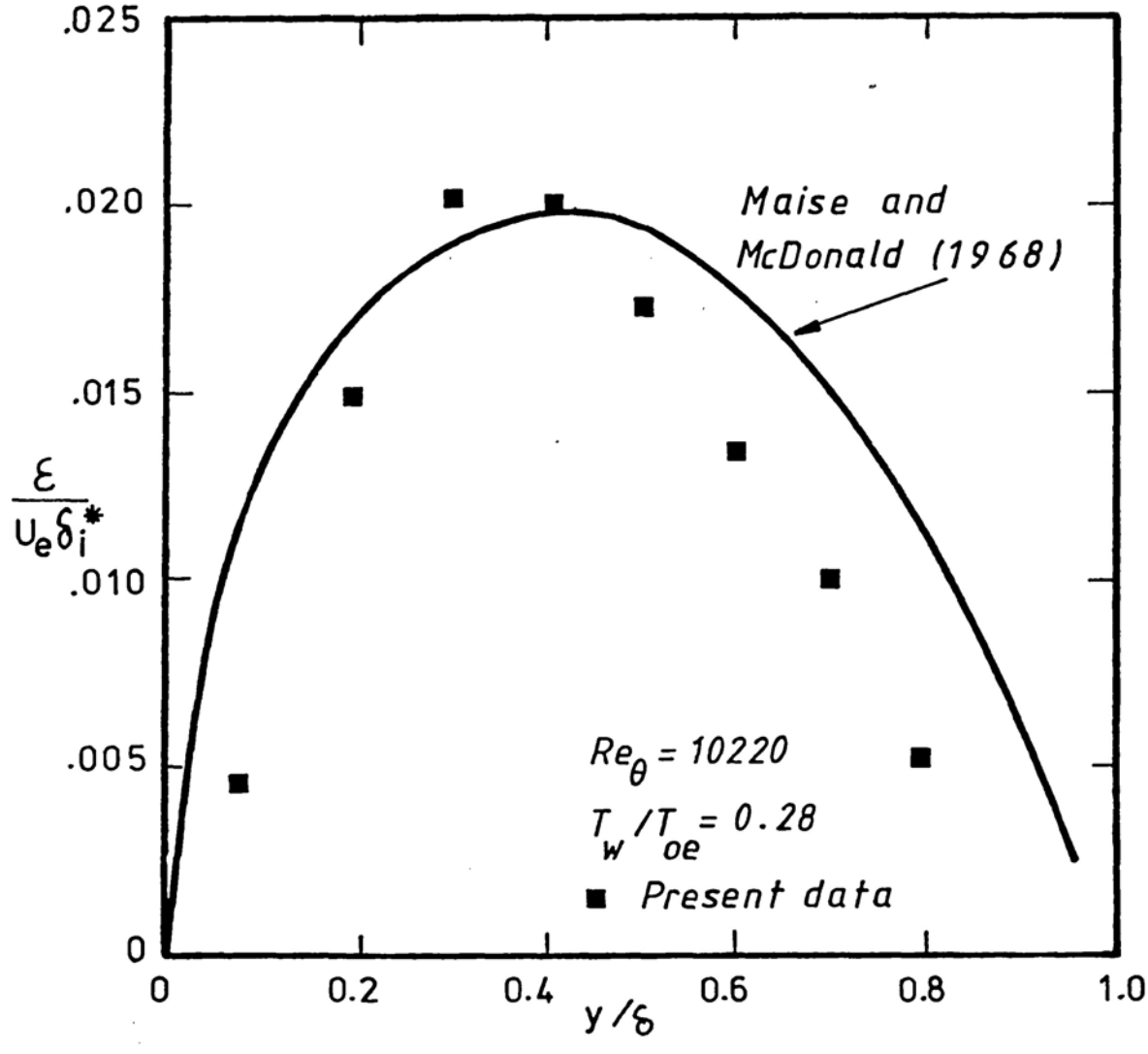
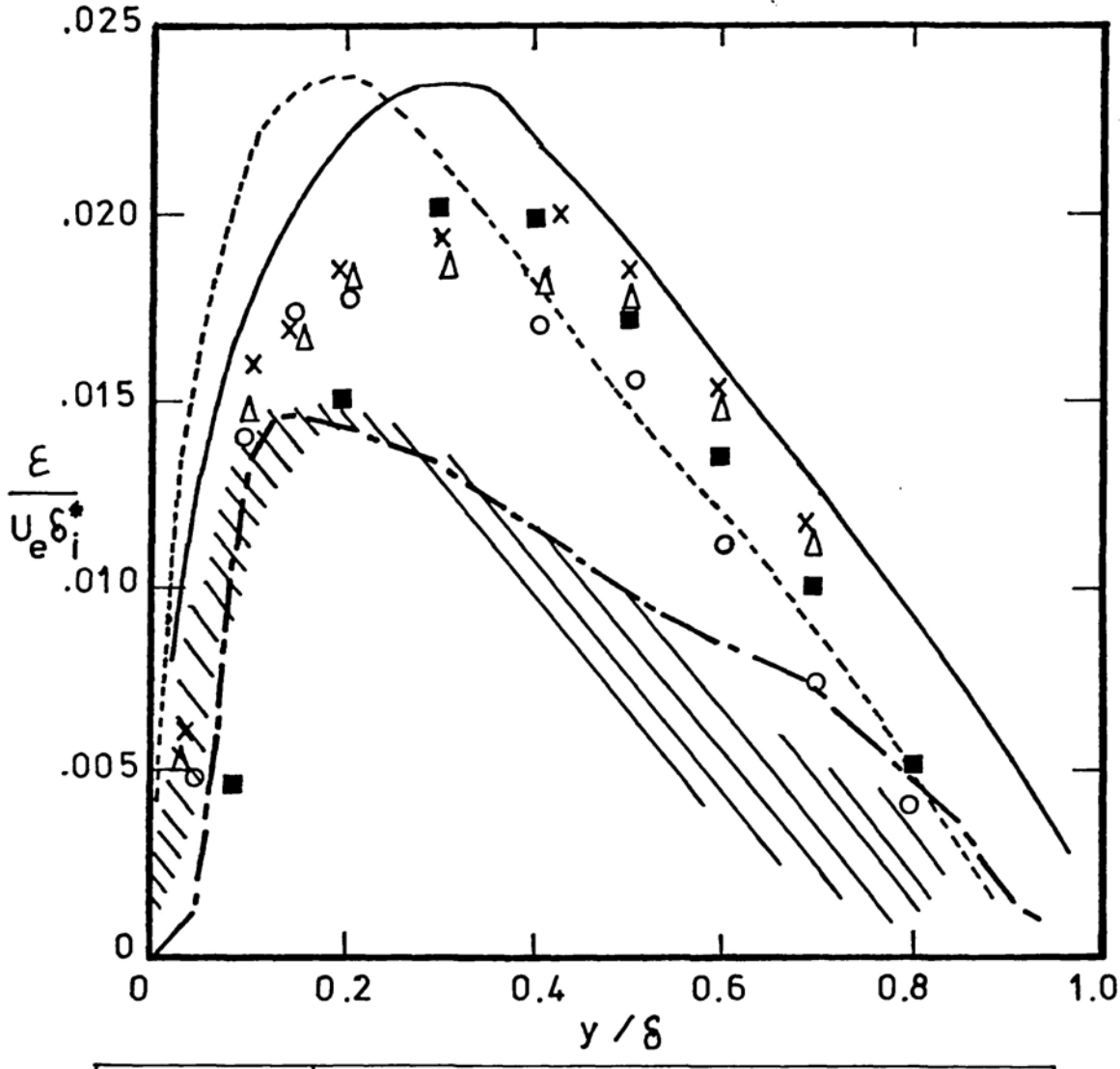


FIG. 5-36 EDDY VISCOSITY DISTRIBUTION AT x = 460mm



		M_e	T_w/T_{oe}
o	LADERMAN (1978)	3	0.94
Δ	" "	3	0.71
×	" "	3	0.54
■	PRESENT DATA	9	0.28
– – –	OWEN ET AL (1975)	7	0.43
////	HORSTMAN AND OWEN (1972)	7	0.46
———	WATSON (1977)	11	0.46
------	" "	11	0.49

FIG. 5-37 COMPARISON OF EDDY VISCOSITY WITH AVAILABLE DATA

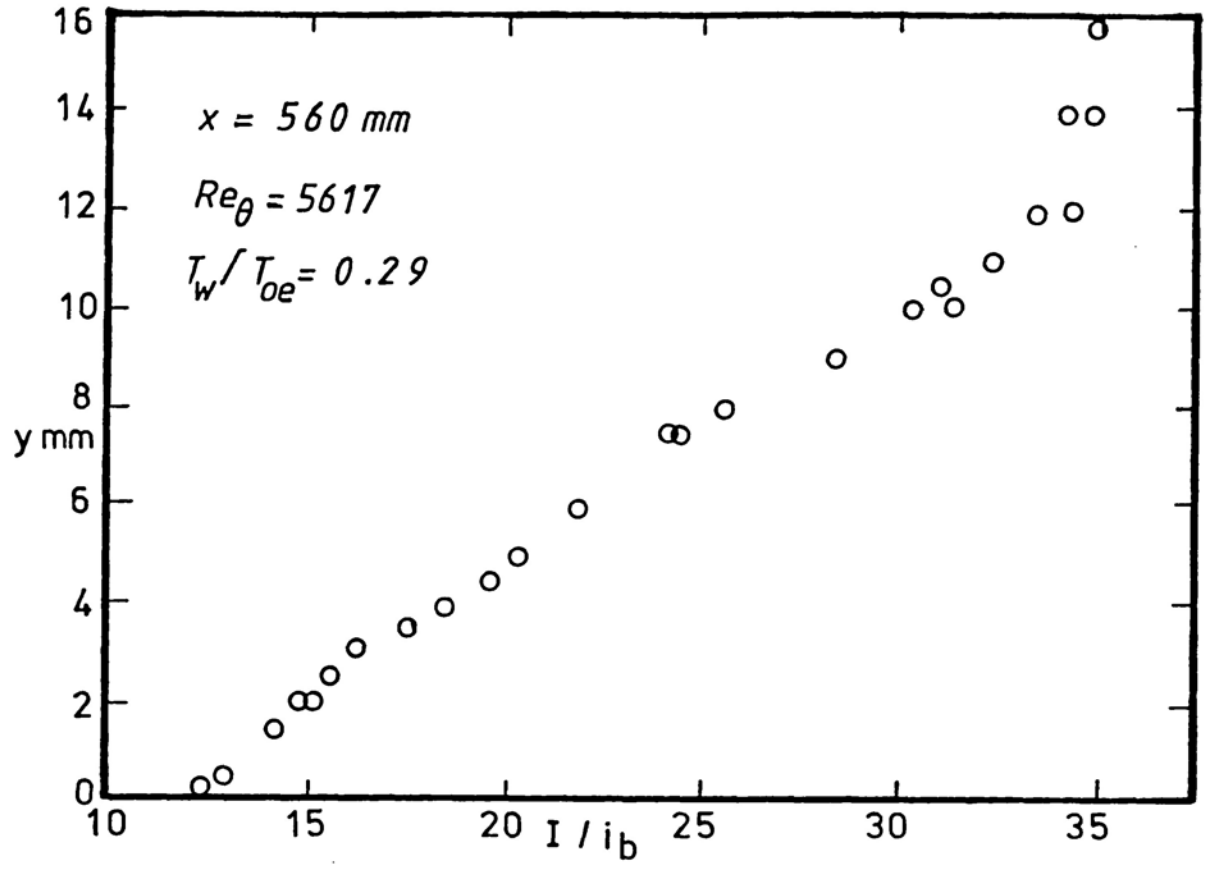


FIG. 5-38 FLUORESCENT LIGHT INTENSITY PROFILE x = 560mm

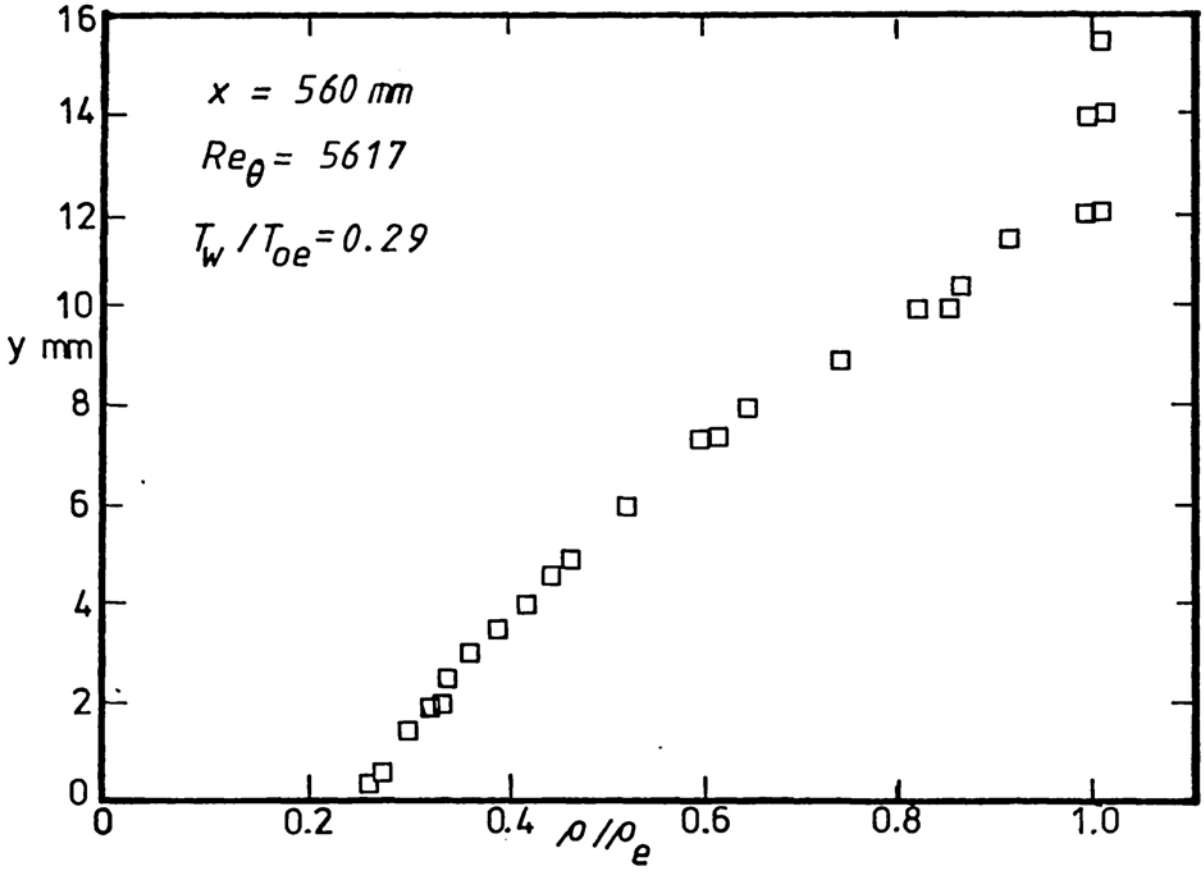


FIG. 5-39 MEAN DENSITY PROFILE x = 560mm

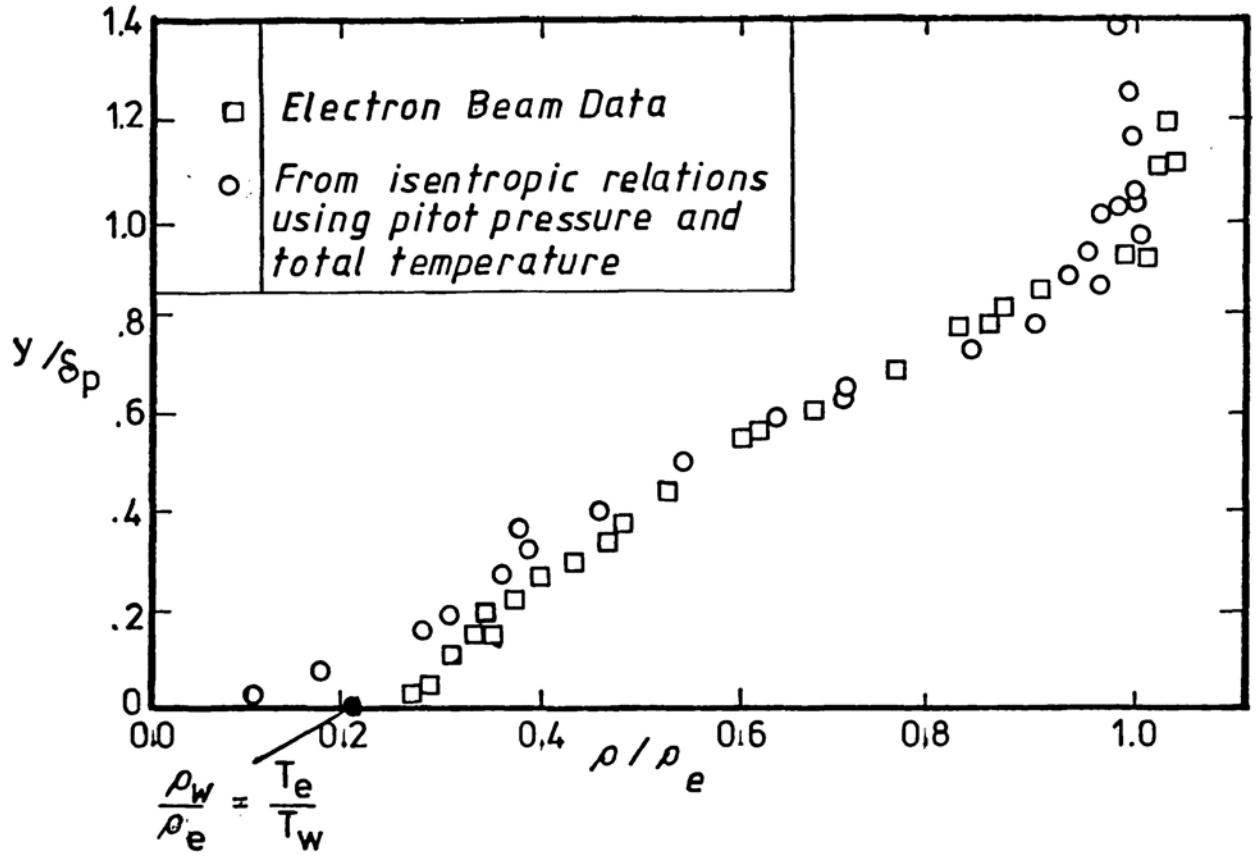


FIG. 5-40 DENSITY PROFILE x = 560mm - COMPARISON BETWEEN ELECTRON BEAM AND CONVENTIONAL PROBES

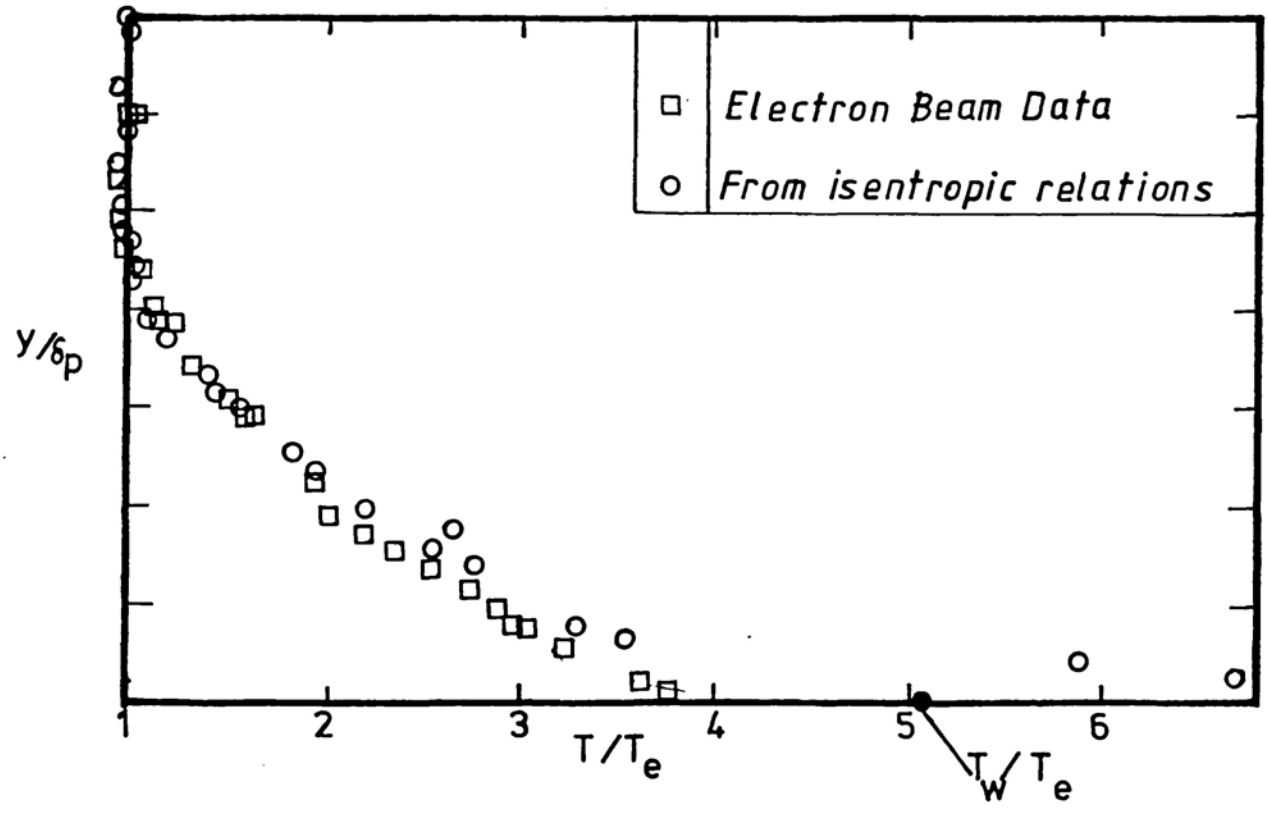


FIG. 5-41 TEMPERATURE PROFILE x = 560mm - COMPARISON BETWEEN ELECTRON BEAM AND CONVENTIONAL PROBES

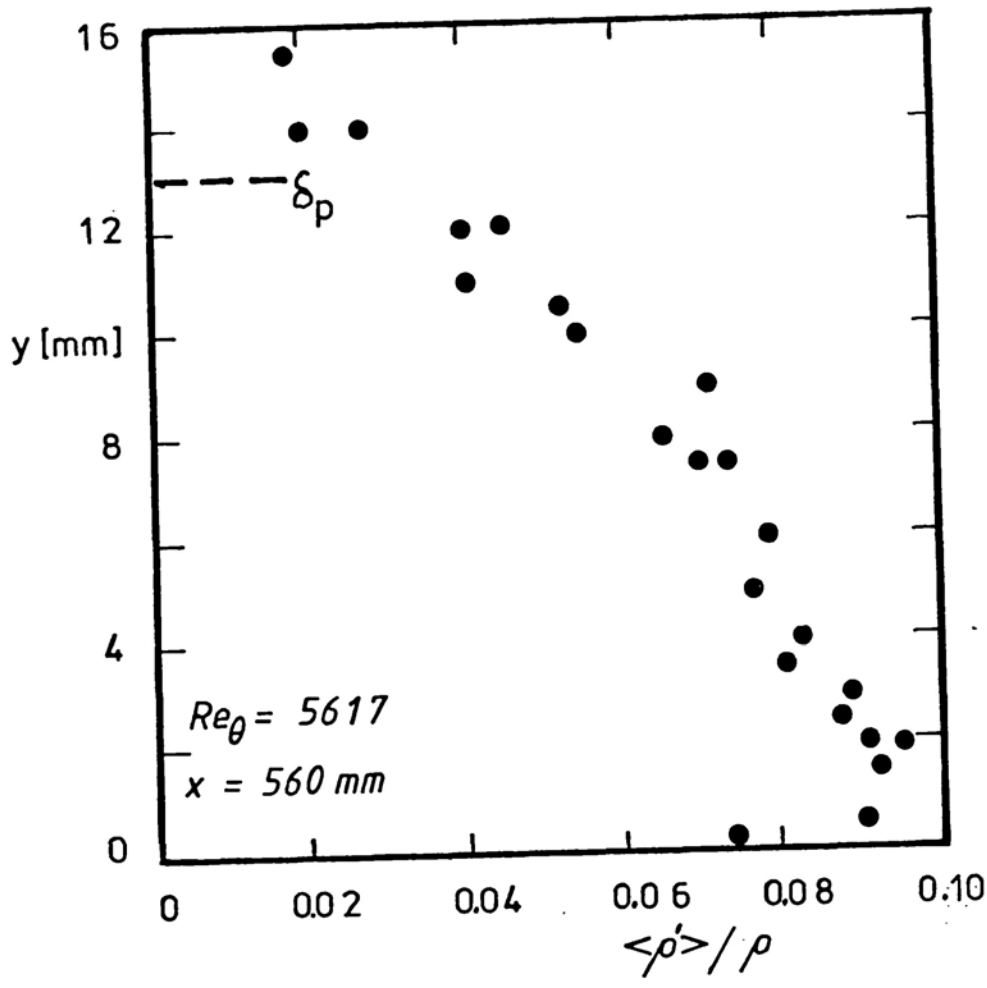


FIG. 5-42 FLUCTUATING DENSITY - x = 560mm

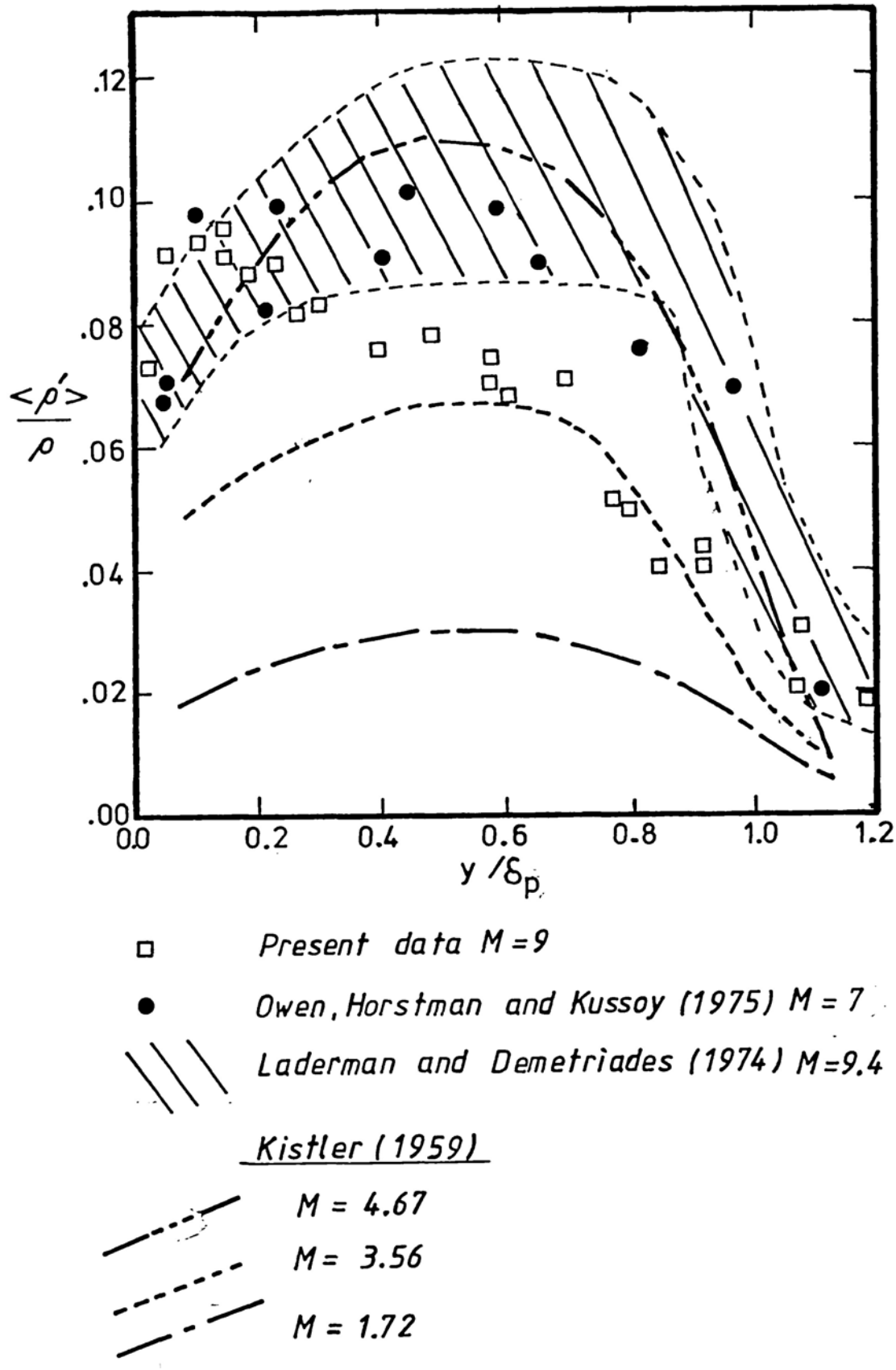


FIG. 5-43 FLUCTUATING DENSITY - COMPARISON WITH AVAILABLE HOT WIRE ANEOMOMETER DATA

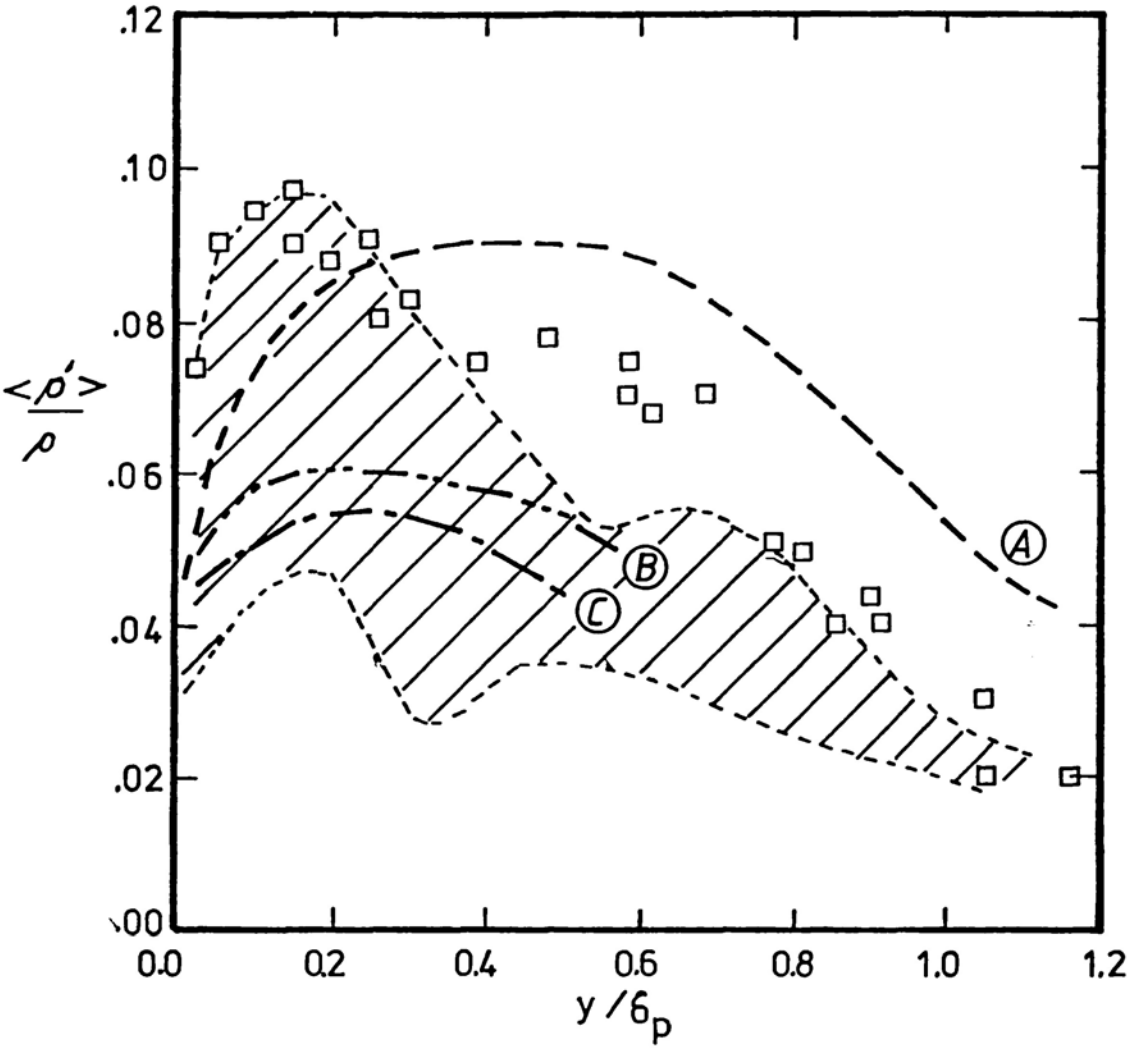


FIG. 5-44 FLUCTUATING DENSITY - COMPARISON WITH AVAILABLE ELECTRON BEAM PROBE DATA

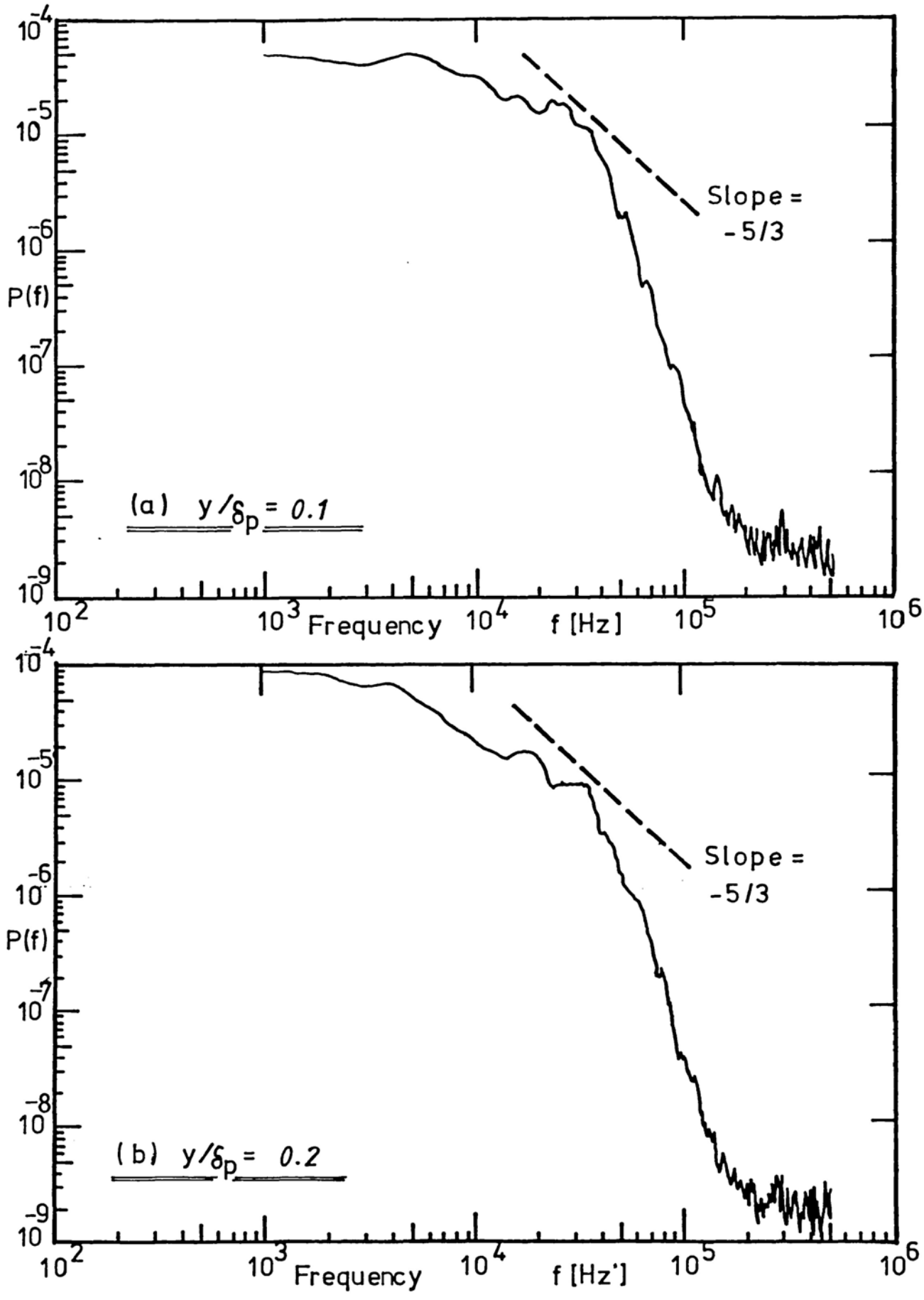


FIG. 5-45 POWER SPECTRAL DENSITY - x = 560mm

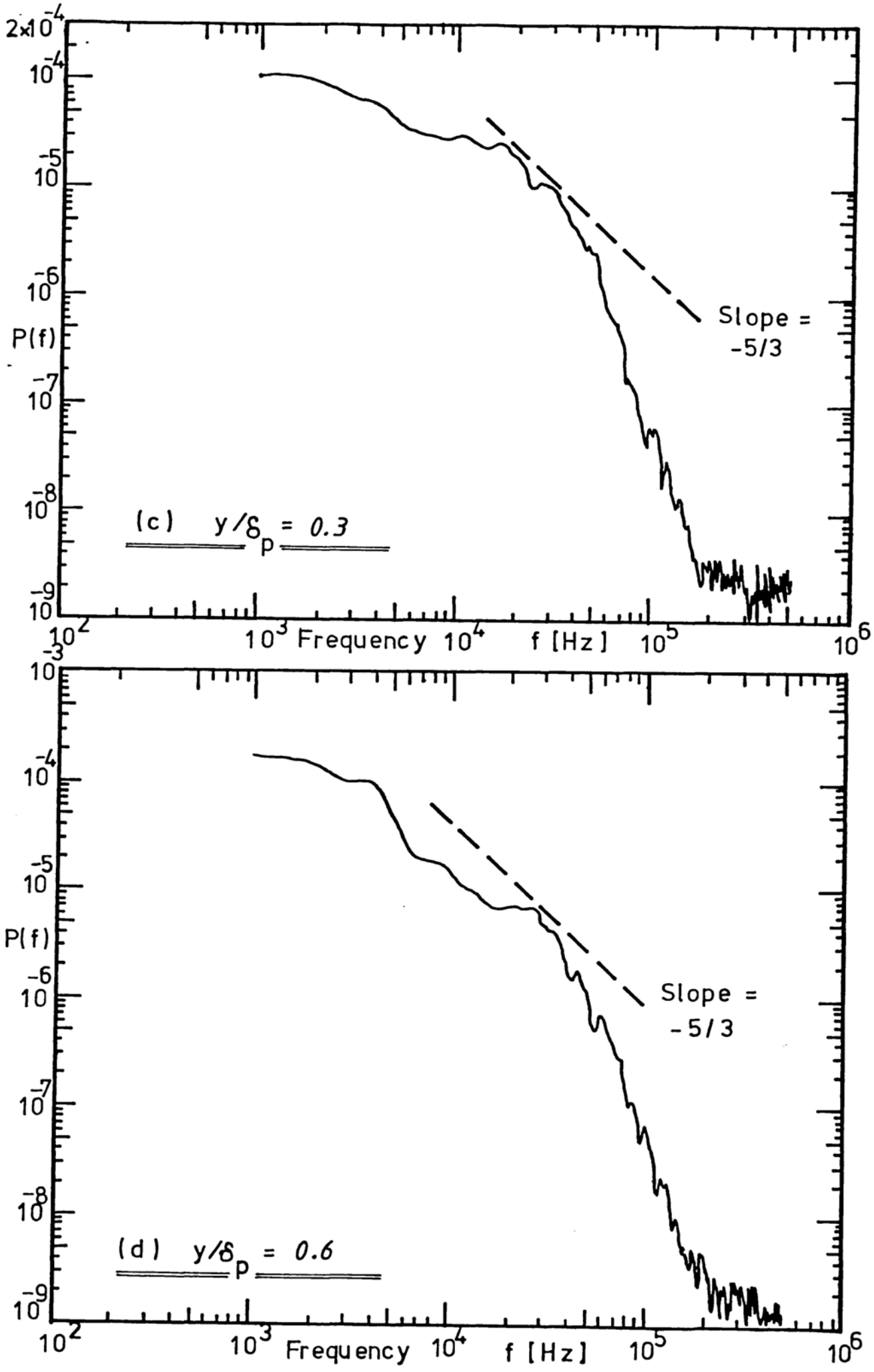


FIG. 5-45 CONTINUED POWER SPECTRAL DENSITY

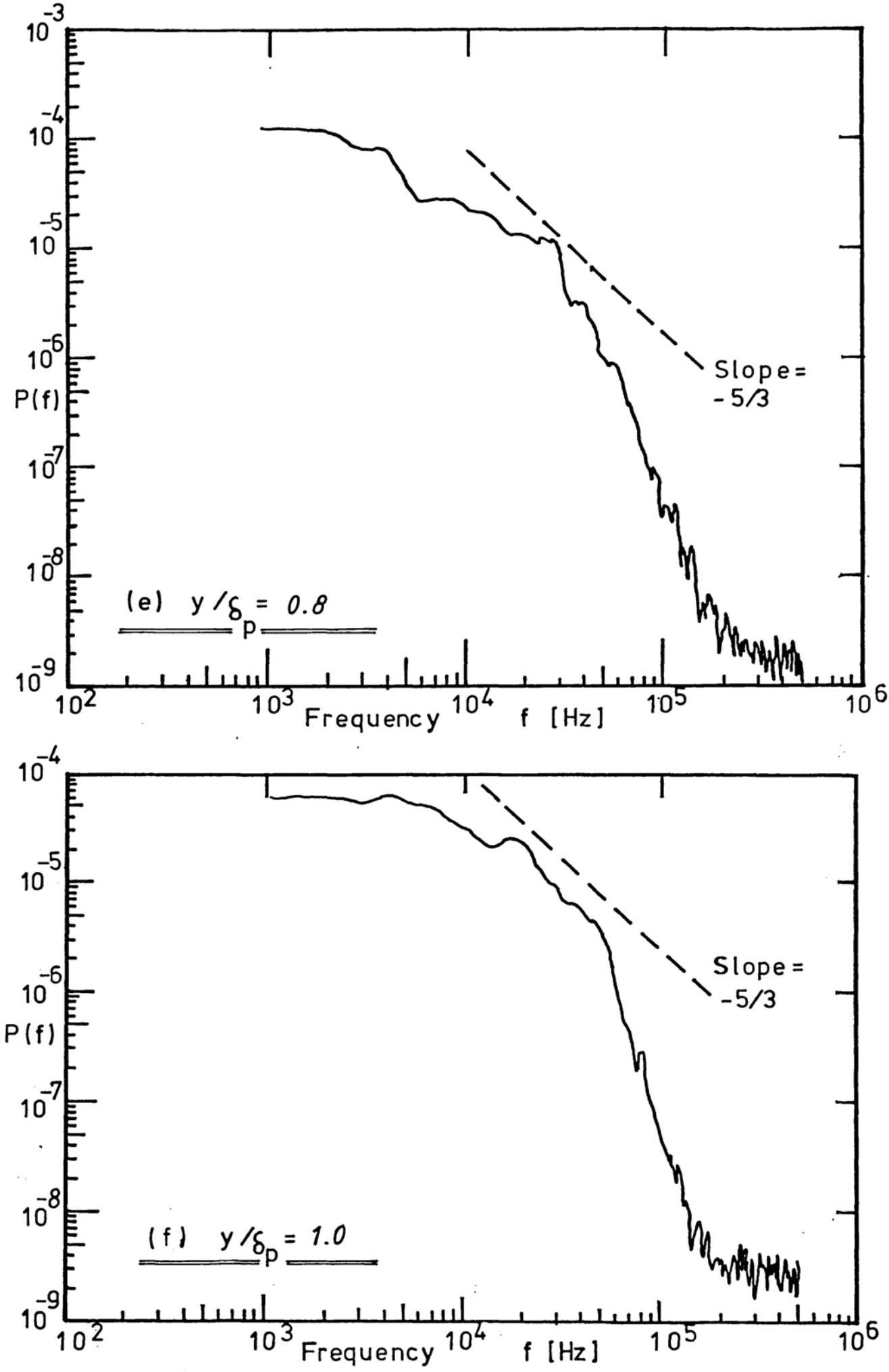


FIG. 5-45 CONTINUED POWER SPECTRAL DENSITY

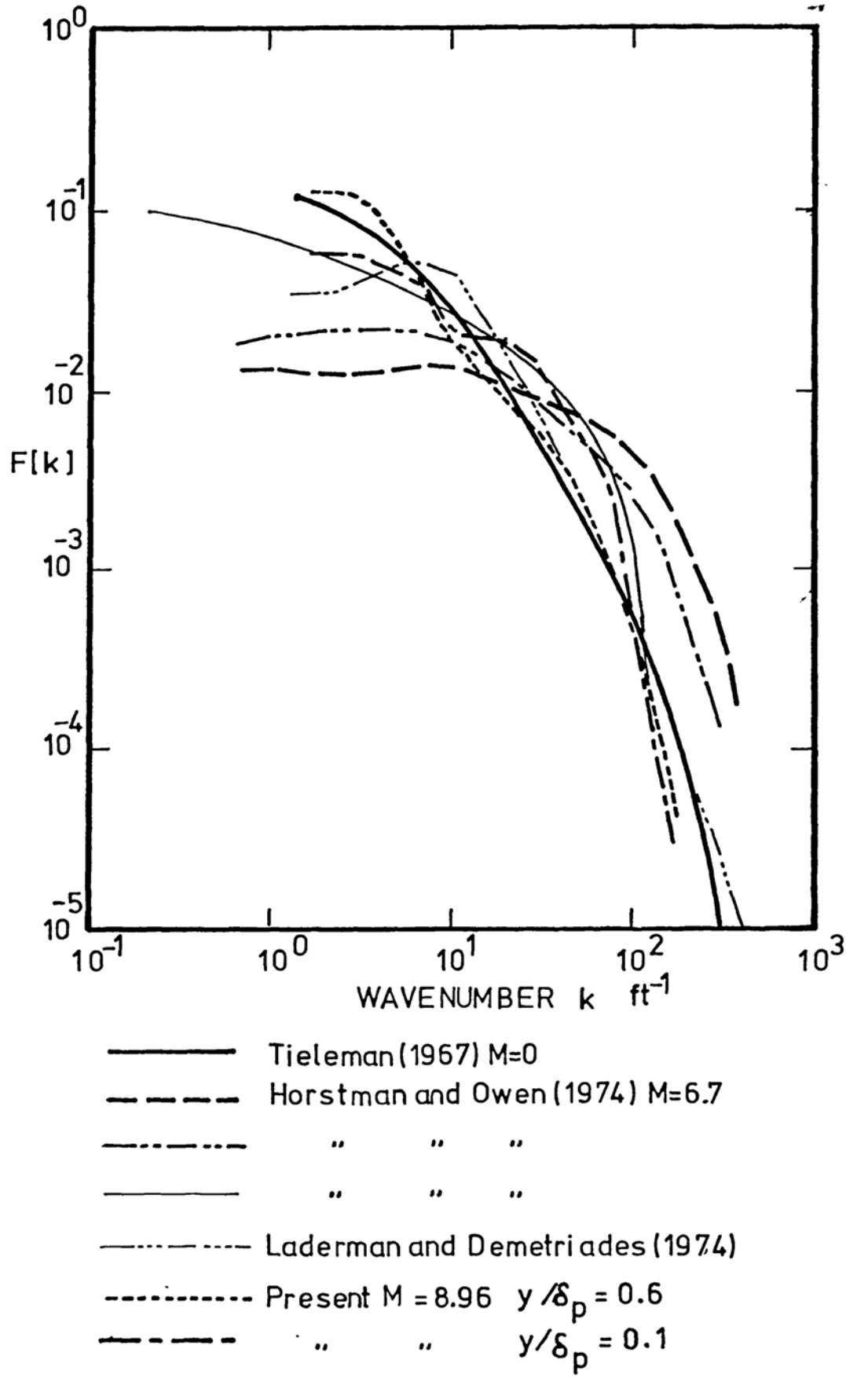


FIG. 5-46 POWER SPECTRAL DENSITY - COMPARISON WITH AVAILABLE DATA (AFTER SANDBORN (1974)

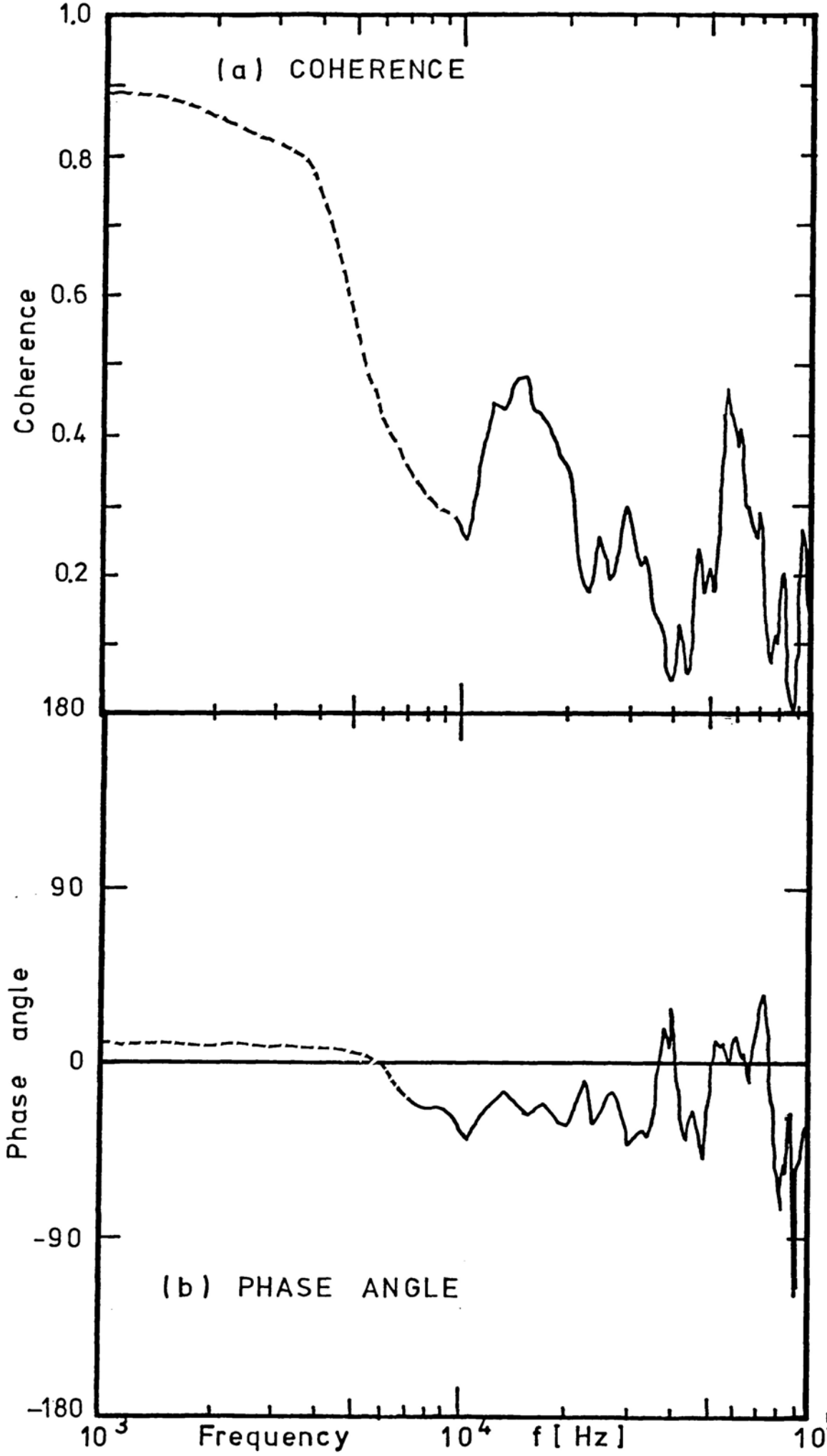


FIG. 5-47 COHERENCE BETWEEN DETECTORS - BOTH FOCUSED $y/\delta_p = 0.1$

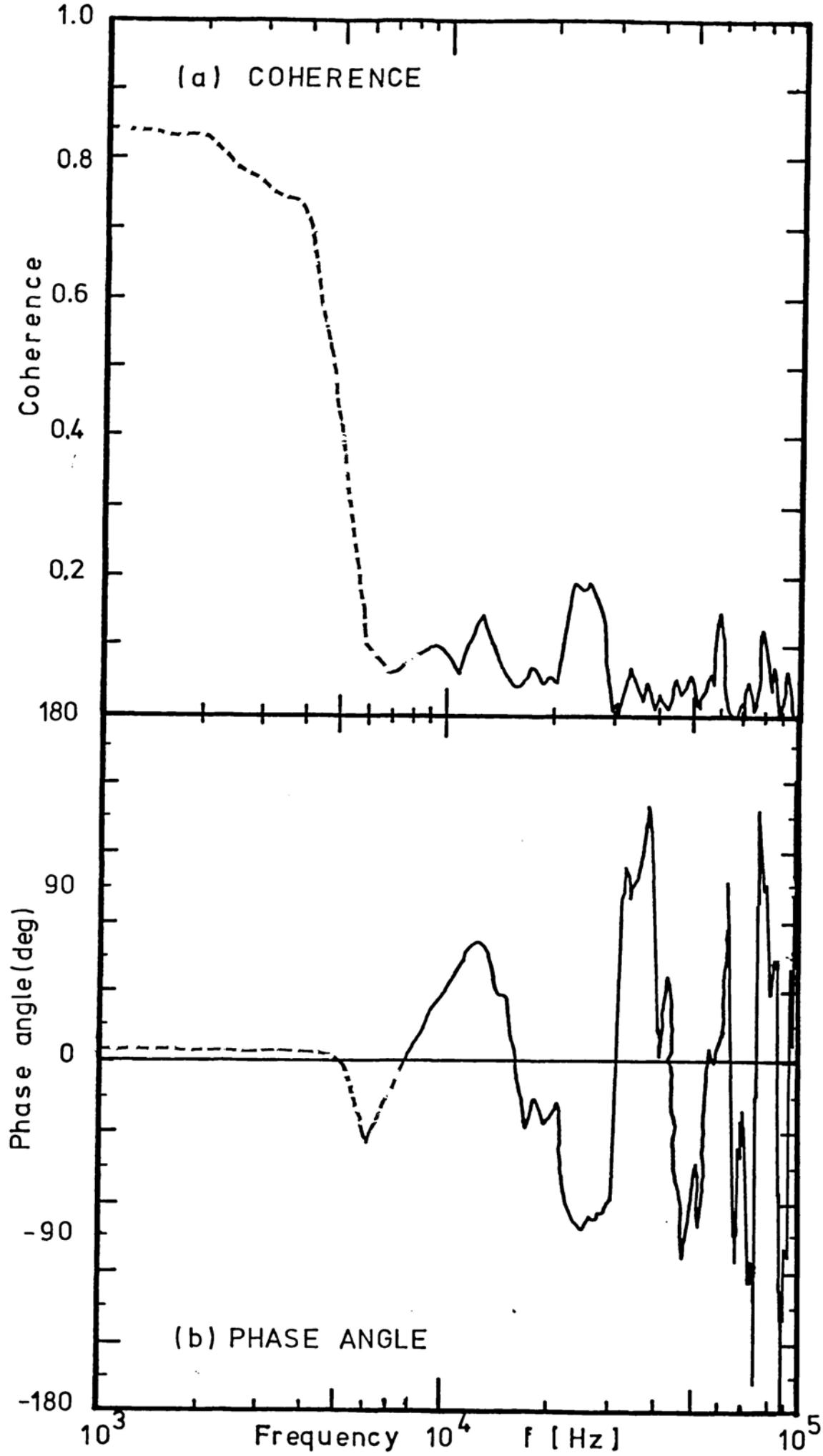


FIG. 5-48 COHERENCE BETWEEN DETECTORS - y/δ_p= 0.1 AND y/δ_p= 0.6

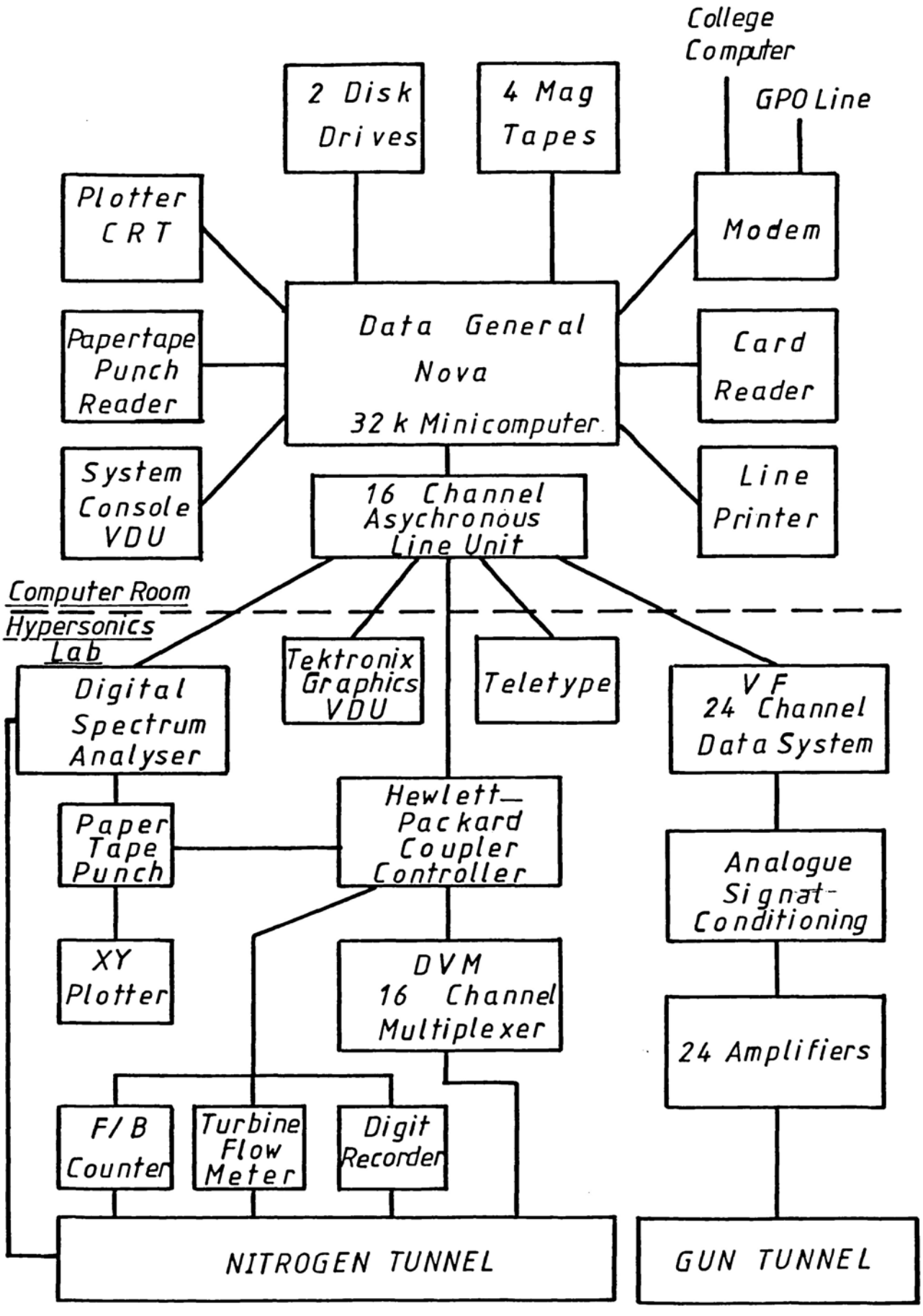


Fig. A1 System Configuration

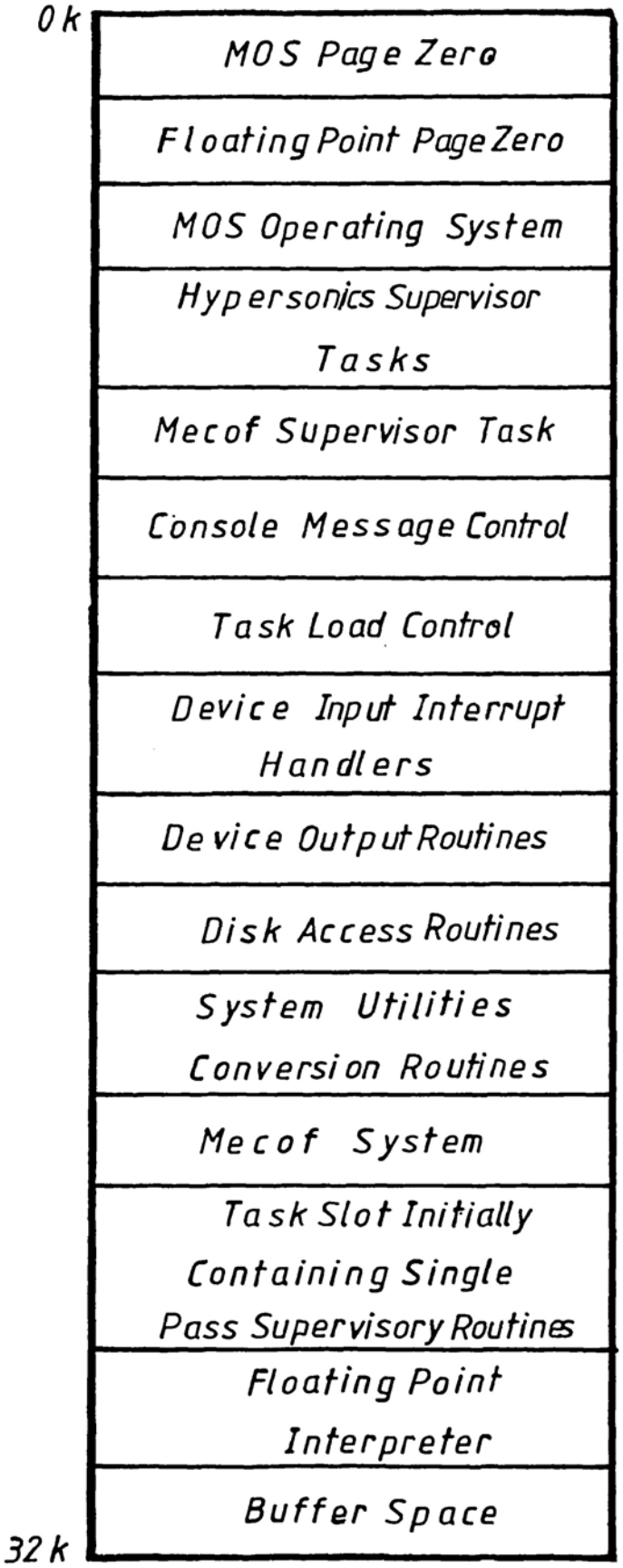


Fig. A2 Core Map

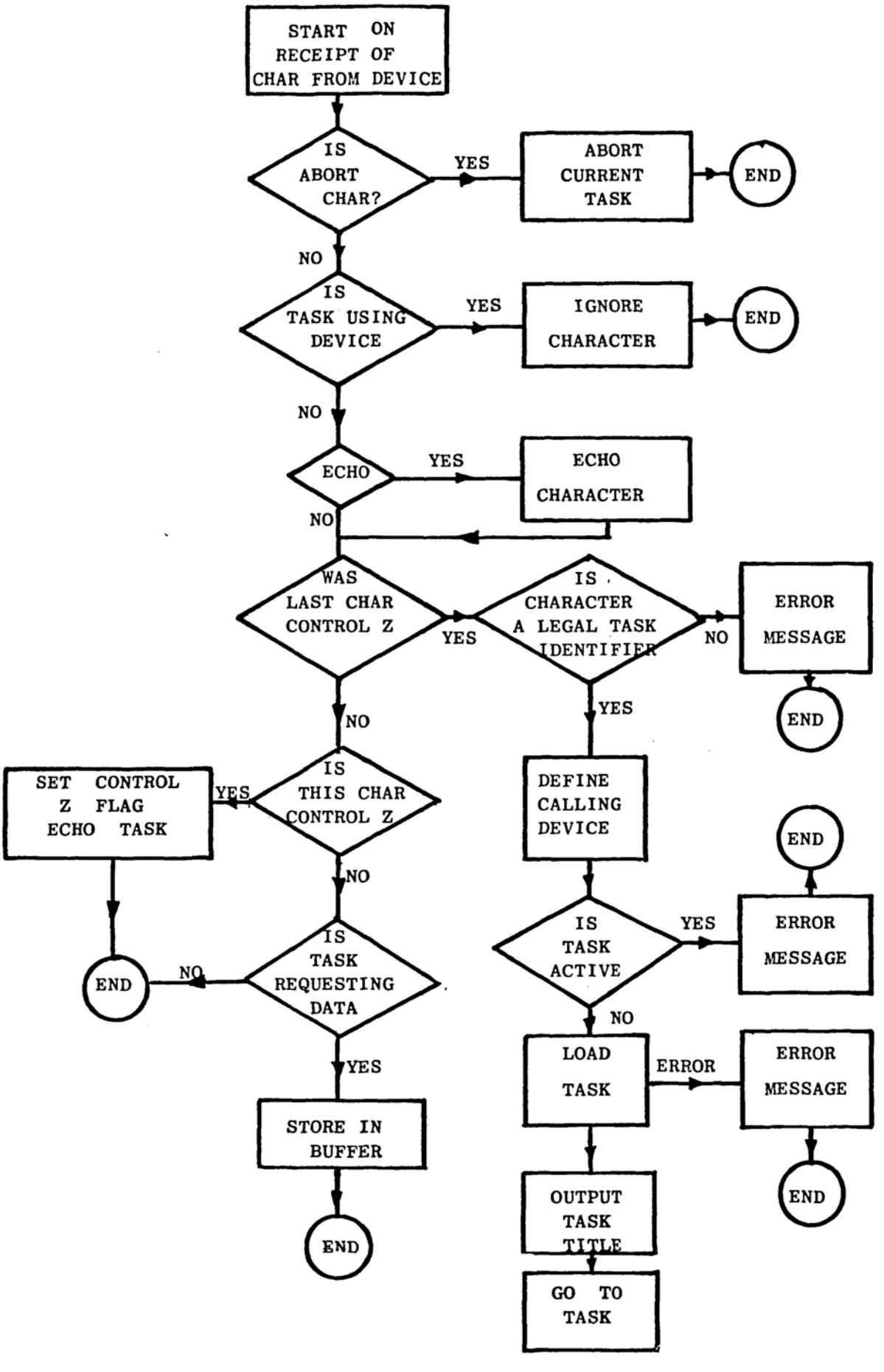


FIG.A3 Master Task

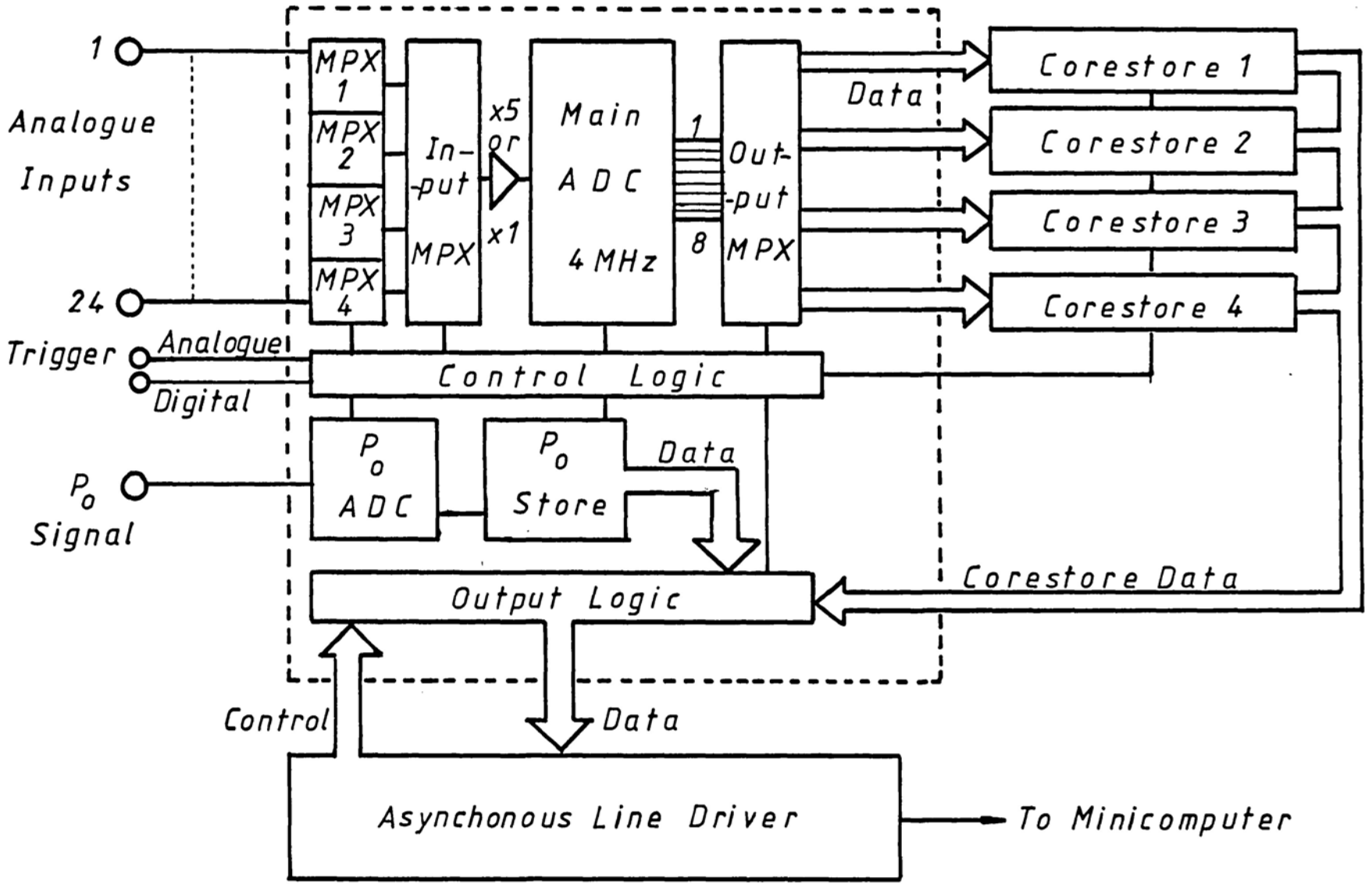


Fig. A4 Gun Tunnel Data System

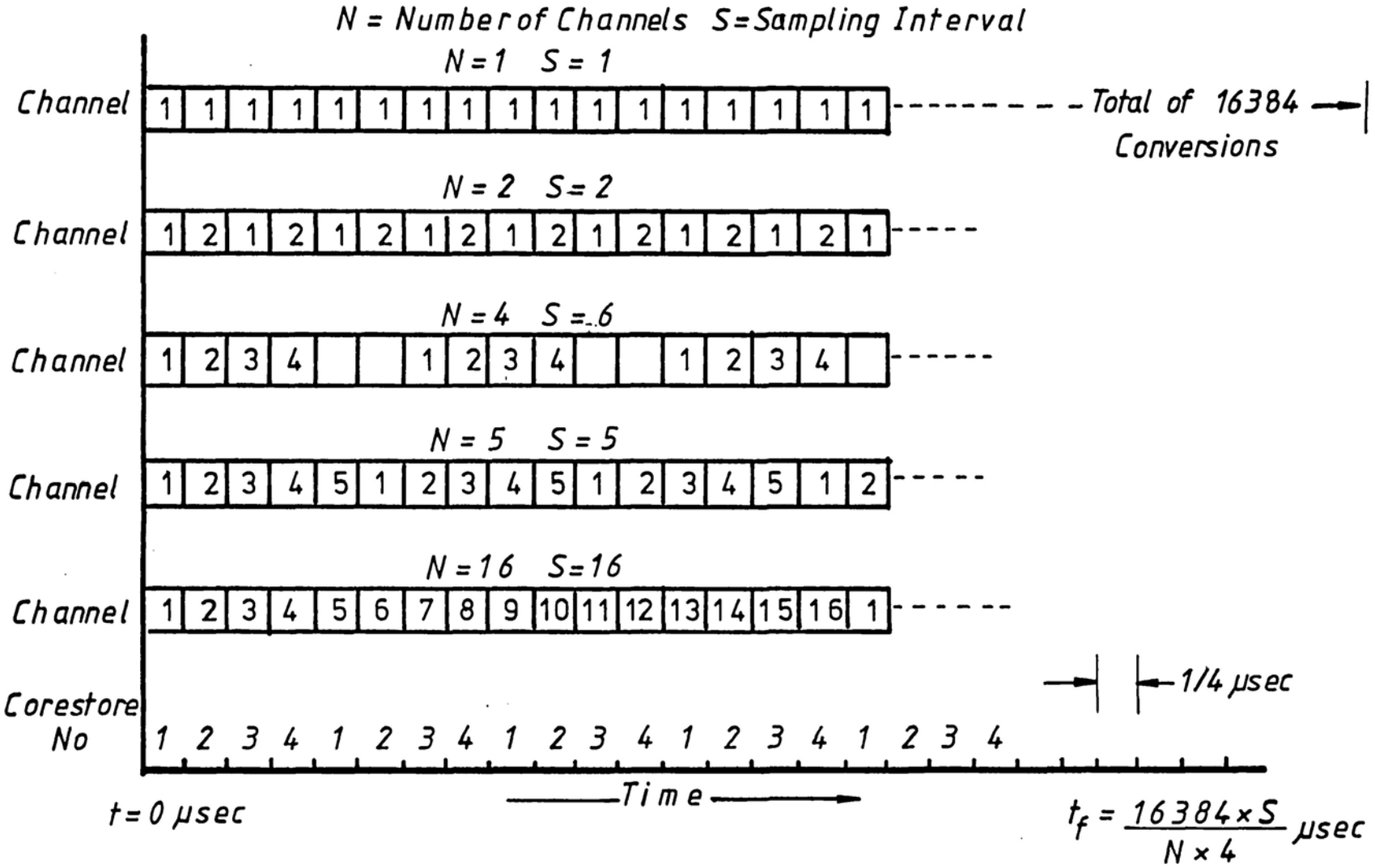


FIG. A5 Timing Diagram

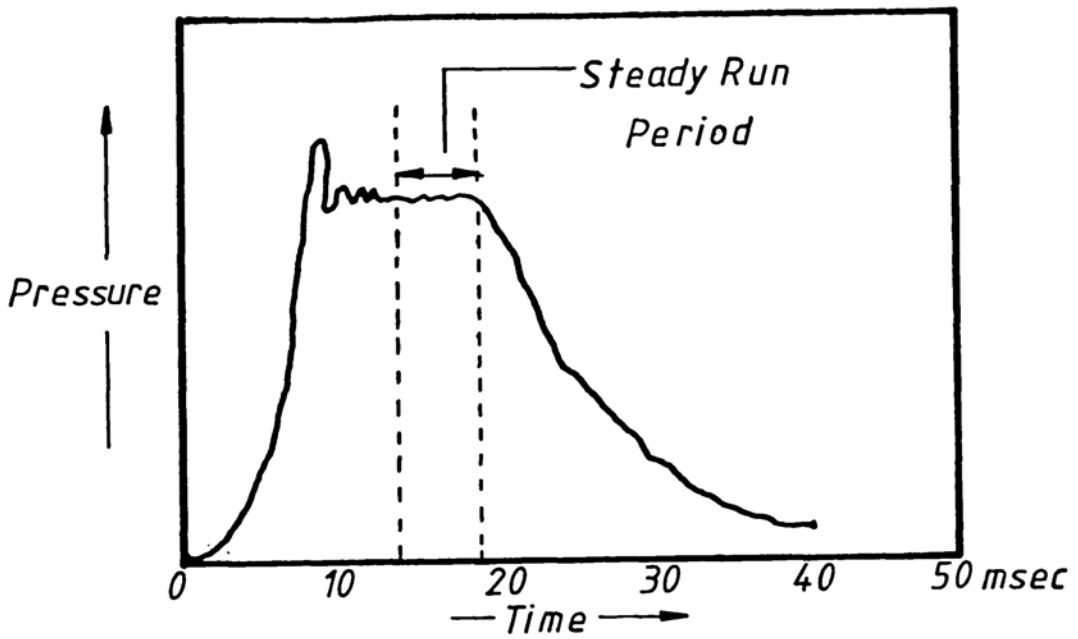
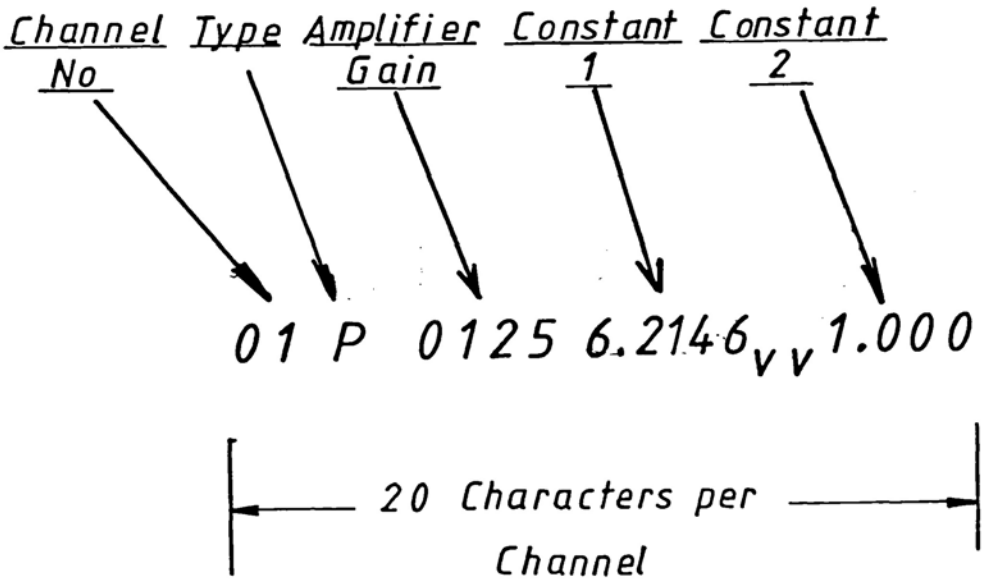
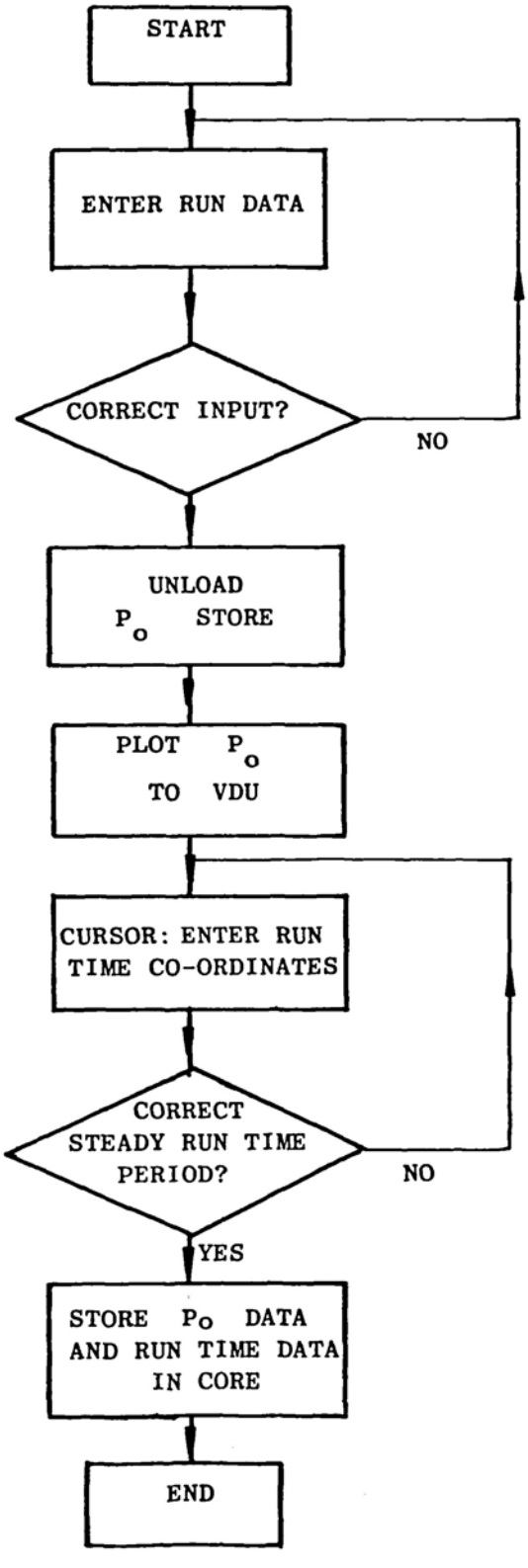


FIG. A6 Typical P_o Pressure Trace



[V = space]

FIG. A7 Organisation Of Channel Calibration Data [Task G]



Task P

FIG. A8 Task P

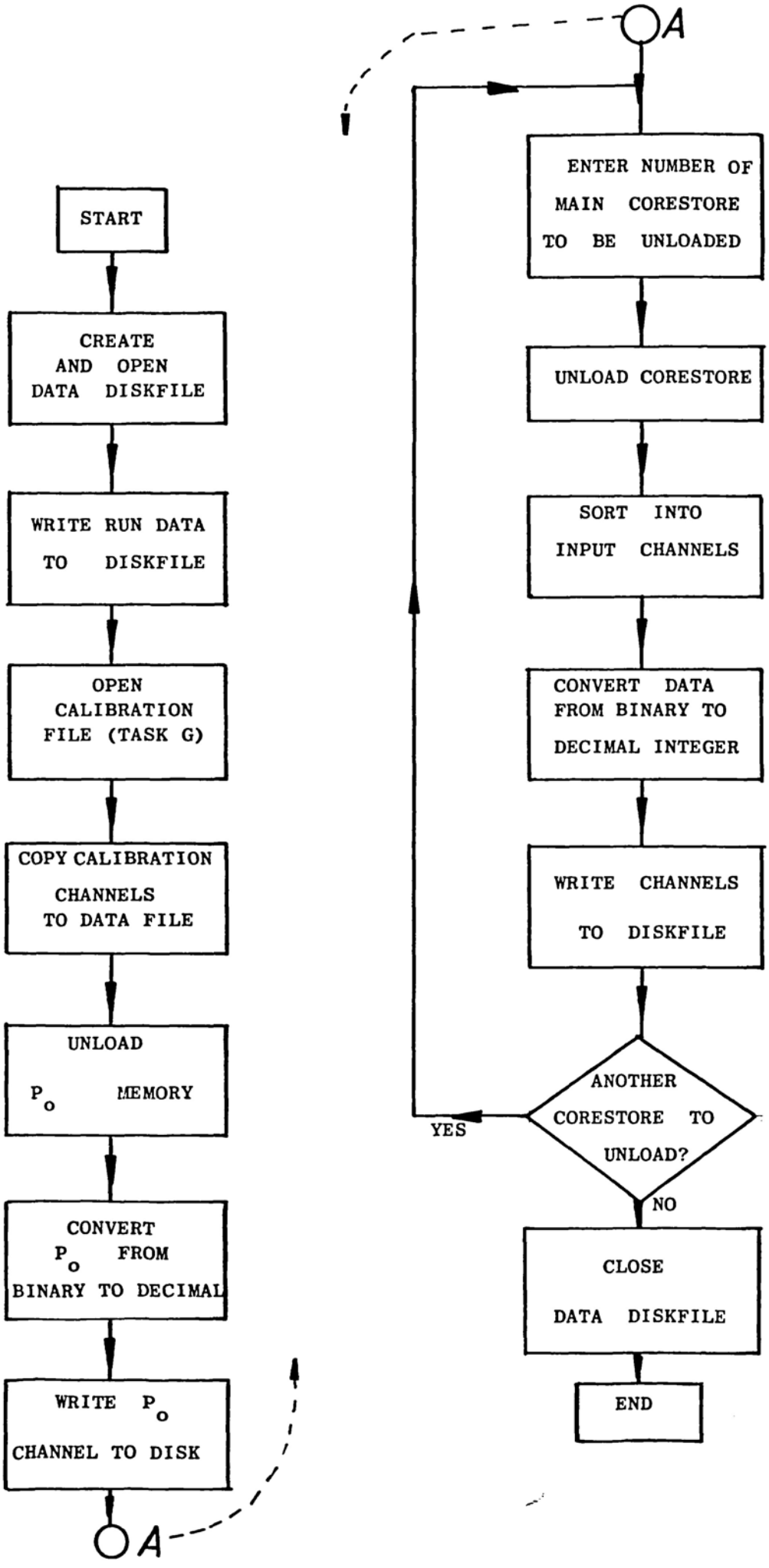

START
CREATE AND OPEN DATA DISKFILE
WRITE RUN DATA TO DISKFILE
OPEN CALIBRATION FILE (TASK G)
COPY CALIBRATION CHANNELS TO DATA FILE
UNLOAD P_o MEMORY
CONVERT P_o FROM BINARY TO DECIMAL
WRITE P_o CHANNEL TO DISK
A
A
ENTER NUMBER OF MAIN CORESTORE TO BE UNLOADED
UNLOAD CORESTORE
SORT INTO INPUT CHANNELS
CONVERT DATA FROM BINARY TO DECIMAL INTEGER
WRITE CHANNELS TO DISKFILE
ANOTHER CORESTORE TO UNLOAD?
YES
NO
CLOSE DATA DISKFILE
END

FIG. A9 Task Q

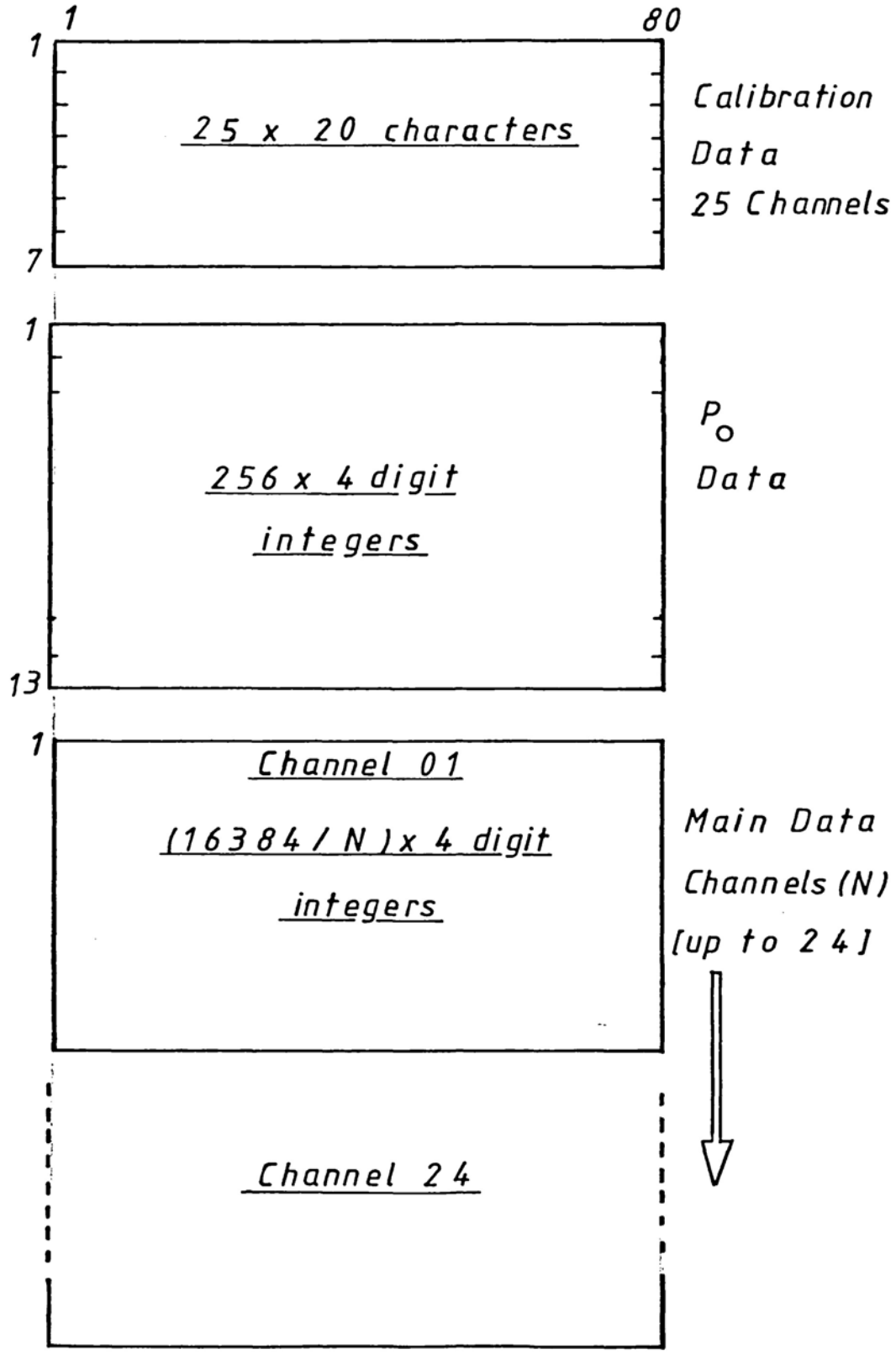


Fig. A10 Task Q Data File Format [80 Column Card Image]

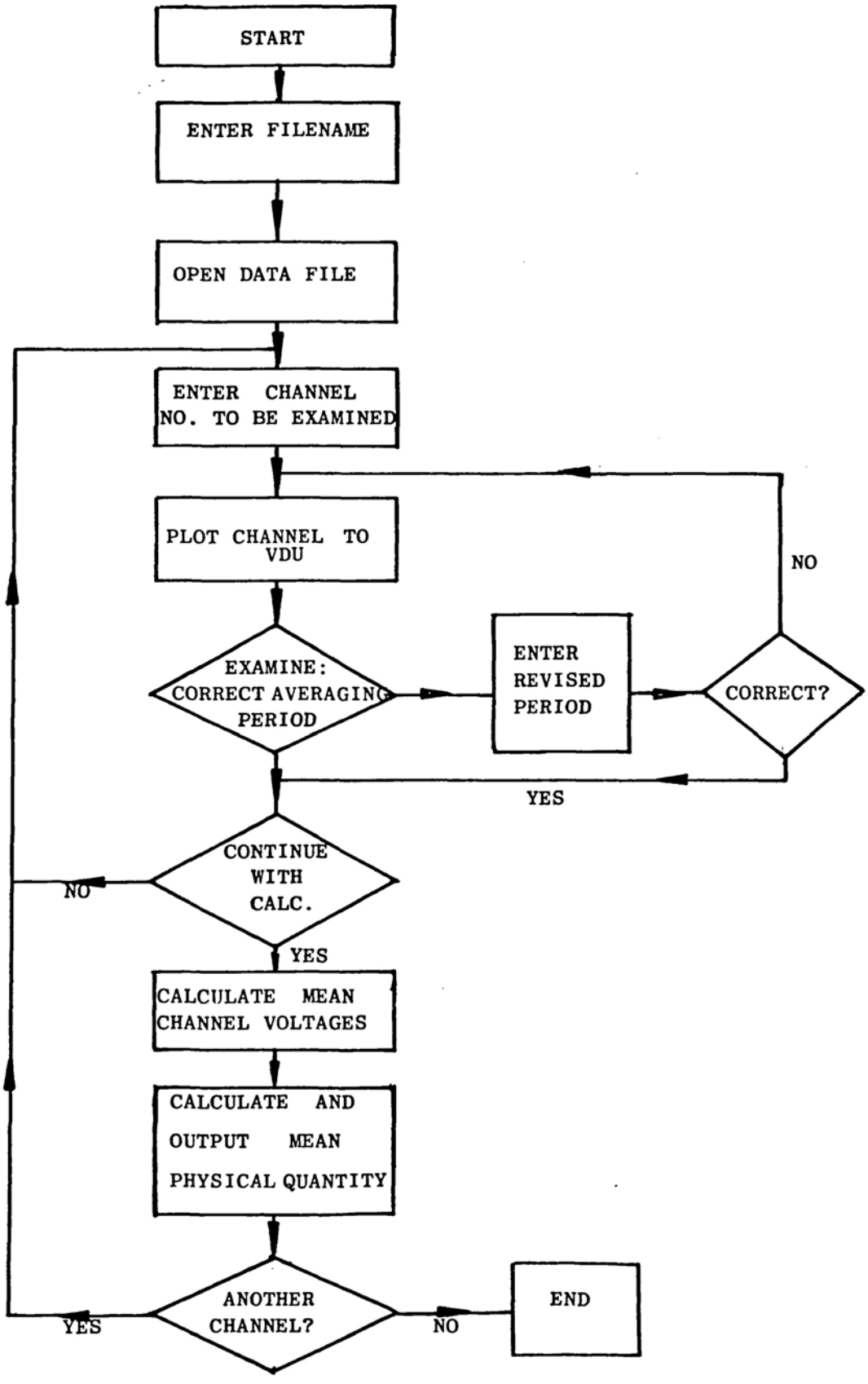


FIG. A11 Task F

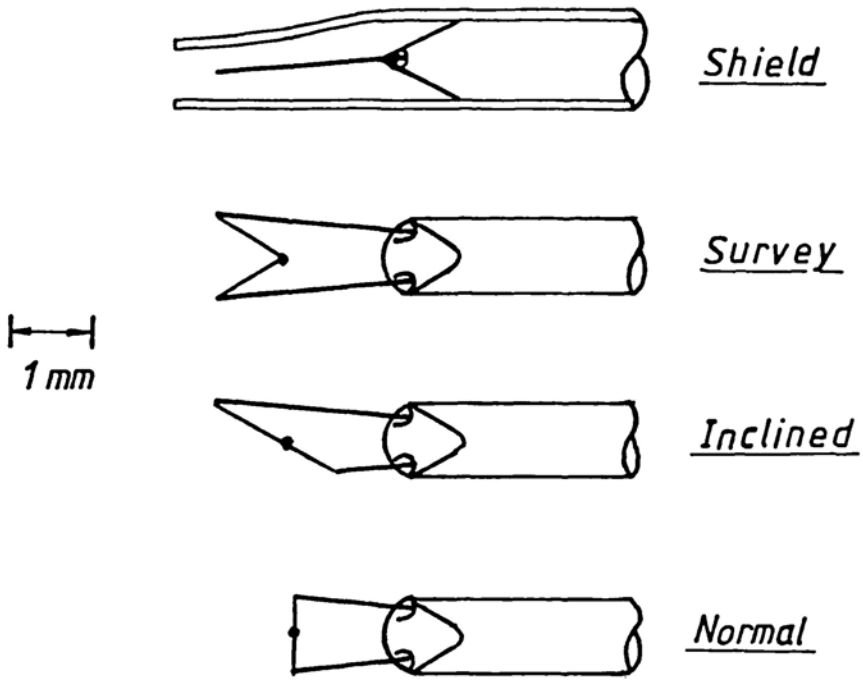


Fig. B1 Calibration Probes

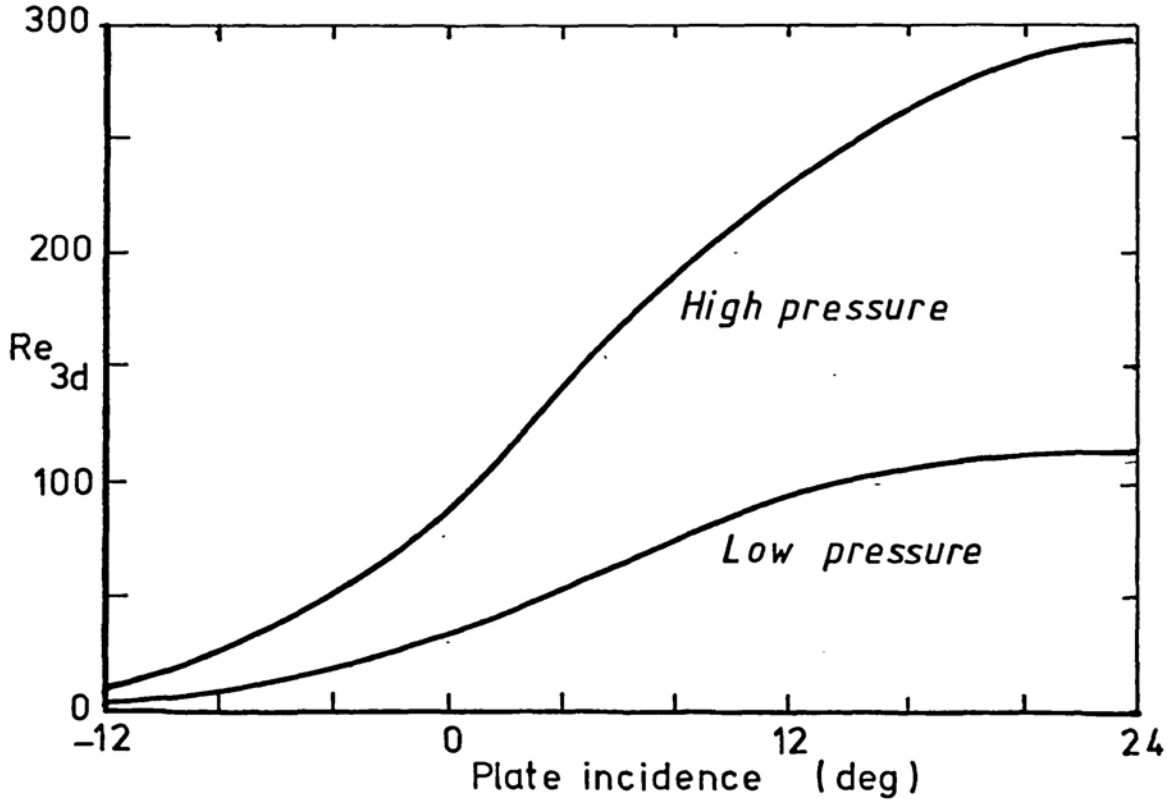


Fig. B2 Variation of probe Reynolds number with plate incidence [sensor wire dia. $1{,}27\times10^{-2}$ mm]

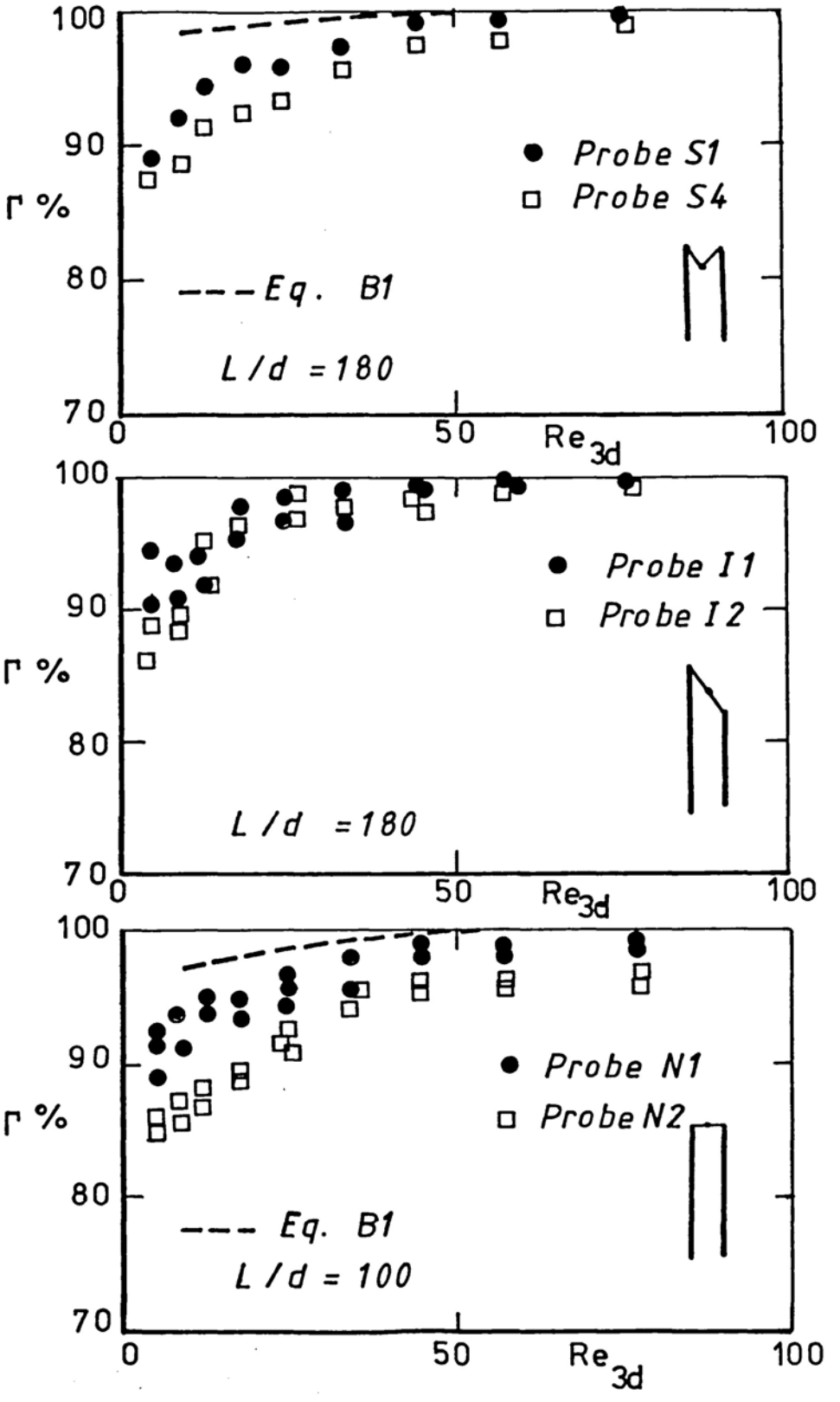


Fig. B3 Calibration data for three probe types